

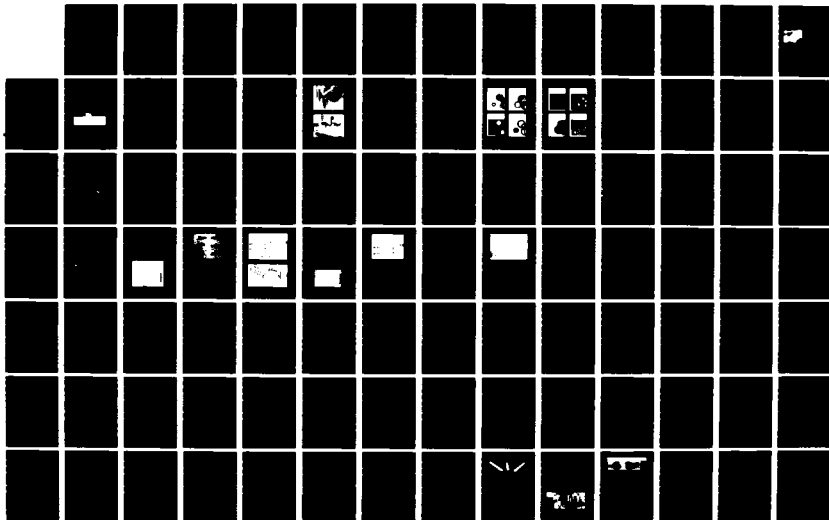
AD-A148 079

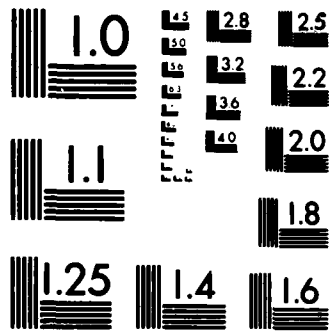
THE SHOCK AND VIBRATION BULLETIN PART 1 OPENING SESSION 1/3
PANEL SESSION SHO. (U) NAVAL RESEARCH LAB WASHINGTON DC
SHOCK AND VIBRATION INFORMAT. SEP 77 BULL-47-PT-1

UNCLASSIFIED

F/G 20/11

NL





MICROCOPY RESOLUTION TEST CHART
NATIONAL BUREAU OF STANDARDS-1963-A

AD-A 148 079

1

Bulletin 47
(Part 1 of 4 Parts)

THE SHOCK AND VIBRATION BULLETIN

Part 1
Opening Session, Panel Session, Shock Analysis
Shock Testing, Isolation and Damping

SEPTEMBER 1977

A Publication of
THE SHOCK AND VIBRATION
INFORMATION CENTER
Naval Research Laboratory, Washington, D.C.



DTIC
NOV 29 1984
A

DTIC FILE COPY

Office of
The Director of Defense
Research and Engineering

Approved for public release; distribution unlimited.

84 11 26 18

SYMPOSIUM MANAGEMENT

THE SHOCK AND VIBRATION INFORMATION CENTER

**Henry C. Pusey, Director
Rudolph H. Volin
J. Gordan Showalter
Barbara Szymanski
Carol Healey**

Bulletin Production

**Graphic Arts Branch, Technical Information Division,
Naval Research Laboratory**

Bulletin 47
(Part 1 of 4 Parts)

THE SHOCK AND VIBRATION BULLETIN

SEPTEMBER 1977

A Publication of
**THE SHOCK AND VIBRATION
INFORMATION CENTER**
Naval Research Laboratory, Washington, D.C.

The 47th Symposium on Shock and Vibration was held at the Albuquerque Inn and Convention Center, Albuquerque, New Mexico on October 19-21, 1976. The Defense Nuclear Agency, Washington, D.C., the Field Command Defense Nuclear Agency, and the Air Force Weapons Laboratory, Kirtland Air Force Base, New Mexico were the hosts.

Office of
The Director of Defense
Research and Engineering



Accession For	
NTIS GR&I	<input checked="" type="checkbox"/>
DTIC TAB	<input type="checkbox"/>
Unannounced	<input type="checkbox"/>
Justification	<input type="checkbox"/>
By	
Date	
Dist	
A-1	

CONTENTS

PAPERS APPEARING IN PART 1

Keynote Address

- IMPACTS OF SHOCK AND VIBRATION CONSIDERATIONS ON WEAPON DEVELOPMENT** xi
Dr. Hua Lin, Assistant Director (Offensive Systems) Office Director of Defense Research and Engineering, Washington, DC

Invited Paper

- NUCLEAR HARDENING IN A MISSILE DEFENSE SYSTEM** 1
Noah J. Hurst, Ballistic Missile Defense Systems Command, Huntsville, AL

Panel Session

- DYNAMICS EFFECTS ON RELIABILITY** 9

Shock Analysis

- SCALING OF STRONG SHOCK HUGONIOTS** 39
W.E. Baker, Southwest Research Institute, San Antonio, TX

- SHOCK SPECTRA AND RESPONSES BY POCKET CALCULATOR** 49
C.T. Morrow, Consultant, Dallas, TX

- STUDIES OF THE TERRADYNAMICS OF A PROJECTILE PENETRATING SAND** 77
L.E. Malvern, R.L. Sierakowski, University of Florida, Gainesville, FL and
J.A. Collins, DLYV/Air Force Armament Laboratory, Eglin AFB, FL

- HARDENED SYSTEM VULNERABILITY ANALYSIS** 87
J.D. Collins, J.H. Wiggins Company, Redondo Beach, CA

Shock Testing

- LABORATORY SIMULATION OF SEQUENTIAL SETBACK AND AERODYNAMIC DRAG EXPERIENCED BY ARMY ORDNANCE PROJECTILES - A DEVICE, THEORY AND DATA** 99
I. Pollin, Harry Diamond Laboratories, Adelphi, MD

BARREL-TAMPED, EXPLOSIVELY PROPELLED ROTATING PLASTIC PLATES	113
F.H. Mathews, B.W. Duggin, Sandia Laboratories, Albuquerque, NM	
SHOCK WAVEFORM TESTING ON AN ELECTRODYNAMIC VIBRATOR	121
W.E. Frain, Applied Physics Laboratory, The Johns Hopkins University, Laurel, MD	
SEISMIC SHOCK WAVEFORM REPRODUCTION AND SHOCK SPECTRA SYNTHESIS ON HYDRAULIC ACTUATOR	133
R.S. Nichols, White Sands Missile Range, NM	

Isolation and Damping

EXPERIENCES ON SHOCK ISOLATION OF EQUIPMENT IN THE SAFEGUARD SYSTEM	151
M.A. Boyd and C.C. Huang, U.S. Army Engineer Division, Huntsville, Huntsville, AL	
ON THE DETERMINATION AND CHARACTERISTICS OF THE CENTER OF ELASTICITY	163
G.L. Fox, Barry Division, Barry Wright Corporation, Watertown, MA	
DESIGN OF ELASTOMERIC COMPONENTS BY USING THE FINITE ELEMENT TECHNIQUE	177
R.H. Finney and B.P. Gupta, Lord Kinematics, Erie, PA	
CHARACTERIZATION OF BULK CUSHION MATERIALS UNDER IMPACT LOADS USING VISCOELASTIC THEORY	189
T.L. Cost, J.D. Dagen, The University of Alabama, Tuscaloosa, AL and J.E. Jackson, Tennessee Valley Authority, Knoxville, TN	
IMPACT RESPONSE MODELING OF BULK CUSHIONING SYSTEMS ON A PROGRAMMABLE DESK-TOP CALCULATOR	197
D.M. McDaniel, U.S. Army Missile Command, Redstone Arsenal, AL and R.M. Wyskida, J.D. Johannes, The University of Alabama in Huntsville, Huntsville, AL	

PAPERS APPEARING IN PART 2

Vibration Analysis

SOME ASPECTS OF VIBRATION CONTROL SUPPORT DESIGN P. Bezler and J.R. Curreri, Brookhaven National Laboratory, Upton, NY
RESPONSE OF A HARDENING SPRING OSCILLATOR TO RANDOM EXCITATION J.T. Kayanickupurathu, Research Fellow and J.R. Curreri, Polytechnic Institute of N.Y., Brooklyn, NY

**NON-LINEAR DYNAMIC RESPONSE OF A MULTI-MASS SYSTEM
WITH GAPS**

B. Koplik, M. Reich, Brookhaven National Laboratory, Upton, NY

AN IMPROVED DERIVATION OF THE DUNKERLEY-MIKHLIN FORMULA

J.E. Brock, Naval Postgraduate School, Monterey, CA

**RECENT ADVANCES IN FAILURE ANALYSIS BY STATISTICAL
TECHNIQUES (FAST)**

W.H. Rowan, TRW Defense and Space Systems Group, Redondo Beach, CA

**ON THE MEAN LIFE EVALUATION OF A MATERIAL WITH IDEAL ELASTO-
PLASTIC BEHAVIOUR, SUBJECTED TO A STOCHASTIC LOADING
PROGRAMME WITH A FINITE NUMBER OF STRAIN LEVELS**

G.A. Philippin, T.H. Topper and H.H.E. Leipholz, University of Waterloo,
Waterloo, Ontario, Canada

**FATIGUE ANALYSIS OF MULTI-DEGREE-OF-FREEDOM SYSTEMS UNDER
RANDOM VIBRATION**

R.G. Lambert, General Electric Company, Utica, NY

**A MATHEMATICAL MODEL FOR THE STRESS AND VIBRATIONAL
ANALYSIS OF THE HUMAN MITRAL VALVE**

J. Mazumdar and T.C. Hearn, The University of Adelaide, South Australia

**THE DECREMENT IN VISUAL ACUITY RELATED TO VIBRATION OF SHAKER,
SEAT, AND OBSERVER'S HEAD**

O.F. Hackett, David W. Taylor Naval Ship Research and Development Center,
Bethesda, MD, W.G. Lewis, Naval Electronics Laboratory Center, San Diego, CA,
R. Langland and T. Harder, Pacific Missile Test Center, Point Mugu, CA

**FREE VIBRATIONS OF UNSYMMETRICALLY LAMINATED CANTILEVERED
COMPOSITE PANELS**

E.A. Thornton, Old Dominion University, Norfolk, VA

**FUNDAMENTAL FREQUENCIES OF ORTHOTROPIC PLATES WITH VARIOUS
PLANFORMS AND EDGE CONDITIONS**

C.W. Bert, The University of Oklahoma, Norman, OK

**DYNAMIC RESPONSE OF LAMINATED COMPOSITE PLATES UNDER
RESIDUAL THERMAL STRESSES**

C.T. Sun, Iowa State University, Ames, IA

**VIBRATION OF COMPOSITE PLATES OF ARBITRARY SHAPE BY THE
METHOD OF CONSTANT DEFLECTION LINES**

S. Dharmarajan and F.H. Chou, San Diego State University, San Diego, CA

COUPLED VIBRATIONS OF TURBOMACHINE BLADES

J.S. Rao, Indian Institute of Technology, New Delhi, India

**ACCELERATION THROUGH RESONANCE OF MULTI-DEGREE OF
FREEDOM SYSTEMS**

**F.H. Wolff, A.J. Molnar and A.C. Hagg, Westinghouse Electric Corporation,
Pittsburgh, PA**

PAPERS APPEARING IN PART 3

Vibration Testing

**COST EFFECTIVELY EXCITING VIBRATION FAILURE MODES FOR
LONG-TIME RELIABILITY DEMONSTRATIONS**

W. Tustin, Tustin Institute of Technology, Inc., Santa Barbara, CA

SELF-TUNING RESONANT FIXTURES

R.T. Fandrich, Harris Corporation, Melbourne, FL

ANALYSIS OF SINUSOIDAL AND RANDOM VIBRATION ENERGIES

J.N. Tait, Naval Air Development Center, Warminster, PA

EVALUATION OF AN ADAPTIVE FILTER AS A DIGITAL TRACKING FILTER

D.O. Smallwood and D.L. Gregory, Sandia Laboratories, Albuquerque, NM

**TOTAL MISSION ENVIRONMENTAL SIMULATION THROUGH DIGITALLY
CONTROLLED ELECTROMAGNETIC VIBRATION**

**D. Hinckley, F.Foley, Boeing Aerospace Company, Seattle, WA and
P. Moseley, W. Ross, Hewlett-Packard Company, Santa Clara, CA**

**A COMPARISON BETWEEN SINUSOIDAL SWEEP AND BROADBAND DIGITAL
TECHNIQUES FOR RESONANCE SEARCH AND TRANSMISSIBILITY
MEASUREMENTS**

P. Moseley, Hewlett-Packard Company, Santa Clara, CA

**MODAL INVESTIGATION OF LIGHTWEIGHT AIRCRAFT STRUCTURES USING
DIGITAL TECHNIQUES**

**R.W. Gordon and H.F. Wolfe, Air Force Flight Dynamics Laboratory,
Wright-Patterson AFB, OH**

DIGITAL CONTROL SYSTEM FOR A MULTIPLE-ACTUATOR SHAKER

D.K. Fisher and M.R. Posehn, Lawrence Livermore Laboratory, Livermore, CA

Instrumentation and Data Analysis

**MEASUREMENT OF ANGULAR VIBRATION USING CONVENTIONAL
ACCELEROMETERS**

**P.W. Whaley and M.W. Obal, Air Force Flight Dynamics Laboratory,
Wright-Patterson AFB, OH**

**THE USE OF A LOW POWER LASER AND PHOTODIODE FOR
DISPLACEMENT DATA**

J.E. Cawthorn, Martin Marietta Aerospace, Orlando, FL

DYNAMIC RESPONSES OF A SOIL COVERED CONCRETE ARCH TO IMPACT AND BLAST LOADINGS

P.T. Nash, US Air Force Armament Laboratory, Eglin AFB, FL and J.H. Smith, W.P. Vann, Texas Tech University, Lubbock, TX

INSTRUCTURE SHOCK ENVIRONMENT OF BURIED STRUCTURES SUBJECTED TO BLAST INDUCED GROUND SHOCK

S.A. Kiger, U.S. Army Engineer Waterways Experiment Station, Vicksburg, MS

CRACK PATTERN OF AN UNDERGROUND, CYLINDRICAL, REINFORCED-CONCRETE STRUCTURE UNDER AN AXIAL BLAST LOADING

L.C. Lee and M.S. Agbabian, Agbabian Associates, El Segundo, CA

FAILURE OF ALUMINUM CYLINDRICAL SHELLS SUBJECTED TO TRANSVERSE BLAST LOADINGS

W.S. Strickland, USAF Armament Laboratory, Eglin AFB, FL, J.E. Milton, C.A. Ross, University of Florida Graduate Engineering Center, Eglin, AFB, FL, and L.J. Mente, Kaman AviDyne, Burlington, MA

EXTENDED TRANSFER MATRIX METHOD FOR FREE VIBRATION OF SHELLS OF REVOLUTION

S. Sankar, Concordia University, Montreal, Canada

A PRACTICAL SCHEME FOR INCLUDING SHEAR WALL (OR FLOOR) STIFFNESS IN FRAME ANALYSIS

R.M. Mains, Washington University, St. Louis, MO

RAIL OVERTURNING

F. Arbabi, Michigan Technological University, Houghton, MI

Systems Identification

APPLICATION OF MODERN PARAMETER ESTIMATION METHODS TO VIBRATING STRUCTURES

W.R. Wells, Wright State University, Dayton, OH

ANALYSIS OF VIBRATION RECORDS BY DATA DEPENDENT SYSTEMS

S.M. Pandit, Michigan Technological University, Houghton, MI

A METHOD OF SYSTEM IDENTIFICATION WITH AN EXPERIMENTAL INVESTIGATION

P.H. Merritt, Air Force Weapons Laboratory, Kirtland AFB, NM and W.E. Baker, University of New Mexico, Albuquerque, NM

A METHOD FOR THE DIRECT IDENTIFICATION OF VIBRATION PARAMETERS FROM THE FREE RESPONSE

S.R. Ibrahim, Old Dominion University, Norfolk, VA and E.C. Mikulcik, The University of Calgary, Calgary, Alberta, Canada

LABORATORY IDENTIFICATION OF THE PATRIOT LAUNCHER STRUCTURE

T.R. Meyer and C.S. O'Hearne, Martin Marietta Aerospace, Orlando, FL

GROUT/SOIL INTERACTION AND GROUND-MOTION MEASUREMENT
M.B. Balachandra and J.A. Malthan, Agbajian Associates, El Segundo, CA

COMPUTER-BASED TRANSPORTABLE DATA-ACQUISITION AND CONTROL SYSTEM
D.K. Fisher, M.R. Posehn, F.L. Sindelar and H.H. Bell, Lawrence Livermore Laboratory, Livermore, CA

Loads and Environments

VIBRATION INVESTIGATION OF A LARGE TRANSPORT HELICOPTER
W.J. Snyder, J.L. Cross and M.B. Schoultz, NASA Langley Research Center, Hampton, VA

AEROACOUSTIC ENVIRONMENT OF A STORE IN AN AIRCRAFT WEAPONS BAY
L.L. Shaw, Air Force Flight Dynamics Laboratory, Wright-Patterson AFB, OH

AN INTERIM REPORT ON SHUTTLE ORBITER VIBROACOUSTICS
Vibration and Acoustics Unit, Space Division, Rockwell International Corporation, Downey, CA

PAPERS APPEARING IN PART 4

Structural Dynamics

PREDICTION OF GAS DYNAMIC LASER MOUNTING FORCES USING ADMITTANCE TESTING TECHNIQUES
W.R. Davis, Jr., Air Force Weapons Laboratory, Kirtland AFB, NM and
D.L. Brown, Air Force Flight Dynamics Laboratory, Wright-Patterson AFB, OH

INFLUENCE OF FLUID ON THE DYNAMIC PLASTIC RESPONSE OF A PIPE
M.G. Srinivasan, R.A. Valentin, Argonne National Laboratory, Argonne, IL and
D. Krajinovic, University of Illinois at Chicago Circle, Chicago, IL

A THEORETICAL ANALYSIS OF THE DYNAMIC RESPONSE OF CONSTRUCTION CABLEWAY SYSTEMS
K.C. Tu, Stone and Webster Engineering Corporation, Denver, CO and
R.S. Ayre, University of Colorado, Boulder, CO

EMPIRICAL INVESTIGATION OF WATER-SHOCK LOADING OF A CONCRETE HALF-SPACE
C.R. Welch and L.K. Davis, U.S. Army Engineer Waterways Experiment Station, Corps of Engineers, Vicksburg, MS

THE EFFECT OF EARTH COVER ON THE DYNAMIC RESPONSE OF HARDENED REINFORCED CONCRETE STRUCTURES
R.D. Crowson, and S.A. Kiger, U.S. Army Engineer Waterways Experiment Station, Vicksburg, MS

Computer Applications

**DIGITAL SIMULATION OF FLEXIBLE AIRCRAFT RESPONSE TO
SYMMETRICAL AND ASYMMETRICAL RUNWAY ROUGHNESS**

T.G. Gerardi, Air Force Flight Dynamics Laboratory, Wright-Patterson AFB, OH

**CHIANTI -- COMPUTER PROGRAMS FOR PARAMETRIC VARIATIONS IN
DYNAMIC SUBSTRUCTURE ANALYSIS**

A. Berman and N. Giansante, Kaman Aerospace Corporation, Bloomfield, CT

FREQUENCY RESPONSE ANALYSIS OF COMPLEX STRUCTURES

H.R. Radwan and P. Shunmugavel, Sargent and Lundy, Chicago, IL

**COMPUTER AIDED DERIVATION OF THE GOVERNING DYNAMICAL
EQUATIONS FOR A HIGH SPEED GROUND VEHICLE**

J. Patten and N. Isada, State University of New York

PAPERS APPEARING IN SUPPLEMENT

**STABILITY OF NEW LIGHTWEIGHT 203MM (EIGHT INCH)
HOWITZER IN SOILS**

H.M. Cole, Naval Surface Weapons Center, White Oak, Silver Spring, MD
and J.C.S. Yang, University of Maryland, College Park, MD

**APPLICATION OF LIGHT-INITIATED EXPLOSIVE FOR SIMULATING
X-RAY BLOWOFF IMPULSE EFFECTS ON A FULL SCALE
REENTRY VEHICLE**

R.A. Benham, F.H. Mathews and P.B. Higgins, Sandia Laboratories,
Albuquerque, NM

KEYNOTE ADDRESS

IMPACTS OF SHOCK & VIBRATION CONSIDERATIONS ON WEAPON SYSTEM DEVELOPMENT

(Keynote Speech delivered to 47th Shock & Vibration Symposium,
October 19-21, 1976; Albuquerque, N.M.)

It is a pleasure for me to be here on the 30th Anniversary of the founding of your Symposium, dedicated to the exchange of information on Shock & Vibration research and test results. I am particularly pleased to have the opportunity to share with you, for this 47th session, some of my thoughts on the Impacts of Shock and Vibration Considerations on Weapon System Development.

Having been trained formally as an aeroelastician and structural dynamicist, I have enjoyed for several years direct association with shock and vibration work in the earlier days of my career. The personal involvement of those years and my later jobs in weapon system development made me keenly aware of the fact that:

- Shock and vibration integrity is every bit as important to a silo-based ICBM as its warhead yield or its guidance accuracy, so that the vital prelaunch survivability of the ICBM can be preserved.

- Shock and vibration integrity is every bit as important to a penetration bomber as its weapon load or its unrefueled range, so that the MTBR (mean time between repair) can be lengthened and the O&M (operation and maintenance) costs can be minimized.

- Shock and vibration integrity is every bit as important to a submarine on patrol at sea as its navigation fix or its secure long-range command, control and communication system; so that the submarine can withstand the depth charge shocks and can reduce the emission of the tell-tale acoustic signals generated by vibration onboard.

In many instances, unfortunately, the shock and vibration effort has been treated as a peripheral activity. Too often, it is tolerated as a necessary evil simply because there is a specification requirement. Other times, the effort is mounted on an ad hoc basis, because the weapon system finds itself in "trouble."

Not infrequently in a major program, the Shock and vibration work has been inflicted with over-effort and under-management. The former gave rise to accusations of esoteric "hobby-shopping"; the latter resulted in inadequate attention and support from the top management. Either case would short-change the weapon system effectiveness or would incur unwarranted costs.

The challenge that we face and the tasks that are ours should be:

- To transform shock and vibration effort into a well-planned activity; and,

- To incorporate shock and vibration integrity as an integral part of a weapon system capability.

Let me expound on this further by examining the most important factors in evaluating weapon systems. These, I would call my three "A's," namely:

- Ability — to perform a given mission. This is the basis of the system requirement. Its payload and range, its penetrativity against defense and its delivery accuracy, etc.

- Availability — to execute the mission at desired time. This is much more than a date for initial operation capability; it considers whether a system has too high an out-of-commission rate due to needed repairs, retrofits, or other reasons.

- Affordability — to own the system for carrying out its mission at desired time. This is becoming an increasingly important consideration because of the many demands made on the Nation's resources from other-than-defense programs e.g., HEW, HUD, etc. and because of other weapon needs within the overall defense budget.

The impacts of shock and vibration considerations on the first two "A's" are apparent. On the third "A," the impact is not that direct. It could cost extensively to retrofit fixes after a system was deployed when shock and vibration deficiencies were discovered after the fact. It would cost unnecessarily if shock and vibration specifications imposed undue performance penalty or RDT&E expenditure. In certain instances, shock and vibration cost is the program cost. An example in point is the MINUTEMAN Silo Upgrade, which, by the time the program is completed, will have cost the Air Force up to one billion dollars. Thus, the impact on Affordability is indeed very significant.

The shock and vibration integrity affects a weapon system not only in its R&D phase but also in the ensuing procurement and maintenance cycles. Inappropriate or inadequate considerations could impose unnecessary costs. The

common of such cost raisers are: unrealistic specifications, lack of design tradeoffs to include shock and vibration consideration, uncertainty in performance verifiability, and ill-conceived test programs.

Of the four items mentioned, an unrealistic specification is probably the worse offender. Figure 1 is a photograph of an E-O Guided Munition in the PAVESTORM III program, designed to be carried on a standard wing rack by an airplane such as an F-4. A vibration qualification test criteria was first established according to MIL-STD-810B for hard-mount equipment pod, shown as the top curve in Figure 2. Upon test, the equipment failed to qualify. Rather than to redesign and repackage the equipment, the designer consulted the shock and vibration engineer and wisely decided to look into some vibration environment measured during flight tests of similar vehicles in similar



Figure 1 — E-O Guided Munition — PAVESTORM III

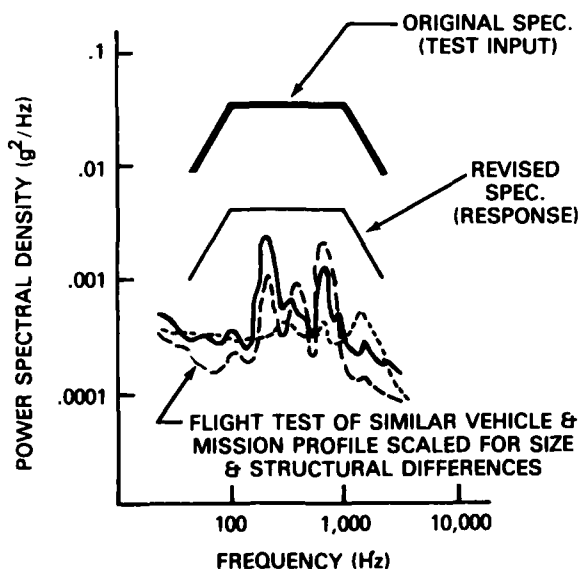


Figure 2 — Vibration Qualification Criteria

flight profiles. By scaling these data according to size, weight and structural differences, the lower group of curves in Figure 2 was obtained. This more accurately represents the environment that the E-O equipment would experience, including the attenuation by structural and other damping effects. The revised specification for a qualification test was then established, shown as the middle curve in Figure 2 and the equipment was "qualified" accordingly. In the subsequent twenty-three flight tests there were no equipment failures.

That was indeed a story with a happy ending. More often than not, however, conservative criteria are not challenged and a redesign would be made to meet such conservative criteria, resulting in unnecessary cost and weight penalty. To avoid undue conservativeness in specifications, one must be able to predict the environment with high confidence and eliminate the need to hedge the design by a large margin. Better prediction techniques are not limited to better analysis or simulation capability. Rational extrapolation from limited testing to predict the design integrity is a fruitful area for research.

Another approach in avoiding undue conservativeness is to treat the shock and vibration consideration from a probabilistic point of view. To insist on a "worst case" environment with near-zero probability of occurrence is unwarranted and unrealistic.

A third approach for avoiding undue conservativeness is to conduct early simplified tests of design concepts to place bounds on the shock and vibration problem. Such simplified but well-thought-out tests would be invaluable in the concept screening process for the system design. These tests would also provide tradeoff data for configuration testability. A readily "testable" configuration enhances design confidence and reduces the pressure to overspecify for a larger design margin.

As common as the over-conservative specification in raising system cost is the lack of design tradeoffs to include shock and vibration considerations. Every design is a compromise of many factors in its tradeoff study. Such a study can hardly be comprehensive because the degree of relevance and significance may not be well understood during the early design stage. However, costly mistakes have been made by neglecting the details of shock and vibration considerations.

Figure 3 shows a cut-off view of the Launch Equipment Room (LER) of a MINUTEMAN ICBM silo. Various equipment racks, surrounding the missile, are mounted on the LER floor. To protect the equipment from the postulated ground shock threat, the LER floor is isolated with a design goal not to exceed 10 g's on the equipment. A prototype isolator was designed, depicted by the left hand sketch in Figure 4, assuming that high frequency motion was of little importance. This prototype isolator was fabricated and tested with the resulting transmissibility shown as the dotted curve in Figure 5. After the isolator was committed to production, a Value Engineering change was made to save production cost by replacing the massive cast retaining plugs with lighter and lower-cost forged tang attachment, depicted by the right hand sketch in Figure 4.

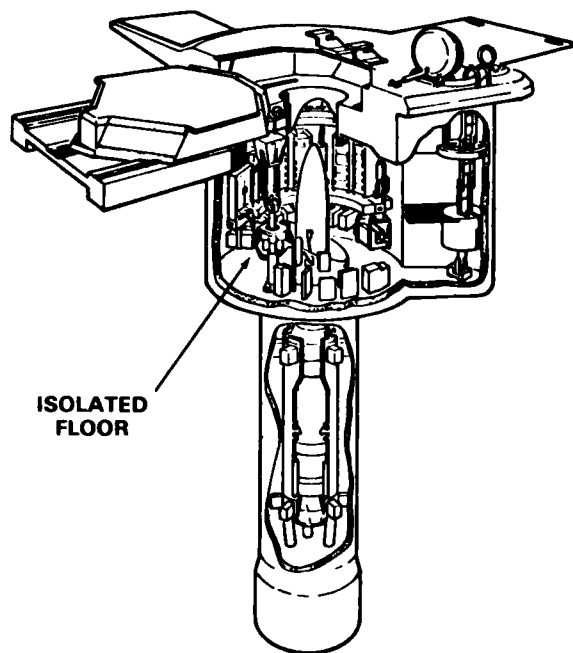


Figure 3 - MINUTEMAN Silo

Since this change did not involve any impacting parts, the new design did not undergo any further examination by the shock and vibration expert until its qualification test, showing a transmissibility as indicated by the solid curve in Figure 5, which exceeds the design goal. Costly redesign and tooling followed. Hindsight indicated that the light attachment excited the "surge mode" of the spring at its upper attachment point because the "mass damper" of the heavy cast plug was removed. If the shock and vibration staff had followed up the design change and, if a conceptual test had been conducted, millions of dollars would have been saved by the well-intended Value Engineering change.

While this instance illustrates insufficient shock and vibration effort, many other instances can be cited to show that the important shock and vibration considerations are simply neglected in a design tradeoff. Most of you must have some such experiences in one manner or the other and have had to come up afterwards with a "fix" for shock and vibration integrity incurring some otherwise unnecessary cost.

To me, the shock and vibration expert should contribute to and participate in the design tradeoffs as a mandatory part of good engineering practice. He should examine the specification levels, keeping them within reasonable bounds; he should help the design in developing concepts with inherent shock and vibration integrity, he should estimate verification test costs and compare them with the costs of other parametric design considerations.

All designs are truly creative art, with no rigid rule or exact formula to follow. Some designs are good. Some, due to a set of constraints or unforeseen circumstances,

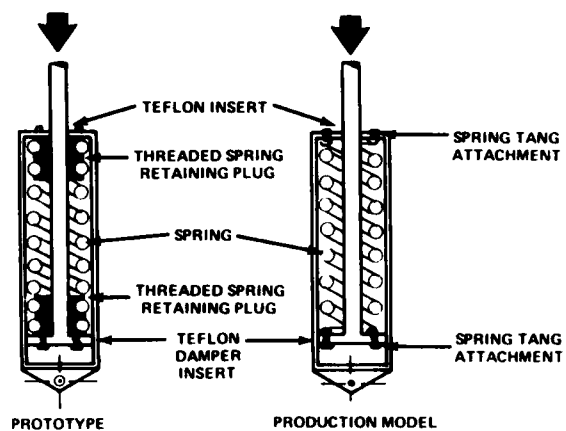


Figure 4 - LER Shock Isolator

ended up in a situation far less than satisfactory. Returning to the three "A's" mentioned earlier, unsatisfactory shock and vibration designs are such that: -

- Ability - incapable of withstanding the shock and vibration environment.
- Availability - causing a delay of system IOC or imposing system shut-downs for retrofits.
- Affordability - incurring unnecessary RDT&E costs and subsequent engineering change costs.

Perhaps I can cite an example to illustrate some of the relevant points. Figure 6 shows a photograph of the Safeguard PAR (Perimeter Acquisition Radar) building in Grand Forks, N. D., the top of the radar face reaching five stories high. Housed in the building are the various equipment for the radar operation. Some of the equipment racks are shown lining up to the right in Figure 7. The floor of the building is isolated from ground motion by a number of massive isolators hung from the ceiling shown at the left in Figure 7. Not all equipment in the building are in neatly packed racks. In fact, some are heavy and comparatively large in size. Figure 8 shows a typical example - a 6000 lb. gas turbine ten feet long, four feet wide, and 3-1/2 feet high. The room that houses this equipment and others is called the TSE (Tactical Support Equipment) room. The TSE room design proves to be an educational story.

Several constraints and guidelines were imposed on the TSE room design during the early 1960s. First, standard commercial equipment was to be used and was to be procured by open bid according to performance specification. Secondly, the hardness level was to be achieved by floor isolation only. And the program schedule was such that the brick and mortar work was literally cast in concrete before the TSE to be housed in the building and protected by the isolated floor were completely specified. The practice of open bid by performance specification further compounded the difficulty because the configuration of the winning bid may not match the assumed weight, size and fragility. This indeed happened. Isolators had to be redesigned and

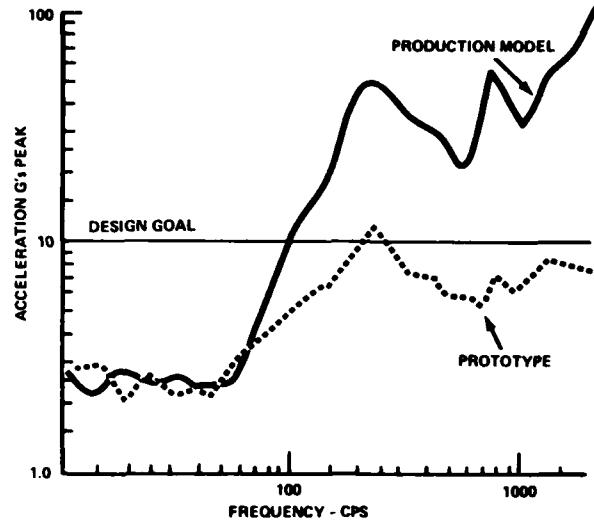


Figure 5 — Isolator Transmissibility



Figure 6 — Safeguard PAR Building

replaced at considerable expense to cost and schedule. There were even "comical" incidences such as the builder putting in some piping conduits in the space reserved for ground shock rattle space. These conduits, of course, had to be rerouted.

More details of this TSE story probably will be covered by the paper entitled "Experience on Shock Isolation of Equipment in the Safeguard System" by Michael Boyd and Charles Huang which appears in the Isolation and Damping Section of this volume. The moral of the story, however, can be generalized. The shock and vibration effort in a weapon system development should be not only adequate but also timely.

The process of weapon system development can be separated in four phases, depicted by the middle row of the block diagram in Figure 9. In the first phase, concepts are created to fulfill the mission requirement. After screening of these concepts, one or more promising candidates are developed in details in the Advanced Development Phase. Tradeoff studies are made iteratively to examine the merits and the disadvantages. Performance of each concept is analyzed or simulated by scaled tests. In the next phase, Validation, full scale tests in realistic, or as realistic as possible, environment are conducted to validate the performance, the cost, and other uncertainties in the system design. Only after this Validation that the weapon system is committed to Full Scale Engineering Development. In the latter

The DASA (Now Defense Nuclear Agency) TREE Handbook was born during the SAFEGUARD design, testing, and parts-screening phases. Contribution to knowledge of Transient Radiation Effects on Electronics was mutual between SAFEGUARD and DNA in those days, when the terms "according to good practice" and "according to the TREE Handbook" became synonymous.

Component hardware and circuits were designed in terms of makeup and operating conditions according to usage that would contribute to hardness as far as such ways were known as time went on.

While testing of pieces of equipment from lower to higher complexity proceeded, the results of hardware responses were fed back to adjust component and subsystem usage to continually changing system performance requirements. That is the nuclear program and to an extent, the system and its usage were changed by what we learned.

Assessments of subsystem hardness were reported periodically or as they were completed, and served to evaluate and correct test plans at agency and command levels, assuring consistency with program objectives in scope and priorities. The overall plans for testing were summarized in nuclear portions of the SAFEGUARD System Master Plan.

I have been speaking of testing and test programs as if all one had to do to determine hardness were to expose a component to a test such as an atmospheric nuclear detonation. I plan to correct this over-simplification before going very much further.

Reviewing groups were chartered by management and the Department of Defense to furnish guidance in the nuclear efforts. These are shown in Figure 3. The project officers groups were jointly represented by the Department of Defense and the Energy Research and Development Administration Laboratories responsible for warheads such as the Sandia Laboratories in Albuquerque and Livermore, the Lawrence Livermore Laboratory and the Los Alamos Scientific Laboratory.

Contractors and other agencies involved in the development of the system, such as the Corps of Engineers (Huntsville Division), the SAFEGUARD Communication Agency (Fort Huachuca) and the Army Munitions Command (Picatinny Arsenal), also prepared hardness test plans for the nuclear effects to meet our overall guidance under our Master Plan, and included effects on intra-site and inter-site equipment. Picatinny Arsenal had the task of adapting the missile and guidance communication systems to the warhead firing apparatus, and the arming, timing, safety assurance, and destruction mechanisms.

Figure 4 contains a summary of our final Nuclear Hardness Assessment Report. Details of work are contained in it. It is a blank copy of the matrix of subsystems and components as rows, together with nuclear weapons effects or imposed environments, as columns. It is used with the numbers of all the blanks to list hardness factors and levels of confidence to which they had been determined. The

- DIRECTOR, DEFENSE RESEARCH AND ENGINEERING
 - DEFENSE SCIENCE BOARD
 - VULNERABILITY TASK FORCE
- (JOINT) PROJECT OFFICERS' GROUPS
 - SPARTAN AND SPRINT NUCLEAR VULNERABILITY AND EFFECTS WORKING GROUPS
- SAFEGUARD SYSTEM OFFICE (SAFSO) VULNERABILITY WORKING GROUPS
 - STRUCTURES
 - BLAST AND SHOCK
 - ELECTROMAGNETIC PULSE (EMP)
 - TREE

Figure 3 — Responsible Reviewing Groups

shaded elements represent effects that do not apply to the corresponding components. There is a total of 70 effects on components shown that did require determination.

Hardness Factor was defined as the ratio of the threshold level of susceptibility to the required hardness level. An equivalent way of saying this is that the Hardness Factor is the ratio of the environment level that a component just fails to withstand to that which must be withstood for success of the mission.

The confidence levels seldom could be expressed any more closely than "high," "moderate," or "low." In some instances, when it was necessary to calculate probabilities of failure rather than simply hardness factors, a numerical level of confidence was produced. The reason for calculating such probabilities was that there were times when it appeared that the requirements were not going to be met, so we made haste to find out what the chances of survival were under those circumstances. It always made the picture look better, because the probabilities of not completing the missions successfully always turned out to be very low. But eventually all of the hardness factors turned out to be on the safe side even in the worst cases, and the probability considerations became unnecessary, though still informative. They became what we might have had to gamble with, but even then not at a very great risk.

When you combine Air Blast, Building Rotation, and the mechanical effects of X-rays as parts of Shock and Vibration, the subject of this Symposium constitutes the broadest of the environmental considerations to our SAFEGUARD System. This would be true whether the weapons were nuclear or not. The remainder of the effects are more or less peculiarly nuclear.

"Electromagnetic Pulse," (EMP) includes several electromagnetic effects having somewhat different causes, but having in common the results that all of them can induce potentially damaging currents in electrical signal cables leading to electronic devices. To oversimplify the descriptions and save time: Transverse EMP is like strong radio waves being propagated from a burst. Radial EMP is similar, but like electrons streaming. IEMP, nowadays more

INVITED PAPER

NUCLEAR HARDENING IN A MISSILE DEFENSE SYSTEM

NOAH J. HURST
Ballistic Missile Defense Systems Command
Huntsville, Alabama

The Missile Defense System referred to in the title is the SAFEGUARD Ballistic Missile Defense System. It was an innovative system and continually created the state of the ABM art from its beginning up until the time of SALT I. It evoked much nuclear hardness effort and hardness testing along the way.

There may be a good many of you who have had to build systems to withstand nuclear weapons at some stand-off distance and who have had experiences similar to those that we have had in the development of the SAFEGUARD System. When I say "withstand nuclear weapons," I imply our definition of hardness, which states that the effects from friendly or enemy weapons will cause no unacceptable degradation of system performance or objectives; i.e., the system may fail but already have met its objective before failing. Or, if the objective is just deterrence, we have less to worry about.

Before any consideration of nuclear effects on the system began, the missile system that was to teach us the subject of nuclear hardening was being developed with a history roughly like that shown in Table 1.

This picture leads on into the SENTINEL and SAFEGUARD phases and toward eventual deployment.

The necessity to pay attention to the ability to survive in nuclear environments was first recognized in NIKE-ZEUS in the period from 1957 to 1963. But the first actual nuclear hardness requirement placed was on NIKE-X radars in 1963. Hardening requirements were given full emphasis throughout the entire missile system since 1968.

It was realized that, in addition to the survival of the system—other advantages are to be gained by being able to operate closer to bursts of our own weapons—that is, under what are called "fratricidal" conditions (Figure 1).

Table 1 — Development of the Nike Missile System

1955	NIKE - II
1956	NIKE - B
FEB 1957	NIKE - ZEUS
JAN 1963	NIKE - X

Closer burst spacings allow more simultaneous intercepts of incoming warheads—either by more attacks on each warhead or by covering more warheads.

Understanding the environments which would have to be provided for as capabilities to be built into the various parts of the system was the first recurring step in the design of hardening procedures. This was part of a learning process and feedback loops that you will see reiterated in the outline of the hardening process (Figure 2).

Piece-parts were selected for known hardness in inherent properties and against effects of known importance. Later on, screening by actual sampled or total individual testing or sometimes control of manufacturing processes, had to be undertaken for some parts.

- SURVIVAL OF SYSTEM
- CLOSER BURST SPACINGS AND SHORTER STAND-OFF WITHOUT FRATRICIDE
- MULTIPLE INTERCEPTS
- MULTIPLE WARHEAD KILLS

Figure 1 — Importance of Hardness

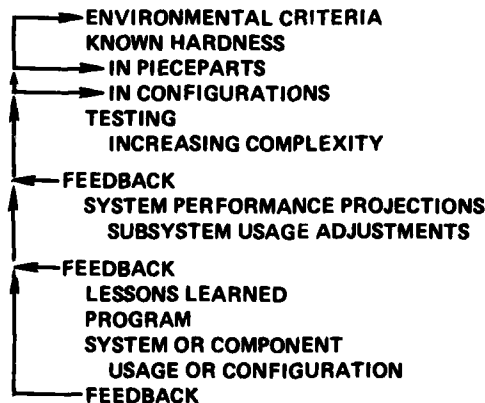


Figure 2 — Hardening Procedures

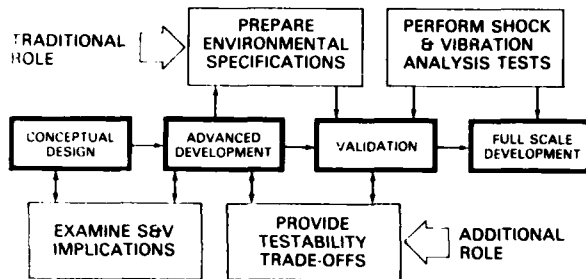


Figure 9 — Shock & Vibration Efforts in Weapon System Development Process

phase major funding is allocated, hardware are prototyped for further testing, and the weapon system design is developed to a degree of maturity demonstrably ready for production.

Traditionally, the shock and vibration consideration plays its role according to the two blocks on the top row in Figure 9. Environmental specifications are requested during the Advanced Development Phase. Analysis of the design and tests are conducted later for the shock and vibration integrity as defined by the specifications. The procedure is generally one way; either from the designer to the shock and vibration expert or vice versa. Seldom does the shock and vibration expert get involved before the Advanced Development Phase.

To realize fully the benefit of shock and vibration efforts, additional tasks should be added as shown in the lower row in Figure 9. Here the process is a two way

iteration. Helpful considerations are included earlier, the benefit of which is self-evident.

In summary, I would like to leave with you these thoughts. Affordability is increasingly a primary concern for every weapon system development and shock and vibration inputs should be included in the early tradeoffs to lower the overall costs. The shock and vibration community can better contribute to the efforts by assuming additional roles in timely manner in all phases of the system development, and by pursuing advance research in analysis and in testing so that design integrity can be preserved without resorting to overly conservative specifications and/or expensive test programs.

Again, I appreciate the opportunity to address the 47th Symposium for the specialists in this complex and vitally important shock and vibration field. You come here not only to learn about the latest research results in the advancing state-of-the-art; but also, perhaps more important, for personal contact with your peers so that the "hard to come by" experience can be exchanged, cooperation of common endeavor can be arranged, and innovative concepts and approaches can be explored. For indeed, the synergetic total of individual efforts will benefit more, not only to the shock and vibration community but also to the Nation at large.

From the titles listed in your program, I am sure that you will have three most interesting and fruitful days ahead. I wish you all the success in meeting the objective of this Symposium.



Figure 7 — Interior of PAR Building



Figure 8 — Gas Turbine on Isolated Floor

frequently included in what is called System-Generated or SGEMP, results from ejection of electrons from the materials of cavities subjected to very sudden radiation. SAFEGUARD can claim (or lament) the first recognition of the existence of IEMP, which came about as the explanation of some extraordinarily high magnetic fields and currents encountered in SPARTAN missile experiments during underground nuclear testing.

Calculations corroborated the observations before very long, but for more than a year there was much skepticism and disbelief of whether the right hypotheses were being drawn and the phenomena were real. They are real enough to be calculated regularly nowadays in satellites at radiation intensities several orders of magnitude lower than those that were dangerous to the SAFEGUARD components.

This is probably a good place to point out differences in method between just "testing" and the means of arriving at hardness evaluations. The difference—at least since our country's agreement not to detonate any more nuclear test weapons in the atmosphere—arises from the fact that there almost never is a nuclear test environment available to simulate the real thing. If the intensity can be attained, the pulse duration is too long, for an imaginary instance; or how do you get the right distribution of energies of rays or particles; or the rise time and the balance between thermal and shock are wrong, and on and on.

I can think of one simulation facility that was big enough and accurate enough to test our missiles against one nuclear effect almost completely. The ARES Facility of the Air Force Weapons Laboratory at Kirtland Air Force Base, New Mexico, gave conclusive results on the hardness of SPRINT and SPARTAN against EMP. Its confirmation

of our ability to calculate the effect accurately also contributed toward the only general method of ascertaining hardness, a method that was to be the principal resource in our assessment of the entire system. This was the use of mathematical analyses to predict the outcome of exposure to inadequate simulations, where demonstration of the accuracy of the calculations proved the validity of predictions for real environments. It was the answer and will continue to be. Improvements are always to be sought, and the indirection of the method may make it remain a little too vague for some people to feel safe with, but it has done a good job for us.

We achieved an instance of a triumph during the pursuit of improvement in capability of calculating cable currents induced by Internal EMP. It was the first time that Maxwell's equations were solved in a computer program in three dimensions with self-consistency and for a field in the presence of a plasma. This was accomplished at a particularly sensational time for our contractor's researchers who did it, in that a forecast of its possibility 14 years in the future appeared in a scientific magazine about that time.

Some of the simulation facilities not yet mentioned that were used were:

1. Neutron and gamma radiation facilities such as laboratory reactors, linear electron accelerators, and flash X-ray machines (actually generating gamma rays).

2. The Nevada Test Site was used for underground nuclear test events simulating all effects. These had the advantages of possibilities of convincing realism in many environmental effects at one time. They were our only good producer of X-rays and of pulses correct for IEMP.

	NUCLEAR ENVIRONMENTS AND EFFECTS												
	EMP	REMP	IEMP	NEUTRON AND GAMMA	X-RAY		AIR BLAST	THERMAL	DUST	EJECTA	DEBRIS	SHOCK AND VIBRATION	BUILDING ROTATION
					RADIATION	Mechanical							
SPRINT MISSILE													
SPARTAN MISSILE													
SPRINT GROUND SUPPORT EQUIPMENT													
SPARTAN GROUND SUPPORT EQUIPMENT													
MISSILE SITE RADAR EXPOSED EQUIPMENT HOUSED EQUIPMENT													
PERIMETER ACQUISITION RADAR EXPOSED EQUIPMENT HOUSED EQUIPMENT													
DATA PROCESSING SYSTEM													
COMMON EQUIPMENT													
EDM TACTICAL SITE FACILITIES													
SATCOM COMMUNICATIONS													
MISSILE FIELD CIRCUITS													

NOT APPLICABLE

Figure 4 - Matrix of Nuclear Weapons Effects on Systems or Components

They had some important disadvantages, too, such as they were expensive, they required multiple simultaneous experimental set-ups for "bracketing" inaccuracies in exposure, and the "button could be pushed" only once, unlike with laboratory simulators.

3. High explosives and laboratory shock and vibration test equipment which I can leave to the imagination of this one audience. This audience contributed to our programs, and their imagination was used to advantage, too.

4. Laboratory current injection sources for inducing or simulating the introduction of currents into electronics by all types of EMP and IEMP.

The following is an example of tests that were performed for us under DNA's auspices. The rocket sled track at Holloman Air Force Base was used to simulate the flight of a missile through the shock waves from four detonations of high explosive. The first detonation was broadside to the missile in open air, and the other three were in shock tubes to guide the shock at different angles with the missiles' own shock waves and direction of motion.

The missile nose cone was instrumented with pressure transducers to measure the total pressure incident on the surface, equal to the combined effects of the cone's own shock wave with that coming from the outside burst.

The explosions were timed so that the missile passed through the external shock waves at the right places. These tests were conducted to determine whether an enhancement of surface pressure occurred when the shock waves from the missile and from an external burst were superimposed. It was shown by calculations that this was possible at some angles to the blast.

The broadside shock was generated by the overhead aerial burst and it arrived as the missile passed directly underneath.

It can be seen in Figure 5 how the results of the sled tests were used to remove some uncertainties arising from different methods and assumptions in calculating predicted

incident shock pressures for the sled tests. The test results showed that the unexpectedly high predicted pressure enhancements are hardly detectable in real transit and will not be stressing in normal operation.

This last series of developments came as the last words for SAFEGUARD and the future for offspring systems. It shows the increasing possibility of emphasis on calculating capability with not so much expensive testing. The SAFEGUARD effort had a great deal of actual test experience to contribute.

We used the multiburst computer simulation code "IDEA" (not an acronym) to predict the overpressure fields for four bursts in a row. We also used the Air Force multiburst simulation, LAMB (Low Altitude MultiBurst) to predict overpressure, density, particle velocity, and dynamic pressure fields. Radiation and thermal multiburst calculations included are based on an advanced version of the ATR ("Air Transport of Radiation") code.

IDEA is programmed on the CDC 7700 Computer of the BMD Advanced Technology Center and uses the Color Graphics interactive capability obtainable at the ATC Advanced Computer facility. It is interactive, so that parametric studies can be performed rapidly. It has proved to be of great value as a development tool for Air Force Weapons Laboratory improvements to LAMB in that problems with theory have been readily apparent in the visual displays.

A sequence of computer generated overpressure fields is shown for four 0.5 KT bursts detonated in the sequence: Two at time = 0, one at 0.1 seconds, and one at 0.2 seconds. Figures 6-12 show the overpressure field at various times after the bursts. Figure 13 shows the air density 0.6 seconds after the bursts. The air density and the overpressure fields are depicted in color and each color represents a band of overpressure or air density. There are 15 color combinations possible on the ATC color graphics. This simulation is state-of-the-art and is constantly being upgraded with improvements in LAMB by the Air Force Weapons Laboratory. It has played a primary role in the development of multiburst models and will continue to do so.

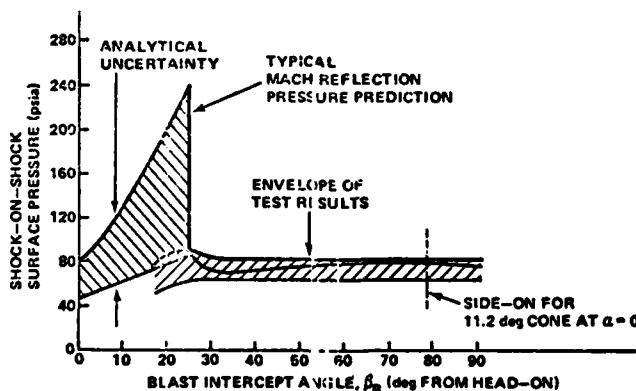


Figure 5 - Typical Shock-on-Shock Pressure Prediction for Sled Test Experiment

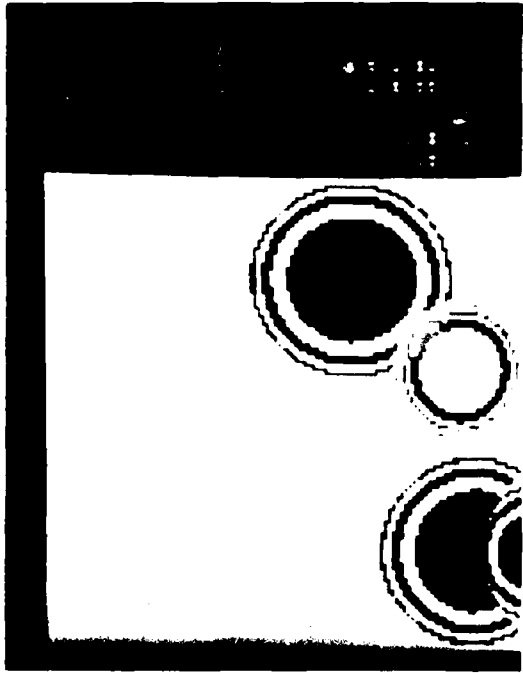


Figure 6 — Overpressure Field 0.2 seconds After Burst

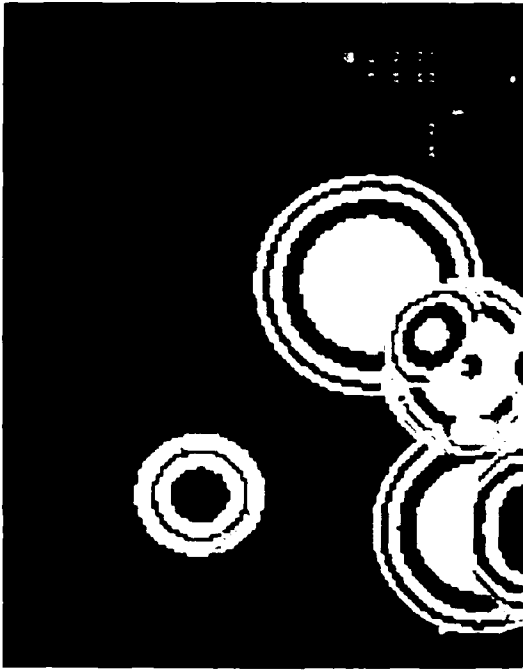


Figure 7 — Overpressure Field 0.3 seconds After Burst

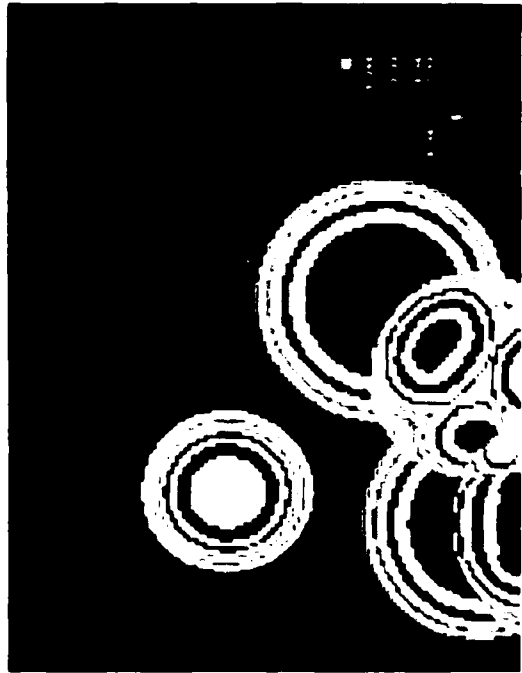


Figure 8 — Overpressure Field 0.4 seconds After Burst

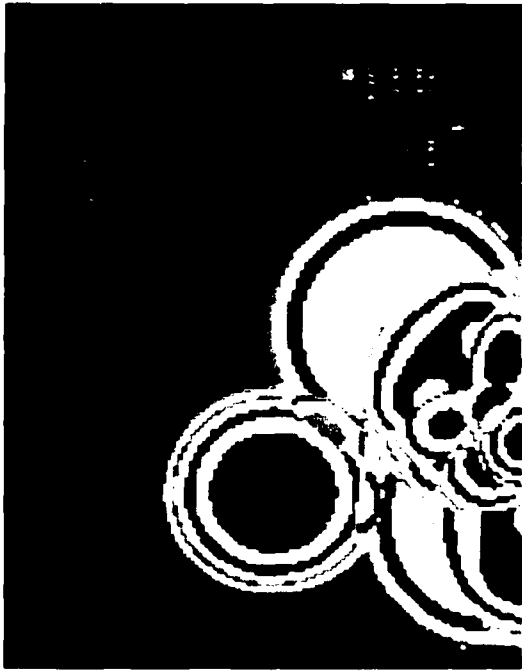


Figure 9 — Overpressure Field 0.6 seconds After Burst



Figure 10 — Overpressure Field 0.8 seconds After Burst



Figure 11 — Overpressure Field 1.0 seconds After Burst



Figure 12 — Overpressure Field 2.0 seconds After Burst

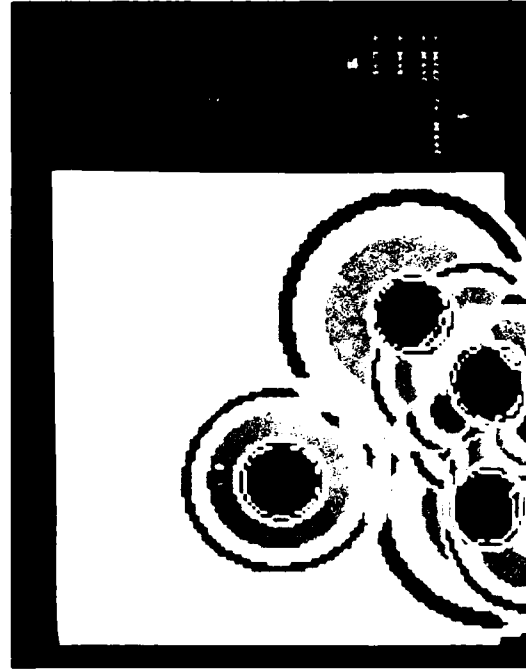


Figure 13 — Overpressure Field 0.6 seconds After Burst

My summary could be a statement of the main lesson that we learned, and it could be in the form of an appeal to save money in future systems by being less hesitant than we were to make design changes early whenever it is known that hardness can be improved by them.

It would be hard to forget that there is a financial tendency to want to make a system work or fly first, regardless of whether it can survive weapons effects, and

that early choices adding a few hundred dollars per vehicle can cost hundreds of times as much if you wait and have to make them retrofits.

Knowledge of good practice was improved greatly by our system building, testing, and research.

The lessons that we learned were many and often expensive, and will bring beneficial savings in the future.

PANEL SESSION

DYNAMICS EFFECTS ON RELIABILITY

Moderator: Robert N. Hancock, Vought Systems Division

Panelists: Michael A. Condouris, U.S. Army Electronics Command
Fort Monmouth, New Jersey
Clark Beck, Boeing Aerospace Company
Seattle, Washington
Allen Curtis, Hughes Aircraft Company
Culver City, California
Joe Popolo, Grumman Aerospace Corporation
Bethpage, New York
Howard Schafer, Naval Weapons Center
China Lake, California
Jon C. Calkins, Pacific Missile Test Center
Point Mugu, California

Mr. Hancock, Chairman (Vought Systems Division):
I work with dynamics. For the last year, I have chaired an IES project on reliability testing, working with the Joint Logistics Commander's Electronics Reliability Workshop. Beginning next to me, the panelists and their speaking topics are: Michael Condouris from the U.S. Army Electronics Command; his topic will be "Helicopter Life Cycle Environments." Seated next to him is Clark Beck from Boeing Aerospace, who will speak on "B-1 Avionics Reliability Qualification." Next to him is Allen Curtis from Hughes Aircraft, who will speak on "Feedback from Field Environments." Joe Popolo will speak on "Combined Environment Testing." Howard Schafer, on "New Specification Impacts." Jon Calkins, from the Pacific Missile Test Center will speak on "Studies of the Sparrow Missile Reliability Under Dynamic Loading."

I will start with a brief summary of some of the recent activities of the Tri-Services in reliability developments. At the 45th Shock and Vibration Symposium in Dayton, the Shock and Vibration community was introduced to some new ideas in the reliability game within the government by Col. Ben Swett, who was followed by Jack Short. I was quite impressed by some of the ideas Col. Swett proposed. At that time a key idea was to cut operational and maintenance (O&M) costs by improving reliability. That required moving some of the O&M costs up to the front end, the RDT&E phase of procurement. A significant change in this thinking has taken place in just the past few months. It has been decided within the DOD that the O&M savings cannot be sold to Congress for two reasons: First, it is doubtful that O&M reductions will actually occur; we are not going to close down a certain number of bases and lay off maintenance personnel, nor will we cease ordering spares. The second reason is you cannot use proposed money downstream to add to procurement costs now. The current thought is we have so much money for procurement, that's it, let's hold on to the minimum dollar. So the present thinking is based on a 1972 survey of industry which showed that 30% of the procurement dollar

went into contractors proving that they had done what they actually did, that is, in the form of proof tests, documentation, inspection and redundant exercises. Col. Swett indicated that we should look at this 30% figure as a possible maximum for application to improve reliability during RDT&E. The IES working group has estimated the facility costs for combined random testing, including all production burn-in, at around \$300,000,000 and we are presently looking at ways to reduce this figure.

There are several aspects of the reliability problem throughout the procurement cycle. I would like to look briefly at Col. Swett's idea, which is still sound, and go through one of these procurement cycles with you so that you can perhaps put it in better context and try to avoid making a heated point of argument about a "demo" test when actually we are talking about a production screening test. I want to aim this discussion toward dynamics and the principal thought toward reducing some of the redundant test costs. Col. Swett said that the reliability standard, MIL-STD-781, and the environmental testing standard, MIL-STD-810, were actually in two separate worlds within the Air Force Systems Command, and that holds true for the Army, Navy, and practically all aircraft companies. The missile side of the house is a slightly different situation, I think it grew up principally under NASA. If you look at some of the separation points in Figure 1, military specifications, Air Force regulations, organizational structure, the type of product that is produced, viewpoints, attitudes, and terminology, I underlined the term "attitudes" because I think that is a key element in why we run tests, whether it is to meet the letter of a specification or actually invoke some reliability attainment, the thought was that we are spending too much on assessments and ignoring actual attainment. Within the DOD, there was some thought given as to what might be done to improve the situation (Figure 2). One of the principal thoughts was to combine the testing insofar as possible. Cancel some of those tests in MIL-STD 810; that is don't repeat sequentially what you have done in combination. Get away from the sequential

PROBLEM
 "RELIABILITY" (781) AND "ENVIRONMENTAL TESTING" (810)
 ARE TWO SEPARATE WORLDS WITHIN AFSC.
 THEY ARE SEPARATED BY
 MIL SPECS AND STANDARDS
 AIR FORCE REGULATIONS
 ORGANIZATIONAL STRUCTURE
 PRODUCT TYPE
 VIEWPOINTS, ATTITUDES & TERMINOLOGY

RELIABILITY (781) IS: WELL ORGANIZED SIDELINE TO EQUIP DEV STATISTICS UNREALISTIC TEST CONDITIONS POOR PREDICTOR OF TRUE MTBF (OPTIMISTIC BY 10 X)	ENVIRONMENTAL TESTING (810) IS: LEFT TO SPO'S AND AFCMD MAINLINE OF EQUIP DEV SPEC COMPLIANCE UNREALISTIC TEST PROCEDURES NO PREDICTOR OF TRUE MTBF (NO RELIABILITY DATA OUTPUT)
--	--

Figure 1 - (From Swett, 43rd S & V Symposium)

EQUIPMENT LEVEL DT&E PROGRAM (PROPOSED)

TEST CONDITIONS AND PROCEDURES

COMBINE PERFORMANCE, RELIABILITY, AND ENVIRONMENTAL QUALIFICATION TESTS INsofar AS PRACTICAL:

- o SELECT STRESS TYPES AND LEVELS
- o DESIGN PROCEDURES TO MAXIMIZE DATA

CANCEL TESTS SUBSUMED BY COMBINATION

EMPLOY COMBINED-STRESS TESTING FOR:

- | | | |
|-------------------------|---|------------|
| o PARTS RATING | } | |
| o EVALUATION TEST | } | PROTOTYPE |
| o QUALIFICATION TEST | } | |
| o SCREENING ("BURN-IN") | } | |
| o PRODUCTION SAMPLING | } | PRODUCTION |

Figure 2 - (From Swett, 43rd S & V Symposium)

test idea and use actual combined mission profile environments. Let us try to fly the "beast" in the laboratory. He was talking at the time doing this on both a prototype base and a production hardware. There were a number of revision activities planned by the Tri-Services Reliability Workshop Organization (Figure 3). Some of these have progressed to a certain extent and those of you who work with reliability testing will be interested in the present status of these standards. MIL-STD-781 has been circulated in two draft forms within the Navy and to industry and it was also mailed to six professional societies the most of the DOD organizations that contributed comments on the last draft; there will also be an 800-page booklet containing those comments. It was planned that there would be a Navy coordination meeting November 22-23, a Tri-Service coordination meeting about December 1, an industry coordination meeting December 3-6, and the minutes would be distributed about December 17. He wants to send the standard to the print shop by January 1. Looking at some of the conflicts between what the present standard says, what DOD has voiced in the form of policy, what Navelex and the Army would desire, I don't think they are going to

MIL-STD-781C + 800 pps Comments Mailed 10/15
 Navy Coordination Nov 22-23
 Tri Service Coordination Nov 30 - Dec 1
 Industry Coordination Dec 3-6
 Minutes Distribution Dec 17
 Print Jan 1

- MIL-STD-785 - Revise FY77
- MIL-STD-721 - Draft Spg. 77
- MIL-STD-1635 (EC) - Rel Dev Test To Industry - Nov 1
- MIL-STD-756 - Awaiting Funds
- MIL-STD-781d - Draft Under Contract Issue 79
- MIL-STD-810C - Rumbblings at Aberdeen

Figure 3 - Status of Standards Revisions, 10/76

meet the final print date of January 1. The best estimate is it would need one more iteration past this one.

They plan to revise MIL-STD-785 in FY 77 which started October 1 and this is the controlling document for aircraft electronics reliability. They expect to revise MIL-STD-721, which is a definition document, in the spring of 1977. MIL-STD-1635 is an Electronics Command standard for reliability development testing as opposed to reliability demonstration testing and it is expected to be issued to industry for comment about November 1. MIL-STD-756 is awaiting funding. MIL-STD-781D, which is a total rewrite and a replacement for MIL-STD-781C, is under writing contract; they expect to issue their first draft in 1979. I just noted that there was a plan to combine MIL-STD-810 and MIL-STD-781 but I don't have any official word on the plans for revision or combination of those two standards.

It might be a good idea to keep these questions in mind, some of these stem from the DOD activity (Figure 4). We put three of these in the preliminary program. How elaborate do we have to be on the 100% production screening tests? Do we need random vibration or do we need pneumatic tapping? Is complex motion of any type satisfactory? When are multi-axis vibration tests justified, that is, at what systems level and what category of tests? When can we use acoustics tests as a forcing function in lieu of a shaker? What can the role of dynamic environments be in

- HOW ELABORATE FOR 100% PRODUCTION SCREENING?
- WHERE ARE MULTIAXIS VIBRATION TESTS JUSTIFIED?
- WHEN USE ACOUSTIC TESTS IN LIEU OF VIBRATION TESTS?
- ROLE OF DYNAMIC ENVIRONMENTS IN COMPUTER AIDED DESIGN?
- WHAT IS THE UNCERTAINTY BAND WITHIN WHICH WE OPERATE?

Figure 4 - Session Questions

the computer aided design program? I have a little trouble visualizing this myself. In that context we should probably start looking in terms of "what is the uncertainty band within which we operate the dynamic systems?" In many cases in the past we have taken the maxi-max condition, envelope multiplied by factors 2 1/2, because in some cases we didn't really know what we were doing, fill the airplane full of lead, and then insist that the "black box" be tested within 1/2% accuracy.

I thought we might flip through this equipment cycle which runs down the page with time. I have tried to state a specific or principal goal for each phase (Figure 5). Under the R&D issues, I put some of the big buzz words that have been mentioned within the DOD and other places the past year. Life cycle costs, which we just said is a paper tiger, computer aided design, research, and the reliability warranty concept; what we are saying is there are not enough hard pieces of evidence yet to say that any one of these has efficacy over another or whether it is definitely the way to go in some cases. That is in the R&D category, which is pre-procurement. We have generally assumed that piece parts and components have been thoroughly and adequately tested before they come to us so that we concentrate principally at the equipment design level in most of our correspondence over the past two years. I want to flag three things in the design phase. Dynamics typically sets up design requirements. They participate, or should participate, in the design to meet

R&D Issues	Life Cycle Costs
	Computer Aided Design
	Combined Environment Reliability Testing
	Reliability Warranty
	Mission Profile Testing
	Test & Evaluation Gap
	Realistic Environment Prediction
Piece Part Testing	
Component Testing	
Design	Set Design Requirements
	Design to meet Requirements
	Design Review - weak pt. ident & correction
Equipment Test	
	Development - to acquire empirical design information
	Engineering Development
	Environmental Qualification
	Reliability Growth - TAAF - required Duane tests ?
	Reliability Demo - in lieu of Reliability Warranty (Customer design acceptance)
	Screening - eliminate production line workmanship defects
	Burn In - mission profile?
	Production Sampling
	Acceptance
Subsystem Integration Test	
System Test	
Field Deployment - Field evaluation, data collection (prediction verification, data bank)	
	- Field Failure analysis & correction

Figure 5 — Equipment Production Cycle

these requirements, particularly in regard to isolators or protection against the dynamic environments, and finally they participate in a design review which has a purpose of weak point identification for possible correction. When we get to the test phase, I split these test pieces into development, "reliability demo," and screening. The principal goal of development testing is to acquire empirical design data, then we can identify engineering development, environmental qualification testing, and reliability growth testing. The question mark that I put after "test analyze and fix" is the Duane Curve applicable to military electronics circuits. The original Duane Curve was based, I think, on test of equipment which in all cases generated its own environment such as jet engines or APU's. In "reliability demo" tests, we are assessing for ourselves the ability of the equipment to stand up, its ability to meet its guaranteed MTBF, or as stated in the parentheses after that, it is in lieu of a reliability warranty, it acts as a customer design acceptance test. The principal function of a screening test would be to eliminate production line workmanship defects. We have "burn-in" production sampling and acceptance that might be sub-categorized or they might all be the same. Does it make sense to do mission profile testing for your screening tests? What does the dynamics man say about that idea? Or, does it make more sense to do some of these tests at the sub-system integration level or even at the systems test level? I could see, for example, the efficacy of acoustics exposure over shaker tests perhaps at the systems level, and maybe at the sub-systems level. Finally, field deployment which has as its purpose field evaluation, data collection, predictions, verification, the forming of a data bank for the next series of equipments and field failure analysis and correction.

Col. Swett defined some problems in this area as being both administrative and technical and he was speaking from the DOD standpoint, talking about the bad specifications, good intent but bad tests, etc. In some industrial organizations segregation of disciplines contributes to the same problems. For example if disagreements arise between the vibration specialist, and the statistician, who may be in the reliability organization on how certain tests should be performed, or their function, or the detailed test plans, they may have to go to a vice presidential level to get that question resolved. That vice president is usually not very interested in an argument between a statistician and a vibration specialist. This is an example of an administrative problem. I don't have too many suggestions for its possible resolution, but it is a problem to be recognized and dealt with both in the government and industry.

Mr. Condouris (U.S. Army Electronics Command): About a year ago when we received MIL-STD-810C, and with our desires as an Army subcommand to have improved relationships between demonstrated and field data on electronic equipments, we proceeded to review existing helicopter vibration data (1) (2) (3) (4) with a goal of coming up with improved testing techniques, we also reviewed recently published reports on field failures (5). We arrived at certain conclusions: (a) In instances where large differences, on the order of 10-1, between demonstrated and field data existed, they became more like 3-1 when they were normalized. (b) Failures due to vibration were second to those caused by temperature. (c) There is a

need for a more meaningful demonstration test and better field equipment failure data gathering. The possibility for developing a mission profile was also strongly emphasized by many, whatever the desire, there was no doubt to prove that MIL-STD-781C requirements for test establishment for MTBF were needed.

Mission profiles (6) were looked into for Army helicopters, keeping in mind that we are interested in vibration data for general types of electronic equipment, that is, those which would be used in many helicopters with varied missions and in a different location within each. Very shortly after reviewing these documents it became apparent that to settle on a mission profile for equipment that might be in use in today's helicopter for up to ten years might be undesirable and it may be even dangerous. Let us look at one report on helicopter flight profiles.

Figure 6 shows six helicopters which were used both in Southeast Asia and the Continental United States. The right side of the graph shows the percentage of time each helicopter spent on various types of missions. We have in the first block the ascent, the second is maneuver, third is descent, and the last is steady state. To the left we have

the open blocks which show the fatigue spectrum for that particular helicopter. If you note the UH-1's in the lower portion of the graph, one was flown in CONUS, that's the upper one, and the bottom one was flown in Southeast Asia. You can see the marked differences in the percentage of time spent in maneuvers for the aircraft flown in CONUS as against that in Southeast Asia. Also, compare these two graphs with the supposed fatigue spectrum for the particular helicopter. You will note that the maneuvers have taken a large portion of the time, up to 73% in the CONUS, whereas in Southeast Asia for the UH-1H, you have about 73% as against the 80% in the fatigue spectrum. Similarly, if you look at the CH-47 helicopters, the second and third from the top, these are cargo-type helicopters. One is armed, the lower one was armed in Southeast Asia; there we also notice a large difference in percentage of time spent in maneuvers for the armed helicopter as against that which was used in straight cargo service. Also, in the cargo helicopter, the ascent and descent are larger than the fatigue spectrum. The UH-1's were similarly armed in Southeast Asia. Weaponry on these ships, from the UH-1 all the way through the CH-47, ranged from small caliber arms, 20mm cannon, grenade launchers, and others. It is evident in this comparison that fatigue spectra for aircraft which, for example, show 63-83% of steady state utilizations for these helicopters, in actual use run from about 12-60%. Maneuver allocations from 2-29% in the fatigue spectrum are again in actual field conditions from 1-75%.

I am sure that prior to the Southeast Asia Conflict, one would have predicted that standard electronic equipment would be exposed to this array of weaponry and combination of helicopter missions. The lesson learned is that a mission profile of today for a given helicopter could be quite different from that of one in actual combat.

A logical next step would be to review existing helicopter vibration data which we did. The OH-6 light observation helicopter, UH-1C and the H-16 helicopters were chosen because they represent a good cross-section of the largest number of helicopters within the Army arsenal. The UH-1C is a cargo litter type, and the H-16 is a gun ship. Also, considerable data had been taken on these three aircraft in a joint effort between the Army and the Air Force. An example of these data are shown in the next few figures. All three of these helicopters used weaponry.

Figure 7 shows the vibration environment over the entire UH-1C helicopter. This particular helicopter used the 7.62mm machine gun, 2.75 inch rocket launchers, and 40mm M-5 grenade launcher. The data are plotted in the lower portion are the minimum, the average (next line up), 90 and 99% occurrences, and maximum. All the data in the following figures will be in this kind of display. In Figure 7 I am using the entire helicopter with gunfire to show what the maximum environment would be in a UH-1C gun ship. There are peaks that exceed the MIL-STD-810C envelope. However, if we look deeper into the report and to our data taking, we find that the vibration environments were well within the envelope where the electronics are normally mounted except for a couple of points. I would like to call particular attention to the average plots in this graph and those that are to follow, that is, the solid line which was drawn right below the 1g line. In this particular curve the average is less than 1g.

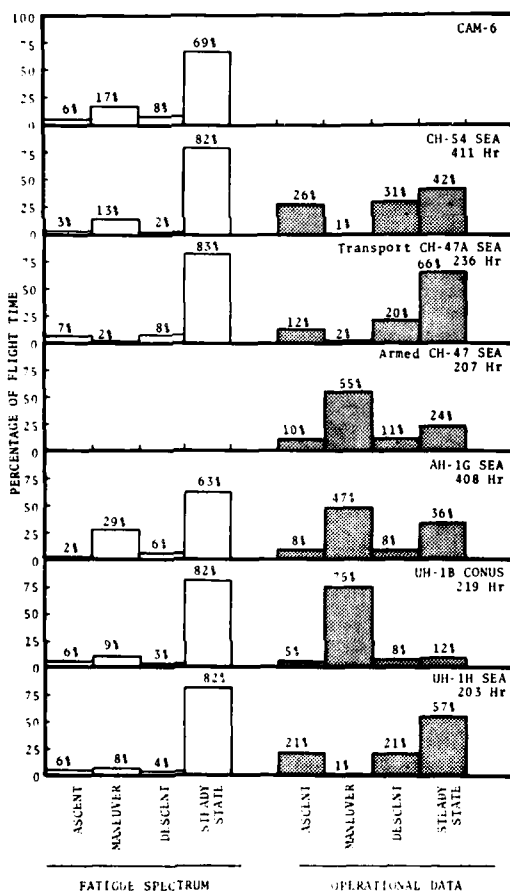


Figure 6 - Comparison of Operational Data and Fatigue Spectra for Various Helicopters.

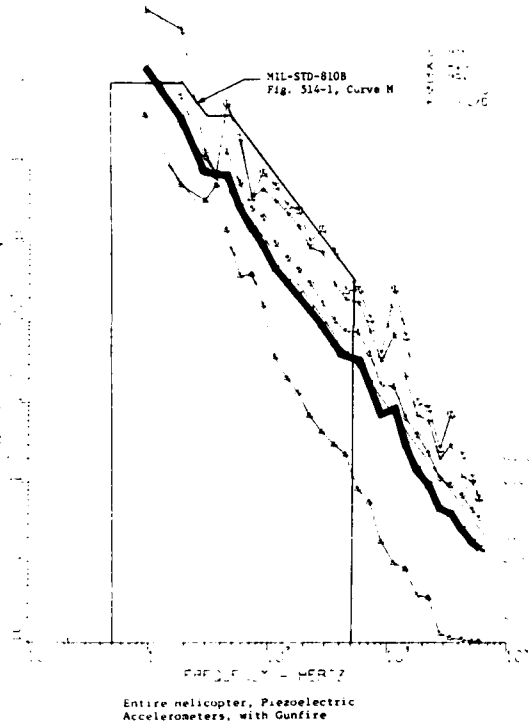


Figure 7 — UH-1C Helicopter

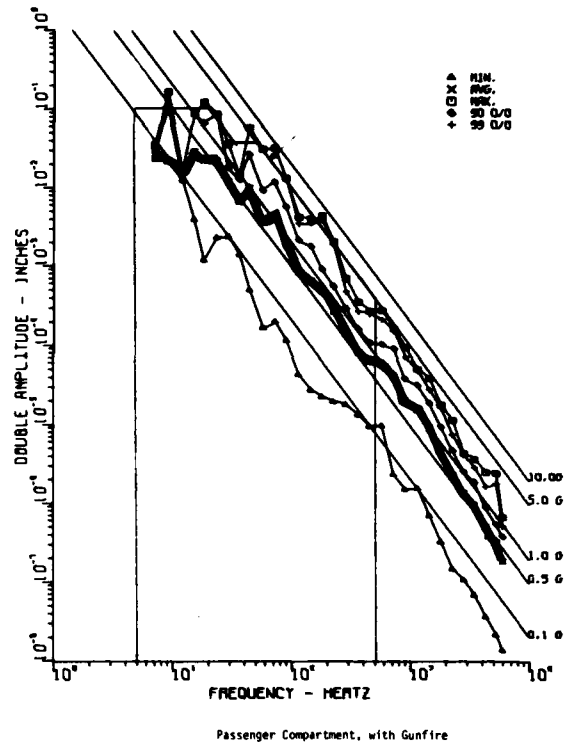


Figure 8 — OH-6 Helicopter

Figure 8 shows the vibration environment with gunfire of the OH-6 helicopter in the passenger compartment. In this plot only the 7.62mm weaponry is used. Here again, the average vibration data are essentially below 1g. In Figure 9 we again have the OH-6 with gunfire. In this instance we are in the nose section and cockpit. Here again, the vibration level is slightly above 1g except on the lower end where we see two data points with average peaks at less than 4G's.

Figure 10 shows the vibration environment of the gun ship, the AH-1G "Cobra" helicopter. This particular helicopter was armed similar to the UH-1C that is we had the 7.62mm weaponry, the grenade launchers, and the rockets. We flew many many missions and we have thousands of feet of tape on this particular helicopter. We had diving maneuvers, "falling leaves," flying backwards, sideways, 90° angles, etc. Figure 10 shows the vibration environment of an entire helicopter without gunfire and this particular figure shows the comparison of the spread of data that occurs when one considers only gun firing versus total flight of an aircraft. The bottom line contains minimum points that were picked in this particular run and the upper lines are the maximum points. The average is below 1/2 g. Figure 11 shows the vibration environment for the same helicopter, but this time with gunfire and it is the overall data throughout the whole helicopter. It includes data taken at the tip of the tail, on top of the engine, up forward near the weaponry, on dashboard equipments, and the rear tail. Here, the maximum to minimum plots have less spread, however the average in general is higher than

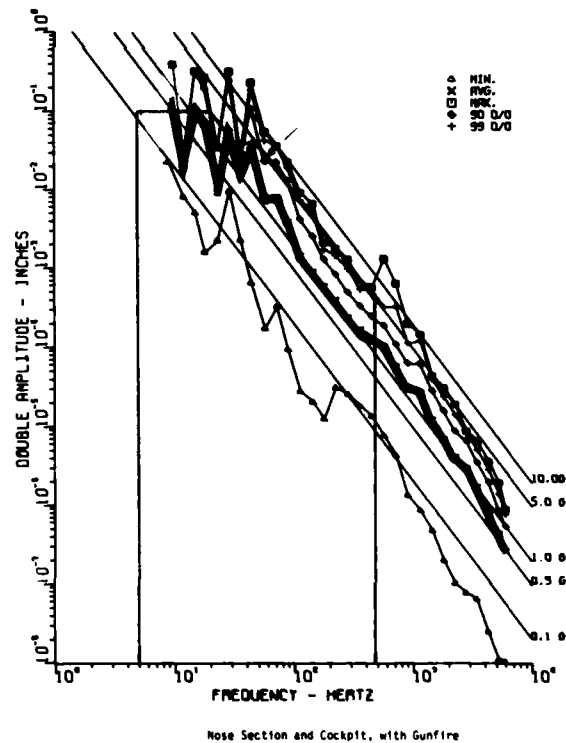


Figure 9 — OH-6 Helicopter

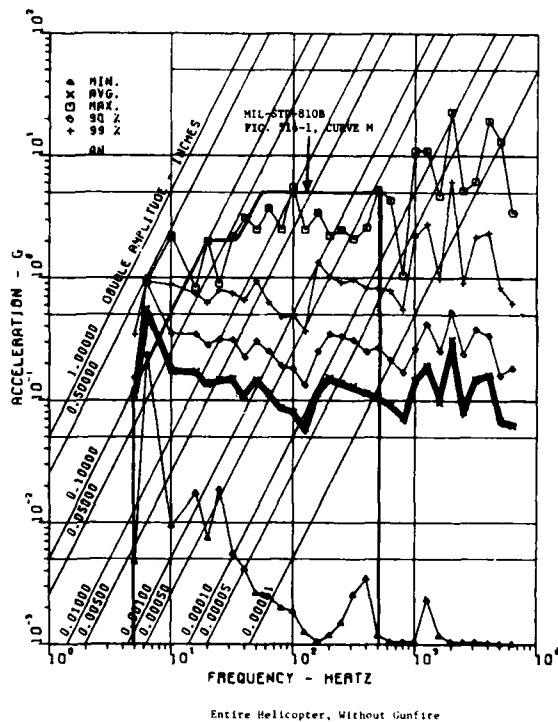


Figure 10 - AH-1G Helicopter

without gunfire but still less than 1/2 g. Without gunfire, the average is lower, but with the gunfire of the average increases. Figure 12 shows the vibration environment in the nose and cockpit sections of the same aircraft between fuselage stations 0-170 and this is without gunfire. The average data line is low, less than 0.2g, and from about 200 hz up, it falls very rapidly to below .01g. Figure 13 shows the vibration environment in the nose and cockpit sections, fuselage stations 0-170, with gunfire. In this plot the spread between the maximum and the minimum is larger than without gunfire. The average plot is higher but still lower than 1/2 g.

Figure 14 shows the data taken in the fuselage sections in the aft electrical compartments, between stations 271 and 390, without gunfire. The data in this plot are shown as an average of less than 0.3g. Figure 15 shows data that were taken in the same electrical compartment with gunfire and the average plots are again below 0.5G.

We look at this data and say what kind of a test do we want? If we consider failure due to fatigue, then there are some fairly reliable analytical treatments of complex vibration data particularly for sinusoidal or narrow band random vibration that boil down to simply needing to know only the mean average amplitude or frequency. Proceeding with this assumption, we considered the average vibration values of these three types of helicopters. We also felt that we wanted the simplest and least costly test if at all possible, keeping in mind that a random type vibration could well be a possibility. We are also desirous of not selecting a vibration test that repeated the design test evaluation, which is

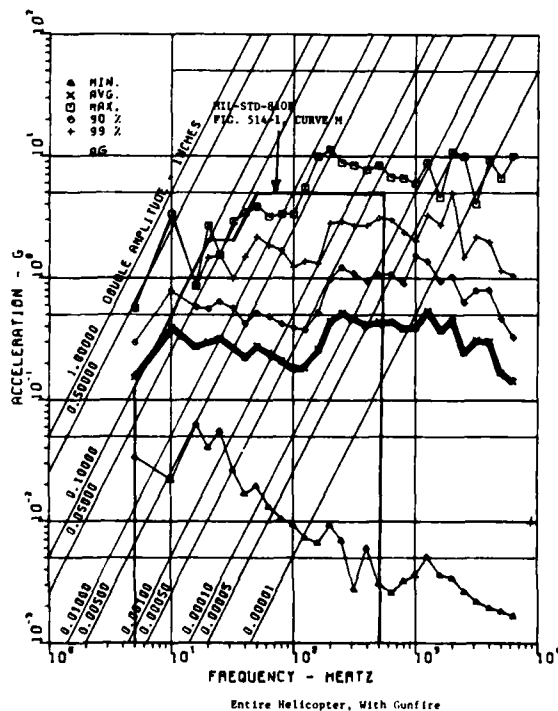


Figure 11 - AH-1G Helicopter

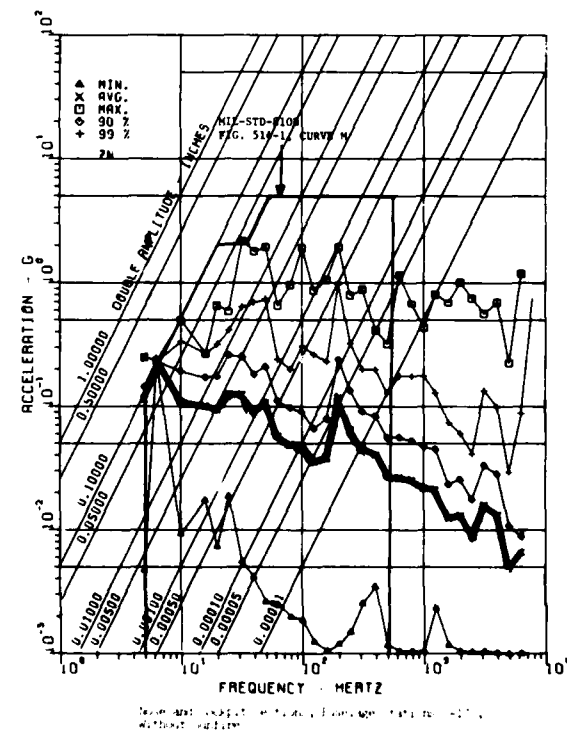


Figure 12 - AH-1G Helicopter

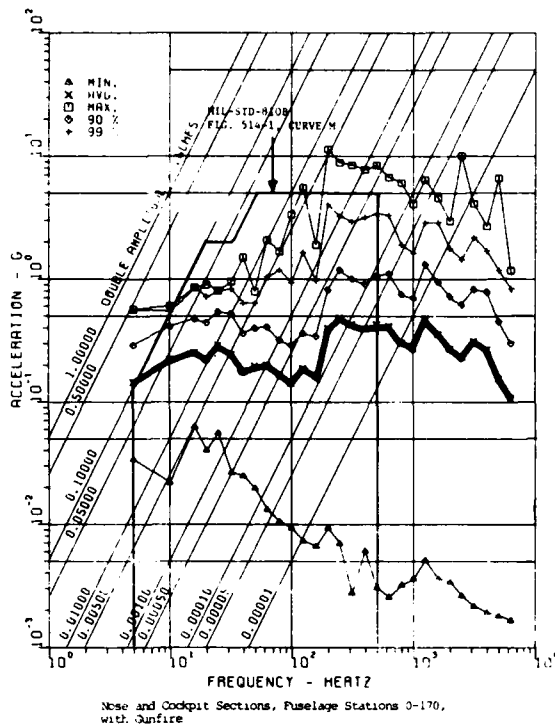


Figure 13 - AH-1G Helicopter

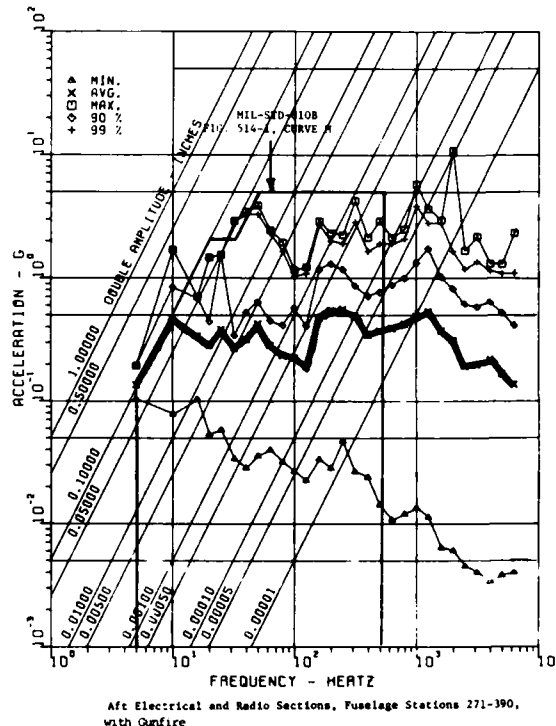


Figure 15 - AH-1G Helicopter

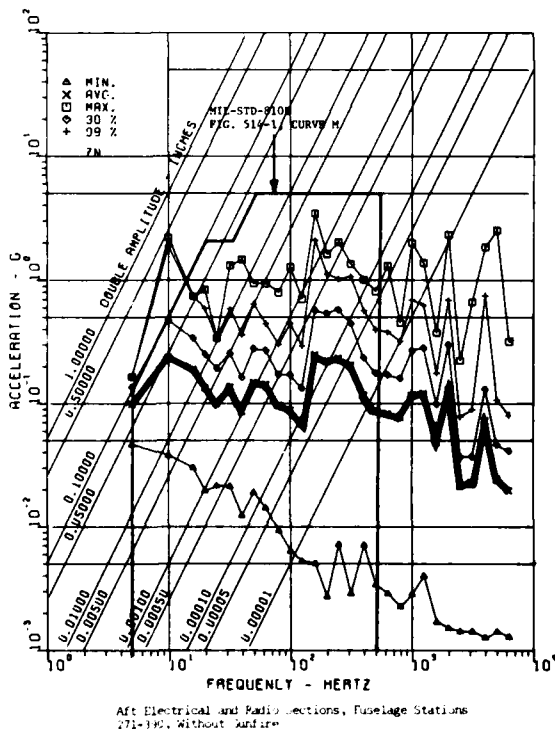


Figure 14 - AH-1G Helicopter

for the most part an aggravated test intended to evaluate a design in a relatively short test time. Based on the above, we chose a 50-minute sinusoidal sweep from 5 to 500 Hz and back to 5 Hz at 1.5g maximum. This is for electronic equipment in helicopters. We expect adjustments and refinements after first-equipment tests. We feel that a key point in establishing a good MTBF test is that if we are getting roughly about a 3-1 relationship between demonstrated and field values with the present requirements of 2.2 g's at a non-resonant frequency between 20 and 60 Hz, then it appears that a slight increase in the dynamic environment could very well satisfy the need for a better test. The real proof of this can only be realized by using the above with proper testing techniques and accurate failure data gathering.

Mr. Kidd (Bell Helicopter): Why were all of the filter slots filled with data?

Mr. Condouris: In this case we swept from 5 up to 5000 Hz using bandwidths of about 20 Hz on the low end and moving up to about 100 Hz on the upper end. Wherever we saw distinct peaks, we included them. If you look at a PSD of this particular data, you would see that they consist primarily of discrete frequencies, mainly the blade passage frequencies and their harmonics. As you get up to the higher end, the sinusoids start to disappear and the data become more complex. It is not pure random. You are seeing the plots for various windows across the frequency spectrum.

Mr. Kidd: Up to about 500 Hz, or at least to 300 Hz, is it mostly discrete frequency?

Mr. Condouris: That is correct.

Mr. Kidd: A random vibration man looking at this would take that to be broadband data of some kind all the way across the frequency spectrum.

Mr. Condouris: I don't think it is.

Mr. Kidd: Well, it is not. Sandia drew that conclusion in a paper that was presented about two years ago that helicopter vibration was primarily random vibration, which it is not, it is primarily discrete frequency vibration.

Mr. Condouris: If you look at the PSD, you see discrete frequencies across the whole bandwidth, a sort of low level type of mixed vibration data.

Mr. Kidd: The helicopter vibration space is a 17 dimensional continuum. What is the correct way to sample that space and how many times are we going to have to sample it before we really come up with a table-pounding position on how to describe that space for specification purposes, particularly in connection with mission spectra with regard to MIL-STD-781C? I think you are looking at a lot of data, we have looked at a lot of data, you and I have talked a little bit but we haven't talked nearly enough. I think we need to come to a good agreement at some point on some dialogue on this mission spectrum. The fatigue people, the FAA, the military, and industry have been talking about mission spectra for fatigue purposes for 20 years. I think it behooves us and others to do the same so that we can get a data bank that we will all agree on, a mission spectrum that we will all agree on, or at least the methodology for a mission spectrum. Do you agree to that?

Mr. Condouris: I agree. I would say that one of the biggest problems we have is trying to get people to get away from peaks for reliability testing because even in our engineering tests, we don't include some of them. We would have nuts and bolts leaving the plant after a demonstration test if we went for those peak values that are shown. We are looking in a simple fashion, since we are using an average and we hope to equate the average data to fatigue values, the proof as I see it is testing. We have to start somewhere; I would suggest that we start with the sinusoid, that would be the first step; that would be the simplest test. Let us get some "black boxes," which we are trying to do, take some that have been in the field already and run this test and come up with some sort of a demonstrated value. This would be with or without temperature. Temperature would play an important part, a combined environment would have a significant effect on this demonstrated value.

Mr. Beck (Boeing Aerospace Co.): A little background. Rockwell International builds the B-1 aircraft, Boeing builds the offensive avionics for that aircraft. We recently went through a study for the Air Force on reliability qualification testing. First, I want to acquaint you with the number of "boxes" that we are talking about and the groupings of these boxes, how much they weigh, how long we are going to test them, and then will tell you how we arrived at the vibration test that we recommended to the Air Force.

There are what we call functional groups and individual "black boxes," line replaceable units (LRU) (Figure 16). In group 1 we take 28 LRU's and play them as a system. These 28 LRU's are located throughout the aircraft, so they are in four areas where the vibration level is different from the design standpoint and these 28 boxes weigh 830 lbs. Group II of that functional group consists of 6

	FUNCTIONAL GROUPS	INDIVIDUAL LRUS*
QUANTITY LOCATION WEIGHT	GROUP ① 28 LRUS 4 AREAS 830 LBS GROUP ② 6 LRUS 2 AREAS 142 LBS	7 LRUS 3 AREAS 15 TO 61 LBS
ENVIRONMENTS	RANDOM VIBRATION TEMPERATURE CYCLE	
TEST HOURS	GROUP ① 1570 HRS GROUP ② 1175 HRS	3500 TO 5000 HRS
TEST ITEMS	2 OF GROUP ① 2 OF GROUP ②	7 TO 10 OF EACH LRU
TIME/ITLM	GROUP ① 785 HRS GROUP ② 588 HRS	500 HRS/LRU

*LRU = LINE REPLACEABLE UNIT = "BLACK BOX"

Figure 16 - B-1 Avionics RQT Concept

LRU's which are in two areas of the airplane and they weigh 142 lbs. That is a functional group where you play it together as a system. The other type is individual LRU's, there are 7 of those, a Doppler Radar, a computer, they are in 3 areas of the aircraft and they weigh anywhere from 15-61 lbs. each. We suggest that these items be subjected to random variation and temperature. The Air Force would like to see Group I go through 1570 hours of testing, Group II, 1175 hours of testing and the individual LRU's, 3500-5000 hours of testing. The number of test items include two aircraft sets of Group I, two aircraft sets of Group II, and 7-10 of each of the LRU's.

We have what I call drivers, or some constraints or ground rules that we have to live with and Figure 17 shows how we handle these. The Air Force wants realistic correlation between tests and operational reliability. Our reply was that you need to impose the same vibration on the test item that it sees in the airplane, and that is essentially random vibration. It should be combined with a

temperature test of some sort because in our design tests, these were the two most common failure modes, temperature first and then vibration. We have to use available test facilities. Some of this will be done at Boeing, the systems or the functional tests, but some of the others will go out to vendors and if one goes to vendors, we don't want to buy new equipment. We have to have an option of running sinusoidal vibration test even though we don't like it as well. We want to minimize this environmental test time because this program would run about a year and a half and in order to do that, we will only run a vibration test in one axis, we will widen our tolerances, we will run to vibration and temperature tests only (we will not include humidity or other tests), and we will use large vibrators so that we can get as many test articles on the table as we can at one time. Another constraint is that we want to use these test articles and put them back on a production airplane. We don't want to buy an extra set of test articles for this so we have to anticipate vibration failures and plan to refurbish.

DRIVER	RESULT
o REALISTIC CORRELATION BETWEEN TEST AND OPERATIONAL RELIABILITY	o RANDOM VIBRATION TEST BASED ON FLIGHT DATA COMBINED WITH TEMPERATURE TEST.
o USE AVAILABLE TEST FACILITIES	o OPTION TO RUN SINE VIBRATION TEST INSTEAD OF RANDOM
o MINIMIZE ENVIRONMENTAL TEST TIME	o ONE AXIS VIBRATION WIDER TOLERANCES VIBRATION AND TEMPERATURE ONLY USE LARGE VIBRATORS
o USE RQT ARTICLES ON PRODUCTION AIRCRAFT	o ANTICIPATE VIBRATION FAILURES AND PLAN TO REFURBISH

*RQT = RELIABILITY QUALIFICATION TEST

Figure 17 - B-1 Avionics RQT* Test Drivers

Let me describe how we arrived at the vibration environment. Figure 18 shows a typical mission for the B1 aircraft; on the vertical scale is dynamic pressure, on the horizontal scale is time. The peak on the right is the maximum dynamic pressure and the airplane is exposed to it for about 14% of the time; but from the fatigue standpoint that contributes 90% of the damage, so initially, we plan to use this region to derive our environment levels and our test times. Looking at some of the environments we are fortunate since we are flying three airplanes and we have accumulated several thousand measurements from the airplanes already. Figure 19 shows some early data that we had taken and I have picked the zone which is the lowest vibration area of the airplane and this is in the nose. This is an envelope of the data that were taken at a relatively low dynamic pressure-250 PSF. There is a pod on the airplane, which lets down and which tends to create a high vibration environment in that area; also opening the bomb bays will cause high vibration. These are the two types of data that we have plotted in Figure 19. We used six transducers and we measured in three directions. The dashed lines show the data and the solid line shows the envelope that we chose; the high peaks are due to some environmental control system and as far as we can tell,

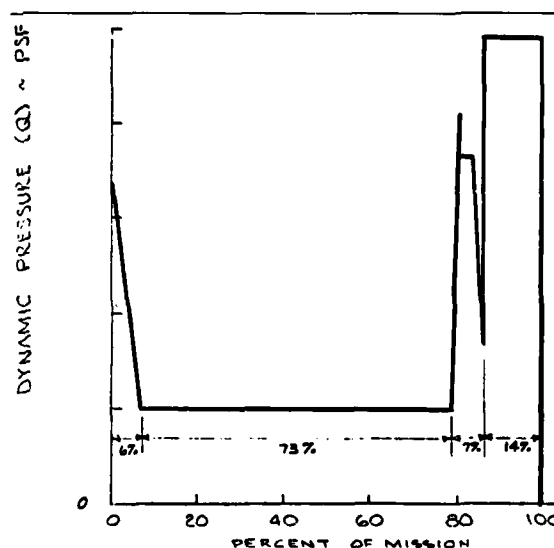


Figure 18 - Variation of Dynamic Pressure (Q) During a Typical Mission.

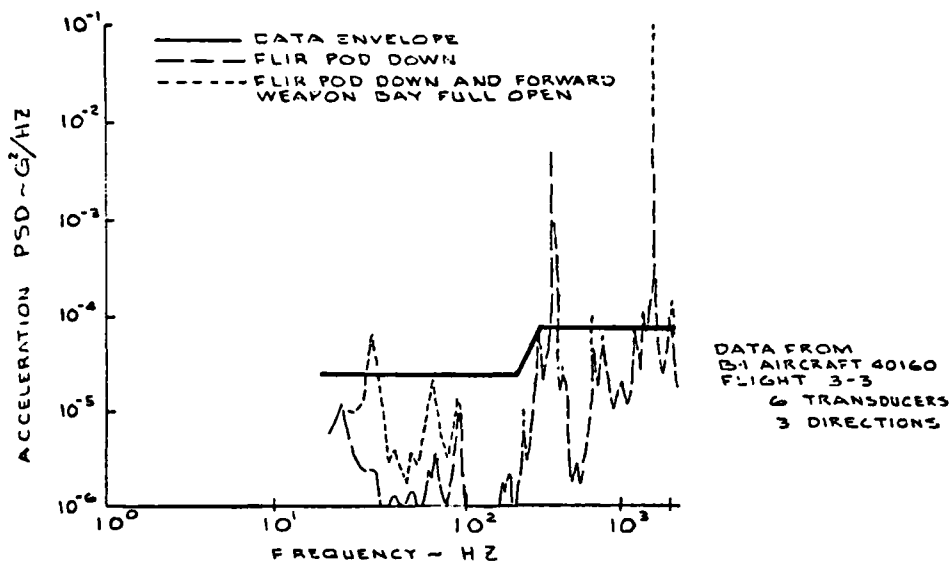


Figure 19 - Zone A Data and Data Envelope, Flight @ Q = 250 PSF.

they are not going to bother us so we are not going to stick them in the test. We will impose a broadband random vibration requirement there. The highest vibration area is in the bomb bay. The effects of opening the bomb bay doors and of lowering the FLIR pod cause the maximum vibration. Figure 20 shows the data and the envelope that we propose for that test.

We are talking about five zones of the airplane and we finally combined them into two zones or two envelopes that we will test to as shown in Figure 21. The upper line is the envelope for items around the FLIR pod and in the bomb bay. The lower line is the envelope for things in the nose and the crew compartment and forward areas.

We are thinking about a test duration of 75 hours and

we will do a single axis test and we will mount the equipment on the vibrator in the axis that we think will produce the highest vibration response.

So, how do we come up with time? Remember Figure 18 where we had 14% of the time at high Q? Figure 22 shows that we will put nine minutes of vibration on for every Reliability Qualification Test (RQT) operating hour; so we are talking about 500 hours per LRU. The airplane goes on one mission about every eight hours and 1.2 hours of this mission is at high Q flight. That was how we arrived at the test duration of 75 hours.

The fact that they want to re-use these LRU's on production airplanes raised the question can we do that from what we presently know about them? Therefore, we had

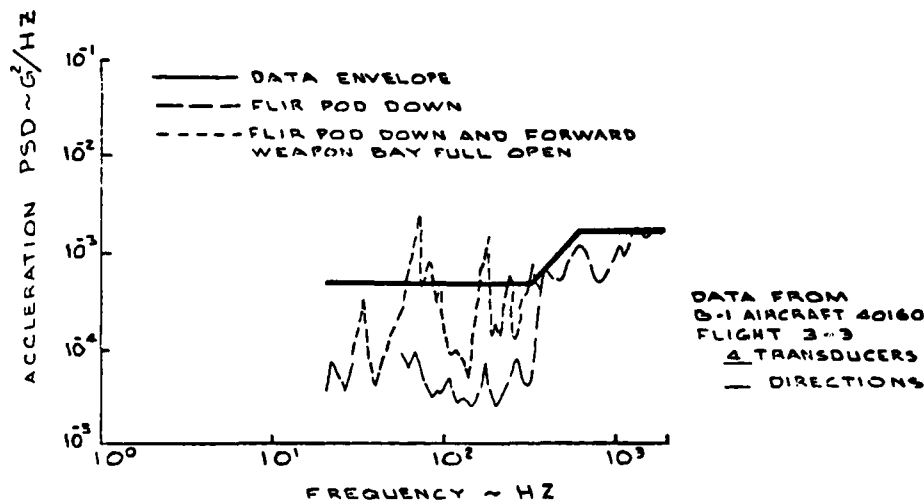


Figure 20 - Zone K Data and Data Envelope for Flight @ Q = 250 PSF.

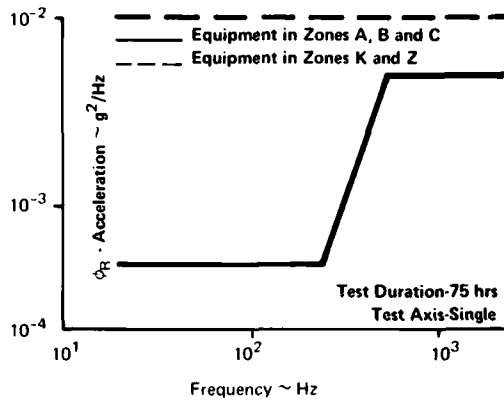


Figure 21 - Recommended RQT Vibration Environments

VIBRATION TIME = 9 MINUTES/RQT OPERATING HOUR

$$\frac{500 \text{ RQT HRS}}{\text{LRU}} \times \frac{1 \text{ MISSION}}{8 \text{ HOURS}} \times \frac{1.2 \text{ HRS OF HI Q FLIGHT}}{\text{MISSION}} = 75 \text{ HRS LRU}$$

$$\frac{75 \text{ VIBRATION HRS}}{500 \text{ RQT HRS}} \times 60 \text{ MINUTES} = 9 \text{ MIN/RQT HR}$$

Figure 22 - RQT Test Duration

to go back and determine what this means from a fatigue standpoint, that is what were they designed to in terms of level and time? Figure 23 shows the comparison of the design envelope for zone A, in the forward part of the airplane and this is the envelope that we will test to. The margin is pretty good, this is the minimum ratio and that is all we really looked at. Figure 24 shows the comparison for the high vibration area. The minimum ratio was picked at 20 Hz because a lot of equipment is mounted on vibration isolators. We evaluated the fatigue life of these items using the relationship in Table 1 which comes out of a paper by Meeker and Piersol. This relationship relates the reliability test time to the design test time, the design test

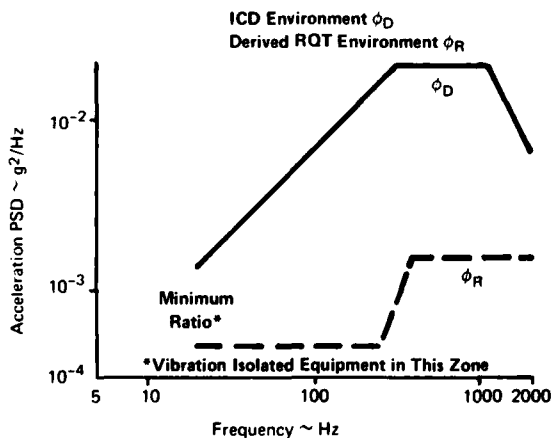


Figure 23 - Comparison of ICD and Data Envelope-Zone A

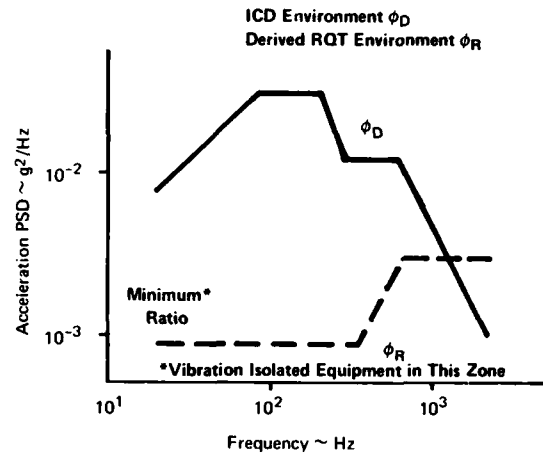


Figure 24 - Comparison of ICD and Data Envelope-Zone K

TABLE 1
Expected Time Before RQT Vibration Failure - T_R^*
Combined RQT Envelopes

Zone	Figure		Minimum Ratio		T_R (Hours)	
	ϕ_D	ϕ_R	Hz	ϕ_D/ϕ_R	N = 8	N = 2.4
A	C11	C16	20	3	1.7	31
B	C12	C16	300	24.5	18.3	81000
C	C13	C16	50	7	4.5	740
K	C14	C16	20	7.6	4.9	1000
Z	C15	C16	50	8	5.2	1220

ϕ_D Design Vibration PSD
 ϕ_R RQT Vibration PSD
 T_D Design Vibration Time (1/2 Hour)

$$*T_R = T_D [\phi_D/\phi_R]^{B/N}$$

B = 9
N = Noted (Meeker & Piersol)

level, the reliability test level, and there is a factor for damping and the S-N curve, that is what the B-N factor is. We evaluated this formula for values of N = 8 to N = 2.4 and we bracketed that because that is where we think those values lie. Based on the design for zone A, we would expect these things to last from two hours to 31 hours, however, we are testing them to 75 hours. Zone K is the one where we had the high envelope and we expect that a "black box" would last from 5-1000 hours and here again, we are testing for 75 hours. This tells us that our design tests show that we cannot get through this reliability test without failures, therefore, we recommended to the Air Force that they should be prepared to refurbish these "black boxes" before they put them back on the airplanes.

The last item concerns random vibration test tolerances (Figure 25). I don't believe MIL-STD-781B or MIL-STD-781C have tolerances in them, but knowing how big our

o WHY REQUIRED - FACILITATE TESTING OF LARGE NUMBER OF LRUs ON A SINGLE FIXTURE.

o RECOMMENDED TOLERANCES.

FREQUENCY BAND	TOLERANCE
20 TO 300 HZ	± 3 dB
300 TO 2000 HZ	± 6 dB
EXCEPT THAT DEVIATIONS AS LARGE AS +6/-12 dB SHALL BE ALLOWED OVER A CUMULATIVE BANDWIDTH OF 200 HZ	
OVERALL GRMS LEVEL	$\pm 15\%$

Figure 25 -- Recommended Random Vibration Test Tolerances.

fixtures are going to be and how much trouble you can have in trying to equalize a fixture, we will open up the tolerances so we don't spend all of our lives trying to work on fixtures. Effectively, this gives the tolerances for various frequency bands and if you look at MIL-STD-810, you can see that we have doubled the tolerances.

Mr. Hancock (Vought Systems Division): Do you have any idea how much difference opening the tolerance band has in your cost?

Mr. Beck: No.

Mr. Kidd (Bell Helicopter): Your second slide (Fig. 17) in the left hand top corner said something about realistic correlation. What do you mean by that?

Mr. Beck: I used the "Combined Environmental Reliability Testing" article that was written by Prather and Earls (7) as an example where they found that the reliability they measured in the field was only about 1/4 of what they demonstrated in the lab.

Mr. Kidd: You are going to keep books on your failures? When you get through, are you going back and say something about the realism of what you did? Are you going to try to certify this realism in some way?

Mr. Beck: No. We are trying to make a test that will give realistic results; whatever the test shows, we want to be able to say that the results are realistic. If you went out in the field and made measurements, you would find MTBF numbers that were similar to those that we found in this test.

Mr. Kidd: I am rather skeptical and I think you are presenting another formalism. I mean, you have a formal procedure and you say this is what I am going to call realism. When you get out in the field, I am very doubtful that you will be able to know if a delta definition of this type will give you some delta improvement in reliability. I don't think so, do you?

Mr. Beck: No. I think that all that will come out of this test is if we apply the environments in this way and if we have a failure, then we should expect the same MTBF in the field. If you don't like that number, if it is too low, then you should do something to the equipment to make it higher.

Mr. Kidd: But then only time will tell whether this helped it or not.

Mr. Beck: That is right and if they make the change, you will never know whether it was there in the first place or not.

Mr. Kidd: I think the main thing that bothers me is the way we are using this work "realism"; I can see people taking third, fourth, and fifth derivatives of an original function that you did not know within 100% anyway. It will add a lot of costs without corresponding returns as far as I can see if we are not very careful about what we say realism is. Somebody ought to define realism. In your case, is realism what you did?

Mr. Beck: We should not expect to get realistic reliability results from a 20 to 60 Hz sinusoidal vibration test.

Mr. Kidd: Maybe that is as realistic as what you are going to do.

Mr. Beck: No, I don't think so. We know this environment, we had the benefit of measuring it on the airplane. One point is does the environment make any difference at all? It might not make any difference to the thing.

Mr. Green (General Dynamics, Fort Worth): How do you plan to compensate for the isolators on the equipment that was isolated? Do you plan to put random vibration through the isolators, or block the isolators? How do you handle that problem?

Mr. Beck: There were shock mounted items in that area in the two graphs that I chose. Most of these items, I'd say 80%, are not isolated. If they are isolated, the environments would be presented at the bottom of the isolator. That is, they were measured at the bottom of the boxes.

Mr. Green: Really it amounts to what you are obligated to do. You can't think that anybody could force or expect you to put the random vibration directly into the equipment in order to ferret out workmanship problems or anything of that nature? Is the shock mount a part of the system?

Mr. Beck: Yes, it is a part of the system.

Voice: What is the rationale for single axis testing?

Mr. Beck: We went to single axis testing primarily because if you put 10 or 15 items on a fixture, which we will do in order to cut down test time, we do not want to be spending time moving the shaker from an upright position or switching it 90° on a table.

Voice: This means if you have one type of LRU, you will put three items on the table with one in each axis?

Mr. Beck: No. It means that we will pick the axis which we think will give it the highest vibration response.

Voice: How will you determine that?

Mr. Beck: From what we know about the equipment.

Voice: Inside or outside?

Mr. Beck: Inside. We have analyzed them and we have made measurements on them. You get a feel for where the worst response is.

Voice: What was the customer's reaction to this?

Mr. Beck: The Air Force? They did not care, anything to save money, I think, since we are in a money-saving mode these days. It also depends on to whom you talk in the Air Force. If you talk to the airframe section, where the vibration specialists are, you might get a different answer than if you talk to the avionics people who are trying to get a "black box" out to do a job.

Dr. Curtis (Hughes Aircraft Co.): We should keep two questions in mind: The first question is if we go to a lot of time and effort to bring a lot of realism into reliability development and reliability demonstration tests, and then presumably screening tests of the rest of the product as it comes off the line, can we really solve the problems that have brought all this to sort of national attention in the last year or two? The second question is how are we going to measure what we got for our money or how well we did? I am afraid that while Col. Swett did us a real service in getting some attention for a change, because I can remember that over a number of years where we have tried to get money to do things that we thought would improve things and we did not get a whole lot of attention, now maybe we have more than we can really stand. But if we have this attention and we work hard and then several years from now it looks as if everything is just about the same as has been before, then a few people may be disappointed.

Last year in San Diego a colleague of mine, Dick Baker, talked to a similar panel session about a study we have had for the Rome Air Development Center on the operational influences on reliability of avionics. A paper by Dick Baker and George Kern, based on this study, is in the September/October Journal of the IES (8). I would like to remind you of a couple of things that we found in that study. This study was brought about because of this "alleged discrepancy" of the factor of 10 between demonstrated reliability and field reliability. Figure 26 which is taken from reference (8), summarizes a year's worth of Air

Force 66-1 failure data and it turns out that it really was not quite 10-1; there were instances where it was as high as 20-1 in certain pieces of equipment and others where it was 2-1. But if you average it out over a lot of equipment in different airplanes, in different commands, if you compare it to demonstrated MTBF, it is about 6-1, and that is shown on the left-hand side. If you compare the predicted MTBF versus field MTBF, the ratio is about 7 1/2 to 1 which says that some of us are optimists. But then if you go carefully into it, it turns out that 6-1 is based on "comparing apples and oranges" and if you get the comparison reduced to "comparing apples to apples" or "oranges to oranges," then it is only a factor of about 2 1/2 to 1 between what we see in the field and what we have demonstrated in the laboratory. These are demonstration programs run under the MIL-STD-781B type testing. It is the only kind of equipment which had such a formal demonstration test. A fair part of the problem is really semantic, it is how you keep score. When you do it in the laboratory, you count operating time, the Air Force 66-1 data are all based on flight time, that is, a large part of this discrepancy. So now you are left with a factor of 2 1/2 to 1 to worry about. You see that the remaining part is divided roughly 50/50 into two other things. One is called "Due to Operational Factors," the other is called "Due to Environmental and Other Factors." You could substitute "miscellaneous" for that or "undefined." The operational factors sort of split into two groups: One is called the maintenance handling factors, this is the replacement rate for the equipment and it is also a function of where it is repaired. The other part is things like the utilization rate, the mission duration, and factors that are concerned with how the equipment is used, half of this remaining variation and that is about as close as you can get.

The only thing we really pulled out of this that you could point towards environmental factors is this summary table (Figure 27) which is a comparison of what we have seen in fighters versus bomber and transport systems. (This was also taken from the previous reference.) "F3" is a sort of a field MTBF after you have taken account of the definitional factors and operational factors, etc., "D" is the demonstrated MTBF, "P1" is a predicted MTBF, "R" is the required MTBF. That was in the contract. We see again, on taking rather broad averages, that the discrepancy between field experience and the demonstrated MTBF is about 2.7 for equipment in fighters as opposed to about

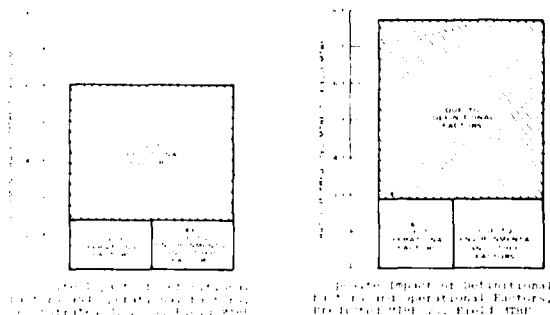


Figure 26 - Composite Impact of Definitional and Operational Factors.

Fighter Systems		Bomber/Transport Systems	
$\frac{F_3}{D}$	= .37 (2.7:1)	$\frac{F_3}{D}$	= .79 (1.3:1)
$\frac{P_1}{F_3}$	= .33 (3:1)	$\frac{P_1}{F_3}$	= .73 (1.4:1)
$\frac{F_3}{R}$	= .46 (2.2:1)	$\frac{F_3}{R}$	= .95 (1.1:1)

Figure 27 - Composite Field MTBF Ratios for Equipments Associated with Fighter Systems and Bomber/Transport Systems.

1.3 for equipment in bombers. However, those weren't the same pieces of equipment since we did not have enough data to only look at equipment that was common to both kinds of aircraft. You might be tempted to say sure you can expect that because fighters go to higher Q's, they are higher performance airplanes, that must all be due to the environment. But if you look carefully, you better not jump to that conclusion because fighters have shorter missions than bombers, the utilization is different, and they are maintained differently. Certainly, not all of that is due to the environment, however, it may be an indicator. I think what I'm trying to illustrate in Figures 27 and 28 is that with the way in which we presently keep score in the field, it will be very very difficult for us to sense that we have made any improvement in reliability by going to a great deal of extra effort. We won't be able to do this just by the normal score-keeping methods presently extant in the Air Force, at least.

As regards what percentage of the problem we might hope to work on, Figure 28 shows a pie chart which I reproduced from a study that was completed by Grumman Aerospace for the Air Force Flight Dynamics Laboratory (9) in which they tried to ascribe or look at the percentage of failures which were due to environment versus non-environmental causes, and roughly 52% of them were ascribed to the environment. This was for equipment on one or two Navy Aircraft. There is a report by Dave Earls from the Air Force Flight Dynamics Laboratory in which he tried to bound the problem; I think he came up with a lower bound of 14% of the failures that could be ascribed to environmental causes and an upper bound of 60% and this was obtained by looking at the typical failure data which he gathered in the "66-1" reports. If you look at the failures due to environmental effects, what percentage of those are due to vibration? We are down to 14%, which is not a tremendous piece of that pie, but even if we could completely eliminate all failures due to vibration by doing a 100% job, somehow, it says that maybe we can solve 14% of the problem or eliminate 14% of the failures. But if you remember Figure 26 where we have a factor of 2 1/2,

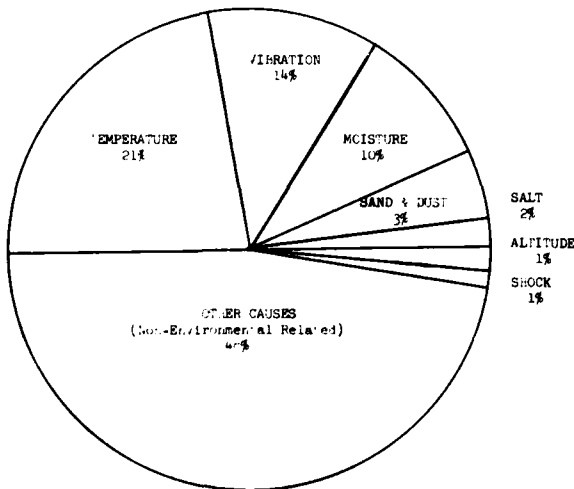


Figure 28 - Total Field Failure Distribution

which is just from score-keeping, again, it will be very difficult to sense that we have done anything worthwhile, unless we do something to improve the score keeping. The center column in Figure 29 which comes from the same Grumman report (9) shows another part of the problem. You look at the vibration failures and it tells us which ones were failures that had not been revealed by the qualification test. Presumably that is a deficiency in the "that" test, that by improving it, you could have found those failures versus those that had been actually found but somehow were not completely fixed because they still re-occurred in the field. These are roughly 50 percent and they illustrate a problem that we are going to have if we run a reliability demonstration, test or a reliability development test on one or two systems. Some people will look at it as being an extended burn-in test and by the time you are through with that, those one or two systems are probably in pretty good shape. But how do you get the factory to produce pieces of equipment that are equally well-screened and burned in serial number after serial number, block after block, month after month so that we don't have this same chart again? We look and see what happens in the field and say that happened in the reliability development test. Again, it is not obvious that we will solve the problem by increased testing in the laboratory.

Mr. Hancock (Vought Systems Div.): I have heard it said that there was disagreement with the 14% in that report. Thinking about it somewhat, I suppose one would be forced to inquire as to the possible failure mode and its relevance as to whether they were vibration causes in the failures. Do you have any comment on the 14% accuracy?

Mr. Condouris (U.S. Army Electronics Command): Amplifying what you have said, we have been thinking about this in the same way. We feel that we did not want to jump into anything and get into exotic testing to take care of that 14%. We have talked a lot about differences between demonstrated and field values of like 10-1, 3-1 and 2 1/2-1. If my memory is correct, I recall seeing some reports where it has been the other way around where we had better reports in the field MTBF than we had demonstrated. This is a little turn on what you are talking about, possibly the data taking and the gathering of data are

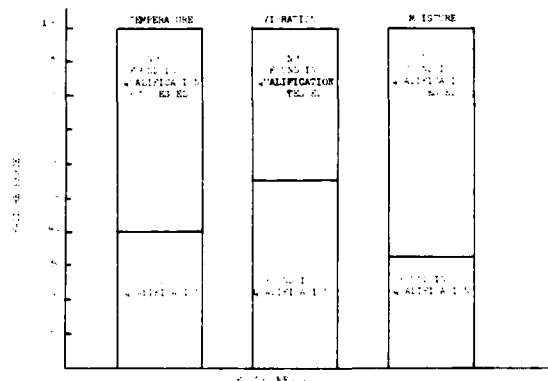


Figure 29 - Relative Field Failure Distribution by Qualification Test History for Primary Environments.

different for one equipment. It was not just a small percentage, I recall one report in which we had hundreds of hours difference the other way around where the field MTBF was better than the demonstrated MTBF. There is a lot to be looked at in this analysis we just made about getting down to that small difference that appears at the end. I concur with what you have been saying in that respect.

Mr. Popolo (Grumman Aerospace Corporation): Allen Curtis made a point about the fact that percentage-wise, it does not seem as if we have a big problem and maybe we will spend a lot of dollars to resolve something that really is not as serious as we think it is. But I can tell you as far as Grumman is concerned, the guy who pays my salary is complaining quite a bit about all of the problems we are having with our equipment and I don't really care whether someone is incorrectly evaluating the failures in the field; we have failures and the failure rates are very very high, therefore we must be doing something wrong. Even if you examine the manner in which the field information is evaluated, and as Allen Curtis has pointed out, it does not look as bad as we think it is, it is still there, therefore I think we should incorporate some sort of change to eliminate those failures because we cannot keep aircraft up in the air. We have been very fortunate with some of the type aircraft that we build, ECM type and multi-mission type, where eventhough we may not be able to accommodate the prime mission, we can still get our aircraft airborne because of its other multi-mission capability. I feel sorry for some of the other aircraft manufacturers who have a single-mission type aircraft where they cannot get them up in the air, so we may look a little bit better than most but the problems are real because the more multi-mission work that you do, the more equipment is involved, therefore more problems result. It is there unless we are being hornswoggled somewhere.

Howard Schafer (Naval Weapons Center): We are discussing dry statistics here, failure tags that are sent back by the "white hat" in the Navy, or the field, or the Air Force technician. Something that has to be kept in mind, we find that some systems have better reliability out in the field than they had in the plant. I spent about a third of my time overseas during this last war trying to ferret out the environmental failures and I found, in some cases, we were getting better reliabilities on avionics and weapons systems in the field than had been predicted. It was caused "dyke pliers." They were finding that they were having so much trouble keeping the systems up, that on an aircraft carrier on Yankee Station, the men would go in with "dyke pliers" and cut the system out so no failures came back. In the depots they are saying we have a good MTBF on this particular "black box" and when the people ask why, "We cut that system completely out." The second point I want to bring up is it is easy to sit back and take dry statistics when we are dry here and say we only have 2-1, but I had something thrown at me at Da Nang in the Marble Mountain Days by some pretty good Marines that were trying to keep their aircraft up. They said they have two check-out sets on Sparrow. "Our Sparrows will check out good on one and bad on the other. You are a guy from China Lake, tell me which one do I believe?"

Mr. Hancock (Vought Systems Division): On that same point, Col. Swett said perhaps there should be no correlation between test results, the way tests had been conducted, and field results.

Voice: Did I understand that Figure 30 showed that 60% of the vibration failures were of items that were found in the qualification test? In starting to work with reliability, I find that the reliability people use a term "non-relevant" and qualification people use the term "random failure." If you look through many reports, you see these types of things and I think that might account for some of that 60%. We need to ferret these out if we can.

Mr. Curtis: Another outcome of our study was that there was a good correlation if the percentage of failures in the demonstration test that were classified as "non-relevant" was small; then the ratio of the field failure rate to the demonstration test failure rate would be small. Another way of saying that is that the more of those failures you rationalize away, that is not going to make them not happen in the field.

Mr. Popolo (Grumman Aerospace Corporation): I am going to talk about two subjects. One of them is combined environment testing and the second one is using random vibration for screening. We finished it about two or three years ago and I will only present the Grumman recommendations.

Starting with the combined environment testing, the question is where do we have to use it? We all know that it is very expensive, a lot of equipment is involved such as chambers and exciters, etc. We have searched the literature and we also did some in-house testing; however I will present an out-of-house recommendation and an in-house recommendation. A paper by Coren, Cotlier, and Conrow (10) presents the results of combined environment testing. The authors looked at different areas, combinations of vibration with high and low temperatures and humidity as evaluated on various type "black boxes," components and electronic assemblies such as radar systems containing switches, relays, etc. The other report is by George Hirschberger from Grumman who is very active in reliability (11). This ECP-425 is something that we use in the Navy, it is an engineering change proposal which is a way of getting some additional funding on a present program.

RESULTS FROM REF 10

	COMBINED VIBRATION AND LOW TEMPERATURE				
	% OF ITEMS FAILED UNDER			SYNERGISTIC EFFECT	SYNERGISTIC EFFECT AS % OF SUM OF INDIVIDUAL ENVIRONMENTS
	COMBINED ENVIRONMENT	TEMPERATURE ALONE	VIBRATION ALONE		
ACTUAL DATA					
Air Group I	0.310	1.159	0.049	-0.898	-74.3
RELAYS	0.397	0.935	0.078	-0.614	-60.7
SWITCHES	0.026	0.163	0.007	-0.144	-84.7
Air Group II	0.001	0.004	0.014	-0.017	-94.4

DATA ALSO EQUIVILIZED TO A COMMON OCCURENCES BASIS AND A COMMON TIME BASIS

Figure 30 - Failures Due to Combined Environments

In this case the work was done on one of our A6A derivatives which was an EA-6A, an electronic counter-measures type aircraft. The purpose of this program was basically to eliminate that small percentage of field failures that was keeping our aircraft on the ground. We went through a very extensive step-stress program to try and determine "what's going on." That unit was supposedly reliability demonstration tested; it was acceptance tested; it had gone through qualification tests, but it still did not work in the aircraft. We started to look at these areas maybe there is a problem in combined environments. Perhaps we should not have performed vibration tests alone or temperature tests alone; perhaps we should have combined them and then try to determine the fragility level for the equipment. It is really a shame because it is after the fact, all of these things should have been resolved beforehand.

Figure 30 is taken from reference (10). I imagine most of you are familiar with the term "synergistic." What was interesting in this particular paper is that on this one combined environment of vibration and low temperature, they first evaluated the various type failures for various types of equipment, as well as components, and in turn they came up with a series of a percentage of failures for a combined environment condition. Then they did a temperature test alone and you can see that it is a fairly sizeable change, and then they ran a vibration test alone. They actually came up with what they call a negative synergistic effect; by including the combined environments, they actually found fewer failures than were actually found when they tested the units separately. They basically ratioed not just the effects from the actual data by itself, but they also equalized the common occurrences as well as the common time bases. All that resulted was the percentage of negative synergistic effects reduced. We at Grumman ran a similar type of test program during that step-stress work that we did on the EA-6A and we found that after spending all the large numbers of dollars to put these combined environment facilities together that we were eventually running out of money. We tried to do some short-circuiting by not doing combined environments and the results of our work indicated that there really was not any advantage, we got just as many failures whether we combined our environments or whether we ran them separately. This made our program managers very happy because now they could save some money. In conclusion, using reference (10), the negative synergistic effect created by combinations of environments caused a reduction in the overall stress and we did not see any advantage to it at all. Where should we use combined environment testing? Our conclusions and our recommendations to the industry are, if there is nothing to be gained during the development of a piece of equipment, and if you really want to determine the worst effect, then do not use combined environments for your acceptance, development, and qualification tests; but, use it during reliability demonstration because that is the real animal, that is the one we are trying to simulate, and if there is a negative synergistic effect, then that is the way we should rate our equipment. That is also the way the reliability and MTBF should be evaluated.

The next subject I have is the work that was done by our reliability people, again in conjunction with our dynamics people and our test people, to determine the

effectiveness of random vibration. This was started around 1970-71, after we spent considerable time on our LEM program for NASA; we used random vibration to do all types of acceptance screening as well as qualification testing. There was not very much of an argument about whether we used sine or random vibration, the world at that time was talking random vibration and all of the space programs still use random vibration. Our management would have rather stayed with the sinusoidal testing but they were forced to random testing by NASA. Based on those very successful results, and based on our failures in the field on all of our electronic equipment, we said let's try something else, let us go to random vibration, but how do you sell it? How do you go to your program manager and say I want you to spend this money to do this type of testing? We did get some funding and we ran a test program and I have the results of that test program.

We had excessive workmanship failures and I am only talking about screening for acceptance. The subject does not deal with reliability demonstration or "burn-in." After going through all of the vibration tests, sinusoidal testing of MIL-STD-781 for acceptance, and even going through the sinusoidal "qual" testing of specifications such as MIL-E-5272 and MIL-T-5422, we wound up with a high percentage of failures. By the way, MIL-STD-810 was not a governing specification on the A-6 and its derivatives because it is basically a 1959 vintage aircraft which has gone through five iterations. Every time a new iteration would come up, the government or the program people made us work to the initial contract specification. At the present time the EF-111 is the only aircraft where MIL-STD-810 is invoked and it is our ECM type aircraft that we are building for the Air Force. We tried to put together various types of specimens, and it numbered approximately 100 different type specimens, in which we would primarily look at failures associated with items such as solder joints, chafed leads and the like, strictly workmanship failures; those were the failures that caused many problems. We also found out that as far as temperature testing was concerned, the acceptance, the reliability demonstration, and the qualification testing did work to extremely high as well as extremely low temperatures, -65° to 160° F (-54 to 71° C). We were accelerating the failure modes during the lab testing in the original qualification program at these extremes but we still had failures; so that is why we felt that maybe our problem was that we did not have the right vibration screening. Figure 31 shows the laboratory and field test results on an Ad converter. We had gone through various units in the laboratory at the manufacturer's plant. Within the first 100 hours, there were a considerable number of failures that were picked up and repairs were made, but once the equipment got into the field we did not really solve the problem they reappeared, and in some cases at a greater rate, in other cases, not at all. We did a good screening job, but there were no failures over 700 hours so we thought that we must be doing something wrong.

We went further, we posed an advanced development program and it was bought off. The purpose was to determine the vibration environment. Would it be sinusoidal, both a fixed frequency and swept, or random? Which would be the most effective way to get the workmanship failures out? We incorporated five difference

A-D CONVERTER TEST & FIELD RESULTS

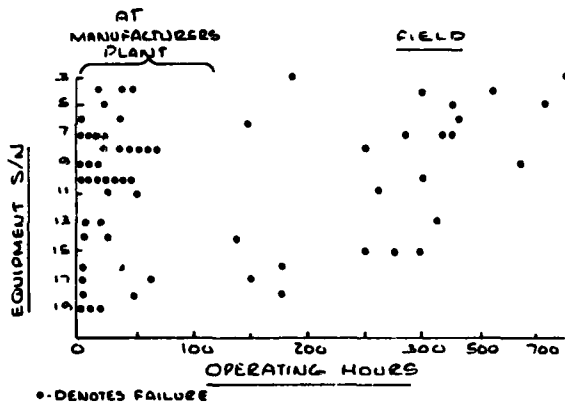


Figure 31 - A-D Converter Test and Field Results

generic type failures that we are most familiar with and they were improper component mountings, poor solder techniques, printed circuit wiring flaws, improper stripped and routed wires, and inadequate tightening of structural components and mounting hardware. We put in known failures, now the idea is how do you find them? We ran the original acceptance or screening test which comes from MIL-STD-781, where we chose a non-resonant frequency between 20 and 60 Hz and that testing is generally done between 1-1/2 to 2 g. We knew that did not work, so we went to a higher level. We chose 50 Hz for our fixed frequency at an input of ± 5 g. Our swept frequency range was 5-500 Hz and it was chosen primarily because our equipment was only qualified for 500 Hz. The third approach was to use an acceptance test spectrum that was developed on one of our space programs, .04 g^2/Hz with the necessary 3 db per octave rolloff which comes out to be a 6.0 g RMS overall value (Figure 32). We had a difficult time trying to convince some people to go that route because we were exceeding 500 Hz. We were able to use

TEST INPUTS

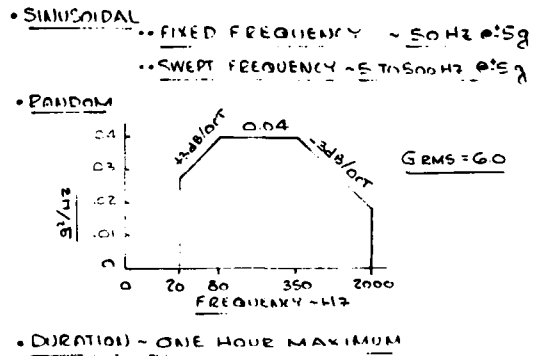


Figure 32 - Vibration Test Inputs

the merits gained during the space program that convinced management to at least try it to see where we were going to go.

These are our results (Figure 33). We plotted the efficiency percentage which is basically that we know what our failures were, we know the number of failures that we could possibly have in each particular piece of equipment, and how many of these come out within the particular type of vibration input over a period of time. Most of the work was done in excess of an hour but, for discussion purposes, I cut it off at an hour. The standard original acceptance test input at the fixed frequency did not give us anything at all, we learned absolutely nothing from the MIL-STD-781 input. Then we went up in steps; first we did the 1 1/2 g sine sweep and the solid line is just a soldered joint and the dash line is the component mounting. During the sine sweep at 1 1/2 g, we started to get failures and it is obvious what happened. We still wanted to run sinusoidal vibration tests to see how high we would have to go to get the same results. The next series of tests was to compare the fixed frequency input at 5 g at 50 Hz and again there were no failures. Then, we started looking at swept sinusoidal vibration. We started to excite the

COMPARISON OF TYPICAL ACCEPTANCE TEST LEVELS

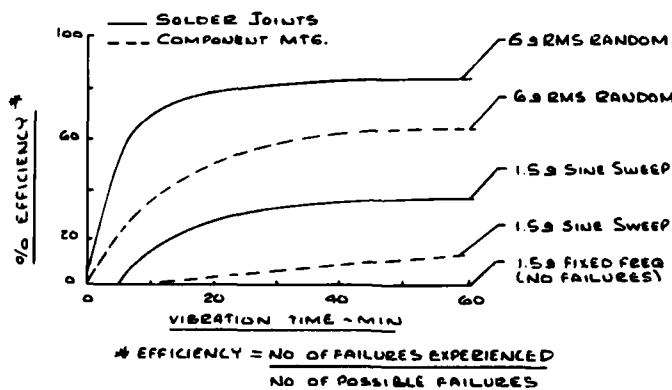


Figure 33 - Comparison of Efficiency of Typical Acceptance Test Levels in Producing Failures.

other modes that are present in the design, in this case using 5 g at the fixed frequency, and some failures started to appear around 25% (Figure 34). And here is a 5 g sine sweep relative to the solder joints and it is similar to the previous curve; Figure 34 also shows the effect of the 6 g RMS random vibration on the component mounting and the solder joints. Within 10-15 minutes of test time, we started to get something around 80% of the failures and by extending the test time, we did not really find that many more. We thought that was very enlightening also hopefully it was a way of convincing people that if we went to random vibration, we would try to reduce our cost by cutting down the test time rather than go for hours and hours at fixed frequencies. They still were not convinced, they wanted us to go further, they wanted us to stay with sinusoidal testing because all of the equipment was qualified to that and it does not cost any more money. So we went further and Figure 35 shows the same 6 g RMS results. Comparing those to the failures from a 10 g sine sweep and from a 12 g fixed frequency at 50 Hz, I think it is quite intuitive to all of us, considering a non-resonant frequency

for an extended period of time, you are not going to have any problems. Maybe we knew that answer before we started but we had to convince somebody.

Even with a 10 g sine sweep which, as far as I was concerned, was the wrong way to go because we knew that the unit is only qualified to 10 g and we have exposed it to 9 hours of testing which is the standard "MIL-Spec." requirement, half hour resonant dwell and one hour cycling periods; we knew we would damage that unit and even though we got some nice screening results, we would probably damage some other parts of the major components which we are not trying to evaluate at this time. That was supposed to have been done during the qualification test, we were concerned with workmanship.

From the results of the test there is no question in our minds that we should be definitely going to random vibration, but we have had considerable contractual difficulties in trying to force our vendors to go to the random vibration acceptance test even though it has been proven

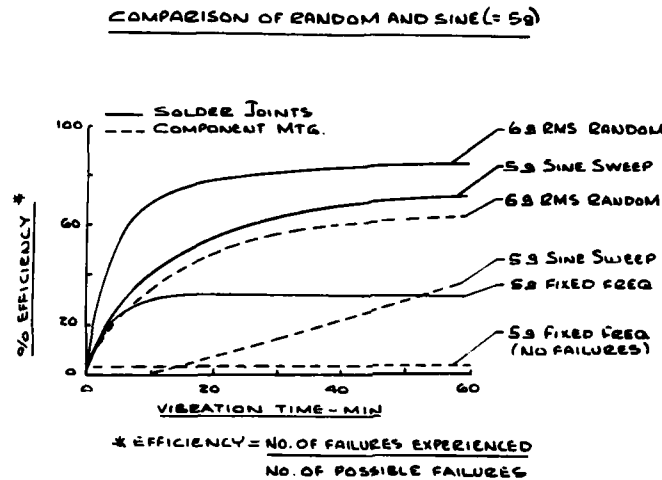


Figure 34 - Comparison of Efficiency of Random and Sinusoidal Vibration in Producing Failures.

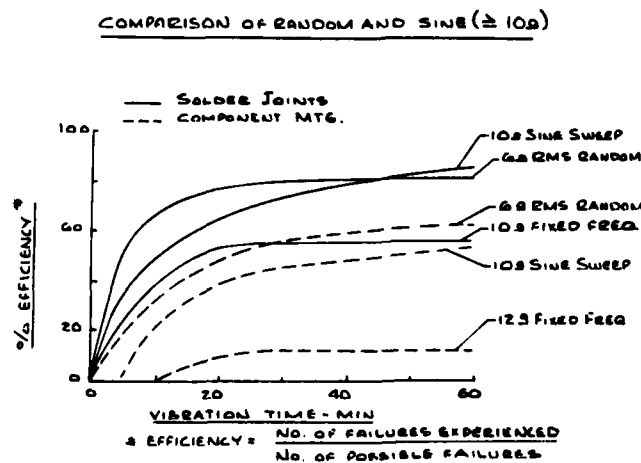


Figure 35 - Comparison of Efficiency of Random and Sinusoidal Vibration in Producing Failures.

extremely successful. We have units we could not get in an airplane, if they turned the key they would fail. After going through all of the acceptance and qualification testing, and by subjecting that same unit to a 10 minute random vibration screening test at the level that I pointed out before, the workmanship failures appeared immediately. We did that first at Grumman and from there we convinced the "powers-that-be" that it should really be done at the vendor. We had the same problem that most of you people have had in that they do not have random vibration systems; in some cases, they had to buy them, in other cases they had to go out to some of the other test facilities and pay to have the work done. When it finally got down to the wire where we were not able to sell aircraft, we cannot get rid of them they won't fly over the fence, we had to do something so we came up with this idea. I do not think it is revolutionary and I do not know if the different type of work that was done to get us where we are now has ever been shown in this manner. The other most interesting and I think the most cost conscious feature, which makes all of the managers happy, is that if you can get those failures out in a very short period of time, you will save a lot of money.

Mr. Silver (Westinghouse): It seems you had a negative and positive synergism involved; your negative synergism was in the temperature test area and your positive synergism was in the vibration test area. It seems as if the temperature failures that occurred when you were not vibrating must be of the nature of non-making contacts which were eliminated when vibration was applied. I think there can be very little doubt that there is more total stress when you have stretched components due to temperature and additive stress due to the dynamic input.

Obviously you get that positive synergism in one case, and a negative synergism in the other. That seems to infer that you should have combined temperature and vibration in qualification and that you should have separate temperature tests because there are failures that can occur in temperature that would not occur when the environments combined.

Mr. Popolo: I disagree because the purpose of qualification testing is to test for a very short period of time at an accelerated level. If you are going to aggravate that situation by entering another discipline, I think you are being unfair to the system. We recommend that the reliability demonstration test is the only place where you should be able to use combined environments. Those are real numbers, they should be real numbers. That first report was by another East Coast aerospace company, Grumman's work did not support the negative synergistic effect. We found it didn't make any difference, we still produced the same number of failures.

Mr. Calkins (Pacific Missile Test Center): I would like to review two studies that we did at PMTC on reliability testing. One was a comparison of random vibration using mechanical shakers versus acoustic testing for the simulation of captive carry vibration as a technique for reliability testing. The second part is the review of a study that we did on reliability accelerated testing on the Sparrow Missile.

The Sparrow Missile is basically 144 in. (3.7m) long, 8 in. (0.2m) diameter, and weighs approximately 500 lbs. (227 kg) (Figure 36). On the far right corner we have the configuration that was used on both the F-4 and the F-14 for captive carry of this missile. It is semi-submerged and

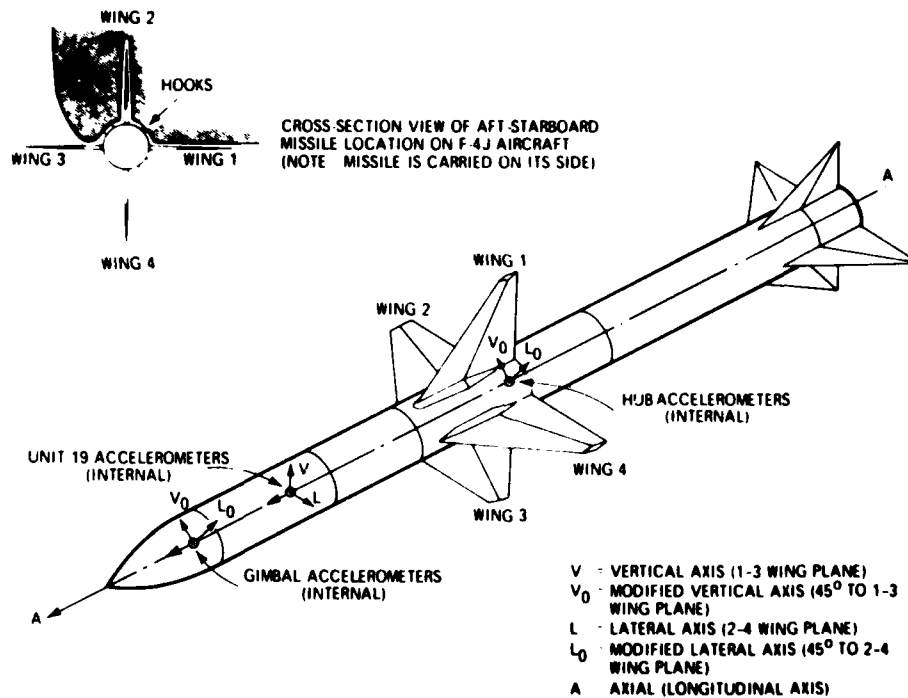


Figure 36 - Instrumented Sparrow Missile

the supporting hooks are 45° to the wing plane. We instrumented this missile in three different areas: the gimbal which is up forward in the nose cone with a tri-axial accelerometer, the mid-section with the tri-axial accelerometer, and right behind the wings with a hub accelerometer. We then took this missile and measured the environment on the F-4 aircraft, we covered the flight envelope from approximately Mach 0.8 to 2.0 and the Q envelope from approximately 600-1800 PSF ($2.9 \times 10^4 - 8.7 \times 10^4$ Pa). (Figure 37). We then took this data from the flight test, reduced it into rms levels and also PSD form, brought the flight test missile back into the laboratory, and did a series of experiments using random vibration on a shaker, acoustic excitation, and combined acoustic and vibration excitation to see what was the most accurate technique to simulate the measured captive flight levels. On the right side are the measured spatial distributions which are the rms levels for each of the orthogonal axes from captive flight (Figure 38). The same information is presented for the laboratory tests. We quantified this information, talking about the top one first, into rms error; the laboratory simulation on the longitudinal or axial vibration, showed an rms error of approximately 7 db. The next two setups were a transverse shaker with a connecting rod and a collar with the missile supported by Bungee cord. This technique performed almost as well as the bottom technique, which was acoustic excitation with an augmented shaker in a lower frequency spectrum below 100 Hz.

We also did another comparison using the spectral information from the captive flight test (Figure 39). The solid line is actually the captive flight data, the next line, the dash and the dot, is the vibration test, the third line is the acoustic test. We realize they are all very close so we once again quantise the information by the partitioning out of all the PSDs into fifty 40 Hz increments then compare it to the simulation of the flight test information to get an rms error, once again for each one of these techniques. The vibration technique showed about 5.7 db error versus 4.6 db error for the total spectrum for acoustic testing. The next phase of the program was to use the simulation and evaluate the exaggeration factor for random testing (Figure 40). This is a good technique if you are used to using accelerated testing to reduce costs by reducing test time. We started with the center relationship presented by Allen Curtis in SVM 8 (12). Knowing that the PSD level is proportional to g^2 , we came up with the second relationship which is between acceleration at a g level and the MTBF. Knowing this relationship, we proceeded to modify the vibroacoustic facility adding an RF chamber and test sets so that we could accurately measure the time of missile failure in the laboratory (Figure 41). We also set up a functional simulation which was a method to test the missile in a dormant environment, that is, we set up one in a separate area away from the vibration or the acoustic testing to measure the failure rate of the missile at 0 g (Figure 42). We proceeded to test the missile at 0 g level, 1 g, 2 g, 3 g, and 4 g. This is the information we obtained in

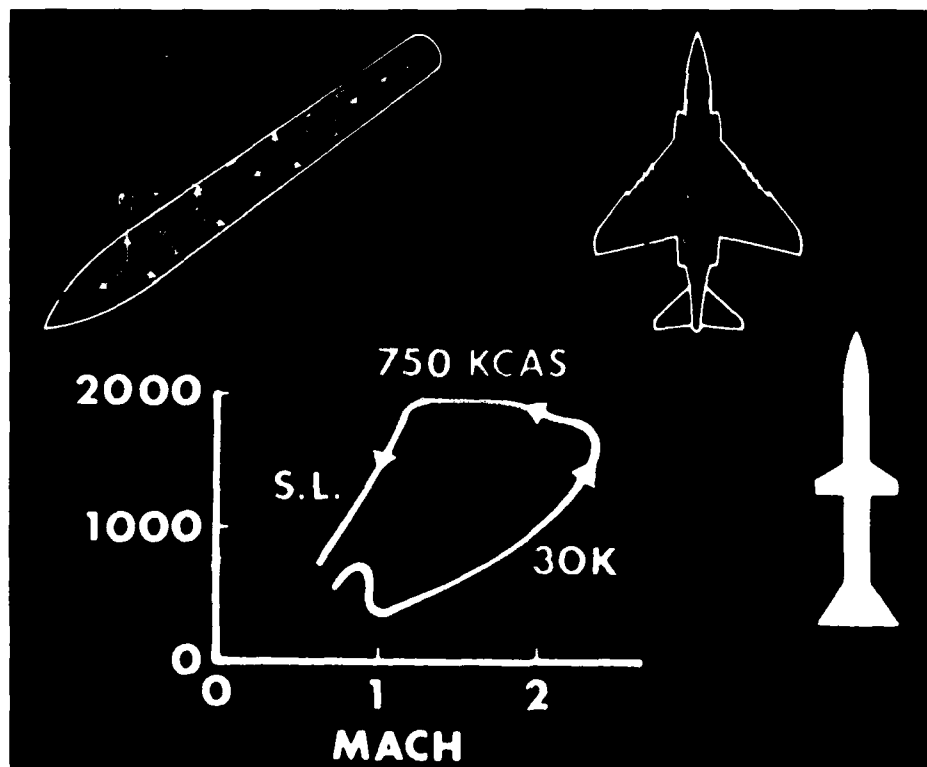


Figure 37 - "Q" Envelope versus Mach Number or Sparrow Missile.

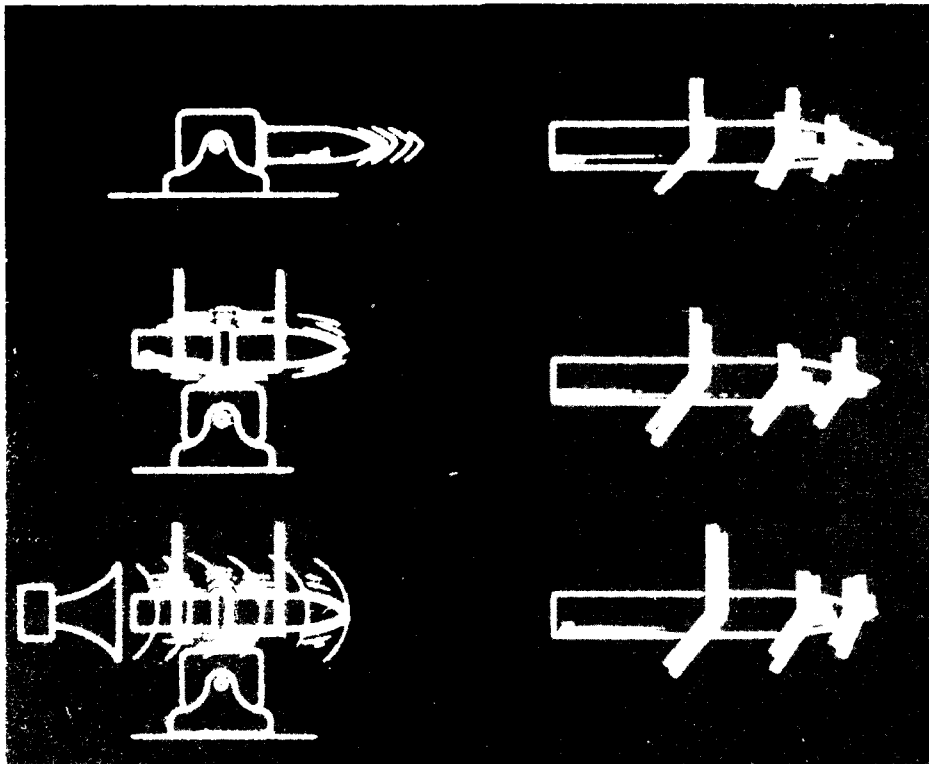


Figure 38 — Spatial Distribution of Vibration on Sparrow Missile.

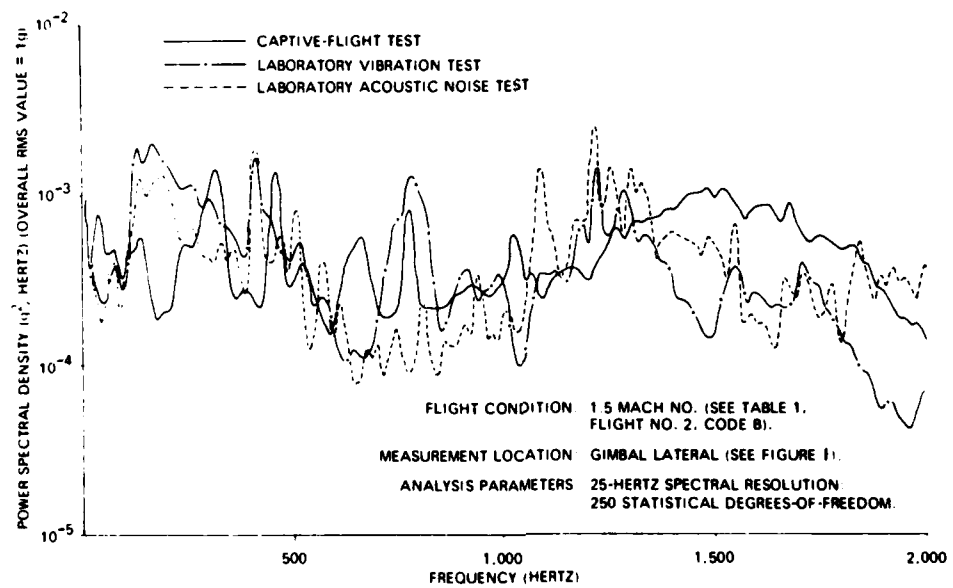


Figure 39 — Comparison of Captive Flight Test Data with Laboratory Vibration Test and Laboratory Acoustic Noise Test Simulations.

$$\frac{MTTF_2}{MTTF_1} = \left(\frac{W_1}{W_2} \right)^{\frac{b}{n}} = \left(\frac{g_1}{g_2} \right)^{2 \frac{b}{n}}$$

SINCE; $W \approx g^2$

Figure 40 - Exaggeration Factor for Random Testing

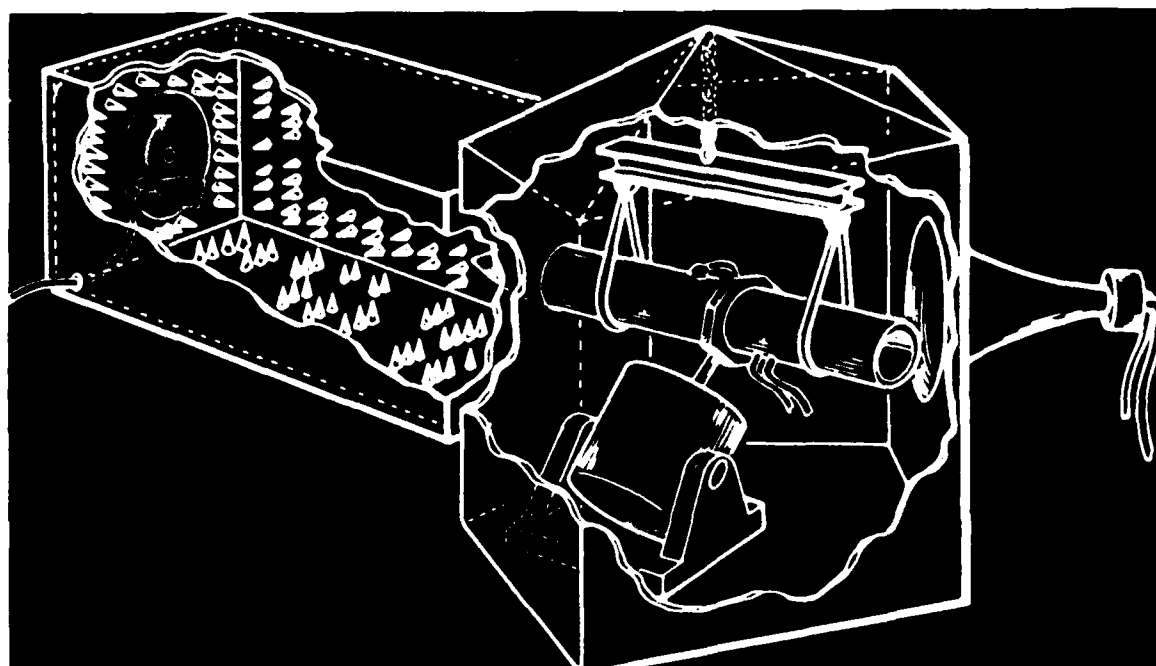
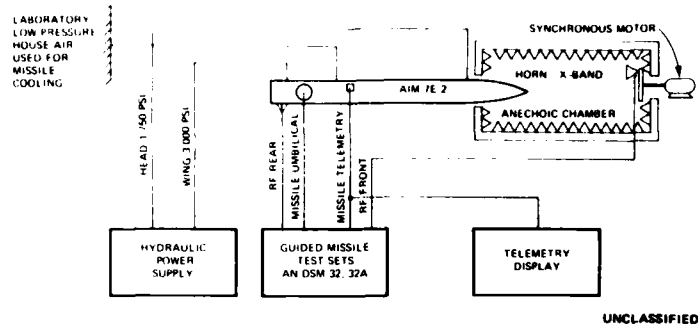


Figure 41 - Combined Environment Test Facility for Sparrow Missile.



UNCLASSIFIED

Figure 42 - Missile Functional Simulation

groupings. Table 2 shows that at 0 g we ended up with MTBF at 322 hours, 1 g, 91 hours, 2 g, 64 hours, 3 g, 10 hours, and at 4 g, about 4 hours. We plotted this data and we used the least squares fit to obtain a function describing the relationship between acceleration and the MTBF (Figure 43). You can remove the exponent, reapply it to the original equation and we end up with an acceleration factor of 4.2 on MTBF testing for the Sparrow Missile (Figure 44).

There is one more area to consider and that is types of failures due to accelerated testing. Basically we started out with five different groupings of data from 0-4 g vibration test levels. If you look at Table 3, you will notice that what we expected was that mostly the 0 g level entirely, we had mechanical wear out. As you progressed across the chart, we went from capacitive to solid-state elements to a predominant distribution of vacuum tube failures. It is a little disconcerting because we then looked at the fleet distribution of failures which is shown in Figure 45, and when you overlay that on the distribution of failures from our testing, you realize that it is not a good distribution below 1 g or above 3 g. So we settled that on accelerated

TABLE 2
Times-To-Failures for Different Vibration Levels

Times-To-Failure in Hours at Various Test Levels						
0 g	1 g	2 g		3 g	4 g	
86.0	2.0	0.5	44.5	0.5		
122.0	13.0	5.5	50.0	0.5	0.5	1.5
341.5	45.0	14.0	77.0	15.0	0.5	2.5
394.5	165.5	20.2	89.0	27.5	1.0	4.5
669.5	233.5	21.0	106.5		1.0	5.0
		38.5	135.5		1.0	5.5
		40.0	135.5*		1.0	7.0*
					1.5	10.0
					1.5	26.0
average = 322.70	average = 91.80	average = 64.74		average = 10.88	average = 4.375	
AOV F Value = 13.05; 1% Critical F Value = 3.83						

*Testing terminated without failure.

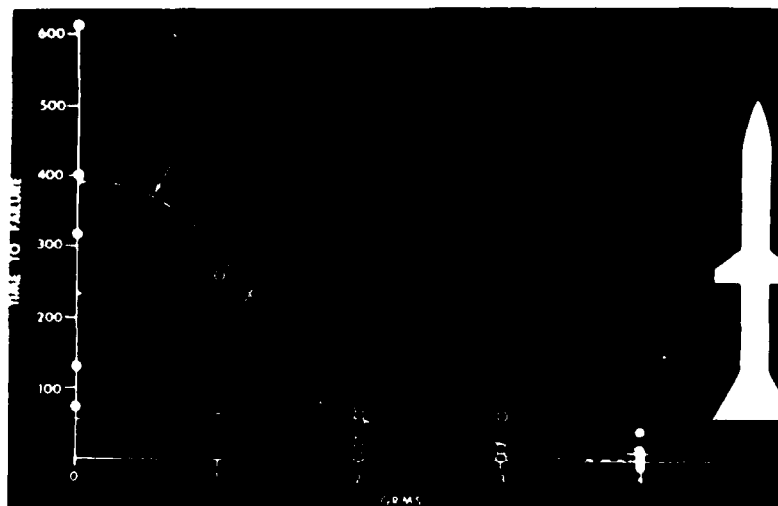


Figure 43 - Time to Failure versus Acceleration

$$\frac{MTTF_2}{MTTF_1} = \left(\frac{g_1}{g_2} \right)^{4.2}$$

Figure 44 — Accelerated Testing Relationship for Sparrow Missile.

testing for the Sparrow Missile we should probably limit our acceleration levels from 1-3 g rms if we want to duplicate the failure types that were predominant in fleet. We came to the conclusion that vibroacoustic excitation provides the best simulation of captive flight vibration levels in terms of spectral and spatial distribution and vibration levels strongly influence both the mean time to failure and the types of failure. We also came up with more questions and these are some of the ones that we have not answered yet. What do you do about frequencies above 2500 Hz? Should the temperature effects be included? What about free flight vibration?

Howard Schafer (Naval Weapons Center): One thing we learned when China Lake was started, try to determine some of the problems facing the tester and the criteria type, which was brought out in a meeting at the Naval Ordnance Laboratory, White Oak, MD, where my division head brought together all nine Director of Navy Laboratory laboratories environmentalists. We could not understand what was happening on the first day of the conference, there was no communication. It boiled down to the fact that we as environmentalists do an extremely good job of talking to ourselves, however, we do not really have a good idea of where we fit in the overall procurement cycle, where our funds really come from, when we should jump into the procurement cycle and the like so Crill Maples cut that meeting somewhat short and went into what a procurement cycle really is. I brought a very simplified procurement cycle, this is Figure 1 from MIL-STD-1670

(Figure 46) which is what we think is the missing link between MIL-STD-210, or science, and MIL-STD-810 which is testing, to put all of our documentation on somewhat the same footing.

Any program has initiation, we have to put out proposals and we have to get them back; the vendor or contractor, whether it is government or industry, has to tell the procurer what he will do and how. Somehow we get down to a validation phase and then full-scale development. We usually get in at full-scale development or at the back end of the validation phase; somebody will bring a basketfull of something to our laboratory and say "test it." We will usually ask how should we test it, and they say you are the tester, you tell us how, what is the best way to test. That is about three years too late! If we, as environmental types, get in at the program initiation, we can then tell the project manager what has to be done and what it will cost; now we have a chance to get funds for those new vibration systems that we have discussed obliquely today, where if we wait until full-scale development, we do not have a chance of getting any new instrumentation unless we dislocate either time on the program or the money scale on the program. In essence, if you keep this type of thing in mind, figure out where you fit into it, you will do yourself and the program quite a favor.

The next thing I found that we had to do was to define what reliability means both in the overall context of the program and also in our working context. It is pretty hard

TABLE 3
Effect of Vibration Test Level and Component Type on Sparrow Missile Failures

Vibration Test Level (g _{rms})*	Time To Failure in Hours by Component Type					Test Terminated Without Failure (Hours)
	Mechanical Wearout	Electro-Mechanical	Passive Elements	Solid State Elements	Vacuum Tubes	
0	86.0	122.0				
	341.5					
	394.5					
	669.5					
1			45.0	2.0	233.5	
				13.0		
				165.5		
2		44.5	14.0	0.5	5.5	193.5
		135.5	40.0	20.2		
			50.0	21.0		
			135.5	77.0		
3		0.5	0.5	15.0	27.5	
		4.5	10.0			
4		5.0			0.5	7.0
					0.5	
					1.0	
					1.0	
					1.0	
					1.5	
					1.5	
					1.5	
					2.5	
					5.5	
				26.5		

*Average of Vertical and Lateral Measurements on Hub Assembly

for you and I to determine what it means in the overall context, so I got a little help from the Defense Management Journal. Col. Swett passed this out as a sample at the April 1976 meeting of the Institute of Environmental Sciences and I want to read a small excerpt from Robert N. Parker, Principal Deputy Director for Defense Research and Engineering (13). "The basic concept is to combine performance, reliability, and environmental testing insofar as practical in the same test chamber and to program in the chamber to simulate the real field environment rather than the artificial profiles defined by the general specification." That is what top management has to say. Those are real good motherhood statements and all of us probably kind of agree with them but how do you put them to work? We go down one more layer of management and, quoting from Mr. Willoughby's article in the same Journal (14): "A crucial factor in testing is the environment, only if the factory test conditions duplicate or exceed the field environment will the testing be truly effective in insuring that specified performance or reliability requirements will be met after deployment." There are three major factors which play strong roles in insuring the adequacy of testing: (1) An accurate mission environmental profile and that has

to be done in the request for proposal area, if we do not do it there, we are years too late. (2) An integrated test plan which sets up logical progressive sequence of testing at increasing levels of assembly and environmental complexity in accordance with the mission profile. That would be done somewhere in that validation phase and possibly in full-scale development. (3) Operational test and evaluation by the government to give the product its first exposure to the real mission environment. Once we have gotten there, it is too late for the designer. It is the old adage, if we don't do the first two first, we never have enough time or money to do it right, we always have money to redesign. Now we get down to the middle management's look. The Naval Air Systems Command was jumped very hard when they found that you could take some of our good aircraft on an aircraft carrier on a non-combat type cruise, come back and you would have to off-load about 2/3 of the aircraft out of the squadron by crane. With this being the forcing function, they decided to take a look at some of the "buzz words" in middle management that will lead us to getting reliability or thinking through what is really our philosophy of testing and reliability together? This is called the "Navair New Look." What is the working tier

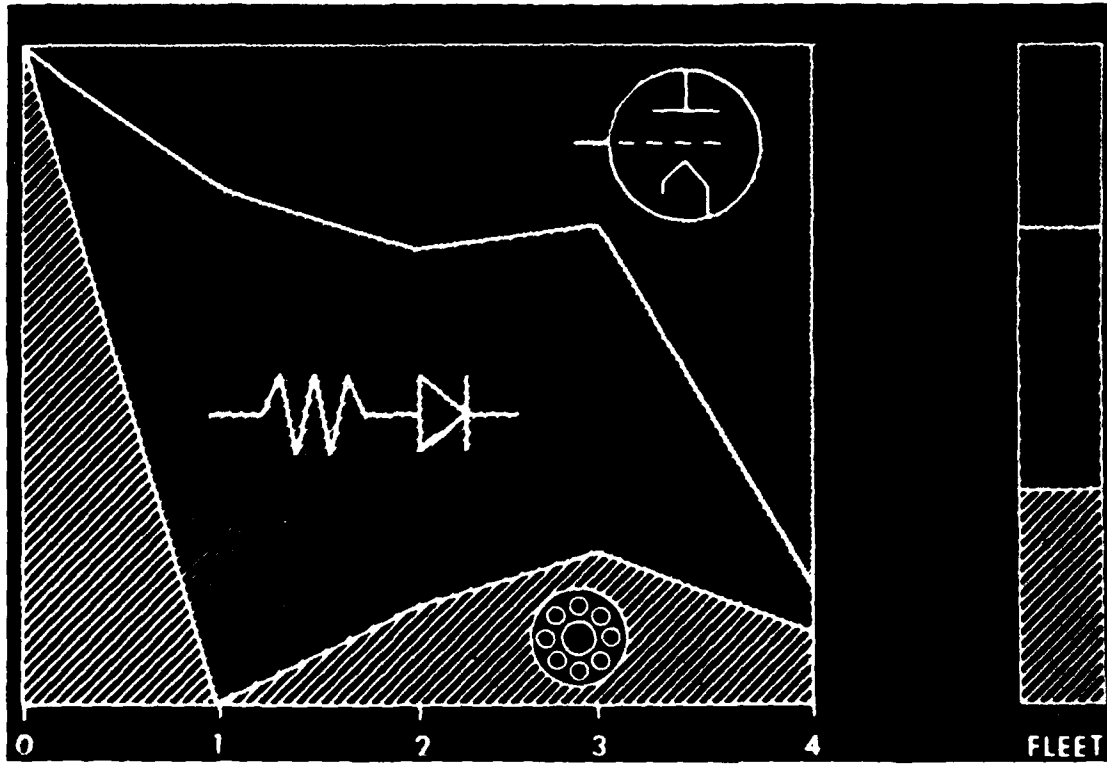


Figure 45 - Fleet Distribution of Failures

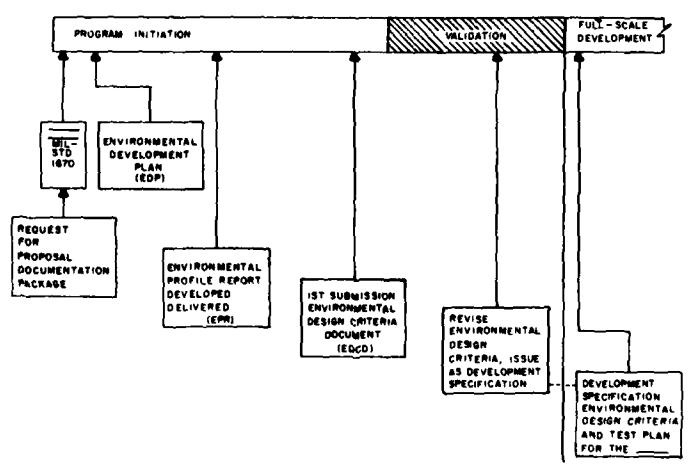


Figure 46 - Documentation Development Sequence

philosophy? In other words how do we get a handle on this so we can know why we are doing something instead of doing something by rote?

The rest of the presentation breaks down to some questions that I would like to ask you, and it is up to you to give the answers; I need the answer. Do we communicate with project personnel and administration or do we just talk to ourselves? How many of you really made an effort to learn what the language or the work patterns of the administrator, the project engineer, and those other than testers and environmental types really mean? How can we interpret our parochial language into language that these people will understand so that we are really communicating? Have we learned where and how to fit into the procurement cycle or do we sit back and when the rice drops into our "rice bowl," we eat. When our "rice bowl" is empty, we are out on the streets and it is too late to go back and ask where we fit into the procurement cycle. Some place we have to take time out while our "rice bowl" is still full and ask where do we fit in the procurement cycle. How can we really do something for the administrator and project personnel? Have we really defined our philosophy of the environment? Have we ever stopped to think of the type of tests we do for qualification, for engineering development, and for reliability demonstration? You can name them as well as I. What are we really expecting to get out of those tests? Are we testing something because somebody has dropped some rice in our "rice bowl" or are we testing something to make that a better unit for that sailor in the field or that airman? Know why each test is done and what useful information will be gained. We take MIL-STD-810 or MIL-E-5272 and we rotely take procedures such and such and do something with it. When I wrote the environmental criteria for the second stage Saturn in our engineering development laboratories at North American Aviation, I had people ask me "you want me to pass this or fail this" in the dynamics area? In other words, if you are a good boy and you do not get on my nerves, I will screen it and it will go. If you need punishment, I can fail anything you bring to the laboratory. How many times has this been our attitude? Do we really know how our actions will save the project and the company both time and money? Why did they hire me in the first place? If I am a project engineer, what does the environmentalist really have to offer me in a way of assuring that a piece of equipment is going to do what the Department of Defense is buying it for? The next thing I have to ask myself is am I spending too much time on arguing amongst my peers? How can I better use methods 514, 519, 501, in MIL-STD-810, or whatever document we are talking about? Should I have so many db per octave roll off or something else like this? Is the test we are using even applicable, even something that has anything to do with the particular piece of equipment that we are testing? It comes down to a question Crill Maples asks, "how many times have we gone out and measured something with the micrometer and come back to the laboratory or wherever and laid it out with a yardstick, and then when it is all said and done we cut it off with a broad axe?"

Mr. Hancock (Vought Systems Division): We opened with a general overview; we got into some of the detail, not

exactly agreeing with each other. I think we have seen three or four different, if not conflicting, approaches and findings here and we closed out with Howard's restatement of some of the initial problems that we are all trying to attack and the ones that are going to be facing us over the next several years. There will be many changes. I do not quite frankly see the total revision of MIL-STD-785 concepts within the foreseeable specifications future. A number of contracts are in existence now and are essentially picking up the concepts that are extant in MIL-STD-781C as mostly constrained by money. I think this is going to be an active working area for at least another five years. It will be in a constant state of flux.

Mr. Silver (Westinghouse): In our meeting on Monday afternoon, we talked about data banking of environmental criteria. In our business we feel that we are getting inadequate definition of our environments to respond to our proposals and also to do the continuing work, I consider this to be the largest stumbling block to making progress in the area. We cannot test to reliability, to realism, if we do not know what realism is. I have addressed this question to a number of people and I have wondered how might be the best way to handle it. I would like to propose that we start some sort of a funded study task through the Joint Logistics Chiefs or however we could start this. But the process is available and I think that the means are at our disposal to do this task; it would be a tremendous task with legal and technical difficulties throughout. But I do not think we will make very much progress in improved reliability without doing realistic testing and without realistic definitions.

Mr. Schafer: That is very intuitive. About 1959-1960 when I started trying to get something in the thermal area, I found that something was wrong. As you have very well indicated with your questions, something is wrong! The only thing I have been able to put my finger on over the last decade is that if we want to talk about reliability, structures, warheads, or aircraft, there is a desk some place in the Army, Navy or Air Force that we can go to that has that as their function. You cannot find the word "environment" any place in the DOD structure. Therefore, the first thing that we as a group, the IES as a society, and I would hope with the backing of some of the other parent societies, should do is to bring this to the attention of the Army, Navy and the Air Force that we must have an "Environmental Desk." We have pushed for this sort of thing inside the Department of the Navy for some time, but it is a situation of prophet having no honor in his own country to some extent. One of the things being thought about by Col. Swett and some in the Navy is can we somehow bring to the realization of the reliability desks that the environment is but a subset of reliability and have them open this up for discussion where 6.2 or 6.3 funds could be provided for such things? But the first thing we have to do is have some point of contact somewhere. In regard to data banking, we find that it is pretty difficult to do because data banks by definition are turned over to statisticians and librarians in general. We find that the statisticians and librarians again do not converse in environmental terms nor in engineering terms. They have difficulties finding engineers that will give their time to interpret for them in their language what categories should

be put down. Sandia's data bank is one of the best and it is open for general usage. To put together another data bank, I have seen both industry and governmental agencies fall flat on their face because of the people that are hired to run the data bank. Secondly, what is the thrust of the information that is necessary. The Fleet Missile System Analysis and Evaluation Group (FMSAEG) has a tremendous data bank in the Navy at Seal Beach, but the information comes from the people in the field who do not understand the format, the content, or the context of what the engineer wants. The engineer does not understand why the field man does not understand that and there is a complete lack of communication. If we push for data banks, we have to get our philosophical house in order and once we have defined what the problem is in our own terms be able to articulate it; then I think we should be able to push forward.

Mr. Kidd (Bell Helicopter): I would like to add to that. You quoted Willoughby as saying that the test ought to duplicate or exceed the environment. I guess it is this environment thing again, when he uses those words that way; I wonder if they have any meaning at all? I have a little device in a "black box." It is on one of 400 of the same type aircraft. It will go through life and go out the other end of the system in 20 years. Are we really going to press this issue of realism? If we are, then we will have to describe this thing accurately, look at the 35 dimensions of this space, tell ourselves how we will sample it, how we will condense the information, how it relates to this little point inside that "black box" on one of 400 ships. It is a lot of effort. Or we can take the other tack and we can get together and say that realism is hopeless, we will go for standardism. We will agree at this convention that we will do it this way and then we will tell everyone don't argue with us, do it this way. I think that will be cost effective because you won't spend endless hours in debate and discussion. It will be cheap and easy because everyone can learn to "do it by the book." We have to clear up whether we do one or the other.

Mr. Popolo (Grumman Aerospace): I do not think you really meant what you said. I think realism is definitely the name of the game. I think standardization is baloney. I think we have been living under standardization for 25 years. I think at Grumman we have been building equipment not for standardization as the old "MIL-specs" have recommended, but we have realized that our equipment is so sophisticated that if it is flown in an F-14 for example, it probably will never fly in a KC-135, an A-7, or an F-4 because it is designed specifically for the F-14 just as the ECM equipment is designed specifically for the A-6 and an EA-6A. That permits us to design a piece of equipment to a specific environment not a standardization. We zone our aircraft and we design the unit to fit in a particular area in the airplane. The only way we can relocate it is by possibly considering that if we put it in a compartment whose environment is more severe than the environment that the original equipment was designed for is by entertaining some sort of attenuation method, whether it be damping or isolation. If you really look at equipment packaged in aircraft, it does not have that much latitude. Our engines take up 50% of the airplane, therefore all of our equipment bays are in the forward area, which we know is a less benign

area. It has been very helpful that we have been able to design equipment to just meet a specific requirement even though someone says I am from the government, I am buying a piece of equipment, and I want to be able to use that 20 years from now in some new iteration of the aircraft. That won't happen. There will be so many changes in the state of the art that equipment, other than an aircraft communications system, which would be standardized from aircraft to aircraft, or a seat, which is always in the same spot, it is not in the tail end of the airplane it is in the cockpit. I think if we go that way, we can sell the realism. But if we are going to fall back to standardization, we will just lose everything we are trying to gain.

Mr. Heber (Heber Engineering): I have to support Dave Kidd in some of his statements. When we run tests, we cannot use the word "realism." The very fact that we go into the laboratory means that we are avoiding realism; we cannot run a test that lasts for the duration of the life of the average "black box," so we have to come up with exaggeration factors and these are by nature unrealistic. In addition, most of our dynamic tests are run on fixtures which have effectively infinite impedance and this is not realistic. Even with these constraints, what is their purpose in order to get repeatability from one test lab to another? If you go to more sophisticated tests, so-called realistic tests which include combined environments, it is a very seductive idea; but even in a simple test, such as a single axis vibration test, you have to rely on things that you cannot specify, such as the fixture designer, the fellow who maintains the equipment, and the fellow who instruments the test article. It is difficult enough to get good reliable repeatable tests under these conditions of single axis testing alone. When you go to multiple axis testing, or combined environments, you have to realize the real fact that when you do this, you will reduce your possibility of repeating the tests from one test set up to another, much less from one laboratory to another. If you feel that combined or "more realistic" environments are going to give you best results, you have to take into account the fact that the control of the test is bound to deteriorate and you will have to come up with a balance or a trade off between those two facts.

Mr. Hancock (Vought Systems Division): If we take a look at the individual test phases that I tried to list earlier, each of those test phases has an optimum; we have to optimize on something, cost, the total environment including the possible use of the "white hat," long-term storage, and a few other things. If we look from the piece part all the way up to the systems level, that has a value. One of the confusing points is that these tests have not been clearly stated in terms of purpose. We must state the purpose of the test before we start it; we should do the best job we can to exercise the potential failure modes at all steps along the way. It is difficult for me to buy off on standardization as opposed to the tailored environments that have been discussed recently by this environmental study group for the Joint Logistics Commanders.

Mr. Schafer (Naval Weapons Center): In amplification of Bob's remark, one of the concepts we have been playing with for a while is this word "standardization." It is a big word in Washington, it has been big for quite a while, you

will find standardization groups in all areas of life although it again turns out to be "spec" writers who are not technical people. Is there some way we can take that word and twist it to our own meaning and our own use? If we can standardize on something technological, then maybe we can get an understanding of testing in the context that Bob just brought up, that is what we are using tests for. One of the ways that we have decided to use standardization in the missile industry is we will standardize on the response of the overall missile at the skin line and from there we will diverge our criteria as we go to the piece part or to a component inside of the missile. Under the old standardization context, we used method X X X from some standard and put the piece part, the component, and the whole missile through that same g^2/Hz type format, and shake them all the same. However, under this concept of all of them being standard, you find out that you are giving much too much energy to one area and maybe not enough to the

other. If we say that we will standardize in our environmental criteria determination work on hypothetically the skin of the aircraft or the skin of the missile, and from there with whatever fudge factors are necessary come up with the power spectral densities on into the piece part, now we have true engineering standardization and this can be sold. We sold it on the concept, but it was not carried through on major missile programs or other smaller programs.

Mr. Kidd (Bell Helicopter): I agree a whole lot with MIL-STD-1670 it is standardization but there is flexibility in it because you have a loop all during that development time. Then, the gentleman who presented the B-1 data I do not think what you are doing is realistic but it is a useful formalism that seems to get us somewhere and I will buy it.

REFERENCES

1. Gluitz, K. J. and Condouris, M. A., Vibration and Acoustic Environment of UH-1C Helicopter configured with and using the M-5 and M-21 Armaments, Technical Report ECOM-4019, U.S. Army Electronics Command, Fort Monmouth, NJ (1972)
2. McIntosh, V. C. and Bolds, P. G., Vibration and Acoustic Environment of OH-6A Helicopter configured with and using the XM-27 Armament System, Technical Report AFFDL-TR-81, Air Force Flight Dynamics Laboratory, Wright-Patterson Air Force Base, Ohio (1975)
3. McIntosh, V. C. and Bolds, P. G., Vibration and Acoustic Environment of AH-1G Helicopter, Technical Report AFFDL-TR-75-17, Air Force Flight Dynamics Laboratory, Wright-Patterson Air Force Base, Ohio (1975)
4. Burt, J. W. and Condouris, M. A., Cockpit Vibration Environment with and without gunfire for AH-1G, OH-6, and UH-1C Helicopters, Technical Report ECOM-4126, U.S. Army Electronics Command, Fort Monmouth, NJ (1973)
5. Hirschberger, G. and Dantowitz, A., Evaluation of Environmental Profiles for Reliability Demonstration, Technical Report RADC TR-75-242, Rome Air Development Center, Air Force Systems Command, Griffiss Air Force Base, NY (1975)
6. Johnson, R. B. Jr.; Clay, L. E.; and Meyer, R. E., Operational Use of UH-1H Helicopters in Southeast Asia, USAAMRDL Technical Report 73-15 U.S. Army Air Mobility Research and Development Laboratory, Fort Eustis, VA (1971)
7. Earls, D. L. and Prather, D. K., Combined Environmental Reliability Test (CERT) for Avionics Subsystem, Journal of Environmental Sciences 19 (2), pp 11-14 March/April 1976
8. Baker, R. L. and Kern, G. A., Operational Influences on Reliability, Journal of the Environmental Sciences 19 (5) (September/October 1976)
9. Dantowitz, A.; Hirschberger, G.; and Pravidlo, D., Analysis of Aeronautical Equipment Environmental Failures, Technical Report AFFDL-TR-71-32 (May 1971)
10. Coren, G.; Cotliar, W. and Conroe, D., Predicting Environmental Interaction, Presented at 6th Annual Reliability and Maintainability Conference, Sponsored by SAE/AIAA/ASME, Cocoa Beach, FL (July 17-19, 1967)
11. Hirschberger, G., Step Stress Program, Grumman Aerospace Corporation, Report ECP 425 (1971)
12. Curtis, A. J.; Tinling, N. G.; and Abstein, H. T. Jr., Selection and Performance of Vibration Tests, Shock and Vibration Monograph 8, Shock and Vibration Information Center, Naval Research Laboratory, Washington, D.C. (1971)
13. Parker, R. N., R & D Emphasis on Reliability, Defense Management Journal 12 (2), p 19 (April 1976)
14. Willoughby, W. J., Reliability by Design, Not by Chance, Defense Management Journal 12 (2), pp 12-18 (April 1976)

SHOCK ANALYSIS

SCALING OF STRONG SHOCK HUGONIOTS

W. E. Baker
Southwest Research Institute
San Antonio, Texas

Within the last two decades, many careful dynamic experiments have been conducted to measure the properties of solid and liquid materials subjected to strong shock waves. Under the extreme pressures of these tests, all materials behave like compressible fluids. The properties of these strongly-shocked materials are usually termed "shock Hugoniots," and are given in the alternate forms of shock velocity as a function of particle velocity, shock pressure as a function of particle velocity, or shock pressure as a function of density increase. Despite a wealth of data in the literature, there seems to have been no systematic attempt to apply similitude methods and determine whether some simple scaling law is valid. This paper presents a scaling law for strong shock Hugoniot properties of a wide variety of solids and liquids. The law is developed and compared with literature data. Agreement is shown to be excellent for a two-parameter fit of dimensionless groups, and good for a one-parameter fit. The author suggests that the law can be used to predict Hugoniots for untested materials, or to aid in planning tests of new materials.

INTRODUCTION

Within the last two decades, many careful dynamic experiments have been conducted to measure the properties of solid and liquid materials subjected to strong shock waves. Most of these data were obtained with contact explosions using plane-wave-initiated precision charges in contact with the target material [1] or with contact explosions used to drive flyer plates into target plates [1,2,3], or by impacts of flyer plates accelerated by light gas guns [4]. The tests require plane and normal or nearly normal impacts or shock incidence, accurate control of high to very high impact velocity, and sophisticated instrumentation to obtain simultaneous measurements of shock velocity and particle velocity induced by the impacts or explosive shocks. Under the extreme pressure of these tests, all materials behave like compressible fluids. Experimentally obtained shock properties are now available in the literature for very many initially solid materials [1-6], and some liquids [1,7].

The properties of these strongly-shocked materials are usually termed "Hugoniots" or "shock Hugoniots," because the equations of continuity of mass, momentum, and energy through discontinuities in fluids on which they rely so heavily were first formulated by

Hugoniot [8]. Two of these equations, specialized to strong shocks, are

$$P = \rho_0 U u \quad (1)$$

$$\frac{\rho_0}{\rho} = 1 - \frac{u}{U} \quad (2)$$

where P is pressure, ρ is density, ρ_0 is initial density of unshocked material, and U is shock velocity. (In the context used here, strong shocks imply pressure several orders of magnitude above yield stresses for solids. In general, these pressures are of the order of megabars, i.e., 10^{11} Pa.) The experimental data consist of measured combinations of U and u up to as high a velocity as can be obtained experimentally. Figure 1 shows a typical plot of raw data for Fansteel 77 (90% W, 6% Ni, 4% Cu) from Ref. 4. Using data points similar to those of Fig. 1, the Hugoniot can be presented, with the aid of Eqs. (1) and (2), as plots of shock pressure vs particle velocity (Fig. 2) or shock pressure vs compression (Fig. 3). Figure 1 also indicates an empirical fit to Hugoniot data which is widely used. It is

$$U = C + Su \quad (3)$$

Combined with Eq. (1), this gives

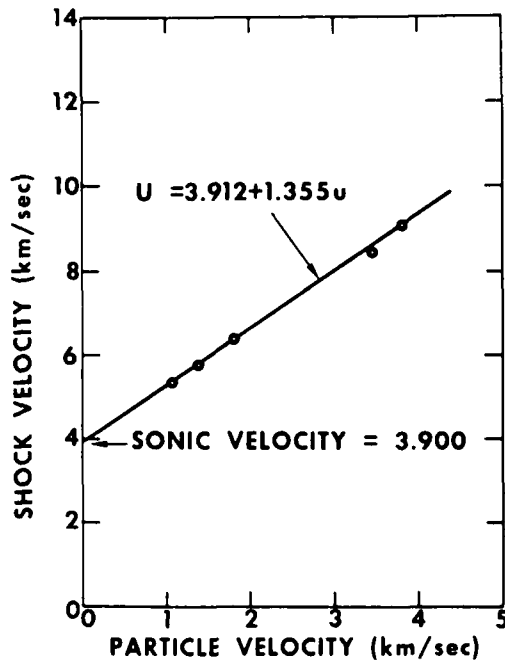


Fig. 1 - Shock velocity vs particle velocity for Fansteel 77 (Ref. 4)

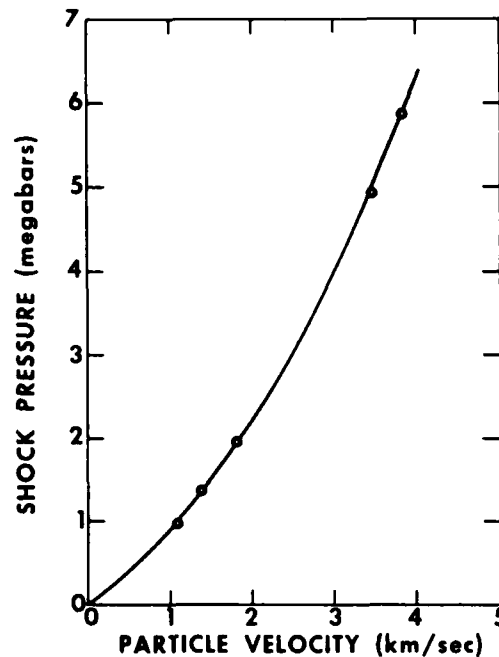


Fig. 2 - Shock pressure vs particle velocity for Fansteel 77 (Ref. 4)

$$P = \rho_0 (Cu + Su^2) \quad (4)$$

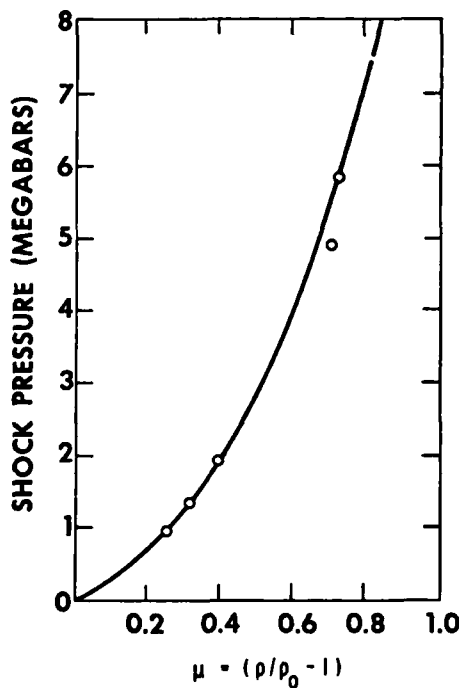


Fig. 3 - Shock pressure vs compression for Fansteel 77 (Ref. 4)

McQueen and Marsh [2] apparently first showed that a linear relationship fitted the U, u data very well for many materials. These authors also noted that the parameter C was essentially sound velocity c_0 in the virgin material. McQueen, et al. [5], have also shown transitions at certain pressures which cause significant deviations from a single linear relationship over the entire range of data. In particular, iron, titanium, zirconium, and hafnium show such transitions. Porous and foamed materials often show [5] nonlinear or bilinear relationships between U and u . But, the vast majority of solids and liquids tested have Hugoniot which fit Eq. (3) very well, often to within a fraction of a percent, over the entire range of measurements.

The Hugoniot data given in the cited references are too voluminous to reproduce in detail here, but selected parameters from experimental fits for materials with a wide variety of physical characteristics are given in Table 1. Although not noted in the literature, this author was struck by the small range of the parameter S , and also by the apparent lack of attempts to apply scaling laws for prediction of Hugoniot from a mass of data which exhibits marked similarities independent of material properties. Scaling has been applied to the problem of hypervelocity impacts of small projectiles into extended targets [9,10,11], but

TABLE 1
Some Representative Hugoniot Data*

Material	Density ρ_0 , g/cm ³	Parameter C, mm/ μ sec	Parameter S (dimensionless)
1. Uranium	18.90	2.60	1.45
2. Palladium	12.00	4.05	1.50
3. Brass	8.41	3.75	1.45
4. Iron	7.84	3.80	1.62
5. Marble	2.70	4.00	1.32
6. Granite	2.63	2.10	1.63
7. Limestone	2.60	3.50	1.43
8. Plexiglass	1.18	2.78	1.30
9. Water	1.00	1.70	1.70
10. Silver	10.49	3.24	1.59
11. Gold	19.24	3.07	1.56
12. Cadmium	8.64	2.44	1.67
13. Cobalt	8.82	4.75	1.33
14. Chromium	7.10	5.22	1.47
15. Copper	8.90	3.96	1.50
16. Molybdenum	10.20	5.16	1.24
17. Nickel	8.86	4.65	1.45
18. Lead	11.34	2.03	1.52
19. Tin	7.28	2.64	1.48
20. Thorium	11.68	2.13	1.28
21. Titanium	4.51	4.78	1.09
22. 5083 Al	2.66	5.30	1.37
23. PMMA	1.18	2.70	1.54
24. Mineral Oil	0.87	2.19	1.52
25. AZ31B Mg	1.78	4.65	1.20
26. Fansteel 77	16.89	3.91	1.36

* Sources of data: Materials 1-9, Ref. 1; materials 10-21, Ref. 2; materials 22 & 23, Ref. 6; materials 24 & 25, Ref. 7; and material 26, Ref. 4.

not to Hugoniot of materials. This paper presents a scaling law for material Hugoniot, and compares its predictions with literature data.

MODEL ANALYSIS

Model analysis (or similitude analysis) yields dimensionless groups of physical parameters which must be kept invariant for similitude or scaling of a physical system or problem. The techniques are well described in texts on similarity methods [9], so the results of the analysis for shock Hugoniot will be given here with no intermediate details.

The parameters assumed to be important in the current problem are listed in Table 2, together with their four basic dimensions in an F, L, T, θ (force, length, time, temperature) system. These 14 parameters are grouped into five basic physical properties of the virgin material, the constitutive properties of shocked material, three basic physical quantities, and four response parameters. An additional basic property, the bulk modulus B of the virgin material, could have been included,

but it is superfluous because it is uniquely defined by ρ_0 and c_0 through the equation*

$$B = \rho_0 c_0^2 \quad (5)$$

The 14 parameters, less four basic dimensions, yield 10 dimensionless groups, or pi terms. This model law can be expressed in the following functional form:

$$\left. \begin{array}{l} U/c_0 \\ \theta C_p/c_0^2 \\ \rho/\rho_0 \\ P/\rho_0 c_0^2 \end{array} \right\} = f_1 \left(\frac{P}{\sigma_y}, \frac{u}{c_0}, \frac{n}{c_0^2}, \frac{C}{c_0}, s, \frac{Ut}{L} \right) \quad (6)$$

This manner of presenting a model law is somewhat optional, but it implies that the four scaled properties on the left hand side of the

* Note that B has dimensions F/L².

TABLE 2
Physical Parameters Assumed to Describe Shock Hugoniot

Parameter	Symbol	Dimensions	Description
Initial density	ρ_0	FT^2/L^4	Basic properties of virgin material
Initial sound speed	c_0	L/T	
Characteristic stress (for solid)	σ_y	F/L^2	
Specific heat	C_p	$L^2/\theta T^2$	
Heat of fusion	n	L^2/T^2	
Constants in Eq. (3)	$\left\{ \begin{array}{l} C \\ S \end{array} \right\}$	$\left\{ \begin{array}{l} L/T \\ --- \end{array} \right\}$	Constitutive constants for shocked material
Characteristic length	L	L	Basic physical quantities
Time	t	T	
Temperature	θ	θ	
Shock velocity	U	L/T	Response parameters
Particle velocity	u	L/T	
Density	ρ	FT^2/L^4	
Pressure	P	F/L^2	

equation are dependent variables which are each different functions f_i of the six dimensionless parameters on the right. The law does not tell us what these functions are; the functions must be determined by analysis or experiment or both. Without further restriction or consideration, this model law is too general to be of much use. Fortunately, the Hugoniot equations, the empirical equation (3), and other physical evidence can be used to drastically reduce the size of this function space.

Let us consider first the scaled physical properties P/σ_y and n/c_0^2 . Because we are studying strong shocks, the pressure behind the shock must be much greater than any characteristic stress in the initially solid material, i.e.,

$$\frac{P}{\sigma_y} \gg 1 \quad (7)$$

As long as this inequality is maintained, we need not keep P/σ_y identical in two scaled experiments (in titanium, for example, we must be above the phase transition). Heats of fusion n have been shown (see Ref. 12 and Chapter 8 of Ref. 9) to be very nearly proportional to the square of the sound velocity in most solid materials. Therefore,

$$\frac{n}{c_0^2} \approx \text{constant} \quad (8)$$

and this group is nearly invariant regardless of material.

Consider now the terms involving the properties C/c_0 and S of shocked material. McQueen and Marsh [2], as well as all later investigators [1,4,5,6,7], demonstrate that the empirical constant C is usually very near to sound velocity c_0 in the virgin material. Therefore, we can with very little error assume that

$$\frac{C}{c_0} = 1 \quad (9)$$

From Table 1 we can see that the range for S is remarkably small, considering the very wide variety of materials tested. We can retain S as a dimensionless parameter, or can, with some loss of accuracy, use a mean value and assume that it is invariant. The mean value for materials in Table 1 is

$$\bar{S} = 1.435 \quad (10)$$

Equations (1) through (4) allow us to obtain explicit relations between some of the remaining scaled groups. Dividing Eq. (4) by $\rho_0 c_0^2$ and using Eq. (9), we find that

$$\frac{P}{\rho_0 c_0^2} = \frac{P}{B} = \frac{u}{c_0} + S \left(\frac{u}{c_0} \right)^2 \quad (11)$$

Similarly, Eq. (3) gives

$$\frac{U}{c_0} = 1 + S \frac{u}{c_0} \quad (12)$$

Another useful expression for presenting Hugoniot data in another form can be obtained by algebraic manipulation of Eqs. (1) through (4) and (9). It is

$$\frac{P}{\rho_0 c_0^2} = \frac{\mu(\mu + 1)}{[\mu(S-1) - 1]^2} \quad (13)$$

where

$$\mu = \left(\frac{\rho}{\rho_0} - 1 \right) \quad (14)$$

An alternate form for Eq. (13) is obtained if the parameter

$$\eta = 1 - \frac{\rho_0}{\rho} \quad (15)$$

is used, instead of μ . This form is

$$\frac{P}{\rho_0 c_0^2} = \frac{\eta}{(1-S\eta)^2} \quad (13a)$$

The quantity η is analogous to the Lagrangian strain

$$\eta = \frac{V - V_0}{V_0} = \frac{\Delta V}{V_0} \quad (16)$$

used in solid mechanics, where V_0 and V are initial and final specific volumes, respectively.

Using the results of the above discussion and supplementing by Eqs. (11), (12), and (13), we can reduce the model law in Eq. (6) to

$$\left. \begin{array}{l} U/c_0 \\ \theta C_p/c_0^2 \end{array} \right\} = f \left(S, \frac{u}{c_0}, \frac{Ut}{L} \right) \quad (6a)$$

This law only applies under the restrictions of Eqs. (7), (8), and (9). This states that scaled shock velocity (which uniquely determines scaled pressure and scaled density) and scaled temperature are functions of S , scaled particle velocity, and scaled time. For shock front properties in Hugoniot, time is immaterial, so we can further reduce Eq. (6a) to

$$\left. \begin{array}{l} U/c_0 = f_1 \left(S, \frac{u}{c_0} \right) \\ \theta C_p/c_0^2 = f_2 \left(S, \frac{u}{c_0} \right) \end{array} \right\} \quad (6b)$$

We are primarily interested in the first of these two relationships because it can be directly compared to experimental results. But, we already know its functional form. It is Eq. (12). Acceptable alternate forms are Eqs. (11) and (13).

COMPARISON WITH DATA

The usual methods of presenting Hugoniot data are in plots of U versus u as in Fig. 1, P versus u as in Fig. 2, or P versus μ as in Fig. 3. As noted earlier, once the variation of U with u is determined, the other two methods of presenting Hugoniot follow directly from the two Hugoniot equations (1) and (2). The reduced scaling law in either of these three forms is given by Eqs. (11), (12), and (13). Any of these forms relates one dimensionless physical property in the shocked material to another dimensionless physical property, and the dimensionless constitutive property S . To compare with experimental data, we can present either two-parameter plots such as U/c_0 versus S and u/c_0 , or can collapse the prediction curves into a single one by using an average value \bar{S} for S . Three such curves of scaled parameters for $S = 1.0, 1.435,$ and 1.70 are given in Figs. 4 through 6, corresponding to Eqs. (12), (11), and (13), respectively. Also plotted on these curves are data points from the literature for a wide range of materials* (the literature is far too voluminous to include all data on these plots).

From the three figures, one can see that scaled pressure plotted versus scaled particle velocity is least affected by variation in S , while scaled pressure plotted versus scaled compression is most sensitive. In all plots, the experimental data cluster about the curves for $S = 1.435$, and lie within the limits chosen for S . The points deviating furthest from the mean curve are for titanium. Those furthest to the right, representing largest values of scaled parameters, are for mineral oil. This is not surprising because both ρ_0 and c_0 are small for this material.

CONCLUSIONS

It is apparent from the comparison of scaled Hugoniot data for widely different condensed materials with the scaled curves representing Eqs. (11) through (13) that it is indeed possible to scale strong shock Hugoniot. To account for differences between materials in the dimensionless constitutive property S , two-parameter plots similar to Figs. 4 through 6 are probably desirable. On these plots, lines

*Usual units in the literature are pressures in megabars, velocities in mm/ μ sec, and densities in g/cm³. To render $P/\rho_0 c_0^2$ in these units dimensionless, multiply by 100.

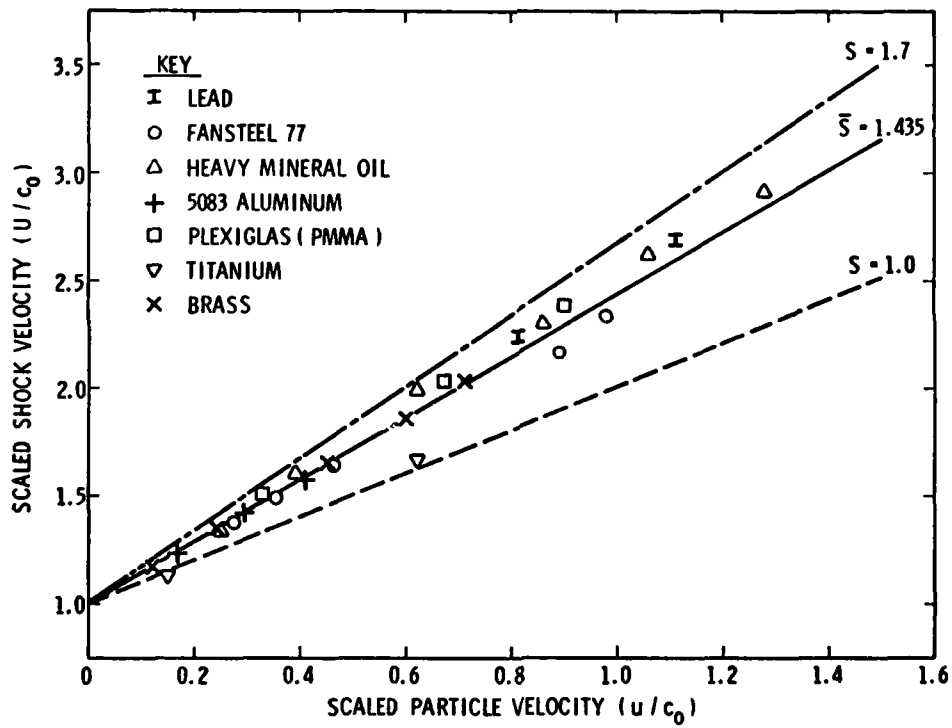


Fig. 4 - Scaled Hugoniot parameters (U/c_0) versus (u/c_0)

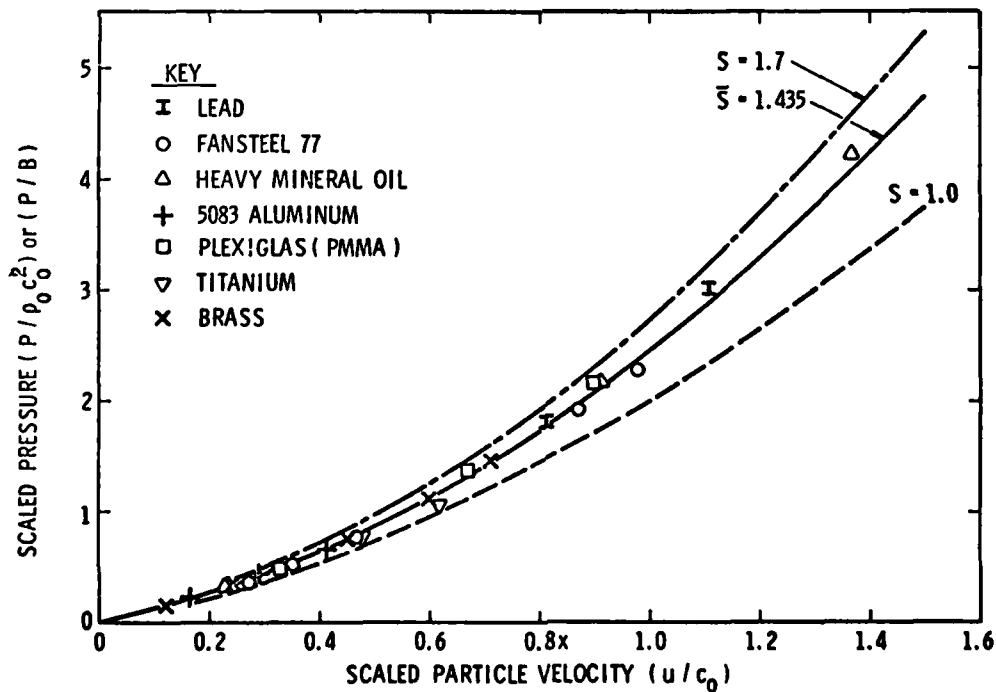


Fig. 5 - Scaled Hugoniot parameters ($P/\rho_0 c_0^2$) versus (u/c_0)

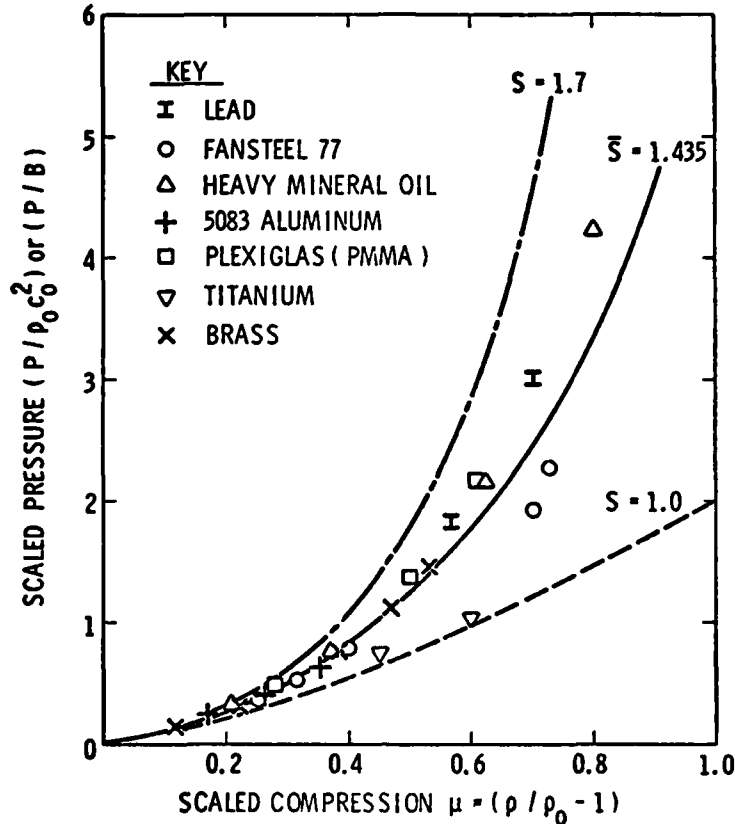


Fig. 6 - Scaled Hugoniot parameters ($P/\rho_0 c_0^2$) versus μ

of constant S for small increments in S would allow easy interpolation of properties for any desired material.

The materials with data points shown in Figs. 4 through 6 were deliberately chosen to give as wide a range in properties as possible. They were not indicative of the vast majority of the data in the literature. Most materials have values for S which are much closer to the mean $\bar{S} = 1.435$ than the limits shown in the figures. Had these data been plotted, dense clusters of points would have surrounded the solid curves for $\bar{S} = 1.435$. Therefore, predictions of shock Hugoniot are accurate enough for many engineering purposes can be made using the solid curves or the equivalent scaled equations. One must know only the initial density ρ_0 and sound velocity c_0 , or alternatively the density and bulk modulus B , to make these predictions. Hopefully, this simple procedure will allow estimation of strong shock properties of solids and liquids which have not been measured without using the expensive and time consuming methods and special facilities required for such measurements. If such tests are needed to obtain these properties more

accurately, predictions from the scaled curves should help in planning the experiments.

The reduced form of the scaling law is, of course, restricted to strong shocks whose strength substantially exceeds yield stresses or transition pressures for solids. Stated in another way, this limits their applicability to materials or ranges of pressure for which the linear relationship between U and u (Eq. (3)) is valid, and for which Eqs. (6), (7), and (8) hold. McQueen, et al. [5], present Hugoniot for a number of foamed, composite, or anisotropic materials which do not follow the linear relationship. So, one should apply the law developed here with care, or realize that it may err, when predicting Hugoniot for such materials. A more general scaling law could be easily derived based on a more complex constitutive equation for shocked materials. It would involve more dimensionless parameters and would therefore require a more complex presentation than the two-parameter one used here. The author's opinion is that improvements in prediction accuracy would be marginal for a more complex law, and he therefore does not recommend it.

Huang [13] has pointed out that the shock velocity U and the empirical parameters C and S can be used to calculate another important parameter often used in strong shock studies, the Grüneisen parameter γ . The conversion equation he gives is

$$\gamma = \frac{U(2U-C)[C + (S-1)U] - \frac{CU}{3}(U-C) - SC^3}{U(U-C)(U+C)} \quad (17)$$

In later work, Huang [14] notes that an average value of γ can be used to characterize strong-shock compressibility for 18 cubic-lattice metals. In some ways, this is analagous to our recommendation of use of an average value $\bar{\gamma}$ to predict shock Hugoniot for unknown materials. One could extend Huang's work and obtain a mean value $\bar{\gamma}$ by fitting Eq. (17) to Hugoniot data for enough different materials. Again, the option to use γ directly or generate a mean $\bar{\gamma}$ is left to the reader.

NOMENCLATURE

P	pressure in shocked material
U	shock velocity
u	particle velocity
ρ	density in shocked material
ρ_0	initial density
C	parameters in empirical fits to Hugoniot data
S	
\bar{S}	average value of S
c_0	sound velocity
μ	scaled compression
σ_y	yield stress
C_p	specific heat
n	heat of fusion
L	a characteristic length
t	time
θ	temperature
η	Lagrangian strain
V	volume
V_0	initial volume
γ	Grüneisen parameter

REFERENCES

1. C. H. Johansson and P. A. Persson, *Detonics of High Explosives*, p. 291. Academic Press, New York, 1970.
2. R. G. McQueen and S. P. Marsh, "Equations of State for Nineteen Metallic Elements from Shock Wave Measurements to Two Megabars," *J. Appl. Physics*, Vol. 31, No. 7, p. 1253, July 1960.
3. A. C. Holt, A. S. Kusubov, D. A. Young, and W. H. Gust, "Thermo-Mechanical Response of Porous Carbon," UCRL-51330, Mar. 1973.
4. A. H. Jones, W. M. Isbell, and C. J. Maiden, "Measurement of Very-High-Pressure Properties of Materials Using a Light-Gas Gun," General Motors TR 65-84, Nov. 1965.
5. R. G. McQueen, S. P. Marsh, J. W. Taylor, J. M. Fritz, and W. J. Carter, *High-Velocity Impact Phenomena*, Chapt. VII, R. Kinslow (ed.). Academic Press, New York, 1970.
6. G. Hauver and A. Melani, "The Hugoniot of 5083 Aluminum," BRL Memo. Rept. No. 2345, Dec. 1973.
7. P. Netherwood and D. Tauber, "The Shock Hugoniot of Mineral Oil," BRL Memo. Rept. No. 2214, Aug. 1972.
8. H. Hugoniot, "Mémoire sur la propagation du mouvement dans les corps et spécialement dans les gaz parfaits," *J. de l'école polytech. Paris*, Vol. 57, 1887, and Vol. 58, 1889.
9. W. E. Baker, P. S. Westine, and F. T. Dodge, *Similarity Methods in Engineering Dynamics*, Chapt. 8. Hayden Book Co., Inc., Rochelle Park, N. J., 1973.
10. W. J. Rae, *High-Velocity Impact Phenomena*, Chapt. VI, R. Kinslow (ed.). Academic Press, New York, 1970.
11. J. K. Dienes and J. M. Walsh, *High-Velocity Impact Phenomena*, Chapt. III, R. Kinslow (ed.). Academic Press, New York, 1970.
12. E. P. Palmer, R. W. Grow, D. K. Johnson, and G. H. Turner, "Cratering: Experiment and Theory," *Hypervelocity Impact Fourth Symposium*, APGC-TR-60-39(I), Sept. 1960.
13. Y. K. Huang, "Direct Method of Calculating the Grüneisen Parameter γ Based on Shock-wave Measurements of Metals," *J. Chemical Physics*, Vol. 51, No. 6, pp. 2573-2577, Sept. 15, 1969.
14. Y. K. Huang, "Analytical Approach to the Shock Compressibility of 18 Cubic-lattice Metals," *J. Chemical Physics*, Vol. 53, No. 2, pp. 571-575, July 15, 1970.

DISCUSSION

Mr. Avrami (Picatinny Arsenal): What do you mean by a strong shock?

Mr. Baker: A shock that is so strong that the pressure is in the megabar region; it is well above "yields" which would be in the low kilobar region.

Mr. Avrami: What is the error bar on your data points?

Mr. Baker: The test is very repeatable for any one material. I did show some data points that were used to draw those curves. If they are repeated, you will find that the error bars are really quite small as long as you stay in the strong shock region. When you get near yield strength or near phase transition in a metal like iron or titanium, then, you don't get these fits and you'll find larger error bars. Some of the compendia reported in the paper have a great deal of detailed data that give these error bars as well as the means.

Mr. Avrami: What happened when you tried to apply your model to the kilobar range?

Mr. Baker: The approximations for strong shocks will go wrong. The general scaling law that I showed earlier would be applicable in the kilobar range because I included parameters that would be in that range. However, it doesn't help you very much because there are many parameters in there that would have to be held constant in order for you to get a comparison.

Dr. Morrow (Consultant): You have been concerned with shock waves in materials. How can your results be applied to damage?

Mr. Baker: The kind of damage that you are concerned with would be wave transmission damage. If one has mechanical impacts, and remember I mentioned earlier that the way one gets these data is to slam one plate of material into another at a high velocity, so there are wave transmission effects. The compression wave reflects from the free surface as a tension wave and it causes spall or high velocity failure of the material. Those are the kind of damage effects we are talking about, not the ordinary low velocity mechanical impacts where we obtain the gross structural response. We are concerned about wave transmission or shock transmission effects in this regime.

SHOCK SPECTRA AND RESPONSES BY POCKET CALCULATOR

Charles T. Morrow
Consultant
Dallas, Texas

Several programs for computation of Fourier and shock spectra (with phase as well as magnitude versus frequency included for one frequency at a time) and single and two-degree-of-freedom responses are given for a card-programmable pocket calculator, along with user instructions and supporting derivations. Not suited for routine data reduction, these programs nevertheless provide the engineer with a convenient means for computation of spectra for selected frequencies and exploration of corresponding test item responses. As yet, they have not been included in the HP-65 User Library. These programs, and similar ones developed in the future, may be helpful in deciding on the best methods of specification of shock severity for environmental test and in providing better design criteria for shock resistance in multiple-degree-of-freedom mechanical systems.

INTRODUCTION

In 1962, by expressing the response of a simple resonator as a Duhamel integral and comparing the form of the undamped resonator response with that of the Fourier transform or spectrum, O'Hara showed that the undamped residual shock spectrum is equal to the magnitude of the Fourier transform of the shock velocity time history.¹ Morrow provided a shortened derivation in 1963,² expressing the relationship in terms of the Fourier transform of the acceleration time history. O'Hara showed, further, that shock responses could be computed by digital integration and that the same methods

could yield a Fourier analysis.

The present treatment is an extension of O'Hara's methods and an adaptation to stepwise insertion of data into a programmable pocket calculator. Such a calculator is too slow for routine data reduction or processing, but it can permit the engineer to sit at his desk and make occasional explorations of spectra and corresponding shock responses. Furthermore, it can be used, for example with a repeated subroutine, to obtain multiple as well as single-degree-of-freedom responses.

Shock spectra are indirect des-

criptions of shock excitations and at the same time indicators of possible responses of a test item. In the former role, they would benefit from a consensus on a limited number of standard usages, together with an appreciation for whatever test item response reproducibility uncertainties may be associated with these. In the latter role, in contrast, they need more variety of approach. They have suffered from too much engineering preoccupation with variations of simple resonator response and too little recognition that the most bothersome failure modes often result from coupling of mechanical resonators.

The calculator programs to be discussed here were developed to provide a means of exploring potential test item responses without the constraint of having to go to the laboratory and depend on laboratory type instrumentation. The availability of such programs for such a purpose may indirectly contribute to the solution of the data reduction and specification problems. In addition, they may provide better design criteria for multiple-degree-of-freedom systems. Shock spectra are not used explicitly in design as much as one might expect. It is more common to design to simpler "equivalent" static loads.

AVAILABLE PROGRAMS

The programs developed so far are the following:

1. Undamped residual and Fourier spectra (Appendix 1). One card. Inputs are step and/or ramp approximations until further excitation is negligible. At the conclusion, spectral phase angle as well as magnitude become available for display.
2. Damped initial, residual and maximum single-resonator responses (Appendix 2). One card. Step inputs only until further response is negligible, or alternately until the residual time interval begins. If the second option is taken, residual response coefficients can be extracted from the memory registers. This second program is useful primarily in providing a more extended sample of possible test item single-resonator responses.
3. Damped double resonator (Appendix 3). Two cards. The model for the computation is shown in Figure 1. The second mass is assumed to be so small that dynamic loading of the first resonator by the second is negligible. The first card is for parameter insertion. The second card, with step acceleration-time inputs only, is for first and second resonator acceleration responses until negligible or until the residual period begins. After shock excitation termination, residual responses may be computed by inputting zero accelerations for successive time increments. However, it is more economical of time and effort when only the second resonator residual response or residual envelope is desired, to proceed to the fourth program cards without otherwise disturbing the data in the memory registers. In any event, if there is any likelihood that the fourth program results may be of interest later, it is well to record the numbers in registers 3 to 8 so that they can be restored later at will. The primary usefulness of this third program is in further extension of the

sampling of possible responses of test items. By permitting computation of responses of even a limited range of coupled resonators, it permits a major advance in realism of physical and mathematical modeling.

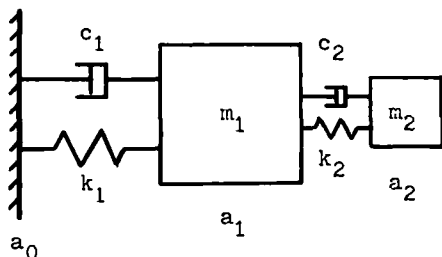


Figure 1
Damped Double Resonator

4. Second resonator residual -- envelope and instantaneous. Five cards. It is important that the value of t_1 used in connection with the first card be identical to that used in the third program, but with the fifth card, the time increment can be changed without introducing error. The first three cards are for reprocessing the parameters and coefficients in the registers. The program will not work if the two resonators are exactly equal in both frequency and damping, so this case must be computed independently when desired (program not given in this paper) or approached as a limit. The fourth card is for computing the envelope of the second resonator residual response, using relatively large time increments -- small only by comparison with the period of the envelope. The fifth card is for the second resonator residual instan-

taneous response if desired. Usable before or after the fourth card, it permits, without deterioration of accuracy, larger time increments than were necessary with the third program. When the resonators are highly damped, it may be of interest to compute instantaneous second resonator residual response while it is rapidly dying away. But, except for the case of highest damping, the envelope, obtained with much less effort, is as adequate for judging the severity of residual shock response. The primary usefulness of this fourth program is again in extending the sampling of possible test item responses.

Figure 2 shows residual response envelopes computed by the third and fourth programs for a 100 g terminal step function (equivalent to a 100 g terminal peak sawtooth if the ramp is of sufficiently long duration compared to the resonance periods of interest, but simpler mathematically). For all cases, the resonance frequencies were $f_1=100$ Hz and $f_2=110$ Hz. The Q values were the same for both resonators, but set successively to 10, 20, 40, and 80. With only a 100 g step excitation of the first resonator, the second resonator peak residual responses were about 320 g, 515 g, 720 g, and 860 g respectively -- surely an incentive for a design change if any of the resonator parameter sets have a chance of being realistic for any coupled resonators in a test item.

Originally it was hoped that the square of the velocity of the second mass, relative to the first, could be integrated as the instantaneous response computations progressed, so as to yield a number proportional to the energy dissipated in

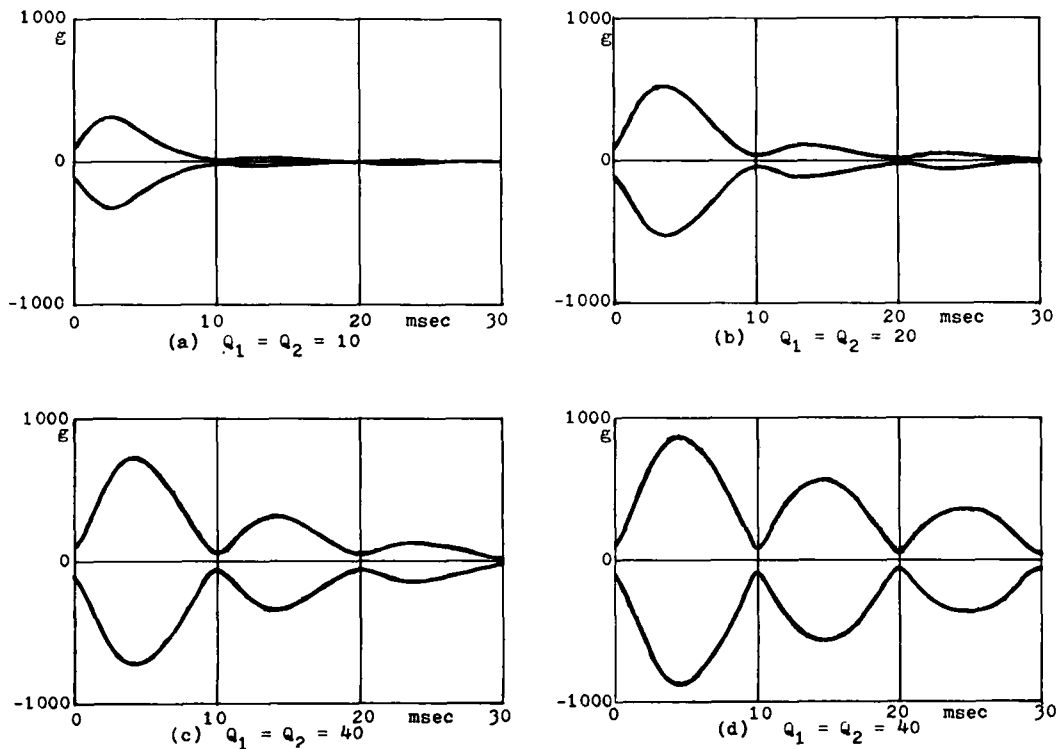


Figure 2
 Envelopes of Second Resonator Residual Responses
 to 100 g Terminal Step Function
 $f_1 = 100 \text{ Hz}$ $f_2 = 110 \text{ Hz}$

the second damped spring. This would have supplemented peak response to provide a more adequate combined indication of shock fatigue hazard, but it was clearly beyond the memory register and program step capabilities of the HP-65 calculator. Anyone who has computed and recorded the complete instantaneous acceleration responses, and has some interest and patience left, could carry out the integration with the aid of a simple supplementary program.

Anyone who has a Hewlett Packard HP-65 calculator and some blank magnetic cards can get started by keying in the programs given in the appendices, checking the program codes for accuracy

of keying, recording on magnetic cards, clipping a corner for erasure protection, and following the user instructions in the appendices. (The programs are not as yet available through the HP-65 User Library.) However, if he encounters any difficulty with very large or very small parameters or acceleration inputs, or for any other reason wishes to improvise on the programs, he should become familiar with the underlying theory.

APPROACH

Any pocket calculator now on the market has extremely limited time-history capability if all data must be stored prior to computation. It becomes necess-

ary to limit preliminary storage to resonant system parameters, plan for sequential inputting of excitation acceleration-time data, and have the calculator respond to each acceleration-time pair by updating a minimum number of coefficients, as well as by computing whatever response may be required for that instant.

Even so, the primary challenge of the present study was to compress the programs within the program step and memory capabilities of the HP-65. Parameter insertions, parameter processings, and coefficient reprocessings for a new type of computation could be allowed to use program segments on as many cards as necessary, but the computations for any set of acceleration-time inputs had to be completed within one card. Subroutines helped to compress such programs within the step capacity.

To overcome the memory register limitation, several procedures were tried as follows:

1. Storage of angles in register 9 between trigonometric computations.
2. Temporary storage and manipulation in the four-register (RPN) stack.
3. Storage of an integer and a fraction, provided they are of the same sign, in the same register, sometimes with multipliers or divisors to decrease truncation error.
4. Storage of numbers in the program after loading from a card, by editing the numbers in at locations marked by pre-assigned labels.

For the programs to be disclosed, the last procedure was the least effective.

It improves data storage only at the expense of extreme penalties in program capacity and is somewhat cumbersome for the HP-65 user.

For exploration of possible test item responses in relation to Fourier or undamped residual shock spectra, ordinarily only a few sets of resonance parameters and a few time histories will be of interest at one sitting. This makes the programs practical. Interpretation of the results is aided by the fact that the coefficient updating routines inherently preserve phase as well as magnitude information.

The foundations for the analysis were the superposition theorem and the known responses of a simple resonator to unit step and unit-slope ramp excitations. The strategy for investigation of coefficient updating was to infer from these responses a plausible mathematical form, with undetermined coefficients, for responses to accumulating successive step or ramp inputs, set $t=t_{k-1}$, where k is the current number of data inputs, superpose the incremental response for $t=t_k$, and derive the coefficient updating formulas.

FOURIER AND UNDAMPED RESIDUAL SPECTRA

The first program, for the computation of Fourier and undamped single-resonator residual spectra, with phase as well as magnitude available to the user, utilizes both step and ramp approximations to the excitation, with the slope corrected to zero after each step, for variable time increments, at the will of the user. This is beneficial for economy of data inputs, especially with simple test pulses. For example, a square wave can be attained by two successive steps of mag-

nitudes equal to the height of the square wave but opposite in sign. A terminal peak sawtooth can be attained by a ramp to the peak value and a negative step to zero. The generation of phase angle information makes either type of spectrum a complete spectral description of the shock, such that a unique excitation acceleration-time history can be reconstructed.

First, let us derive the coefficient updating formulas for step inputs, with k representing the current number of data inputs. The acceleration response of a simple undamped resonator of resonance frequency f_1 to a unit step at time $t=0$ is

$$a_1(t \geq 0) = 1 - \cos 2\pi f_1 t. \quad (1)$$

Therefore, the response to a step of magnitude $a_{0(k-1)}$ at $t=t_{k-1}$ is

$$\begin{aligned} a_1(t \geq t_{k-1}) &= \Delta a_{0(k-1)} [1 - \cos 2\pi f_1 (t - t_{k-1})] \\ &= \Delta a_{0(k-1)} \\ &- \Delta a_{0(k-1)} [\cos 2\pi f_1 t_{k-1} \cos 2\pi f_1 t \\ &+ \sin 2\pi f_1 t_{k-1} \sin 2\pi f_1 t]. \end{aligned} \quad (2)$$

This suggests that the cumulative response to successive acceleration steps through $t=t_{k-1}$ may be of form

$$\begin{aligned} a_1(t \geq t_{k-1}) &= C_{k-1} + D_{k-1} \cos 2\pi f_1 t \\ &+ E_{k-1} \sin 2\pi f_1 t. \end{aligned} \quad (3)$$

We now derive the updating formulas for C_k , D_k and E_k from the t_{k-1} coefficient values. After the next step at $t=t_k$, from Equations 2 and 3, by superposition,

$$a_1(t \geq t_k) = C_{k-1} +$$

$$\begin{aligned} &+ D_{k-1} \cos 2\pi f_1 t + E_{k-1} \sin 2\pi f_1 t \\ &+ \Delta a_{0k} - \Delta a_{0k} [\cos 2\pi f_1 t_k \cos 2\pi f_1 t \\ &+ \sin 2\pi f_1 t_k \sin 2\pi f_1 t] \\ &= C_k + D_k \cos 2\pi f_1 t + E_k \sin 2\pi f_1 t. \end{aligned} \quad (4)$$

This is possible if

$$C_k = C_{k-1} + \Delta a_{0k} = \sum_{k=0}^k \Delta a_{0k} = a_{0k}, \quad (5)$$

$$\begin{aligned} D_k &= D_{k-1} \\ &- (a_{0k} - a_{0(k-1)}) \cos 2\pi f_1 t_k, \end{aligned} \quad (6)$$

and

$$\begin{aligned} E_k &= E_{k-1} \\ &- (a_{0k} - a_{0(k-1)}) \sin 2\pi f_1 t_k, \end{aligned} \quad (7)$$

where $a_{0(k-1)}$ and a_{0k} are respectively the excitation accelerations at $t=t_{k-1}$ and $t=t_k$, with the actual shock acceleration approximated by successive steps.

Inspection of Equation (1) shows the form of Equation (3) is compatible with an initial step at $t=0$. Equation (2) shows that the form is compatible with an initial step at any other time. Equations (4) through (7) show that if the form of Equation (3), or, more simply, the final form of Equation (4), holds for any step input, it holds also for all subsequent step inputs.

After each data input, since only the residual response or spectrum is desired, it is sufficient for the calculator to perform the coefficient updating operations of Equations (6) and (7), without computing each response. The first coefficient, given by Equation (5),

will be zero at shock termination.

Fewer data inputs may be sufficient if the HP-65 user has the option approximating ramp as well as step inputs at any time. Let us now derive the coefficient updating formulas for successive ramps. The response to a unit-slope ramp starting at $t=0$ can be obtained, according to Laplace transform theory, as the time integral of the response to a unit step at $t=0$, as follows:

$$a_1(t \geq 0) = \int_0^t (1 - \cos 2\pi f_1 t) dt$$

$$= t - (1/2\pi f_1) \sin 2\pi f_1 t. \quad (8)$$

Therefore, the response to a ramp of slope γ_k initiated at $t=t_{k-1}$ is given by

$$a_1(t \geq t_{k-1}) = \gamma_k [t - t_{k-1} - (1/2\pi f_1) \sin 2\pi f_1 (t - t_{k-1})]$$

$$= \gamma_k [t - t_{k-1} - (1/2\pi f_1) \cos 2\pi f_1 t_{k-1} \sin 2\pi f_1 t + (1/2\pi f_1) \sin 2\pi f_1 t_{k-1} \cos 2\pi f_1 t] \quad (9)$$

By an argument similar to that used previously, it can be shown that the response after the k 'th data input is

$$a_1(t \geq t_{k-1}) = C_k + D_k t + E_k \cos 2\pi f_1 t + F_k \sin 2\pi f_1 t, \quad (10)$$

provided that the undetermined coefficients are related to those for $t \geq t_{k-1}$ by

$$C_k = C_{k-1} - (\gamma_k - \gamma_{k-1}) t_{k-1} = a_k, \quad (11)$$

$$D_k = \gamma_k, \quad (12)$$

$$E_k = E_{k-1} + (\gamma_k - \gamma_{k-1}) (\sin 2\pi f_1 t_{k-1}) / 2\pi f_1, \quad (13)$$

and

$$F_k = F_{k-1} - (\gamma_k - \gamma_{k-1}) (\cos 2\pi f_1 t_{k-1}) / 2\pi f_1, \quad (14)$$

where

$$\gamma_k = (a_{0k} - a_{0(k-1)}) / (t_k - t_{k-1}). \quad (15)$$

Pressing the appropriate user-definable key (labelled STEP) after keying in a_{0k} results in the coefficient updating operations corresponding to Equations (6) and (7). Pressing another user definable key (labelled RAMP) after keying in the number results in the coefficient updating operations corresponding to Equations (13) through (15). Both C_k and D_k are zero at shock termination.

A ramp can be used immediately after a step without requiring any further complications in the program. However, to simplify using a step after a ramp, pressing the STEP-labelled key after keying in a_{0k} results not only in operations corresponding to equations (6) and (7) but also in setting the subsequent excitation slope to zero and correcting the response coefficients for this by means of Equations (13) through (15). This results in some delay in completing the STEP computations, but the STEP key will be used only once or twice per shock computation if the RAMP key is available.

Accordingly, so long as only residual response coefficients (as opposed to response during the shock, as in some later programs) are desired, a square wave can be generated by two successive step functions of opposite sign. Similarly, a terminal peak sawtooth can be generated by a ramp followed by a negative step. A half sine wave can be approximated by a small number of successive ramps, clus-

tered mostly near the peak of the curve, where the slope changes most rapidly except for the slope discontinuities at beginning and end, and a step input of zero acceleration the instant the final ramp reaches zero, to set the subsequent slope to zero and terminate the pulse. The high frequency Fourier or residual spectra for these simple pulses, or even more complicated pulses, will not be so critically dependent on making a large number of data inputs if both step and ramp are used judiciously.

On completion of data inputs, by pressing the appropriate user-definable key, the calculator can be made to convert the residual coefficients to polar form

$$E_n + jF_n = A_n e^{j\phi_n} \quad (16)$$

and display the undamped residual shock spectrum magnitude A_n for the chosen frequency. Then, pressing keys g x y will make the calculator display the associated phase angle in degrees.^{3,4} Alternately, pressing a different user-definable key can make the calculator compute

$$\begin{aligned} (E_n + jF_n)/j2 f_1 &= (F_n - jE_n)/2 f_1 \\ &= r_n c^{j\theta_n} \end{aligned} \quad (17)$$

and display the Fourier magnitude r_n . Then, pressing keys g x y will make the calculator display the phase angle

$$\theta_n = \phi_n - 90 \text{ degrees.} \quad (18)$$

The two user-definable keys are labelled with abbreviations for residual and Fourier, respectively.

The phase angles ϕ_n and θ_n are rel-

ative to a reference time of $t=0$, the beginning of the shock excitation and the beginning of computation. If the shock were delayed a time t_0 relative to the start of computation, this would decrease ϕ_n and θ_n by $2 f_1 t_0$. Phase shifts relative to a value at some standard frequency, preferably in midrange, will be adequate for use in describing the inherent properties of a shock, if, for example, phase information should ever be incorporated into a specification. Time of initiation is unimportant to shock severity. Such relative phase shifts can readily be obtained by computing ϕ_n or θ_n for the standard frequency and subtracting it from all other phase angles.

DAMPED INITIAL, RESIDUAL AND MAXIMAX

For the remaining programs, the ramp approximation is omitted in order to save on register and program capacity requirements, and the step approximation is used without need for slope correction. When response computations are to be carried out during the shock, several data inputs per resonance period are necessary, so that the advantage of the ramp is somewhat decreased. Eventually, revision of the programs for more powerful card-programmable calculators should permit restoring the ramp approximation.

The second program, for the computation of damped initial, residual and maximax single-resonator responses, involves response computations as well as coefficient updating.

Max and min (negative max) acceleration responses are stored in two registers. At shock termination, when there is a definite ending, these represent posi-

tive and negative initial damped spectra. At response termination, after the inputting of a sufficient number of acceleration zeros, these stored values represent positive and negative maximax spectra, unless the two registers are manually set to zero at shock termination, in which case they yield damped residual spectra. Alternately, at shock termination, the calculator can be made to recall the stored coefficients, which then are residual coefficients, convert them to polar form, and multiply the magnitude by an exponential to yield a good estimate of the residual spectrum.

Inasmuch as the resonator is now damped, Equation (1) becomes

$$a_1(t \geq 0) = 1 - e^{-\alpha_1 t} \cos 2\pi f_1 t, \quad (19)$$

where

$$\alpha_1 = f_1 / Q_1 = c_1 / 2m_1 \quad (20)$$

is the decay constant due to damping c_1 with mass m_1 .

Equations (5) to (7) become respectively

$$C_k = a_{0k}, \quad (21)$$

$$D_k = D_{k-1}$$

$$- (a_{0k} - a_{0(k-1)}) e^{\alpha_1 t_k} \cos 2\pi f_1 t_k, \quad (22)$$

and

$$E_k = E_{k-1}$$

$$- (a_{0k} - a_{0(k-1)}) e^{\alpha_1 t_k} \sin 2\pi f_1 t_k. \quad (23)$$

These are the coefficient updating equations to permit computation of instantaneous response at each t_{k-1} or t_k by the relation

$$a_1(t \geq t_{k-1}) = C_{k-1} + D_{k-1} e^{-\alpha_1 t} \cos 2\pi f_1 t + E_{k-1} e^{-\alpha_1 t} \sin 2\pi f_1 t \quad (24)$$

or

$$a_1(t \geq t_k) = C_k + D_k e^{-\alpha_1 t} \cos 2\pi f_1 t + E_k e^{-\alpha_1 t} \sin 2\pi f_1 t. \quad (25)$$

Equation (24) was the one used in the program, after each t_k input but before the corresponding a_{0k} input. Equation (25) after both inputs would also have yielded the same responses.

TWO-DEGREE-OF-FREEDOM WITHOUT LOADING

The third program provides instantaneous first and second mass responses in a two-degree-of-freedom in which the first resonator is not dynamically loaded by the second, or, in other words, the second mass is negligible compared to the first. This represents a worst case in the natural progression from heavy to light in the sequence from component to subassembly to part -- favorable for static but unfavorable for some dynamic loads because of the amplifications that can take place.

Subroutines suggested by Equations (21) to (24) are adequate for this two-degree-of-freedom system if the first resonator computed response is taken to be the excitation input for the second resonator computation, and the frequency f_2 and decay constant α_2 are interchanged with f_1 and α_1 , respectively, in the appropriate register, before second resonator computation. This is less demanding on data storage capacity than computing second resonator response by single use of a complete formula per excitation data input, especially if first resonator response is also desired. One card is used with parameter insertions and the other with acceleration-time inputs and corresponding computations. There is double

number storage in some registers, with one number stored as an integer and the other stored as a fraction. To help keep the second card program within 100 steps, storing of maximum and minimum values is omitted.

The storage and program step requirements are further eased by restricting time increments to a constant $\Delta t = t_1$, recognizing that responses will be computed only at the ends of such increments, and referring each exponential decay back to $t = t_{k-1}$ rather than to $t = 0$. Instead of Equations (22) to (24),

$$D_k = D_{k-1} e^{-\alpha_1(t_k - t_{k-1})} - (a_{0k} - a_{0(k-1)}) \cos 2\pi f_1 t_k, \quad (26)$$

$$E_k = E_{k-1} e^{-\alpha_1(t_k - t_{k-1})} - (a_{0k} - a_{0(k-1)}) \sin 2\pi f_1 t_k, \quad (27)$$

and

$$a_1(t_k) = a_{0(k-1)} + E_{1(k-1)} e^{-\alpha_1(t_k - t_{k-1})} \cos 2\pi f_1 t_k + F_{1(k-1)} e^{-\alpha_1(t_k - t_{k-1})} \sin 2\pi f_1 t_k. \quad (28)$$

For second resonator updating and response, the equations are identical in form, with $a_2(t_k)$ instead of $a_1(t_k)$, $D_2(k-1)$ and $E_2(k-1)$ as coefficients, and $a_1(k-1)$ and a_{1k} as acceleration inputs. The exponentials $e^{-\alpha_1(t_k - t_{k-1})}$ and $e^{-\alpha_2(t_k - t_{k-1})}$ are constant factors, computed once and stored. Use of either in the response computation and coefficient updating program is by one complete operation, with only one recall from the register per usage.

Inasmuch as the computation pro-

ceeds by successive step approximations to the excitations of both resonators and uses first resonator response as second resonator excitation, a time increment that is not small enough compared to the smaller resonance period affects not only the number of response points computed but their accuracy as well, and especially for the second resonator. The errors in the second resonator response computations are most noticeable at the beginning. A tenth of the smaller period may yield satisfactorily accurate responses after the first such period, but an increment closer to a fiftieth may be necessary if the initial values must also be accurate. An irregular excitation function may require more data inputs than a regular one.

This third program can be made to yield residual responses by inputting successive zeros for acceleration. For example, one can obtain the first and second resonator residual responses to a 100 g terminal step function by storing the number 100 in registers 1 and 2 before loading the second card, and inputting zero accelerations after loading the second card.

SECOND RESONATOR RESIDUAL

However, if only the second resonator residual response or its envelope is of interest, the residual computation is better carried out by the fourth program, about to be discussed, after carrying the third program user operations through shock termination. The fourth program merely evaluates a predetermined mathematical formula, so that accuracy of individual computations is unaffected by time increment size.

For example, the computation of the

first curves of Figure 2 utilized the following operations and numerical inputs:

Load program 3, card 1. .0001 A. 100 B. 10 C. 110 D. 10 E. 100 STO 1 STO 2. Load program 3, card 2. 0 RTN R/S. R/S. 0 R/S. .001 RTN R/S. Load program 4, card 1. .0001 A. etc.

The fourth program uses the results of the third, on the assumption that computations with the latter have been carried out only to the end of shock excitation or until further shock inputs may be considered negligible, or else that the contents of registers 2 to 6 for $t=t_n$ (instant of shock termination) were recorded and have been restored. This fourth program converts the contents to a more suitable form for zero excitation and permits computation of either the residual envelope or the instantaneous residual response, or both.

From Equation (28), the excitation of the second resonator by the first for any $t > t_n$ may be expressed as

$$\begin{aligned} & e^{-\alpha_1(t-t_n)} [E_{1n} \cos \omega_1 t + F_{1n} \sin \omega_1 t] \\ & = e^{-\alpha_1(t-t_n)} [E_{1n} \cos \omega_1 (t_n + t - t_n) \\ & + F_{1n} \sin \omega_1 (t_n + t - t_n)] \\ & = e^{-\alpha_1(t-t_n)} [E_{1r} \cos \omega_1 (t - t_n) \\ & + F_{1r} \sin \omega_1 (t - t_n)], \end{aligned} \quad (29)$$

where

$$E_{1r} = E_{1n} \cos \omega_1 t_1 + F_{1n} \sin \omega_1 t_1 \quad (30)$$

and

$$F_{1r} = F_{1n} \cos \omega_1 t_1 - E_{1n} \sin \omega_1 t_1 \quad (31)$$

Similarly, any persisting response of the second resonator to prior excita-

tion plus any continuing a_{1n} from the last data input is given by

$$\begin{aligned} & e^{-\alpha_2(t-t_n)} [E_{2n} \cos \omega_2 t + F_{2n} \sin \omega_2 t] + a_{1n} \\ & = e^{-\alpha_2(t-t_n)} [E_{2r}^* \cos \omega_2 (t - t_n) \\ & + F_{2r} \sin \omega_2 (t - t_n)] + a_{1n}, \end{aligned} \quad (32)$$

where

$$E_{2r}^* = E_{2n} \cos \omega_2 t_1 + F_{2n} \sin \omega_2 t_1 \quad (33)$$

and

$$F_{2r} = F_{2n} \cos \omega_2 t_1 - E_{2n} \sin \omega_2 t_1. \quad (34)$$

We can now replace $t-t_n$ by t in the final expressions of Equations (29) to (32) if we remember from this point on to measure t from t_n rather than from zero.

We must now replace the continuing a_{1n} from the last data input, by the time-shifted Equation (29), as the excitation of the second resonator during the residual interval, and obtain new updating and response formulas for second resonator responses at both f_1 and f_2 . The first operation is to subtract a step of magnitude a_{1n} from the excitation of the second resonator and correct the response for this.

The response of the second resonator to a positive step of this magnitude is

$$a_{1n}(1 - e^{-\alpha_2 t} \cos \omega_2 t). \quad (35)$$

Therefore, subtracting such a step from the excitation adds a_{1n} to Equation (33) to yield

$$\begin{aligned} E_{2r} & = E_{2r}^* + a_{1n} \\ & = E_{2n} \cos \omega_2 t_1 + F_{2n} \sin \omega_2 t_1 + a_{1n}. \end{aligned} \quad (36)$$

and subtracts a_{1n} from time-shifted Equation (32) to yield the expression

$$e^{-\alpha_2 t} [E_{2r} \cos \omega_2 t + F_{2r} \sin \omega_2 t] \quad (37)$$

The next operation is to find by Laplace transform theory the response of the second resonator to the transient expressed by

$$e^{-\alpha_1 t} E_{1r} \cos \omega_1 t + F_{1r} \sin \omega_1 t \quad (38)$$

from Equation (29) with the origin shifted to $t=t_n$, and add it to Expression (37).

From Appendix 4 of a previous paper⁵, the Laplace transform for Expression (38) is obtained, by summing the transforms for the individual terms, as

$$\frac{\omega_1 F_{1r} + sE_{1r}}{(s+\alpha_1)^2 + \omega_1^2} = \frac{\omega_1 F_{1r} + sE_{1r}}{(s+\alpha_1-j\omega_1)(s+\alpha_1+j\omega_1)} \quad (39)$$

From the same reference, the transfer function for the second resonator is

$$\frac{\alpha_2^2 + \omega_2^2}{(s+\alpha_2)^2 + \omega_2^2} = \frac{\alpha_2^2 + \omega_2^2}{(s+\alpha_2-j\omega_2)(s+\alpha_2+j\omega_2)} \quad (40)$$

so that the transform of the response to be added is the product

$$\frac{(\alpha_2^2 + \omega_2^2)(\omega_1 F_{1r} + sE_{1r})}{(s+\alpha_1-j\omega_1)(s+\alpha_1+j\omega_1)(s+\alpha_2-j\omega_2)(s+\alpha_2+j\omega_2)} \quad (41)$$

Finally, by application of the Heaviside expansion theorem, treated in Ap-

pendix 3 of the same previous paper, the response to be added is found to be, in initial complex form

$$\begin{aligned} & \left[\frac{\omega_1 F_{1r} + (-\alpha_1 + j\omega_1) E_{1r}}{j2\omega_1 (-\alpha_1 + \alpha_2 + j\omega_1 - j\omega_2) (-\alpha_1 + \alpha_2 + j\omega_1 + j\omega_2)} \right] \\ & \times e^{(-\alpha_1 + j\omega_1)t} \\ & + \frac{\omega_1 F_{1r} + (-\alpha_1 - j\omega_1) E_{1r}}{j2\omega_1 (-\alpha_1 + \alpha_2 - j\omega_1 - j\omega_2) (-\alpha_1 + \alpha_2 - j\omega_1 + j\omega_2)} \\ & \times e^{(-\alpha_1 - j\omega_1)t} \\ & + \frac{\omega_1 F_{1r} + (-\alpha_2 + j\omega_2) E_{1r}}{j2\omega_2 (-\alpha_2 + \alpha_1 - j\omega_2 + j\omega_1) (-\alpha_2 + \alpha_1 + j\omega_2 + j\omega_1)} \\ & \times e^{(-\alpha_2 + j\omega_2)t} \\ & + \frac{\omega_1 F_{1r} + (-\alpha_2 - j\omega_2) E_{1r}}{j2\omega_2 (-\alpha_2 + \alpha_1 - j\omega_2 - j\omega_1) (-\alpha_2 + \alpha_1 - j\omega_2 + j\omega_1)} \\ & \times e^{(-\alpha_2 - j\omega_2)t} \Big] (\alpha_2^2 + \omega_2^2) \\ & - e^{-\alpha_1 t} [G \cos \omega_1 t + H \sin \omega_1 t] \\ & + e^{-\alpha_2 t} [I \cos \omega_2 t + J \sin \omega_2 t] \quad (42) \end{aligned}$$

in final trigonometric form.

The first two terms of the initial, exponential, expression have the same least common denominator as the last two terms, which combines with the factor outside the bracket to yield the common factor

$$P = \frac{\alpha_2^2 + \omega_2^2}{[(\alpha_1 - \alpha_2)^2 + (\omega_2 - \omega_1)^2] [(\alpha_2 - \alpha_1)^2 + (\omega_2 + \omega_1)^2]} \quad (43)$$

It follows that

$$G = P \{ E_{1r} [(\alpha_2 - \alpha_1)^2 + \omega_2^2 - \omega_1^2] - 2(\omega_1 F_{1r} - \alpha_1 E_{1r})(\alpha_2 - \alpha_1) \}, \quad (44)$$

$$H = F \{ (\omega_1 F_{1r} - \alpha_1 E_{1r}) [(\alpha_2 - \alpha_1)^2 + \omega_2^2 - \omega_1^2] / \omega_1 - 2\omega_1 E_{1r}(\alpha_2 - \alpha_1) \}. \quad (45)$$

$$I' = P \{ E_{1r} [(\alpha_1 - \alpha_2)^2 + \omega_1^2 - \omega_2^2] - 2(\omega_1 F_{1r} - \alpha_2 E_{1r})(\alpha_1 - \alpha_2) \}, \quad (46)$$

and

$$J' = P \{ (\omega_1 F_{1r} - \alpha_2 E_{1r}) [(\alpha_1 - \alpha_2)^2 + \omega_1^2 - \omega_2^2] / \omega_2 - 2\omega_2 E_{1r}(\alpha_1 - \alpha_2) \}. \quad (47)$$

Now, if

$$I = E_{2r} - I' \quad (48)$$

and

$$J = F_{2r} + J', \quad (49)$$

the total instantaneous residual response of the second resonator is given by

$$e^{-\alpha_1 t} [G \cos \omega_1 t + H \sin \omega_1 t] + e^{-\alpha_2 t} [I \cos \omega_2 t + J \sin \omega_2 t]. \quad (50)$$

The manipulations implied by Equations (36) and (37) are readily performed in the calculator within card 1. The acceleration a_{1n} is added to E_{2r}' but deleted from the memory and not used in any computation based on Equation (37).

After calculator manipulations in accordance with the next two cards to replace the contents of suitable registers with the coefficients G, H, I and J, the instantaneous residual response is computable by Equation (50). However, as this is rather tedious for the HP-65 user, except for the cases of highest

damping and therefore most rapid decay, it is deferred until the fifth card. Computation of the residual envelope, which is less tedious for the user but almost as informative, is made possible by the fourth card, with the use of the same coefficients in conjunction with the derivation to follow. Equation (50) is converted to

$$\begin{aligned} & (1/2)(Ge^{-\alpha_1 t} + Ie^{-\alpha_2 t})(\cos \omega_1 t + \cos \omega_2 t) \\ & + (1/2)(Ge^{-\alpha_1 t} - Ie^{-\alpha_2 t})(\cos \omega_1 t - \cos \omega_2 t) \\ & + (1/2)(He^{-\alpha_1 t} + Je^{-\alpha_2 t})(\sin \omega_1 t + \sin \omega_2 t) \\ & + (1/2)(He^{-\alpha_1 t} - Je^{-\alpha_2 t})(\sin \omega_1 t - \sin \omega_2 t) \\ & = (Ge^{-\alpha_1 t} + Ie^{-\alpha_2 t}) \cos(\omega_1 - \omega_2)t/2 \cos(\omega_1 + \omega_2)t/2 \\ & - (Ge^{-\alpha_1 t} - Ie^{-\alpha_2 t}) \sin(\omega_1 - \omega_2)t/2 \sin(\omega_1 + \omega_2)t/2 \\ & + (He^{-\alpha_1 t} + Je^{-\alpha_2 t}) \cos(\omega_1 - \omega_2)t/2 \sin(\omega_1 + \omega_2)t/2 \\ & + (He^{-\alpha_1 t} - Je^{-\alpha_2 t}) \sin(\omega_1 - \omega_2)t/2 \cos(\omega_1 + \omega_2)t/2 \\ & = M \cos(\omega_1 + \omega_2)t/2 + N \sin(\omega_1 + \omega_2)t/2, \quad (51) \end{aligned}$$

where

$$M = (Ge^{-\alpha_1 t} + Ie^{-\alpha_2 t}) \cos(\omega_1 - \omega_2)t/2 + (He^{-\alpha_1 t} - Je^{-\alpha_2 t}) \sin(\omega_1 - \omega_2)t/2 \quad (52)$$

and

$$N = (He^{-\alpha_1 t} + Je^{-\alpha_2 t}) \cos(\omega_1 - \omega_2)t/2 - (Ge^{-\alpha_1 t} - Ie^{-\alpha_2 t}) \sin(\omega_1 - \omega_2)t/2. \quad (53)$$

Thus, finally, the magnitude of the envelope at any time t, measured from shock termination, is

$$R(t) = [M^2(t) + N^2(t)]^{1/2}. \quad (54)$$

Please note that this, being an envelope, is not necessarily continuous with the instantaneous response at shock termination

CONCLUSION

In spite of the program step and memory register limitations of the HP-65 card-programmable pocket calculator, it has been possible to devise programs, operable at the users desk, that can provide improved insight into single and double resonator responses and their relation to spectra. In principle, the programs could be adapted to a key-programmable calculator without magnetic card storage, but the labor of having to key in such extensive programs each time a computation is of interest would greatly compound the difficulty of using a pocket calculator.

One stimulus for this work was a desire to be able to shift in an arbitrary way the phase versus frequency characteristic of the Fourier or undamped residual shock spectrum and observe the effect on response -- especially second resonator response. This was not achieved but may be solved later through further programming with a more powerful calculator.

More powerful calculators, such as the HP-67 or HP-97, based on essentially the same logic as that of the HP-65, and placed on the market during the preparation of this paper, should make it possible to simplify existing programs by eliminating tricks now necessary to gain adequate information storage, and to make the programs more powerful and versatile. It should be possible to compute Fourier or undamped residual spectra for several frequencies for a single set of acceleration-time inputs. It should be possible to provide for ramp as well as step excitation approximations more generally, so as to decrease the number of data inputs within the duration of the shock excita-

tion. It should be possible to integrate the square of the relative velocity of the second mass while other computations are in progress, so as to obtain conveniently a measure of the energy dissipated in the second resonator. Further, in part by providing for arbitrary phase shifts at the interest of the user, it should be possible to explore more fully the problem of two shocks with identical spectral magnitude curves but different time histories and therefore potentially different test item response severities.

Ultimately, anyone who owns a card-programmable calculator and wants to use it for the study of shocks and shock responses should be given that capability. It is difficult to predict how other calculators, based on different logic than that of the HP-65, HP-67 and HP-97, would compare in computation of shock spectra and shock responses, without buying them and learning how to program them -- an opportunity the present author would be happy to leave to others. If any reader who owns a Texas Instruments SR-52 card-programmable calculator would adapt to it the programs of the appendices, perhaps devise some additional shock programs for it so as to utilize its capabilities to the utmost, and publish his results, he would be performing a useful service for shock and vibration engineers.

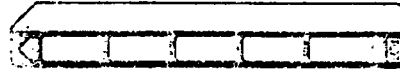
APPENDIX 1

Program and User Instructions for Fourier and Undamped
Single Resonator Shock Spectra

HP-65 User Instructions

Title Residual and Fourier Spectra _____ One Card Page _____ of _____

Programmer _____ Date _____



STEP	INSTRUCTIONS	INPUT DATA/UNITS	KEYS	OUTPUT DATA/UNITS
1	Load Card		<input type="checkbox"/> <input type="checkbox"/>	
2	Input f	f	RTN R/S	
3	Input a ₁	a ₁	A <input type="checkbox"/>	
4	Input t ₁	t ₁	B or C	
5	Repeat steps 3 and 4 for increasing k until a _k becomes negligible or permanently zero		<input type="checkbox"/> <input type="checkbox"/>	
6	Compute residual magnitude and		D <input type="checkbox"/>	Resid Lag
7	Display angle in degrees or		E x2Y	Res Angle
8	Compute Fourier magnitude and		E <input type="checkbox"/>	Fouri Lag
9	Display angle in degrees		E x2Y	Fou Angle
			<input type="checkbox"/> <input type="checkbox"/>	
			<input type="checkbox"/> <input type="checkbox"/>	
			<input type="checkbox"/> <input type="checkbox"/>	
			<input type="checkbox"/> <input type="checkbox"/>	
			<input type="checkbox"/> <input type="checkbox"/>	
			<input type="checkbox"/> <input type="checkbox"/>	
			<input type="checkbox"/> <input type="checkbox"/>	
			<input type="checkbox"/> <input type="checkbox"/>	
			<input type="checkbox"/> <input type="checkbox"/>	
			<input type="checkbox"/> <input type="checkbox"/>	
			<input type="checkbox"/> <input type="checkbox"/>	
			<input type="checkbox"/> <input type="checkbox"/>	
			<input type="checkbox"/> <input type="checkbox"/>	
			<input type="checkbox"/> <input type="checkbox"/>	
			<input type="checkbox"/> <input type="checkbox"/>	
			<input type="checkbox"/> <input type="checkbox"/>	
			<input type="checkbox"/> <input type="checkbox"/>	

HP-65 Program Form Card 1 of 1

Fourier and Undamped Residual Spectra, Step and Ramp Inputs, Page _____ of _____

SWITCH TO W PRGM PRESS [] PRGM] TO CLEAR MEMORY Slope Reset after Step

KEY ENTRY	CODE SHOWN	COMMENTS	KEY ENTRY	CODE SHOWN	COMMENTS	REGISTERS
F	31	Store $2\pi f$ in 1	LABEL	23	Adjust 6 and 7 for	R ₁ $2\pi f$
REG	43		1	01	any change in input	
E	35		RCL 5	34 05	slope	
π	02		gxzy	35 07		R ₂ a_k
X	71		STO 5	33 05		
2	02		-	51		
X	71		RCL 1	34 01		R ₃ t_k
STC 1	33 01		+	81		
R/S	04		ENTER	41		
LABEL	23	Interchange a_k with	ENTER	41		R ₄ t_{k-1}
A	11	a_{k-1} , take difference	RCL 1	34 01		
E	35	and enter twice	RCL 4	34 04		
RAE	42		X	71		R ₅ Y_k
RCL 2	34 02		1	01		
gxzy	35 07		F-1	32		
STC 2	33 02		R→P	01		R ₆ E_k
-	51		CR↑	35 09		
ENTER	41		X	71		R ₇ F_k
ENTER	41		STC	33		
RTN	24		+	61		
LABEL	23	Store t_k in 3 and 4,	7	07		R ₈
E	12	modify 6 and 7 in	CR↑	35 08		
STC 3	33 03	accordance with	X	71		
STC 4	33 04	added step	STC	33		
RCL 1	34 01		-	51		R ₉
X	71		6	06		
1	01		RTN	24		
F-1	32		LABEL	23	Compute residual spec-	LABELS
R→P	01		D	14	trum and display	A a_k
CR↑	35 09		E	35	magnitude (press	B t_k ST01
X	71		REG	41	gxzy to display	C t_k RAMP
STC	33		RCL 7	34 07	angle)	D Resid
+	61		RCL 6	34 06		E Fourier
6	06		F	31		0
CR↑	35 08		R→P	01		1 Slope
X	71		RTN	24		2
STC	33		LABEL	23	Compute Fourier	3
+	61		E	15	transform and display	4
7	07		E	35	magnitude (press gxzy	5
0	00	Reset input slope to	REG	41	to display angle)	6
STC	22	zero	RCL 6	34 06		7
1	01		ONS	42		8
LABEL	23	Store t_{k-1} in 4, t_k	RCL 7	34 07		9
C	13	in 3 and modify 6 and	F	31		
RCL 3	34 03	7 in accordance with	R→P	01		FLAGS
STC 4	33 04	added ramp	RCL 1	34 01		1
gxzy	35 07		+	81		2
STO 3	33 03		RTN	24		
-	51					
+	61					

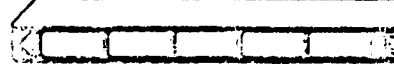
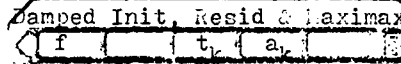
SEE USER MANUAL FOR DETAILS ON MAGNETIC CARD WITH SWITCH SET AT W PRGM

APPENDIX 2
 Program and User Instructions for Damped Initial
 Residual and Maximax Single Resonator Responses

HP-85 User Instructions

For Damped Initial, Residual and Maximax Single-Resonator Response, of _____

Programmer _____ One Card _____ Date _____



STEP	INSTRUCTIONS	INPUT DATA/UNITS	KEYS	OUTPUT DATA/UNITS
1	Load Card		[] []	
2	Initialize		f REG	
3	Input f	f	A []	
4	Input $\alpha = \pi f/Q$		B []	
5	Input first $t_k = t_1$	t_1	C []	
6	Input first $a_k = a_1$, display response	a_1	D []	a_{r1}
7	Repeat steps 5 and 6 for larger k until shock termination or until response termination	t_k a_k	C [] D []	a_{rk}
8	Display a_{rmax}		RTN R/S	a_{rmax}
9	Display a_{rmin} (negative)		R/S []	a_{rmin}
10	If data were entered only until shock termination, display estimate of max residual		[] [] R/S []	Max Resid
11	Display phase angle		ϵ XZY	
			[] []	
			[] []	
			[] []	
			[] []	
			[] []	
			[] []	
			[] []	
			[] []	
			[] []	
			[] []	
			[] []	
			[] []	

HP-65 Program Form Card 1 of 1

Title Damped Initial, Residual and Maximax Single-Resonator Response of _____

SWITCH TO W/PRGM PRESS [] PRGM TO CLEAR MEMORY Step Input Approximations only Init f REG

KEY ENTRY	CODE SHOWN	COMMENTS	KEY ENTRY	CODE SHOWN	COMMENTS	REGISTERS
RCL 7	34 07	Display a_{rmax}	X	71		R ₁ $2\pi f$
R/S	84		RCL 4	34 04		
RCL 8	34 08	Display a_{rmin}	+	61		R ₂ α
R/S	84		ENTER	41		
RCL 6	34 06	Estimate Residual	ENTER	41		R ₃ t_k
RCL 5	34 05		ENTER	41		
g	35		RCL 7	34 07		R ₄ a_k
DEG	41		EX \leftrightarrow Y	35 22		
f	31		ER \uparrow	35 08		R ₅ $\frac{1}{k}$
R \leftrightarrow P	01		STO 7	33 07		
RCL 2	34 02		ER \uparrow	35 08		R ₆ f_k
RCL 3	34 03		RCL 8	34 08		
X	71		EX \leftrightarrow Y	35 24		
CHS	42		ER \uparrow	35 08		
f ⁻¹	32		STC 8	33 08		
LN	07		ER \uparrow	35 08		
X	71		RTN	24		
R/S	84		LABEL 23		Input a_k and update registers 4, 5 and 6	R ₇ a_{rmax}
LABEL 23		Input f, store $2\pi f$ in 1	D	14		
A	11		RCL 4	34 04		R ₈ a_{rmin}
f	31		EX \leftrightarrow Y	35 07		
REG	43		STC 4	33 04		
g	35		-	51		
π	02		E	15		
X	71		ER \uparrow	35 08		
2	02		EX \leftrightarrow Y	35 07		R ₉
X	71		K	71		
STC 1	33 01		ELSTx	35 00		LABELS
RTN	24		ER \uparrow	35 09		A f
LABEL 23		Input α and store in 2	K	71		B α
B	12		STC	33		C t_k
STO 2	33 02		+	+		D a_k
RTN	24		5	5		E $\cos \alpha \sin$
LABEL 23		Input t_k , compute response, store in 7	ER \uparrow	35 08		0
C	13		STO	33		1
RCL 3	34 03	if max, store in 8	+	+		2
EX \leftrightarrow Y	35 07	if min, and display	6	06		3
STO 3	33 03		0	00		4
-	51		RTN	24		5
RCL 2	34 02		LABEL 23		Compute cos and sin	6
X	71		E	15		7
f ⁻¹	32		RCL 1	34 01		8
LN	07		RCL 3	34 03		9
E	15		X	71		FLAGS
RCL 5	34 05		L	01		1
X	71		E	05		2
EX \leftrightarrow Y	35 07		RAD	42		
RCL 6	34 06		f ⁻¹	32		
X	71		R \leftrightarrow P	01		
+	61		RTN	24		

TO EXECUTE PROGRAM INSERT MAGNETIC CARD WITH SWITCH SET AT A PRGM

APPENDIX C
 Program and User Instructions for Damped Double Resonator Instantaneous Response without Dynamic Loading of First Mass by Record

HP-65 User Instructions

Double Resonator Instantaneous Response Two Cards Page of

Programmer Date

Double Res Shock #1 Init&Param
 t₁ f₁ Q₁ f₂ Q₂

Double Res Shock #2 Inst Resp

STEP	INSTRUCTIONS	INPUT DATA/UNITS	KEYS	OUTPUT DATA/UNITS
1	Load Card 1		<input type="text"/> <input type="text"/>	
2	Input t ₁	t ₁	A <input type="text"/>	
3	Input f ₁	f ₁	B <input type="text"/>	
4	Input Q ₁	Q ₁	C <input type="text"/>	
5	Input f ₂	f ₂	D <input type="text"/>	
6	Input Q ₂	Q ₂	E <input type="text"/>	
7	Load Card 2		<input type="text"/> <input type="text"/>	
8	Input t ₀ =0, compute a ₁₀	0	RTN R/S	a ₁₀
9	Compute a ₂₀		R/S <input type="text"/>	a ₂₀
10	Input a ₀₀	a ₀₀	R/S <input type="text"/>	
11	Input t _k =t ₁ , compute a ₁₁	t ₁	RTN R/S	a ₁₁
12	Compute a ₂₁		R/S <input type="text"/>	a ₂₁
13	Input a ₀₁	a ₀₁	R/S <input type="text"/>	
14	Repeat steps 11 to 13 for larger k up to shock termination and then proceed to the fourth program without disturbing the memory registers, or, alternately, continue repeating the steps for still larger k through response termination. (Note that steps 8 to 10 can be omitted if all accelerations are zero until t=0.)	t _{0k}	RTN R/S	a _{1k}
			R/S <input type="text"/>	a _{2k}
			<input type="text"/> <input type="text"/>	
			<input type="text"/> <input type="text"/>	
			<input type="text"/> <input type="text"/>	
			<input type="text"/> <input type="text"/>	
			<input type="text"/> <input type="text"/>	
			<input type="text"/> <input type="text"/>	
			<input type="text"/> <input type="text"/>	
			<input type="text"/> <input type="text"/>	
			<input type="text"/> <input type="text"/>	

HP-65 Program Form Card 1 of 2

The Double Resonator Instantaneous Response, Initialization and Parameter Inputs

SWITCH TO W/PRGM PRESS \uparrow PRGM TO CLEAR MEMORY and Parameter Inputs

KEY ENTRY	CODE SHOWN	COMMENTS	KEY ENTRY	CODE SHOWN	COMMENTS	REGISTERS
\dagger	61	Enter f, input α (or	LABEL	23	Input Q_2 add	R ₁
C	35	Q) RTN R/S read Q	\dagger	15	$\text{Exp}(-\alpha_2 t_1)$ to 8	
π	02	(or α)	\dagger	61		
X	71		X	71		R ₂
R/S	64		2	02		
LABEL	23	Input t_1 , enter twice	\dagger	61		
A	11	and initialize	CHS	42		R ₃
ENTER	41		f \uparrow	32		
ENTER	41		LN	07		
C	35		STC	33		R ₄
RAD	42		+	61		
f	31		C	08		
RDG	43		RM	24		R ₅
RTN	24					
LABEL	23	Input f_1 , store INT				
B	12	$2\pi f_1$ in 7				R ₆
C	35					
π	02					
X	71					R ₇ INT $2\pi f_1$
2	02					+Exp(- $\alpha_1 t_1$)
X	71					
f	31					R ₈ INT $2\pi f_1$
INT	03					+Exp(- $\alpha_2 t_2$)
STC	33					
RTN	24					R ₉
LABEL	23	Input Q_1 , add				
C	13	Exp(- $\alpha_1 t_1$) to 7				
\dagger	61					LABELS
X	71					A t_1 , Init
2	02					B f_1
\dagger	61					C Q_1
CHS	42					D f_2
f \uparrow	32					E Q_2
LN	07					0
STC	33					1
+	61					2
7	07					3
STC	33					4
RTN	24					5
LABEL	23	Input f_2 , store INT				6
D	14	$2\pi f_2$ in 5				7
C	35					8
π	02					9
X	71					FLAGS
2	02					1
X	71					
f	31					2
INT	03					
STC	33					
RTN	24					

HP-65 Program Form Card 2 of 2

Title Double Resonator Instantaneous Response, Step Inputs Page of

SWITCH TO W PRGM PRESS Γ PRGM TO CLEAR MEMORY

KEY ENTRY	CODE SHOWN	COMMENTS	KEY ENTRY	CODE SHOWN	COMMENTS	REGISTERS
RCL	33	Add t_1 to 1	B	12		R1 $\ln t a_{0k}$
+	61		STO	33		$+t_k$
1	01		+	61		
RCL 7	34 07	Update E_{1k} and F_{1k}	5	05		R2 a_{1k}
F-1	32	partially in advance	ER↓	35 08		
INT	83		STO	33		
STC	33		+	61		R3 $-1k$
K	71		6	06		
3	03		ER↓	35 08	Display a_{2k}	
STC	33		R/S	84	Input a_{0k} and update	R4 $-1k$
K	71		f	31	$\ln t a_{0k}$ in 1	
4	04		INT	83		
RCL 7	34 07	Compute and display	RCL 1	34 01		R5 E_{2k}
A	11	a_{1k}	f-1	32		
RCL 3	34 03		INT	83		
K	71		+	61		R6 E_{2k}
EXZY	35 07		RCL 1	34 01		
RCL 4	34 04		EXZY	35 07		
K	71		STO 1	33 01		R7 $\ln 2\pi f$
+	61		-	51	Complete updating	$+ \ln \exp(-\alpha_1 t)$
RCL 1	34 01		RCL 7	34 07	of E_{1k} and F_{1k}	R8 $\ln 2\pi f$
+	61		A	11		$+ \ln \exp(-\alpha_2 t)$
R/S	84		B	12		
RCL 6	34 08	Update E_{2k} and F_{2k}	STC	33		
F-1	22	partially in advance	+	61		R9
INT	83		2	02		
STC	33		ER↓	35 08		
K	71		STC	33		
5	05		+	61		
STC	33		4	04		
K	71		R/S	84	Input 0 or t_1 RPN R/S	
6	06		LABEL	23		LABELS
ER↓	35 08		A	11	Subroutine for cos	A $\cos \theta \sin$
RCL 8	34 08	Compute a_{2k}	RCL 1	34 01	and sin	B Update
A	11		f-1	32		
RCL 5	34 05		INT	83		
K	71		X	71		
EXZY	35 07		1	01		
RCL 6	34 06		f-1	32		
K	71		R+P	01		
+	61		RPN	24		
RCL 2	34 02		LABEL	23		
+	61		B	12	Subroutine for E and	
EXZY	35 07	Update a_{1k} in 2	ER↓	35 08	F update	
RCL 2	34 02		EXZY	35 07		
EX Y	35 07		K	71		
STO 2	33 02		GISTx	35 00		FLAGS
51	51	Complete updating of	ER↓	35 08		1
RCL 8	34 08	E_{2k} and F_{2k}	K	71		2
11	11		RPN	24		

TELETYPE UNIT REQUIRED FOR THIS PROGRAM. CLEAR MEMORY SWITCH SET AT W PRGM

APPENDIX 4
 Program and User Instructions for Second Resonator
 Residual Response, Envelope or Instantaneous 5 Cards

HP-65 User Instructions

Resid Card #1
 t, Comp

Resid Card #2 or #3
 Comp

STEP	INSTRUCTIONS	INPUT DATA/UNITS	KEYS	OUTPUT DATA/UNITS
1	Load Card 1		<input type="text"/> <input type="text"/>	
2	Input t_1 (identical to t_1 of third program) and compute	t_1	A <input type="text"/>	
3	Load Card 2		<input type="text"/> <input type="text"/>	
4	Compute		A <input type="text"/>	
5	Load Card 3		<input type="text"/> <input type="text"/>	
6	Compute		A <input type="text"/>	

Resid (Env) Card 4
 Δt Comp

Resid (Inst) Card 5
 Oort Comp

STEP	INSTRUCTIONS	INPUT DATA/UNITS	KEYS	OUTPUT DATA/UNITS
7	Load Card 4 or 5 (or compute with both in succession) For card 4:		<input type="text"/> <input type="text"/>	
8	Input 0	0	A <input type="text"/>	
9	Compute point in envelope		B <input type="text"/>	R_0
10	Input Δt small compared to $1/ f_2 - f_1 $	Δt	A <input type="text"/>	
11	Compute point in envelope		B <input type="text"/>	R_1
12	Repeat step 11 for multiples of Δt as long as desired For card 5:		B <input type="text"/>	R_k
13	Input 0	0	A <input type="text"/>	
14	Compute response		B <input type="text"/>	a'_{20}
15	Input t'_1 (which may be larger than t_1 in third program)	t'_1	A <input type="text"/>	
16	Compute response		B <input type="text"/>	a'_{21}
17	Repeat step 16 for multiples of t'_1 as long as desired		B <input type="text"/>	a'_{2k}
	Note: Steps 8, 9, 13, 14 can be omitted		<input type="text"/> <input type="text"/>	

HP-65 Program Form Card 1 of 5

The Second Resonator Residual, Initialization, Coordinate Shift, Subtraction of a_{1n} Step

SWITCH TO HIGH PRESS 1 FROM 1 TO MEMORY

KEY ENTRY	CODE SHOWN	COMMENTS	KEY ENTRY	CODE SHOWN	COMMENTS	REGISTERS
LAB 23	23	Input t_1 , enter twice	X	71		R1 t_1
A	11	and compute	-	51		
S	35		SIC 6	33 06		
LAB 42	42		CR+	35 08		R2 a_{1n}
CR+	41		SIC 5	33 05		
CR+	41		RCL 2	34 02	Add a_{1n} to a_{2r}	
RCL 7	24 07	Replace	SIC	33		R3 a_{1n} or a_{2r}
S	12	INT2 $f_1 + \exp(-\alpha_1 t_1)$	+	61		
SIC 7	23 07	by INT2 $f_1 + 1/2 t_1$	S	05		R4 a_{1n} or a_{2r}
CR+	35 08	Replace	RCL	24		
RCL 8	24 08	INT2 $f_2 + \exp(-\alpha_2 t_1)$	LAB 23		$\exp(-\alpha_2 t_1) + 1/2 t_1$	
S	12	by INT2 $f_2 + 1/2 t_1$	S	12		
SIC 8	33 08		CR+	41		R5 a_{2n} or a_{2r}
RCL 1	24 01	Replace $I_{1a_{0n}} + t_n$	RCL	32		a_{2r}
f-1	22	by t_n	f-1	23		R6 a_{2r}
INT	83		S	32		
SIC 1	33 01		L	07		R6 a_{2n} or a_{2r}
RCL 7	24 07	Compute a_{1r} and a_{2r}	CR+	42		a_{2r}
S	13	store in 3 and 4	CR+	35 07		R7 $\ln 2 \pi f_1 + 1/2 t_1$
RCL 3	24 03		f	21		
X	71		INT	83		
CR+	35 07		CR+	35 08		R8 $\ln 2 \pi f_2 + 1/2 t_2$
RCL 4	24 04		CR+	35 07		
f	71		+	61		
+	61		CR+	35 07		R9
RCL 7	24 07		+	61		
C	13		CR+	25 00		
RCL 4	24 04		+	61		
A	71		CR+	24		
CR+	35 07		LAB 23		cos and sin	
RCL 3	24 03		C	13		
-	51		1	01		
SIC 1	33 04		f-1	32		
S	05		CR+	01		
SIC 3	33 05		CR+	24		
RCL 3	24 03	Compute a_{2r} and a_{2r}				
C	13	store in 5 and 6				
RCL 5	24 05					
X	71					
CR+	35 07					
RCL 6	24 06					
f	71					
RCL 3	24 03					
C	13					
RCL 6	24 06					
f	71					
CR+	35 07					
RCL 5	24 05					

- LABELS
- A \cos
 - B $+1/2 t_1$
 - C \cos and \sin
 - D
 - E
 - 0
 - 1
 - 2
 - 3
 - 4
 - 5
 - 6
 - 7
 - 8
 - 9
- FLAGS
- 1
 - 2

HP-65 Program Form Card 2 of 5

The Second Residual: Computation and Storage of x_1 and x_2 - and u_1 and u_2 Page _____ of _____

SWITCH TO W.P.H.M. PRESS 'F' FROM 'I' TO CLEAR MEMORY

x_2 - and u_1 and u_2

KEY ENTRY	CODE SHOWN	COMMENTS	KEY ENTRY	CODE SHOWN	COMMENTS	REGISTERS
RC 2	23	Compute x_2 and store	R	04		R1 x_1
F	11	in 2	RC	24		
F	24	00				R2 x_2
F	41					
F	32					R3 u_1
F	83					
F	71					
RC 2	23	02				
RC 7	24	07				R4 u_1 or u_2
F	41	Compute x_1 and store				
F	32	in 1				
F	32					R5 u_2
F	32					
F	71					R6 u_2
RC 1	23	01				
F	51	Compute z and store				
F	32	in 1				R7 $I_1 = 2\pi f_1$
F	00					$+1/w_1$
F	41					
F	41					
RC 2	24	00				R8 $I_2 = 2\pi f_2$
RC 7	24	07				$+1/w_2$
F	51					
F	32					R9
F	00					
F	61					
RC 2	24	02				
RC 3	24	00				
RC 7	24	07				
F	61					
F	22					
F	00					
F	61					
F	71					
F	05					
1/E	04					
RC	33					
F	00					
RC 2	24	02				
F	32					
F	00					
F	61					
STC	00					
K	71					
RC 7	24	07				
RC	33	Store u_1 in 4				
K	71					

LABELS

- A COND
- B
- C
- D
- E
- 0
- 1
- 2
- 3
- 4
- 5
- 6
- 7
- 8
- 9

FLAGS

- 1
- 2

HP-65 Program Form Card 3 of 5

1. Second Resonator Residual, Summing of Response to First Resonator of Resonator Transient

SWITCH TO PROGRAM MODE, PRESS F, PROGRAM TO CLEAR MEMORY

KEY ENTRY	CODE SHOWN	COMMENTS	KEY ENTRY	CODE SHOWN	COMMENTS	REGISTERS
LABEL	23	Compute	LABEL	23	Subroutine	R1 α_1 of α_2
A	11	Convert coefficients	C	13		R2 α_2 of α_1
-	12	for f_2	RCL 3	34 03		R3 E_{1r} of G
C	13		X	71		R4 E_{1r} of H
DEC	33		RCL 3	34 03		R5 E_{2r} of I
+	61		RCL 2	34 02		R5 E_{2r} of J
5	05		X	71		R7 $1.42\pi f_1$ + $1/\alpha_1$ of
0	14		RCL 4	34 04		$1.42\pi f_2$ + $1/\alpha_2$
-	12		-	51		R8 $1.42\pi f_1$ + $1/\alpha_1$ of
0	71		RCL 1	34 01		R9
0	15		RCL 2	34 02		
DEC	33		-	51		
+	61		X	71		
C	06		2	02		
RCL 1	34 01	Interchange 1 and 2,	X	71		
RCL 2	34 02	2 and 1	+	61		
RCL 2	34 02		RCL	34		
RCL 2	34 02		9	02		
DEC 2	33 07		X	71		
RTN	24 00		RTN	24		
DEC 6	33 08		LABEL	23	Subroutine	
RTN	24 00		D	14		
DEC 1	33 01		RCL 3	34 03		
RTN	24 00		RCL 2	34 02		
DEC 2	33 02		X	71		
0	12	Convert coefficients	RCL 4	34 04		
C	13	for f_1	-	51		
-	14		CHS	42		
-	12		RCL 6	34 06		
X	71		=	61		
0	15		RTN	24		
DEC 4	33 04		LABEL	23	Subroutine	
RTN	24 00		D	14		
DEC 3	33 03		RCL 1	34 01		
RTN	24 00	Subroutine	RCL 2	34 02		
0	12		-	51		
RCL 1	34 01		RCL 3	34 03		
RCL 2	34 02		X	71		
-1	51		RCL 6	34 06		
-1	22		X	71		
RTN	24 00		2	02		
DEC 7	33 07		X	71		
-1	32		+	61		
RTN	24 00		RCL	34		
+	61		9	02		
RCL 6	34 06		X	71		
-1	32		RTN	24		
X	05					
-	51					
RTN	24					

- LABELS
- A Comp
 - B Subr
 - C Subr
 - D Subr
 - E Subr
- 0
- 1
- 2
- 3
- 4
- 5
- 6
- 7
- 8
- 9
- FLAGS
- 1
- 2

HP-65 Program Form Card 4 of 5

Title Second Resonator Residual, Envelope Computation for Page of
 Successive $t = \Delta t^n$

SWITCH TO W PRGM PRESS [] [PRGM] TO CLEAR MEMORY

KEY ENTRY	CODE SHOWN	COMMENTS	KEY ENTRY	CODE SHOWN	COMMENTS	REGISTERS
LABEL	23	Store Δt in 2, 0 in 1	X	71		R ₁ $t=0$ or Δt^n
A	11	1	RCL 0	34 06	Compute $G e^{-\alpha_1 t}$	
STC	2 33 02		C	13		R ₂ Δt or $\frac{INT}{+ \Delta t}$
0	00		RCL 3	34 03		
STC	1 33 01		X	71		
RTN	24		-	51	Take difference	
LABEL	23	Compute	D	14	Compute I_1^2	R ₃ G
B	12		RCL 2	34 02	Remove I_1^2 from 2	
RCL 2	34 02	Store Δt^n in 1	f	31	and add to I_1^2	
f ⁻¹	32		INT	03	compute and display	R ₄ H
INT	03		STC	33	$x(t)$	
STC	33		-	51		
+	61		2	02		R ₅ I
1	01		+	61		
RCL 8	34 08	Compute $G e^{-\alpha_1 t}$	f	31		
C	13		\sqrt{x}	09		R ₆ J
RCL 3	34 03		RTN	24		
X	71		LABEL	23	Compute exponential	
RCL 7	34 07	Compute $I e^{-\alpha_2 t}$	C	13		R ₇ $I_1^2 + f_2$
C	13		ENTER	41		$+ 1/\alpha_2$
RCL 5	34 05		f ⁻¹	32		
X	71		INT	03		R ₈ $\frac{INT 2\pi f_1}{+ 1/\alpha_1}$
+	61	Take sum	X	71		
RCL 8	34 08	Compute $I e^{-\alpha_1 t}$	RCL 1	34 01		R ₉
C	13		X	71		
RCL 4	34 04		INT	03		
X	71		f ⁻¹	32		
RCL 7	34 07	Compute $J e^{-\alpha_2 t}$	INT	03		
C	13		RTN	24		
RCL 6	34 06		LABEL	23	Compute i_1^2 or i_2^2	
X	71		D	14		
-	51	Take difference	RCL 0	34 06		
D	14	Compute $INT I_1^2$ and	RCL 7	34 07		
f	31	add to 2	-	51		
INT	03		2	02		
STC	33		÷	61		
+	61		RCL 1	34 01		
2	02		X	71		
RCL 8	34 08	Compute $I e^{-\alpha_1 t}$	I	01		
C	13		f ⁻¹	32		
RCL 4	34 04		R _→	01		
X	71		ERR	35 09		
RCL 7	34 07	Compute $J e^{-\alpha_2 t}$	X	71		
C	13		ERR	35 08		
RCL 6	34 06		X	71		
X	71		ERR	35 09		
+	61	Take sum	+	61		
RCL 7	34 07	Compute $I e^{-\alpha_2 t}$	f ⁻¹	32		
C	13		\sqrt{x}	09		
RCL 5	34 05		RTN	24		

- LABELS**
- A Δt
 - B COMP
 - C Exp
 - D SUBR
 - E
 - 0
 - 1
 - 2
 - 3
 - 4
 - 5
 - 6
 - 7
 - 8
 - 9
- FLAGS**
- 1
 - 2

HP-65 Program Form Card 5 of 5

Title Second Resonator Residual, Instantaneous Response Page of

SWITCH TO W PROGRAM PRESS [F] [PRGM] TO CLEAR MEMORY

KEY ENTRY	CODE SHOWN	COMMENTS	KEY ENTRY	CODE SHOWN	COMMENTS	REGISTERS
LABEL	23	Store 0 or t_1 in 2.	L	23		R1 0 or $t=t_1-n$
A	11	0 in 1	X	71		
DEC 2	22 02		RC1 1	24 01		R2 0 or t_1
0	00		K	71		
DEC 1	22 01		CRS	42		
RC1	24		F-1	32		
LABEL	22	Compute residual a_{2k}	R	07		R3 0
12			K	71		
RC1 2	24 02		+	61	Sum, display the	R4 0
DEC	22		RC1	24	response a_{2k}	
r	01					
1	01					
RC1 3	24 03	Compute $2\pi f_1 t$				R5 I
RC1 1	24 01					
1	71					
1	01	cos and sin				R6 J
F-1	32					
r	01					
RC1 2	24 03	Multiply by C and D				R7 I, $2\pi f_2$ $+1/2_2$
A	71					
RC1 2	24 03					
RC1 4	24 04					R8 I, $2\pi f_1$ $+1/4_1$
+	61	Sum				
RC1 1	24 01	Multiply by $e^{-\alpha_1 t}$				R9
r	01					
F-1	32					
LABEL	03					LABELS
A	03					A 0 or t_1
RC1 1	24 01					B COMD
A	71					C
0	42					D
F-1	32					E
+	67					0
+	71					1
RC1 7	24 07	Compute $2\pi f_2 t$				2
RC1 1	24 01					3
1	71					4
1	01	cos and sin				5
F-1	32					6
r	01					7
RC1 5	24 05					8
A	71					9
RC1 2	24 02					FLAGS
+	61	Sum				1
RC1 7	24 07	Multiply by $e^{-\alpha_2 t}$				2
r	01					
F-1	32					

REFERENCES

1. G. J. O'Hara, "A Numerical Procedure for Shock and Fourier Analysis", NRL Report 5772, June 5, 1962
2. C. T. Morrow, SHOCK AND VIBRATION ENGINEERING, Vol. 1, Wiley 1963, pp 226 - 229
3. C. T. Morrow, "Energy Absorption and Phase Effects in Shock Excited Coupled Systems", SHOCK AND VIBRATION BULLETIN 45, June 1975, Part 5, pp 19 - 26
4. C. T. Morrow, "Effect of Phase Shift on Shock Response", SHOCK AND VIBRATION BULLETIN 46
5. C. T. Morrow, "Shock Spectra, Residual, Initial and Maximax as Criteria of Shock Severity", SHOCK AND VIBRATION BULLETIN 45, June 1975, Part 5, pp 191 - 205

Please note that Equation (52) of Reference 5 is incorrect.

DISCUSSION

Mr. Dyrdaahl (Boeing Company): How long does it take to perform this calculation?

Dr. Morrow: It depends on which program you use. If you use the first one, which calculates a spectrum at one frequency at a time, then it takes maybe up to 5 or so additional seconds for the computation updating each time you put in acceleration time pair. If you are dealing with 2 degree of freedom systems, it takes longer. Suppose we wanted to obtain the spectrum of a terminal peak sawtooth using the first program; all we have to do is input a ramp to the peak acceleration at a time equal to the duration of that sawtooth and then input a step to zero. This just takes a few seconds after which we take a look at the residual spectrum that we have obtained, by pressing an additional key, or we can press a different key and get the Fourier spectrum. By pressing two additional keys, we can get the phase.

STUDIES OF THE TERRADYNAMICS OF A
PROJECTILE PENETRATING SAND

L. E. Malvern, R.L. Sierakowski
Engineering Sciences Department
University of Florida
Gainesville, Florida 32611

and

J. A. Collins
DLV/Air Force Armament Laboratory
Eglin AFB, Florida 32542

A series of systematic experimental studies has been completed on several 20-mm-diameter terradynamic vehicles with length-to-diameter ratio of 10 and with different nose shapes [blunt ended, double blunt ended (step-tier), and biconic]. Center-of-gravity position was varied by partially hollowing some projectiles. The sand medium was impacted under two conditions [dry (only moderately compacted), and saturated]. Three impact velocity regimes were examined. (approximately 210, 320, 400 m/s) A special feature of the study has been the unusually complete visual recording of the first 1.2 meters of the trajectory by five sequential flash x-rays. This test not only gave very precise position and attitude information of the penetrator but also clearly revealed the sand separation (and possible reattachment). In addition, in some cases a detached "bow wave" was observed ahead of the projectile, which resembled a weak shock wave ahead of a supersonic aerodynamic vehicle. This paper presents data for tests at near zero obliquity for solid projectiles with blunt-ended and step-tier noses, and compares the data with one-dimensional force-law penetration models of the Poncelet type.

INTRODUCTION

The study of the mechanics of high speed earth penetrators, including predictions of depth of penetration, cavity formation, stability, and target interaction has been given in recent years the name terradynamics. While this area of study has been investigated since the early 18th century, technological barriers have hindered experimental programs in assessing models advanced for characterizing penetrator performance. The principal difficulty encountered has been the unavailability of experimental tools for examining the sequential motion of a vehicle passing through opaque loose and/or semicohesive media. More elaborate monitoring tools must be introduced than those used for flow visualization studies of bodies in gaseous or liquid media. The necessity

for generating this experimental data is occasioned by the number of penetrator models requiring this input.

A recent review of the State-of-Art of Earth Penetration Technology by Triandafilidis [1] has categorized predictive penetration techniques according to semi-analytical, theoretical, and empirical models. The semi-analytical technique, which includes the earliest penetration models based upon Newtonian mechanics, such as Poncelet [2], requires experimental data for evaluation of the important penetration constants. So-called analytical techniques, which include the Cavity Expansion [3-5] and Differential Force Law Models [6], rely upon knowledge of constitutive target material properties. The theoretical models proposed [7-9] are based upon continuum mechanics formulations describing the penetrator

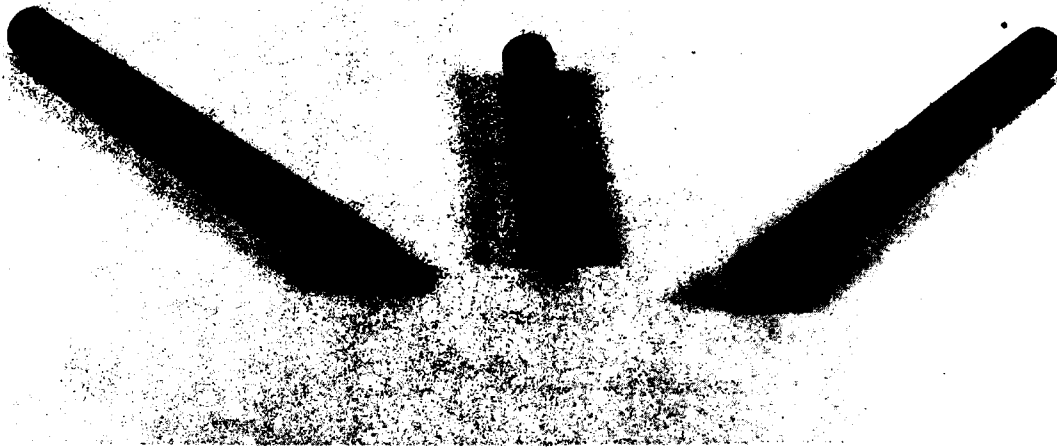


Fig. 1 - Flat Ended and Step-Tier Projectiles Used in Test Program

and target, and rely upon finite difference and finite element computer codes as solution techniques. Finally, empirical techniques based upon extensive laboratory and field testing have been introduced with the most extensive work in this area developed at Sandia Laboratories [10-11].

All of the semianalytical and empirical models require some information on the penetrator and target properties. However, information on the predicted trajectory path has remained somewhat scarce. One of the first techniques used for obtaining transient trajectory information was reported by Allen, Mayfield, and Morrison [12]. A position-time recording of the projectile motion in dry quartz sand was obtained using a photographic-electronic chronograph specifically designed to record the sequential breaking of grid wires in the sand. Another position-time record of vehicle position in a granular medium has been obtained by Hakala [13] using microwave techniques. There has also been a considerable development in on-board sensors sending back data through trailing wires or by telemetry for air dropped penetrators at moderate speeds, and a few laboratory studies monitoring projectile motions by such means as breaking buried wires or screens. Other investigators such as Biele [14] have studied the trajectory of a penetrator by post-test examination of the cavity shape, using probes in-

serted in the cavity and sectioning procedures. A successful method of monitoring the penetrator trajectory using flash X-ray radiography was first noted with isolated success using a single unit by Avco [15] and recently expanded to include three consecutive units by Culp [16].

In the current test program, five consecutively spaced X-ray units have been used to visually record transient positions of the penetrator in a horizontal penetration of the test chamber. The X-ray system consisted of one 150 KV unit and four 300 KV units. Nonspinning projectiles of stable configuration with various nose shapes have been tested in dry and saturated sand at three velocities of near zero impact obliquity. In addition to the X-ray units, which were the most successful data collection tool in these tests, strain gages and pressure sensors on the test chamber walls and floor, and velocity sensing coils for magnetized projectiles have been used as monitoring devices in conjunction with a magnetic tape recording system and subsequently transcribed by a sixteen-channel oscillographic recording system. A comparison of the data collected, for the specimens tested, with classical one-dimensional penetration models is described.

TABLE 1

Test Numbers of Experimental Matrix

Projectile Nose Type	Target	210 m/sec					320 m/sec				400 m/sec			
Flat	Dry Sand	15	16	17	18	19	20	22	23	24	14	25	26	27
Flat	Wet Sand	70	71	72	73	36	37	38	74	76	82	83	84	
Step-Tier	Dry Sand	52	53	54	55	57	56	58	59	61	62	63	64	65
Step-Tier	Wet Sand	42	43	44	45	39	40	41	49	50	51	68	69	

TEST PROCEDURE

Penetration experiments were performed using specially fabricated cylindrical projectiles of diameter 0.02 m and length 0.23 m with two different nose shapes (flat ended and step-tier) as shown in Fig. 1. For all tests, a 1.20 m long by 0.15 m by 0.40 m open-top box was used as the target test chamber with Eglin sand (dry or fully saturated) used as the target medium. For the current tests, the projectiles entered the test chamber in horizontal flight at approximately zero degree angle of incidence.

A matrix table summarizing the types of specimens tested as well as the target conditions is given in Table 1. Detailed descriptions of the tests, as well as tabulated data for these and other tests in the program are given in [17, 18].

Impact projectile velocities were controlled by varying powder load in a primed 20 mm case. The striking velocity was measured by using paper-back velocity screens located at fixed positions near the test chamber entrance. A foil make switch was used to trigger all X-ray units, with the timing sequence of the X-rays adjusted according to the best estimate of time delay as given by the Project Engineer. Fig. 2 shows a general view of the test chamber with X-ray film cassettes mounted along its wall. Two X-ray heads can be seen behind the box, one small 150 KV unit, and one 300 KV unit.

For all tests a magnetic system was used to furnish supplementary velocity information. The steel projectiles were magnetized to a strength of about 150 gauss, as measured at the center of the nose with a Hall-effect gauss-meter. When this magnetized projectile passed

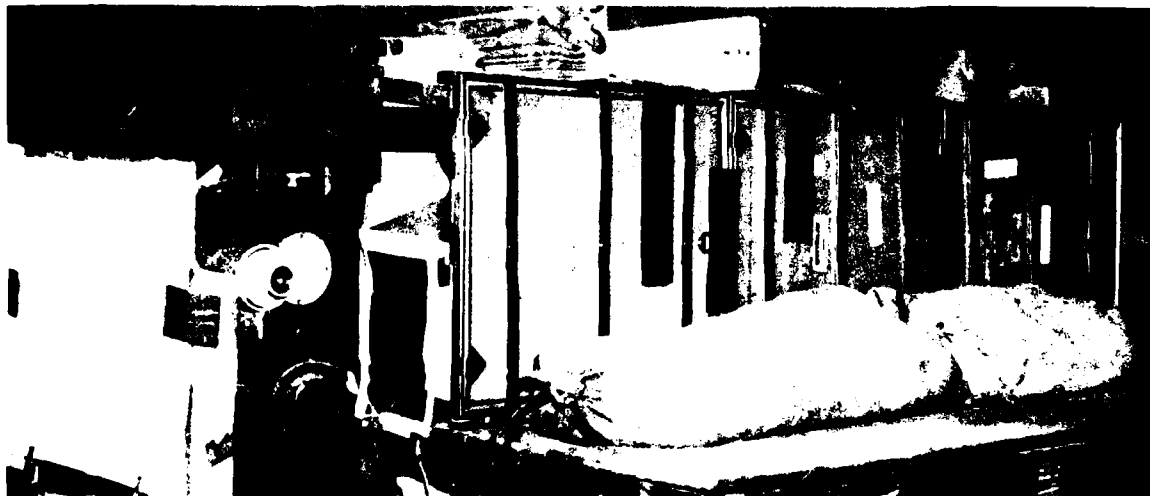


Fig. 2 - Overview of Test Chamber, X-rays, Velocity Screens, and Associated Equipment

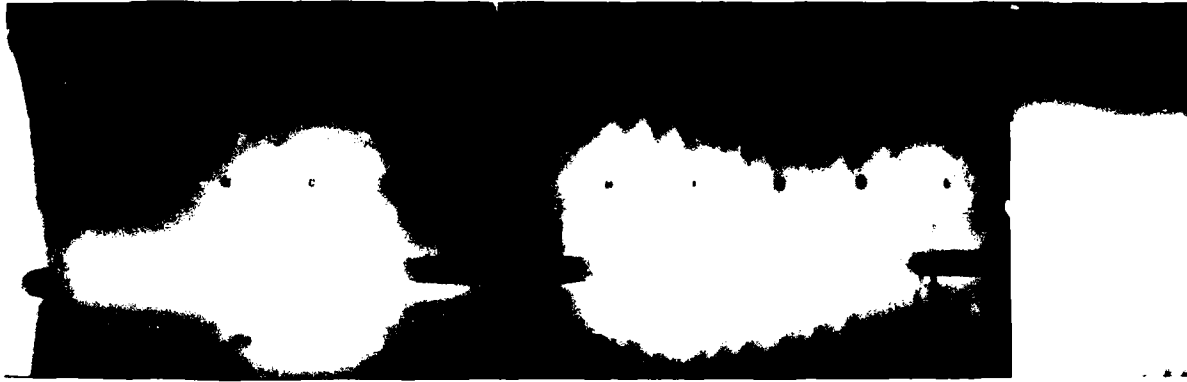


Fig. 3 - Sequence of Shots for Test Number 26, Flat Nosed Projectile in Dry Sand at 400 m/sec.

through a set of round copper-wire coils at fixed intervals along the path, voltage signals were generated, which were recorded without preamplification on the magnetic tape recording system and later transcribed to the oscillograph. Coil size (diameter 0.15 m) was selected in an attempt to provide as sharp a response as possible without disturbing the projectile-target medium interaction. With this coil size the maximum voltage responses occurred when the projectile nose or tail was about 0.02 to 0.04 m from the coil plane, assuming a horizontal projectile passing through the coil center. Variations in recorded velocity caused by path deviations and by variations in location of peak radial magnetic field at the coil were nominally within about five per cent of the measured velocity.

Other monitoring devices used for obtaining information about the transient forces exerted by the sand in these tests were pressure transducers located at the base of the test chamber area, and strain gages mounted to the test chamber side walls. The pressure gages were Bell and Howell Type 4-402-006 pressure transducers with a range of 0-50 psi, while the strain gages were Baldwin-Lima-Hamilton Type A-9-4, mounted at varying intervals along the chamber side walls nominally 0.38 m, 0.69 m, and 0.99 m, as measured from the front of the box. Preliminary analyses of the pressure and strain gage data show reproducibility and consistency in determining the approximate relative position of the projectile while in the test chamber. In addition, the pressure transducer oscillograph trace was found useful as a monitor of the X-ray firing times because of electrical pick-up.

RESULTS AND DISCUSSION

It has been mentioned previously that the most successful tool used for data collection in this series of experiments was flash radiography. For the primary test program of studying blunt and step-tier projectiles fired horizontally at impact velocities of 210, 320, and 400 m/sec. into dry and saturated sand, four or more test replications were made at each impact speed. The use of multiple impact speeds with approximately five X-ray pictures taken for each shot is believed to be one of the most extensive demonstrated uses of flash radiography in terradynamics research. A typical sequence of such shots is shown in Fig.3 for the case of a flat nosed projectile entering dry sand, which corresponds to Test Number 26 from Table 1.

Data was reduced from the X-ray photos by assuming a central flight of the vehicle through the test chamber and measuring the location of the vehicle nose with respect to fixed letter positions on the box side wall (see Fig.3). This recorded information was adjusted to correct for photographic distortion of the plane of the projectile by scaling the true vehicle dimensions with respect to the photographically recorded size. The adjusted data was used to re-evaluate and record both the projectile nose position and the center of gravity position in the plane of the penetrator. This information was then used for calculating the velocity profile of the vehicle through the box, attitude of the projectile, and other trajectory parameters.

In addition to providing an accurate indication of projectile trajectory and attitude, the X-ray techniques provided a means of visually examining the separ-

ation of sand from the projectile and reattachment along the vehicle body. Reattachment was not, however, observed as a recurring event for the projectile nose shapes and velocity regimes tested.

The X-rays did, however, reveal a detached bow wave, Fig. 4, particularly for the higher impact speeds in dry sand. A bow wave in the present context is defined as a density discontinuity moving with the projectile and resembling the detached shock wave ahead of a supersonic aircraft. These bow waves have similarly been observed in the X-rays taken by Culp [16], which with color enhancement techniques have clearly delineated density variations. These results indicate that any penetration model based on the shear zone associated with incompressible plasticity theory must be applied with considerable caution.

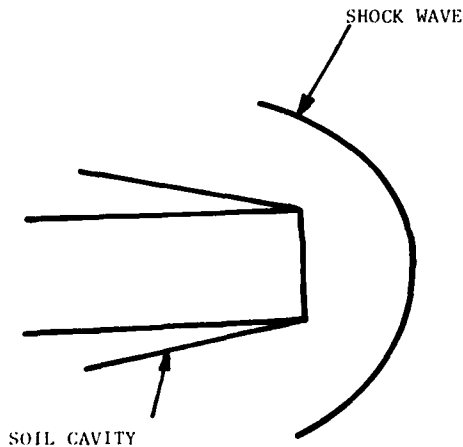


Fig. 4 - Detached Bow Wave for Test Number 14, Flat Nosed Projectile in Dry Sand at 400 m/sec.

For further quantitative examination of the data semi-analytical and empirical equations were considered as follows. The Poncelet force law [2] takes the following form, after division by the mass m of the projectile

$$-\frac{dV}{dt} = A + BV^2 \quad (1)$$

After a variable change, $dV/dt = V dV/dx$, Equation (1) can be integrated to give the following relationship be-

tween x and V if the initial speed was V_0 at x_0 .

$$x - x_0 = \frac{1}{2B} \ln\left[\frac{A + V_0^2}{A + V^2}\right] \quad (2)$$

If the projectile stops at final position x_f , so that the total penetration is $D = x_f - x_0$, then

$$D = \frac{1}{2B} \ln\left[1 + \frac{BV_0^2}{A}\right] \quad (3)$$

and, with $s = x_f - x$,

$$s = \frac{1}{2B} \ln\left[1 + \frac{BV^2}{A}\right] \text{ for } x_0 < x < x_f. \quad (4)$$

The last form is especially convenient for correlating velocity with distances measured back from the stopping point.

In the current test program all observations were made in the region where V was greater than 61 m/s. In that region, as Young [11] has pointed out and as is confirmed by the present results, the constant A in the Poncelet law is negligible in comparison to the inertial drag BV^2 term. Putting $A=0$ in Equation (2) reduces it to

$$x - x_0 = \frac{1}{B} \ln(V_0/V), \quad (5)$$

which is the form of the Poncelet equation actually used for the data analysis.

The constant B is related to the drag coefficient C_D , defined as in aerodynamics, so that

$$\text{Inertial Drag Force} = \frac{1}{2}\rho A_1 C_D V^2 \quad (6)$$

where A_1 is the projected area of the projectile on a plane perpendicular to the velocity and ρ is the density of the medium being penetrated. Thus

$$B = \frac{1}{2m}\rho A_1 C_D \text{ or } C_D = 2mB/\rho A_1 \quad (7)$$

Fig. 5 shows a plot of the position-time curve for Shot No. 26.

The five plotted points are the experimental data determined from the five X-rays of Fig. 3. The two curves are for a cubic interpolation function fitted to the data by a linear regression method and for a Poncelet equation of the form of Equation (5) with x_0 and V_0 given and B determined by a non-linear regression (least squares based on all five points). The two fitted curves essentially coincide during the time of observation, although the cubic begins to diverge unrealistically upon extrapolation outside the interval of observation. This is even more noticeable in

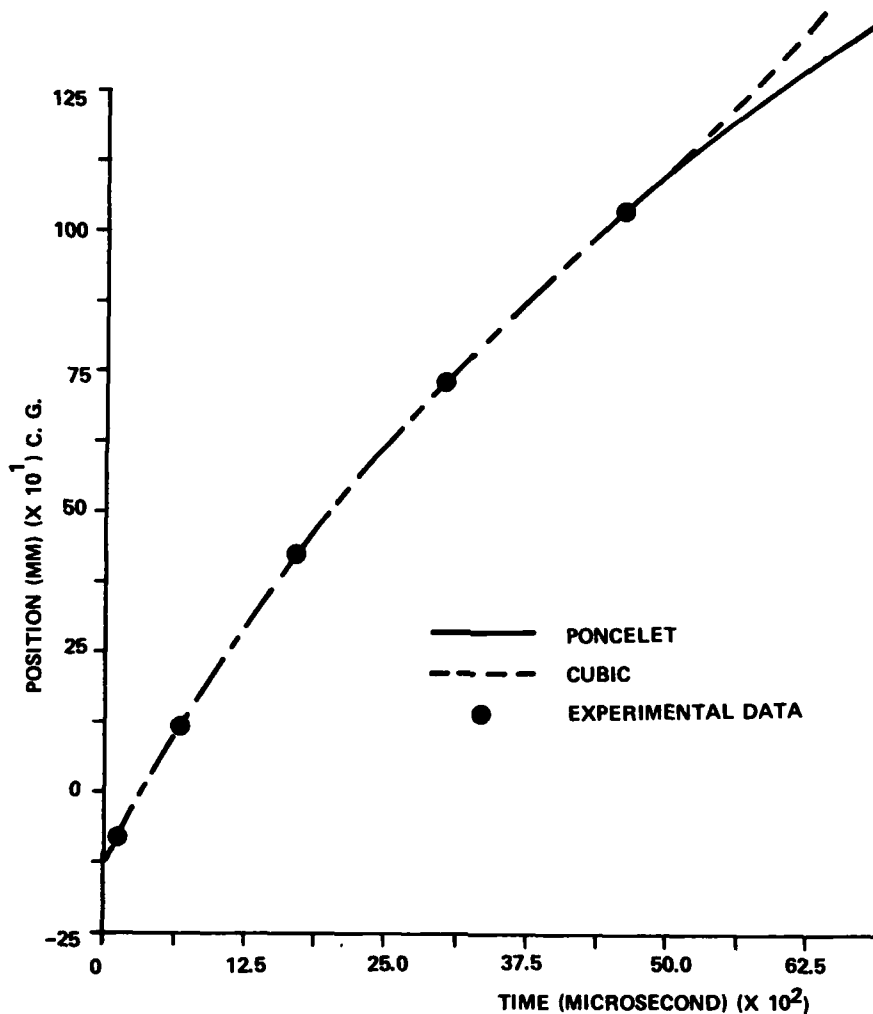


Fig. 5 - C. G. Position Versus Time for Test Number 26, Flat Nosed Projectile in Dry Sand at 400 m/sec.

Fig. 6, which shows curves of velocity versus position. The dashed curve is obtained by differentiating the cubic of Fig. 5, while the solid curve is given by Equation (5). The four "experimental data" velocities of Fig. 6 were obtained by finite differencing the position-time data for the five points of Fig. 5.

A second type of nonlinear regression procedure was also applied based on these four finite-difference velocities V_1, V_2, V_3, V_4 , at positions x_1, x_2, x_3, x_4 without assuming V_0 known. The second nonlinear regression procedure gave

$$B = \frac{(\sum x_i) \left(\frac{1}{4} \sum \ln V_i \right) - \sum x_i \ln V_i}{\sum x_i^2 - \frac{1}{4} (\sum x_i) (\sum x_i)} \quad (8)$$

and then

$$\ln V_0 = \sum \ln V_i + \frac{1}{4} B \sum x_i \quad (9)$$

where the summations go from $i=1$ to $i=4$. The two different methods gave almost the same value of B , and hence of C_D by Equation [7], in most cases. Fig. 7 shows the calculated C_D versus initial impact velocity for 20 of the shots. When the two regression procedures gave significantly different results, the first procedure based on all five data points was used to determine the plotted

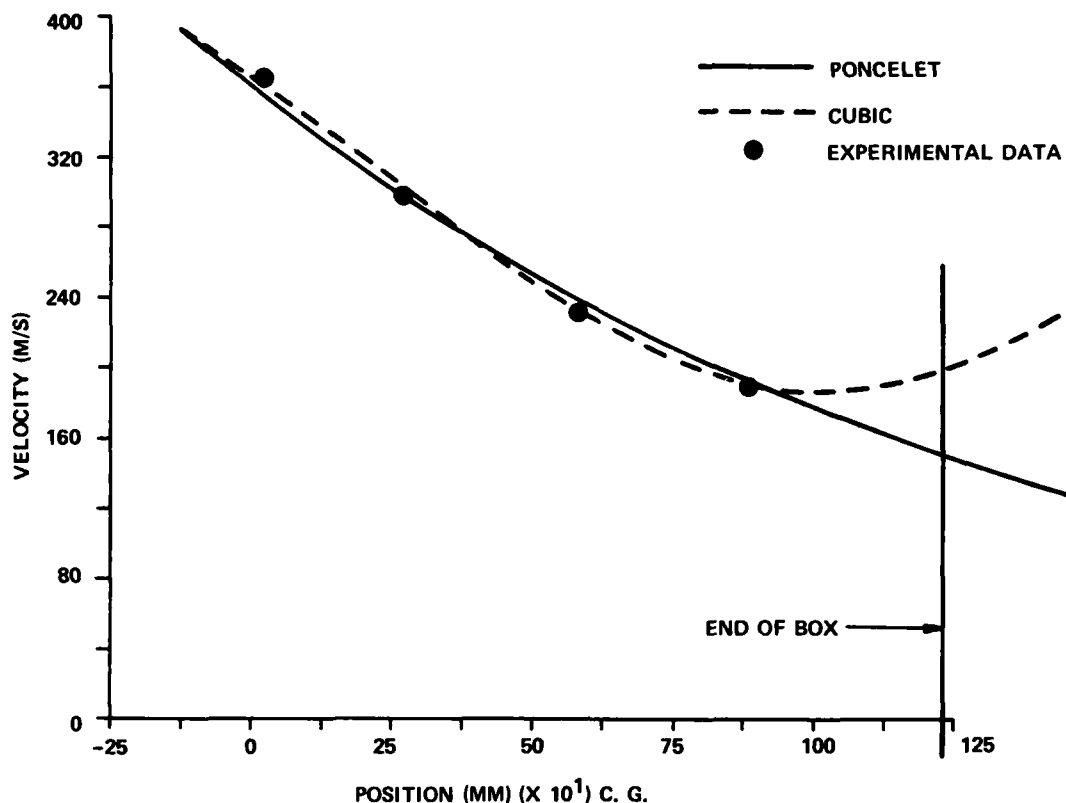


Fig. 6 - Velocity Versus C. G. Position for Test Number 26, Flat Nosed Projectile in Dry Sand at 400 m/sec.

value of C_D .

For shots in dry sand (marked with triangles in Fig. 7) the results show that C_D is almost independent of velocity as observed in these experiments, although there is a slight downward trend of C_D with increasing velocity. The shots in wet sand (saturated) show greater scatter in the calculated values at each velocity and also show a marked decreasing trend of C_D with increasing impact velocity. The downward trend of C_D with velocity was also observed between different segments of the trajectory for a given test [17].

The experimental results were also compared with the Sandia empirical formulas [10,11]. Thus, according to Young [11] the total depth of penetration D is given in terms of the initial impact velocity V_0 by an equations of the following forms (in SI units):

$$D = 0.117 KSN(W/A_1)^{1/2} (V_0 - 31.5) \quad (10)$$

for $V_0 > 61$ m/s

or by

$$D = 2KSN(W/A_1) \ln[1 + 2V_0^2(10^{-4})] \quad (11)$$

for $V_0 < 61$ m/s,

where W is projectile weight, A_1 is cross sectional area, N is a nose coefficient, S is a soil coefficient, and K is an independently determined parameter. Since all impacts in the present study had $V_0 > 61$ m/s, a procedure based on a method used by Young [11] to modify Equation (10) for use with layered media was used to analyze the experiments. Since K, S and N appear only as the product KSN , the procedure followed was to determine the best value of KSN to fit the experimental velocity versus position data.

AD-A148 079

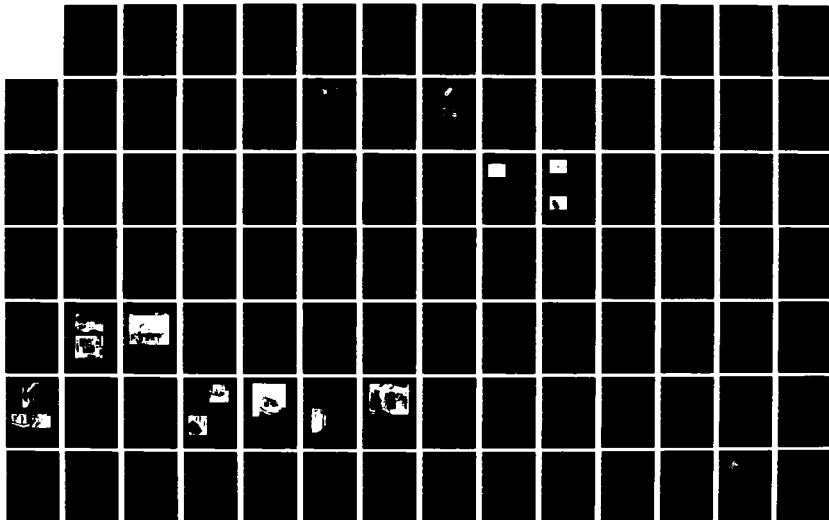
THE SHOCK AND VIBRATION BULLETIN PART 1 OPENING SESSION
PANEL SESSION SHO. (U) NAVAL RESEARCH LAB WASHINGTON DC
SHOCK AND VIBRATION INFORMAT. . SEP 77 BULL-47-PT-1

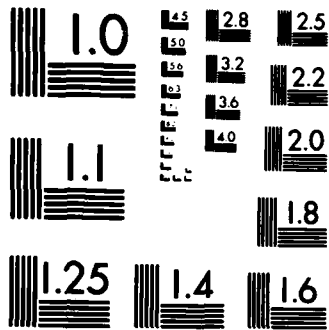
2/3

UNCLASSIFIED

F/G 20/11

NL





MICROCOPY RESOLUTION TEST CHART
NATIONAL BUREAU OF STANDARDS-1963-A

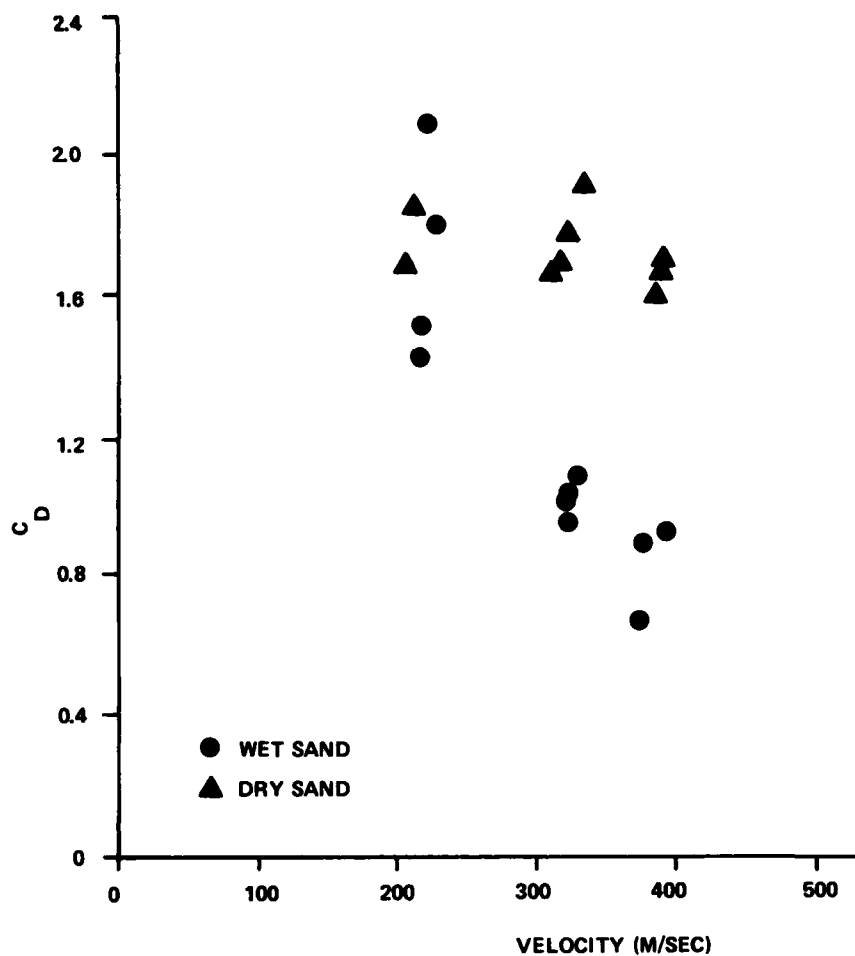


Fig. 7 - Poncelet Parameter C_D Versus Impact Velocity for Flat Nosed Projectile Tests in Dry and Wet Sand

The basis for the application of the Sandia empirical formula to layered media [11] was the assumption of constant deceleration through each layer. Thus, if a_n is the acceleration magnitude nondimensionalized with respect to the acceleration of gravity g (so that $a_n g$ is the dimensional deceleration), then the velocities V_{n+1} at the beginning and the end of a layer were related by

$$v_{n+1}^2 = v_n^2 - 2g[(a_{n-1} + a_n) \frac{L}{2} + a_n(t_n - L)] \quad (12)$$

where t_n is the thickness of the layer, and it is assumed that $t_n \gg L$. For the flat-nosed projectile, with $L=0$, Equation 12 reduces to

$$v_{n+1}^2 = v_n^2 - 2a_n g t_n \quad (13)$$

which is the basis for the following regression procedure to determine the Sandia parameter KSN. Let

$$G_i = v_1^2 / [0.0117 (v_1 - 30.5) (v_1^2 - v_i^2) (W/A)^{1/2}] \quad (14)$$

Then

$$KSN = \frac{\sum (x_i - x_1) (\frac{1}{3} \sum G_i) - \sum (x_i - x_1) (G_i)}{\sum (x_i - x_1)^2 - \frac{1}{3} [\sum (x_i - x_1)] [\sum (x_i - x_1)]} \quad (15)$$

$i = 2 \text{ to } 4.$

A plot of the fitted values of the Sandia parameter KSN for the same shots

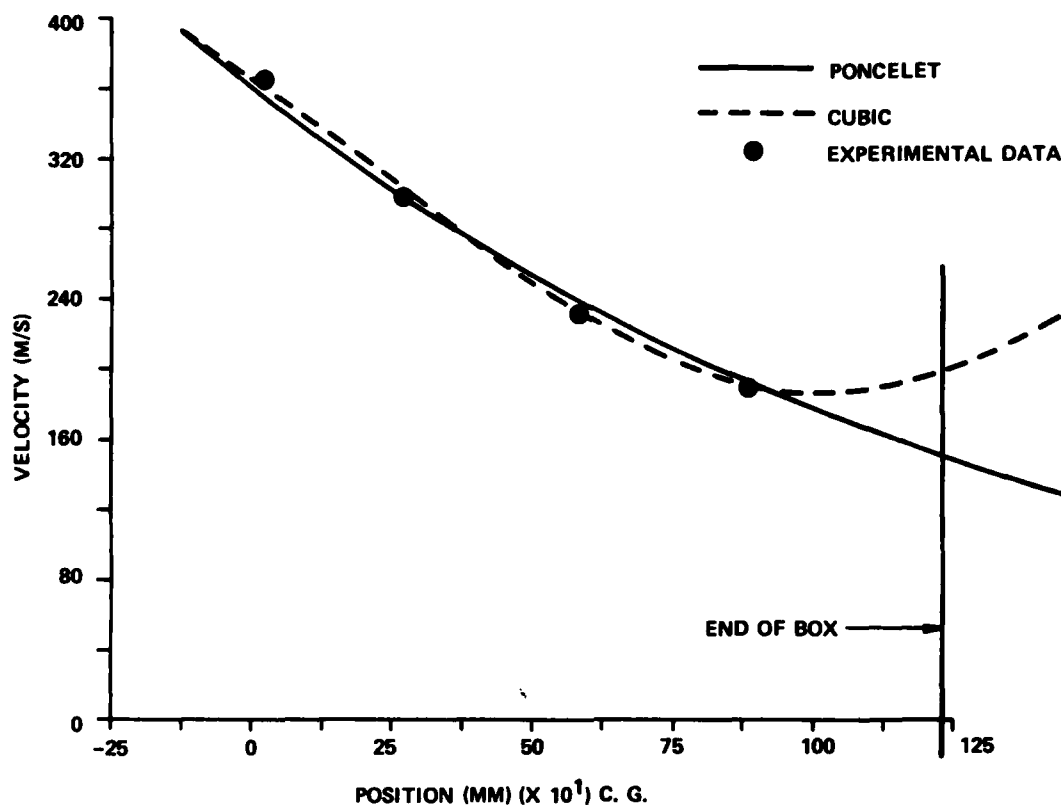


Fig. 6 - Velocity Versus C. G. Position for Test Number 26, Flat Nosed Projectile in Dry Sand at 400 m/sec.

value of C_D .

For shots in dry sand (marked with triangles in Fig. 7) the results show that C_D is almost independent of velocity as observed in these experiments, although there is a slight downward trend of C_D with increasing velocity. The shots in wet sand (saturated) show greater scatter in the calculated values at each velocity and also show a marked decreasing trend of C_D with increasing impact velocity. The downward trend of C_D with velocity was also observed between different segments of the trajectory for a given test [17].

The experimental results were also compared with the Sandia empirical formulas [10,11]. Thus, according to Young [11] the total depth of penetration D is given in terms of the initial impact velocity V_0 by an equations of the following forms (in SI units):

$$D = 0.117 KSN(W/A_1)^{1/2}(V_0 - 31.5) \quad (10)$$

for $V_0 > 61$ m/s

or by

$$D = 2KSN(W/A_1) \ln[1 + 2V_0^2(10^{-4})] \quad (11)$$

for $V_0 < 61$ m/s,

where W is projectile weight, A_1 is cross sectional area, N is a nose coefficient, S is a soil coefficient, and K is an independently determined parameter. Since all impacts in the present study had $V_0 > 61$ m/s, a procedure based on a method used by Young [11] to modify Equation (10) for use with layered media was used to analyze the experiments. Since K, S and N appear only as the product KSN , the procedure followed was to determine the best value of KSN to fit the experimental velocity versus position data.

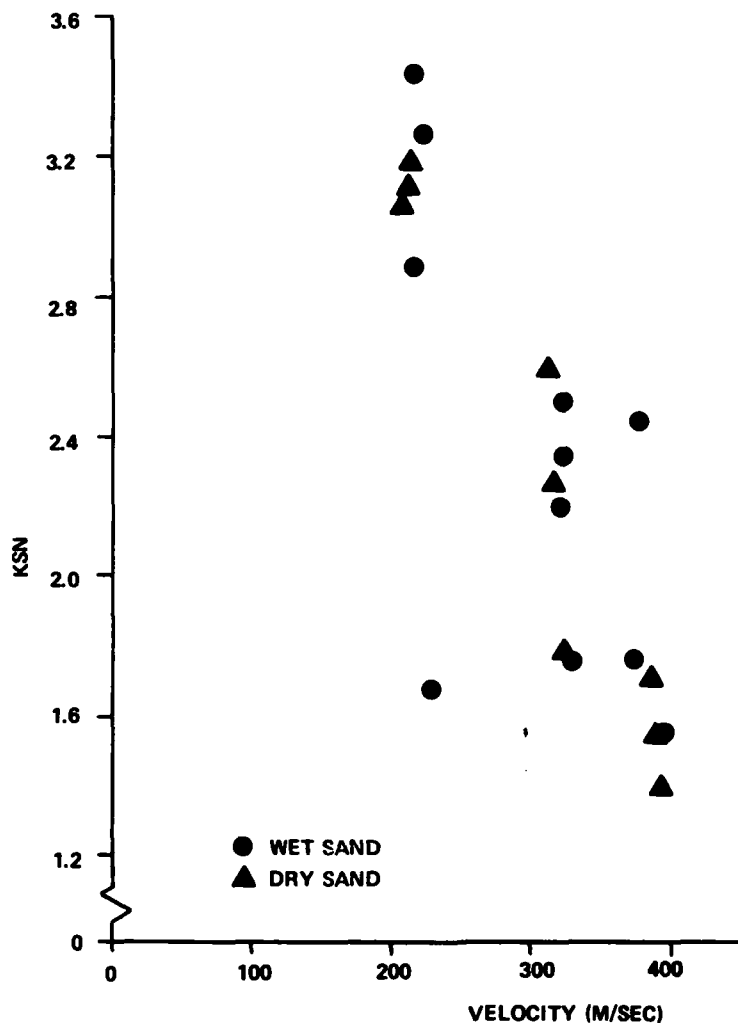


Fig. 8 - Sandia Penetration Coefficient KSN Versus Impact Velocity for Flat Nosed Projectile Tests in Dry and Wet Sand

used for C_D in Fig. 7 is shown in Fig. 8. The fitted values of KSN show a marked dependency upon impact velocity in both dry sand and wet sand. The greater scatter in the fitted values of KSN than in those of C_D indicates that these penetration events are not well characterized by a single value of KSN for each shot. The greater discrepancies with the Sandia equation can be explained in part by the assumption of a constant deceleration magnitude in each segment, in contrast with the Poncelet prediction which does fit the dry sand experimental data very well in these velocity ranges.

CONCLUDING REMARKS:

From the present studies, the following remarks can be made: (a) Successful use of a multiple head radiographic detection system has been demonstrated for granular media, (b) the cavity formation, separation phenomenon, and bow shock wave have been catalogued as a function of initial impact velocity, (c) the classical Poncelet equation has been shown to provide a better fit to experimental data than the single cubic interpolation formula or the empirical model (d) the Poncelet drag coefficient C_D has been found to be velocity de-

pendent, although for dry sand the dependence is very slight in the velocity range observed, and (e) the saturation level of the sand changes significantly the functional dependence of C_D on velocity.

Further experiments and analysis are underway to study the form and meaning of the changes of C_D with velocity, including observations of the low velocity regime as the projectile comes to a stop. Different nose shapes, vertical firings, and water as a target material will be tested to give a better understanding of the mechanism involved in penetration.

ACKNOWLEDGMENT

This research was supported in part by AFATL Contract No.F 08635-75-C-0054. The careful assistance of the support personnel of VITRO in performing of the experimental work at Eglin AFB is gratefully acknowledged.

REFERENCES

- [1] G.E.Triandafilidis: State of the Art of Earth Penetration Technology, TR CE-42(76)DNA-297, May, 1976.
- [2] Poncelet, J.V. Cours de Mecanique Industrielle, First Edition, 1829.
- [3] Rohani, B. "High Velocity Fragment Penetration of Soil Targets." Proc. of the Conference on Rapid Penetration of Terrestrial Materials, Texas A & M University, College Station, Texas, 1972.
- [4] Norwood, F.R. "Cylindrical Cavity Expansion in a Locking Soil." Sandia Laboratories, SLA-74-0201, Albuquerque, New Mexico, July 1974.
- [5] Bernard, R.S. and Hanagud, S.V. "Development of a Projectile Penetration Theory," U.S. Army Engineers Waterways Experiment Station, Report I, Penetration Theory for Shallow to Moderate Depths, Technical Report S-75-9, Vicksburg, Mississippi, June 1975.
- [6] Henderson, D. and Stephens, R.L. "Impact and Penetration Technology" paper presented at the Fuze-Munitions Environment Characterization Symposium at Picatinny Arsenal, New Jersey, by AVCO Corp., November 1972.
- [7] Hermann, W. "A Lagrangian Finite Difference Method for Two-Dimensional Motion Including Material Strength," AFWL, Technical Report

WL-TR-64-107, November 1967.

- [8] Hageman, L.J. and Walsh, J.M. "HELP-- A Multi-Material Eulerian Program for Compressible Fluid and Elastic-Plastic Flows in Two Space Dimensions and Time," Systems, Science and Software, 3SIR-350, Vol. 1, La Jolla, California, 1970.
- [9] Sedgwick, R.T., "Theoretical Terminal Ballistic Investigation and Studies of Impact at Low and Very High Velocities." General Electric Co., Space Sciences Laboratory, Technical Report AFATL-TR-68-61, King of Prussia, Pennsylvania, 1968.
- [10] Young, C.W. "The Development of Empirical Equations for Predicting Depth of an Earth-Penetrating Projectile." Sandia Laboratories, SC-DR-67-70, May 1967.
- [11] Young, C.W. "Empirical Equations for Predicting Penetration Performance in Layered Earth Materials for Complex Penetrator Configurations." Sandia Laboratories, SC-DR-72-0523, December 1972.
- [12] Allen, W.A., Mayfield, E.B. and Morrison, H.L. "Dynamics of a Projectile Penetrating Sand," Journal of Applied Physics, Vol.28, No.3, March 1957.
- [13] Hakala, W.W. "Resistance of a Granular Medium to Normal Impact of a Rigid Projectile", Ph.D. Dissertation, Virginia Polytechnic Institute, Blacksburg, Virginia, June 1965.
- [14] Biele, A., An investigation of the Terradynamic Stability of a Scaled Model Projectile, Masters Thesis, Mississippi State University, August, 1973.
- [15] Hoffman, P.R., McMath, R.R., Migotsky, E., Projectile Penetration Studies, AFWL-TR-64-102, December 1964.
- [16] Culp, M.F.: Submunition Penetration into Tactical Targets, LMSC-D43546, December 1975.
- [17] Malvern, L.E., Sierakowski, R.L., Ross, C.A., Milton, J.A., Ting, C.S., and Collins, J.A. "Study of Penetration Technology", AFATL-76-129, Eglin AFB, Florida, October 1976.
- [18] Collins, J.A. and Sierakowski, R.L., "Studies on the Penetration Mechanics of Eglin Sand", AFATL-76-122, Eglin AFB, Florida, October 1976.

HARDENED SYSTEM VULNERABILITY ANALYSIS

Jon D. Collins
J. H. Wiggins Company
Redondo Beach, California

A procedure is demonstrated for the performance of a survivability analysis of a hardened facility subject to nuclear attack. The methodology of system failure computation is summarized and the process required to define the system and develop the data is discussed. A fault tree methodology is introduced to be used with the identification of system failure. Methods of fragility definition are described and a methodology is discussed for the development of fragility curves and functions from data. Some weapon induced effects (air blast overpressure and ground shock) are discussed in general from the standpoint of formulation and the uncertainties. Examples are given of how to compute nominal values and the associated uncertainties and correlations (covariance). The problem of translating the free field environment to local environment is discussed using two approaches: linear transfer function; and a reduced degree-of-freedom system dynamic simulation.

ANALYSIS OF SYSTEM FAILURE

The objective of this study is to determine how the facility and its functions will survive and operate during and after a nuclear attack. The "system" in this analysis is not just the facility, but also the weapon, the local environment (geology, etc.), the facility structure and all of the elements of the facility.

The ability to evaluate the system properly is dependent upon the accuracy and adequacy of the mathematical simulation. Since the simulation must be made up of mathematical descriptions of all of the critical interactive relationships (impulse, soil conditions, shock isolation, etc.) which characterize the nuclear vulnerability problem, it is very evident that an accurate simulation is generally impossible. However, with certain compromises in the models, it is possible to formulate a workable simulation, which, using a probabilistic approach to represent the uncertainty, can be used to evaluate the system analytically in the absence of real system test data. Thus, a major

point with regard to this discussion is that a system analysis (in this case, a simulation) has to be as accurate as possible, and must simulate analytically all of the critical interactions before it can serve as a useful tool. Note that it can perform no better than the level of understanding gained of the behavior of each of the elements of the system. A system analysis organizes understanding of the system, but does not improve on the knowledge of the individual behavior of the elements. If the hardened system is complex and highly interactive, the model must be able to represent those characteristics. Too much simplification too soon can lead to an erroneous model. On the other hand, complexity can be carried too far when the results of the increased complexity do not have a material effect on the sought after answer. Thus caution must be used in finding the appropriate level of detail.

In 1968, a program (FAST III) was completed which modeled the various elements of the system failure problem. This program has gone through several revisions [1-6], and is now capable of

analyzing a group of facilities being attacked by multiple weapons [6]. FAST is basically a simulation of the failure process. It starts with a specification of the weapon effects, then modifies the weapon effects to be local mechanical effects (acceleration, velocity, etc.)*, determines the failure probability of each component and finally uses a reliability network of the components to establish the probability of system failure. The path of energy from weapon to component is shown in Figure 1. If there were no uncertainty in weapon effects, the basic operation of FAST would be deterministic (other than the computation of failure from the reliability network components). This would mean that only a single chain of computations would be necessary to compute system failure; however, many factors contribute to uncertainty in

*The method is not limited to mechanical effects and has been used successfully to analyze radiation, EMP, thermal and debris effects.

these weapon effects and consequently, they must be characterized by probability distributions.

The system failure probability resulting from the above sequence of computations is a complex function of many weapon effects and can be generally expressed as

$$P_{fs} = P(\text{failure} | x_1, x_2, x_3, \dots) \quad (1)$$

where x_1, x_2, x_3, \dots are the weapon effects.

Since the weapon effects are uncertain and must be expressed by individual or joint probability distributions, $p(x_1, x_2, x_3, \dots)$, we must seek the average or expected value of P_{fs} which is

$$P_{fs} = E[P(\text{failure} | x_1, x_2, \dots)] \\ = \int_{\text{All } x_1, x_2, x_3, \dots} P(\text{fail.} | x_1, x_2, x_3, \dots) \\ \cdot p(x_1, x_2, x_3, \dots) dx_1 dx_2 dx_3 \dots \quad (2)$$

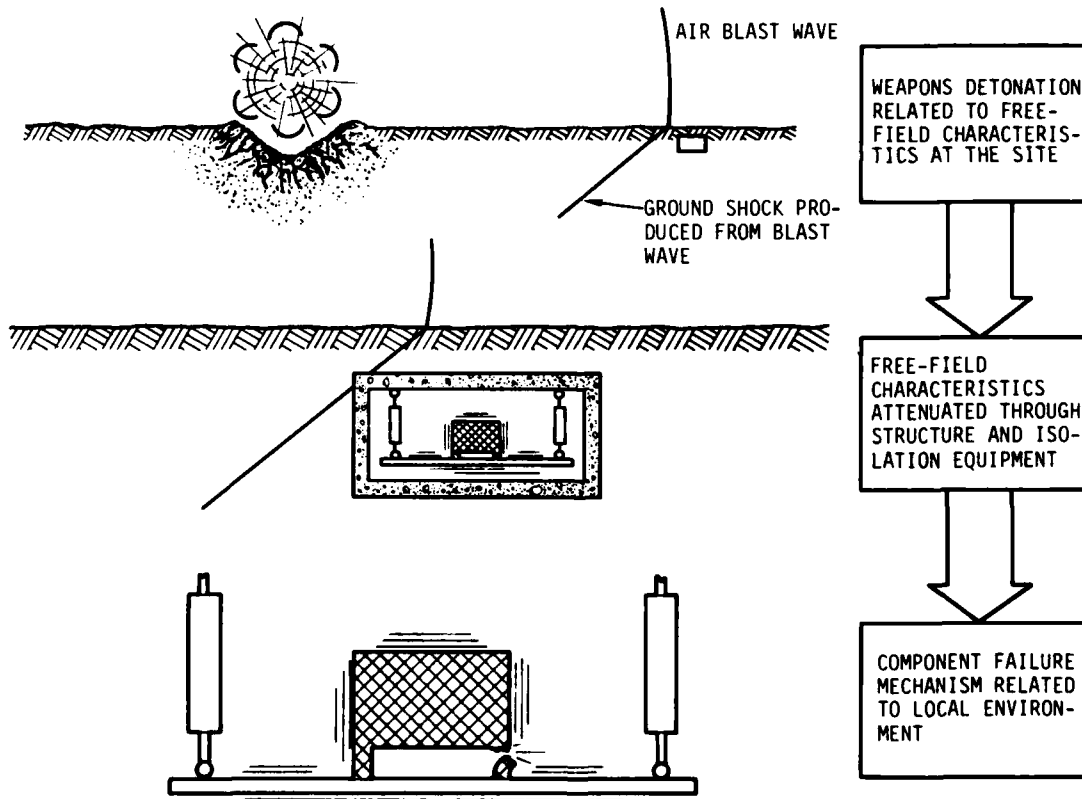


Figure 1. Tracing Weapons Effects to Component Failure

If $P(\)$ and $p(\)$ were simple and separable functions; e.g., $\alpha x_1 x_2 x_3 \dots$, it might be possible to integrate the above multiple integral, but it is not. Consequently a Monte Carlo technique [1] was selected to represent the expectation process. The flow diagram in Figure 2 shows the basic logical procedure to compute P_{fs} . This diagram

does not include the added sophistication of confidence intervals due to model (rather than data) uncertainty, multiple weapons, cumulative damage, etc. which are part of the various versions of the FAST program. However, it does identify the basic procedure which is fundamental to the concept.

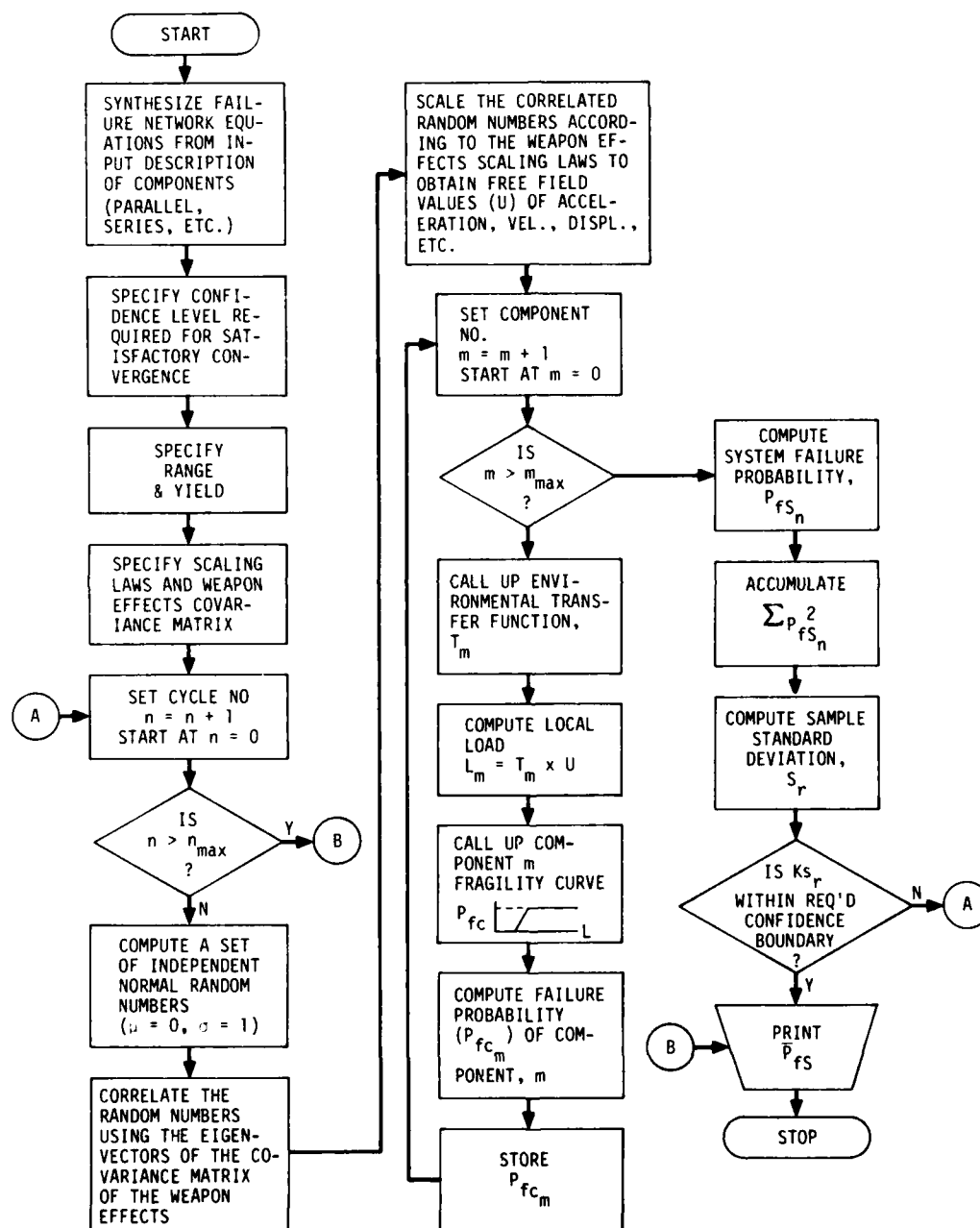


Figure 2. Flow Diagram of System Failure Analysis

IDENTIFICATION AND COMPUTATION OF SYSTEM AND SUBSYSTEM FAILURE MODES

The first step in the evaluation of system failure (or survivability) is the identification of the critical functions of the subsystem and components. If a component or subsystem fails and the system can still perform its functions, then there is less interest in including the component or subsystem in the analysis. Each subsystem is evaluated to determine its role in supporting that function. Redundancy which improves the reliability must be considered and treated in a proper sense.

The method which has been chosen in this study to systematically identify roles, redundancies, and failure modes is the fault tree. In the sequence of analysis steps, the fault tree precedes the reliability network in identifying causation and coupling which lead to system failure. The method is indifferent to the causation of the component failures and therefore some failures may not be due to the nuclear environment. In this case those non-nuclear modes will be removed from the analysis.

A fault tree is a graphical representation of the logic that relates failure to an undesired event. Descriptions of the method and application can be found in a number of texts, one of the more notable of which is the Handbook of System Safety by Hammer [7].

By recording combinations of events in a logic diagram, the technique lends itself readily to the use of probability estimates for elements, subsystems and systems being considered.

The steps used in applying the technique to this problem should be:

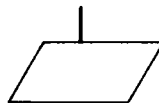
- define the undesired events,
- acquire complete understanding of the functions of the system and the roles of the components,
- construct the fault tree,
- collect quantitative data,
- identify the failure network, the component failure functions, and their failure inducing environments,
- prepare input to the system failure (FAST) program from the above steps.

A typical fault tree is shown in Figure 3 for a failure mode of a diesel engine operating in a hardened facility.

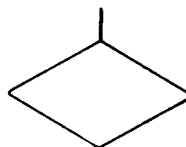
The definitions of symbols as used in this application are as follows:



The circle describes a probabilistic description of the environmental load, contamination, etc.



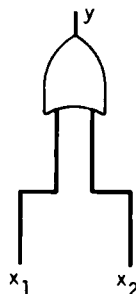
The parallelogram describes the computation of failure probability (using a fragility curve, matrix, etc.) based upon the level of the environment.



A fault event that is considered basic and the possible causes are not developed further, either because the data are available in that form, the event is of insufficient consequence, or the necessary information is unavailable.



Transfer symbol from another fault tree.



OR GATE describing the logical operation where any one of the inputs will cause the output event, i.e., failure of y would occur if x₁ or x₂ fail. The equivalent Boolean expression is

$$y = x_1 \cup x_2$$

or

$$y = x_1 + x_2$$

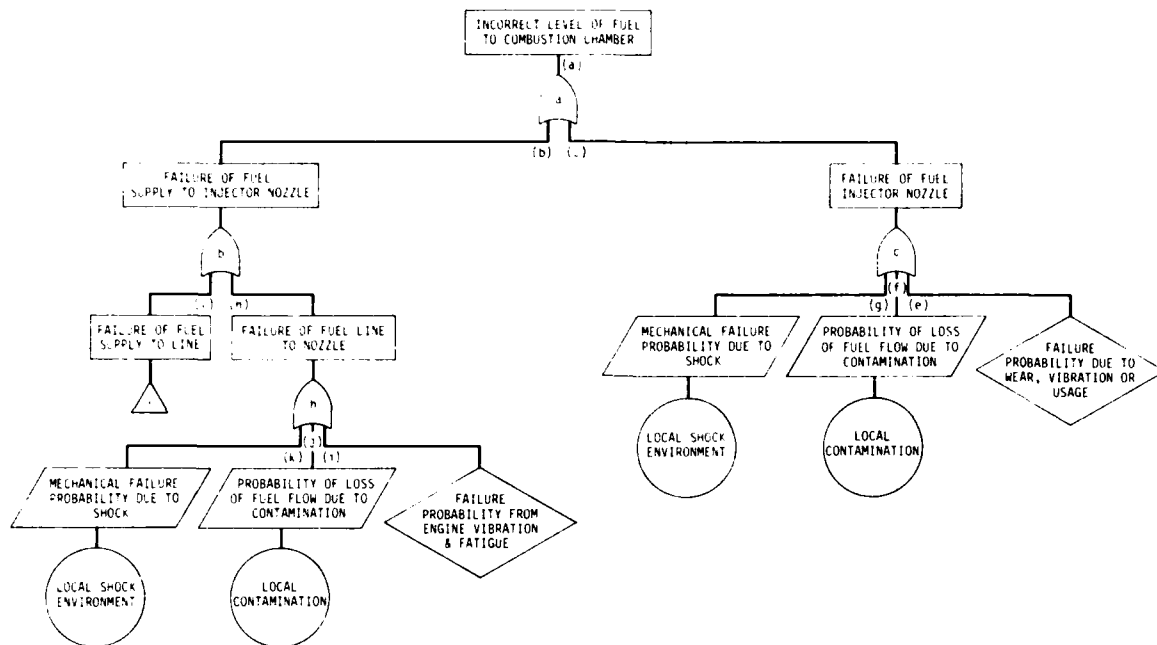
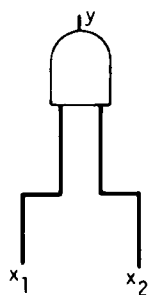


Figure 3. Fault Tree Describing a Cause for Diesel Engine Failure in the PARPP



AND GATE (not shown in Figure 3) describing the logical operation where all of the inputs must occur to produce the output event. The equivalent Boolean expression is:

$$y = x_1 \cap x_2$$

or

$$y = x_1 \cdot x_2$$

In the example, because of the exclusive use of OR Gates, the probability of failure takes the form shown in Equation (3).

$$P_f(a) = 1 - [1 - P_f(l)][1 - P_f(k)][1 - P_f(j)] \cdot [1 - P_f(i)][1 - P_f(g)][1 - P_f(f)] \cdot [1 - P_f(e)] \quad (3)$$

If only the nuclear effects are considered, the equation reduces to

$$P_f(a) = 1 - [1 - P_f(l)][1 - P_f(k)][1 - P_f(j)] \cdot [1 - P_f(g)][1 - P_f(f)] \quad (4)$$

IDENTIFICATION AND QUANTIFICATION OF COMPONENT FRAGILITY

A primary objective of the fault tree analysis is to locate and identify roles of components in the failure process. Once this is done, it is necessary to develop a characterization of the resistance of each component to levels of the critical weapon-induced environments. These environments are frequently dynamic, although there are exceptions such as the accumulation of debris which creates a static load or blockage in critical ducts.

The first step in fragility analysis is the description of the full range of environments which may influence the component. For example, this would mean that the environments must reflect the attenuations and amplifications which occur when the shock strikes and excites the structure and the energy is transmitted to the component. The discussion of the establishment of these local environments is included later in the paper.

The second step in the analysis is to model the motion of the component in these environments and determine the mode of failure; i.e., yield or fracture due to excessive load. Typical failures can be: (1) A shock-isolated platform could exceed the rattle space and bang the structure floor or wall. The banging would produce high local accelerations which could cause inertial loads which would lead to shearing of attachments or electrical connectors. (2) A hard-mounted component could be shaken so that inertial loads cause stresses exceeding attachment or operating element strength.

Situations such as the banging are dependent upon two dynamic measures, displacement (reaching the limit) and velocity (the velocity at the instant the limit is reached). In these situations failure is a joint function of the occurrence of two effects.

Fragility has usually been represented by a cumulative probability distribution function as shown in Figure 4. However, when combined effects lead to the failure, a single curve is insufficient. A modeling procedure suggested in Reference [5] represents the component fragility by two "sub-components" in parallel, one sensitive to displacement and the other sensitive to velocity. In this way the real component will fail only when both the displacement and the velocity have been exceeded. There have been reservations that this "sub-component" approach may not serve every situation. Consequently two-dimensional fragility functions are either built in or can be entered into the FAST programs [5,6] to accommodate other situations.

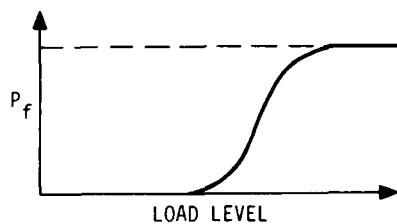


Figure 4. One-Dimensional Fragility

The only accurate way to obtain fragility information is to perform

many tests to failure. However, the cost of the components and systems is such that tests to failure are rarely made and, if so, only a few times. Most components are designed to survive in a specified environment and, when tested in that environment, survive. Therefore, the only real information available on a component is that its failure probability is either zero or very low for loads up to the specification load. Above that level, there is no information. Figure 5 shows the problem of the lack of data to develop the probability of failure function.

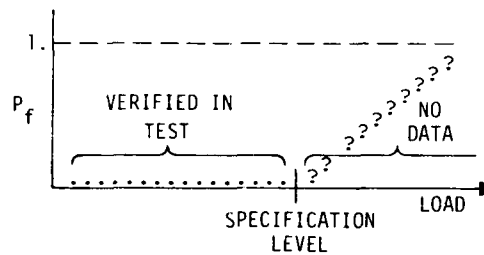


Figure 5. The Data Base for Most Fragility Curves

The discussion above is not a criticism of current practice because testing to failure is too expensive. But, because tests are made only to specification, we must live with the absence of real failure information. The question is how do we estimate the curve in the "no data" region of Figure 5?

The procedure to develop fragility curves analytically can be described by the flow diagram in Figure 6. The first step is the identification of an adequate deterministic model of response. Second, criteria must be established for failure (a maximum displacement, strain, stress, etc.). Then all component characteristics relevant to the deterministic response model must be examined for statistical variation. It is basically these variations plus some uncertainty in confidence in the model and the criteria which produce the uncertainty in failure probability as a function of level of load.

Once these inputs have been identified, a statistical approach can be used which will either by random sampling

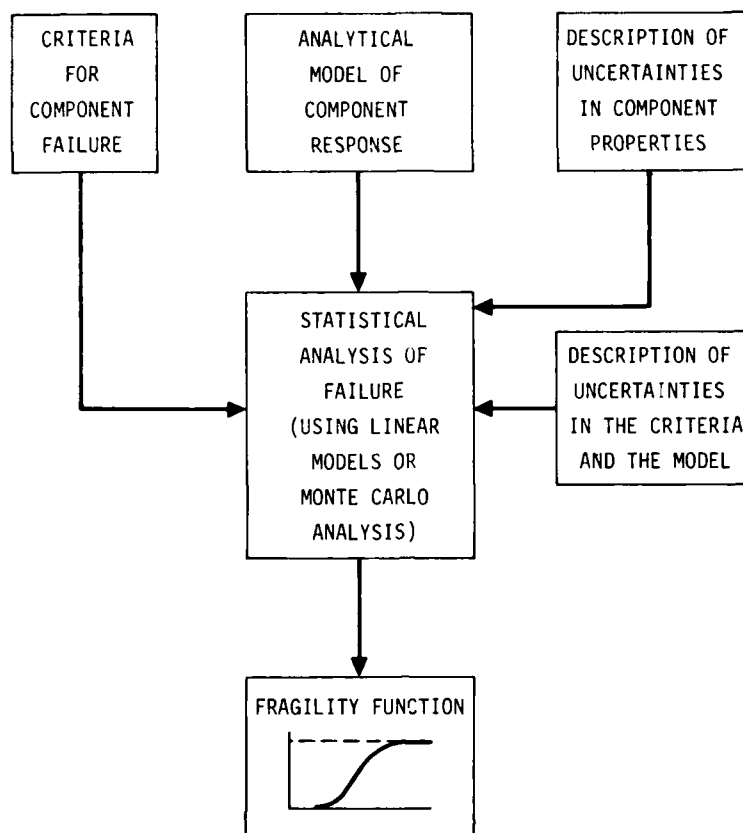


Figure 6. Fragility Function (Curve) Development Procedure

(Monte Carlo) or covariance propagation, produce the desired single or multivariate fragility function. An example of the Monte Carlo approach is presented in Reference [8] for buried cylinders subjected to ground shock. It was found that material properties alone contribute a failure level uncertainty of 15%.

DEVELOPMENT OF WEAPONS EFFECTS DATA

The primary mechanical weapon effects are air blast (overpressure and dynamic pressure), cratering ejecta and ground shock (direct induced, airblast induced and surface outrunning). For reasons of brevity and demonstration of uncertainty and correlation, this discussion will be limited to overpressure, dynamic pressure and direct induced shock.

Overpressure

The sudden release of energy in the nuclear detonation produces extremely hot gases which, in expanding very rapidly, create a very strong blast wave moving out radially from the source. The spherical expansion causes the shock to weaken as it moves and the peak overpressure decreases exponentially with time and distance.

In addition to the primary blast wave, a precursor wave can be formed under certain conditions. If the intense thermal radiation from a nuclear detonation impinges on a heat absorbing surface, a hot thermal layer is formed near the surface. Since the thermal radiation propagates faster than the air blast, the hot layer is formed ahead of the blast wave. The propagation velocity in this layer is higher than that of the blast wave in the

unheated atmosphere. Thus, under certain combinations of yield, height of burst and surface conditions, an additional wave, a precursor, may propagate ahead of the main shock. A full discussion of the blast wave and precursor formation is presented in References [9], [10] and [11].

The purpose of this discussion is to identify the elements of the blast wave and to establish the sources of data from which the time histories can be computed. It is important to note that the shape, period and intensity change with range, and the effect of the direct blast wave must either be computed directly or scaled as a function of range. An example is shown below in Figure 7 of the time history from the same weapon yield and height of burst, but at different ranges.

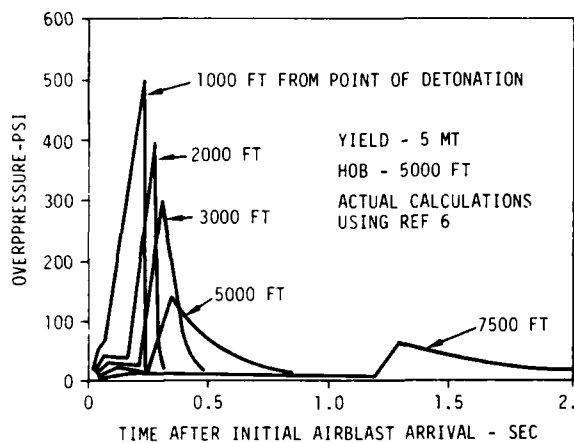


Figure 7. Time Histories of Overpressure for the Same Weapon at Various Ranges

Optimally, these time histories could be incorporated into structure-soil system dynamic analyses to compute the environment at each component directly. The peak local environmental loads could then be plotted as a function of range and fitted with a scaling law. Currently, the system survivability programs use simple exponential scaling laws of the peaks, such as:

$$\left(\frac{E}{E_0}\right) = \left(\frac{W}{W_0}\right)^\alpha \left(\frac{R}{R_0}\right)^\beta \exp\left\{-\gamma\left[\frac{H}{W^{1/3}} - \left(\frac{H}{W^{1/3}}\right)_0\right]\right\} \quad (5)$$

where α , β and γ are scaling factors, E_0 is the baseline value of the local environment, W_0 and R_0 are the baseline yield and range, and H is the height of burst.

Dynamic Pressure

The strong shock moving in still air has the effect of accelerating the air as it passes through it. This air moving parallel to the ground creates a very high wind and aerodynamic load on objects or structures which extend above the ground level. Dynamic pressure is computed by the formula

$$q = \frac{1}{2} \rho V^2 \quad (6)$$

Drag is computed by

$$D = \frac{1}{2} \rho V^2 C_D A \quad (7)$$

where ρ is the atmospheric density behind the shock, V is the air velocity behind the shock, C_D is the drag coefficient of the structure and A is normally the projected area normal to the direction of the airstream.

The dynamic pressure has a time-history shape similar to that of the overpressure, but not as spiked.

The drag on a structure can apply an overturning or a shear load. If dynamics of the structure can be ignored in consideration of shear, then peak dynamic pressure can be used and scaled directly from the peak overpressure using the Rankine-Hugoniot equations [11]. Since shock strength correlates directly with the air velocity following the shock, then peak overpressure and peak dynamic pressure are 100% correlated from a statistical point of view.

Drag coefficients (high Reynolds No.) are summarized for a variety of configurations in Reference [9]. This same document also describes in sufficient detail the procedures required to compute the loads on all faces of a structure.

Modeling Air Blast Uncertainty

The authors are quoted in Reference [9] as saying that overpressure and dynamic pressure can be predicted within a factor of two of the theoretical peak value. This would mean that the true value would range between one-half and twice the predicted value. If the logarithm of the value of overpressure is used, then the factors of two (or one-half) times the overpressure become

symmetrical about the predicted value (Figure 8).

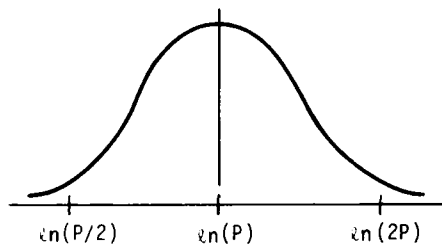


Figure 8. Distribution of Predicted Overpressure

$$z_{.95/2} = \frac{\ln 2p - \ln p}{\sigma_{\ln p}}$$

$$\sigma_{\ln p} = \frac{\ln 2}{z_{.95/2}} = \frac{.693}{1.96} = .354$$

As mentioned earlier for high overpressures, peak overpressure and peak dynamic pressure are 100% correlated, which means that one can be expressed as a coefficient of the other.

$$q = \beta p \quad (9)$$

However, drag on a structure consists of other factors which are independent of overpressure, such as drag coefficient and cross-sectional area. Thus

$$D = q C_D A = \beta p C_D A \quad (10)$$

Representative uncertainties in C_D and A can be expressed as 1.2 or 1/1.2 times the predicted value. Using logarithms again

$$z_{.95/2} = \frac{\ln(1.2C_D) - \ln(C_D)}{\sigma_{\ln C_D}} \quad (11)$$

and

$$\sigma_{\ln C_D} = \sigma_{\ln A} = .093$$

* Note in fact that the multiplier β may have some uncertainty associated with it too, but this uncertainty will be neglected in this example.

To establish the covariance between D and p , find the expected value of the products of their logarithms

$$\begin{aligned} \text{Cov}[\ln D, \ln p] &= E[\ln D \ln p] - E[\ln D]E[\ln p] \\ &= E[(\ln p)^2 + E[\ln C_D \ln p] \\ &\quad + E[\ln \beta \ln p] + E[\ln A \ln p] \\ &\quad - E[\ln D] E[\ln p]] \end{aligned} \quad (12)$$

Since p , C_D and A are all statistically independent and β is a constant, the expected value of the cross products vanish. Hence, after manipulation

$$\begin{aligned} \text{Cov}[\ln D, \ln p] &= \text{Var}[\ln p] - E[\ln p] \\ &\quad \times (E[\ln C_D] + E[\ln A]) \end{aligned} \quad (13)$$

If p , C , D and A are all non-dimensionalized (to factors) such that their mean values are one, then

$$\text{Cov}[\ln D', \ln p'] = \sigma_{\ln p'}^2 \quad (14)$$

and the covariance matrix for D' and p' is

$$\begin{aligned} \begin{bmatrix} \Sigma_{\ln D', \ln p'} \end{bmatrix} &= \begin{bmatrix} \sigma_{\ln D'}^2 & \text{Cov}[\ln D', \ln p'] \\ \text{Cov}[\ln D', \ln p'] & \sigma_{\ln p'}^2 \end{bmatrix} \\ &= \begin{bmatrix} .378^2 & .354^2 \\ .354^2 & .354^2 \end{bmatrix} \end{aligned} \quad (15)$$

where

$$\begin{aligned} \sigma_{\ln D'}^2 &= \sigma_{\ln p'}^2 + \sigma_{\ln A'}^2 + \sigma_{\ln C_D'}^2 \\ &= (.354)^2 + 2(.093)^2 \end{aligned} \quad (16)$$

The correlation coefficient between $\ln D'$ and $\ln p'$ in this case is

$$\rho = \frac{\text{Cov}(\ln D', \ln p')}{\sigma_{\ln D'} \sigma_{\ln p'}} = .937 \quad (17)$$

which means that although the two effects are not 100% correlated, they are very highly correlated.

A convenience of the log-normal distribution is that the uncertainties are dimensionless scale factors with median equal to one. Hence, the covariance matrix in Equation (13) can be used directly for any weapon-induced environment which is directly proportional to overpressure or drag. The covariance matrix can be a direct input into the system survivability program (Figure 2).

Direct Induced Ground Shock

The discussion to follow highlights some of the aspects of the modeling of uncertainty of ground shock without trying to develop detailed deterministic models. This is because the subject is far too complex to be covered fairly here and also because not all of the data necessary are available for unclassified discussion.

The ground shock problem divides into three areas: direct crater induced, airblast induced (superseismic) and surface outrunning. Discussion of all three of these phenomena is included in Reference [9]. This discussion will be restricted to direct induced shock.

Most of the data obtained from direct-induced ground shock have come from contained nuclear tests. Measurements were fairly abundant and the following equations and tables summarize the results from the data [9].

The peak values are generally represented by the following equations [9].*

$$\text{peak vel: } v = v_R \left[\frac{W}{\text{IMT}} \right]^{2/3} \left[\frac{R}{\text{lkft}} \right]^{-2} \quad (18)$$

$$\text{peak displ: } d = d_R \left[\frac{W}{\text{IMT}} \right]^{5/6} \left[\frac{R}{\text{lkft}} \right]^{-3/2} \quad (19)$$

$$\text{peak accel: } a = a_R \left[\frac{W}{\text{IMT}} \right] \left[\frac{R}{\text{lkft}} \right]^{-4} \quad (20)$$

The values for v_R , d_R and a_R for a variety of soil conditions and for contained and near surface bursts are given in Tables 1 and 2. Also included are uncertainty factors which are translated into standard deviations (log-normal) assuming a 95% confidence of these factors.

No covariance (or correlation) data were available from the tabulated information given in Reference [9] or [12]. These correlations could be obtained from reevaluation of the data used to develop the individual uncertainty

*A very comprehensive set of data is available in Reference [12] which may indicate some differences with these expressions for varying conditions and for airblast induced shock.

Table 1. Reference Values for Contained Bursts

	HARD ROCK	SOFT ROCK	ALLUVIUM
v_R , fps	200	80	20
UNCERTAINTY FACTOR	$\times 2.5$	$\times 2$	$\times 3$
σ_{1nv}	.47	.35	.56
d_R , fps	200	160	100
UNCERTAINTY FACTOR	$\times 2$	$\times 3$	$\times 4$
σ_{1nd}	.35	.56	.71
a_R , g	3500	600	120
UNCERTAINTY FACTOR	$\times 2.5$	$\times 5$	$\times 5$
σ_{1na}	.47	.82	.82

Table 2. Reference Values for Near-Surface Bursts

	HARD ROCK	SOFT ROCK	ALLUVIUM
v_R , fps	25	10	2.5
UNCERTAINTY FACTOR	$\times 2.5$	$\times 2$	$\times 3$
σ_{Inv}	.47	.35	.56
d_R , in.	4.5	1	.5
UNCERTAINTY FACTOR	$\times 2$	$\times 3$	$\times 4$
σ_{Ind}	.35	.56	.71
a_R , g	140	25	5
UNCERTAINTY FACTOR	$\times 2.5$	$\times 5$	$\times 5$
σ_{Ina}	.47	.82	.82

estimates. With no further information at this time, it can still be assumed that large peak velocities will be highly correlated with large peak displacements, etc. Hence, it is probably true that the correlation coefficients range from .75 to almost 1.00.

CORRELATION OF FREE-FIELD ENVIRONMENT TO LOCAL ENVIRONMENT

The transfer functions in the flow diagram of Figure 2 are merely scale factors which modify the free-field environment levels to the local environment levels where the critical components are located. In the past these scale factors have been constants which meant that the scaling of local environment to free-field was linear with environmental level. It is possible, particularly in the case of dynamic response to shock, that this linear scaling may be inadequate and a more elaborate analysis may be necessary. Development of the scale factors arises directly from the formulation of the load equations. Where shock spectra are used, structural dynamic analyses are needed to relate the free-field load to the local response.

In the dynamic case, where input forces are uncertain and complex, and the dynamic system (structure, soil medium, shock isolators, etc.) is complex, transfer functions may not offer an adequate means of specifying the local environments. In this situation, a desirable approach is to model the entire system and shake it with the spectrum of inputs and evaluate the resulting local responses statistically. This would mean bypassing the transfer function entirely and creating a set of

weapon induced effects and covariances for each local condition which would scale in some way with range and perhaps yield. A proposed solution would use finite element models of the building and the surrounding soil initially and a system dynamic program such as DYNALIST II [13] to perform the synthesis and response analysis. This approach permits very complex modeling (thousands of degrees of freedom) but, by judicious selection of generalized coordinates and the inclusion of a full damping matrix, reduces the problem to a workable size and still takes into account all the problems of phasing and heavy damping.

COMMENT

Statistical modeling is not a panacea to cover all the problems of poor deterministic models. Good statistical models arise from good deterministic models. Therefore any future system survivability (failure) analysis should be developed from a well conceived deterministic simulation. Then uncertainty can be introduced and the final objective be achieved.

ACKNOWLEDGMENT

The work supporting this paper was performed at the J.H. Wiggins Company under Contract DACA 39-75-M-0295 with the U.S. Army Engineer Waterways Experiment Station, Weapon Effects Laboratory.

REFERENCES

1. J.D. Collins and P.B. Grote, "Ground System Vulnerability Analysis," Technical Report No. 01615-6003-R000, TRW Systems Group, Redondo Beach, CA, May 1968
2. J.D. Collins and P.B. Grote, "Ground System Vulnerability Analysis," Proceedings of the ASCE-EMD Specialty Conference, Purdue University, Lafayette, Indiana, November 1969
3. W.H. Rowan, "Recent Advances in Failure Analysis by Statistical Techniques (FAST), prepared for 46th Shock and Vibration Symposium, San Diego, CA., September 1975
4. W.H. Rowan, "Hardness Evaluation," The Shock and Vibration Bulletin, December 1970.
5. W.H. Rowan, et al., "Failure Analysis by Statistical Techniques (FAST)," DNA 3336F-1, TRW Systems Group, Redondo Beach, CA, October 1975
6. J.D. Collins and Bruce Kennedy, "MX-FAST Computer Program Description," Technical Report No. 75-3031-1, J.H. Wiggins Company, Redondo Beach, CA, July 1975
7. Willie Hammer, Handbook of System and Product Safety, Prentice-Hall, inc., Englewood Cliffs, N.J., 1972
8. D.E. Evensen and J.D. Collins, "Test Planning with Uncertainty," Technical Report No. 76-1270, J.H. Wiggins Company, Redondo Beach, CA, August 1976 (to be released through DNA as DNA 4099F)
9. Robert E. Crawford, Cornelius H. Higgins, and Edward H. Bultman, "The Air Force Manual for Design and Analysis of Hardened Structures," Civil Nuclear Systems Corporation, Doc. No. AFWL-TR-74-102, Air Force Weapons Lab., Kirtland Air Force Base, New Mexico, October 1974
10. H.L. Brode, "Height of Burst Effects at High Overpressures," RM6301, The Rand Corporation, Santa Monica, CA, July 1970
11. "Air Blast Loading in the High Shock Strength Region, Part II, Prediction Methods and Examples," DASA 1460, Defense Atomic Support Agency, Washington, D.C., February 1965.
12. N. Lipner, D.C. Anderson and P.K. Dai, "Ground Motion Environments for Generic Site Conditions," DNA Contract No. 001-74-C-0249, TRW Systems Group, Redondo Beach, CA, December 1975
13. T.K. Hasselman, A. Bronowicki, and G.C. Hart, "DYNALIST II, A Computer Program for Stability and Dynamic Response Analysis of Rail Vehicle Systems," Vol. I, II, Rept. No. 74-1208, J.H. Wiggins Company, Redondo Beach, CA, June 1974

SHOCK TESTING

LABORATORY SIMULATION OF SEQUENTIAL SETBACK AND AERODYNAMIC DRAG
EXPERIENCED BY ARMY ORDNANCE PROJECTILES -- A DEVICE, THEORY AND DATA

Dr. Irvin Pollin
Harry Diamond Laboratories
Adelphi, Maryland

Various testers are used at the Harry Diamond Laboratories to provide simulation of artillery interior ballistic environments (setback, angular acceleration) and exterior ballistic environments (spin, aerodynamic drag). This paper describes the work performed to combine setback and drag into a single laboratory tester in order to simulate these environments sequentially, as they would occur in a real launch. A variety of pulse shapes have been obtained (in this simulator and in other simulators used for setback only) with peak accelerations of 300 to 100,000 g at impact speeds up to 1500 fps and energies up to 55,000 ft-lb. The present tests attained maximum setbacks of 5000 g with a pulse duration of 1.5 ms. A "steady" state drag commenced within 4 ms of the completion of setback and aerodynamic drag up to 30 g was simulated for periods up to 20 ms. Good agreement between test and predicted data was found for both setback and drag. Independent of setback, the simulation of aerodynamic drag can readily be extended to larger drags, longer time periods, or specific drag-time profiles. Data are presented on simulator tests of an Army fuze mechanism, which requires both setback and drag to arm.

1. INTRODUCTION

In the simulation of sequential setback and aerodynamic drag, the projectile (called a bird), having equipment on board to be test evaluated, emerges from a launcher (typically an air gun) and impacts an aluminum honeycomb or wooden mitigator located between the bird and a momentum exchange mass (MEM). The equipment in the bird is mounted so that the impact simulates the setback pulse (acceleration-time trajectory) that occurs in the weapon launcher. The drag signature is simulated thereafter, as is later described. Test data of the bird displacement as a function of time are obtained by a streak photograph, from which setback and drag are determined by double differentiation. The conservation equations of mass, momentum, and energy are solved exactly to obtain the forces acting on and the motions of the bird, mitigator, and MEM as functions of time.

The setback is comprised of essentially three parts: rise, steady, and fall. The rise and steady parts occur during the crushing of the mitigator, and their characteristic features are determined primarily by the bird mass and by the shape, dynamic crush strength and mass density of the mitigator. The fall is controlled primarily by the elasticity of the components at maximum mitigator crush; this may include elasticity intentionally introduced

into the system by incorporating springs into the MEM. By this means, parabolic, trapezoidal, and other pulse shapes have been obtained.

The drag simulation is obtained as follows: The bird emerges from the air gun and impact occurs within an open-ended catch tube of circular cross section, figs. 1a and 1b. (The bird and MEM are circular cylinders). The bird forms a close fit with the inner wall of the catch tube. However, the diameter of the MEM is selected to obtain a desired air leakage into the cavity formed by the bird, tube, and MEM. (The mitigator diameter is small enough not to obstruct air flow between the bird and MEM). The setback pulse is designed so that the bird velocity at the completion of setback is approximately zero, and the bird momentum is transferred to the MEM. The MEM motion increases the length of the cavity, causing the cavity pressure to drop, and gives rise to a pressure differential across the bird. The bird acceleration, or drag simulation, is therefore determined primarily by the relative motion between the bird and MEM, the cavity volume, the air leakage into the cavity, and the bird mass. The MEM mass is much larger than the bird mass so that little change in the MEM speed occurs during drag simulation. Pressure buildup in

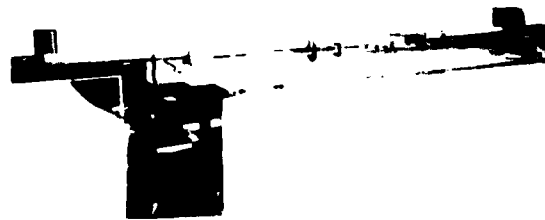


Figure 1a Setback drag simulator

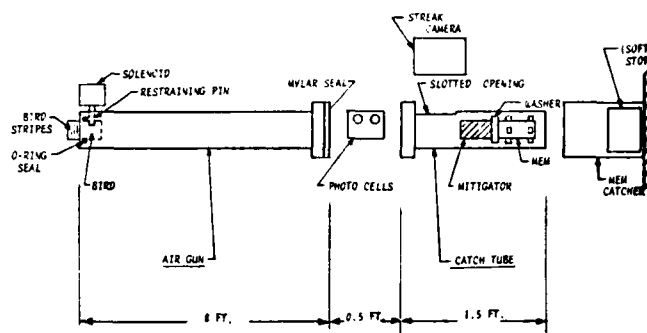


Figure 1b Setback drag simulator (schematic)

the cavity during setback is minimized by the longitudinal slotted opening to the atmosphere in the catch tube that extends from the point where the bird enters the tube to a position near where the bird impacts the mitigator. The drag profile is not significantly changed by moderate variations of the initial cavity volume and pressure.

2. DESIGN OF THE SIMULATOR

In the present tests, an HDL 2.5-in.-diam. x 8-ft-long air gun was used in combination with a 2.5-in.-diam. x 1.5-ft-long catch tube to provide the sequential simulation of setback and drag environments (figs. 1a and 1b). The air gun is sealed at one end by the bird and by a 0.002-in. mylar diaphragm at the other end. A vacuum of about 1 torr is drawn in the space between the seals and, upon release of a restraining pin, the bird is driven the length of the gun and into the catch tube by atmospheric air. In each of 30 tests, the 1.17-lb bird emerged from the gun at a speed of

155 ± 5 fps (table I). In order to avoid any effects on drag by the air flow following the bird down the air gun, the first contact of the bird with the mitigator occurs when the bird is completely inside the catch tube and the gun and catch tube are separated by a distance of 6 in. The bird setback is caused by the crushing of the mitigator, which is located just aft of the slotted opening and which is in physical contact with the MEM. Both the mitigator and the MEM are at rest prior to impact. For a nonelastic MEM (consisting only of a mass without springs), the ratio of MEM to mitigator masses is of the order 100, and the ratio of MEM to bird masses is about 10 for aluminum honeycomb and about 5 for wood mitigators.

The aims of the present tests were to evaluate the simulator and to simulate the setback and drag environments experienced by an arming mechanism being developed for use in Army ordnance projectiles. To this end, the bird was made of Bakelite™, with a diameter of

TABLE I - SUMMARY OF TEST VALUES
USED IN THE SIMULATION OF DRAG
AND SETBACK

Shot No.	Bird Weight lb.	MEM Weight lb.	Washer Diameter in.	Cavity Leakage Area in ²	Impact Speed fps	Bird Speed fps	MEM Speed fps	Mitigator
99	1.17	4.83	2.483	.117	156	-.6	37.9	Wood
100	1.17	4.83	2.483	.117	160	-1.3	38.8	Wood
101	1.17	4.83	2.451	.241	155	.6	36.7	Wood
102	1.17	4.83	2.451	.241	-	.8*	36.7*	Wood
104	1.17	4.83	2.451	.241	-	.8*	36.7*	Wood
105	1.17	4.83	2.451	.241	150	1.5	35.6	Wood
107	1.17	4.83	2.401	.432	157	3.0	37.3	Wood
108	1.17	4.83	2.401	.432	156	3.7	36.9	Wood
109	1.17	4.83	2.350	.622	156	3.5	36.9	Wood
110	1.17	4.83	2.350	.622	157	3.6	37.1	Wood
111	1.17	4.74	2.000	1.443	153	3.8	36.8	Wood
112	1.17	4.74	2.000	1.443	153	3.2	36.9	Wood
113	1.17	11.16	2.483	.117	155	-3.6	16.6	Aluminum
114	1.17	11.16	2.483	.117	154	-3.0	16.4	Aluminum
116	1.17	11.16	2.401	.432	155	3.8	15.8	Aluminum
117	1.17	11.16	2.401	.432	-	4.2	15.8*	Aluminum
118	1.17	11.16	2.401	.432	156	3.6	15.8	Aluminum
119	1.17	11.16	2.451	.241	155	1.1	16.0	Aluminum
120	1.17	11.16	2.451	.241	155	1.1	16.0	Aluminum
121	1.17	4.74	2.00	1.443	155	4.7	37.1	Wood
122	1.17	4.74	2.00	1.443	157	4.1	37.7	Wood
123	1.17	4.83	2.350	.622	155	3.3	36.7	Wood
124	1.17	4.83	2.350	.622	155	3.2	36.7	Wood
125	1.17	4.83	2.401	.432	157	3.3	37.2	Wood
126	1.17	4.83	2.401	.432	157	3.2	37.2	Wood

2.483 in. at the impact section and length of 6 in. (fig. 2). As shown, the bird diameter aft of the impact section was reduced by 0.06 in. so that a stripe pattern attached to the bird did not make physical contact with the wall of the gun or catch tube. (A streak photo of the stripes gives displacement-time data from which the bird setback and drag are obtained by double differentiation). The interior of the bird accommodated two arming mechanisms (fig. 2).

The aluminum honeycomb mitigators had a static crush strength of 2000 psi; each was a cube with a 1.5-in. edge. A light plastic foam strip was taped around each aluminum mitigator to center the mitigator with the axis of the catch tube (fig. 3). The wood mitigators (four marine grade, 3/4 in. fir plywood sections held together with masking tape) fitted snugly into the tube and were 2.9 in. long with an equilateral triangular cross section having an area of 2.0 in.² (fig. 3).

The top and bottom photos show the mitigators before and after impact. To attain approximately zero bird speed following setback, the required weights of the MEM's were 4.83 lb for the wood mitigator and 11.16 lb for the aluminum honeycomb mitigator. (The MEM weights are different because the elasticity of the two mitigators is different). The MEM's consisted of 2-in.-

diam. brass bars with 4 legs at each end (fig. 4). On placing the MEM in the catch tube, the centerline of each MEM was coincident with the axis of the tube.

In the present tests, for the fixed bird and MEM masses, fixed initial relative motion between bird and MEM following setback, and insignificant variations of cavity pressure and volume (with respect to their effect on drag), the drag was determined by controlling the air leakage into the cavity. To accomplish this, an aluminum washer of desired diameter was screwed to the impact end of the MEM (fig. 4). Each washer weighed about 0.09 lb and the mitigator was placed in physical contact with the washer. Air leakage was determined by the size (diameter) of the washer (taking into account the small leakage past the bird into the cavity).

3. COMPUTER PROGRAMS

The computer codes in section 7 are presented for the computation of setback acceleration (code SETBACK for the aluminum mitigator only), which is an adaptation of the computer code VARYB, case A, of Pollin, (Ref 1) and for the computation of the acceleration caused by aerodynamic drag (code DRAG) for both aluminum and wood mitigators. SETBACK is based on the conservation equations for continuity, momentum, and energy. No computer code is available for wood mitigators; here, setback

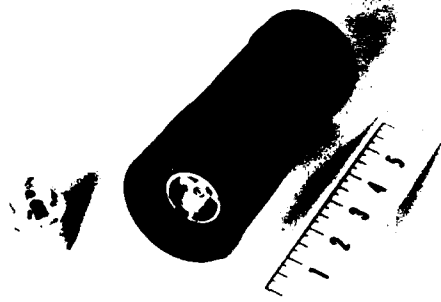


Figure 2 Bird, and safety and arming device



Figure 3 Aluminum honeycomb and wood mitigators

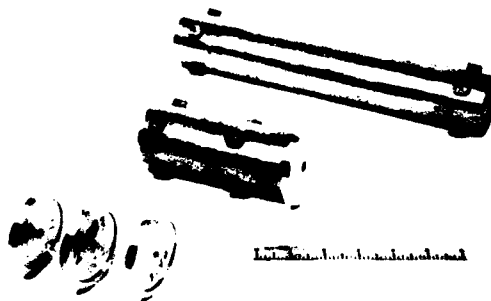


Figure 4 MEMs and washers

designs were based on unpublished HDL experimental data. The termination of the mitigator crush occurs when $U_1=U_2$ at the time denoted by $T=TC$. The elasticity in the mitigator produces additional setback for a time interval at $T>TC$. Empirical data indicate that a linear spring constant formulation yields the proper additional setback acceleration and the time at which setback terminates. The spring constants for the aluminum and wood are based on equal displacements at each end of the mitigator of $C_1=C_2=0.01$ (aluminum) and $C_1=C_2=0.06$ in. (wood) at the time $T=TC$ and for the load acting on the mitigator at that time. To facilitate the recording of streak photo data, the tests were designed so that the bird velocity $U_1 \approx 0$ at the termination of setback. For this condition, the above spring constants were used in SETBACK to determine the appropriate MEM mass for both the aluminum and wood mitigators.

Maximum setback loading is at least 100 times larger than that for aerodynamic drag, and the setback pulse fall occurs in less than 400 μ s; see figs. 5 and 6. Thus, the setback and drag parts of the pulse are clearly distinguishable. The termination of setback marks the commencement of drag. However, because of the reduction of the cavity volume, the cavity pressure rises to about 20 psi during setback (see section 4). Hence, in the computations, the commencement of drag is assumed to occur at the time during the pulse fall where the streak photo data yield $A_1 = -22$ g; this is the bird acceleration caused by a cavity pressure of 20 psi in the absence of setback. The streak photo data give the value of U_1 at the commencement of drag and momentum conservation yields the corresponding value for the MEM velocity, U_2 . The measured length of the crushed mitigator is used to denote the distance separating the bird and MEM at the commencement of drag, from which the corresponding volume of air in the cavity is determined.

3.1 SETBACK FOR ALUMINUM MITIGATORS

The impact of the bird with the mitigator (which is attached to and at rest with the MEM inside the catch tube -- fig. 1b) initiates crushing of the mitigator at its interface with the bird. The crush front, which is the boundary separating the crushed and uncrushed mitigator masses proceeds toward the MEM during crushing.

The dynamic crush force is given by Pollin (Ref 1).

$$F = 1.05 F_0 (1 + 0.5 (U_1 - U_2)/U_0).$$

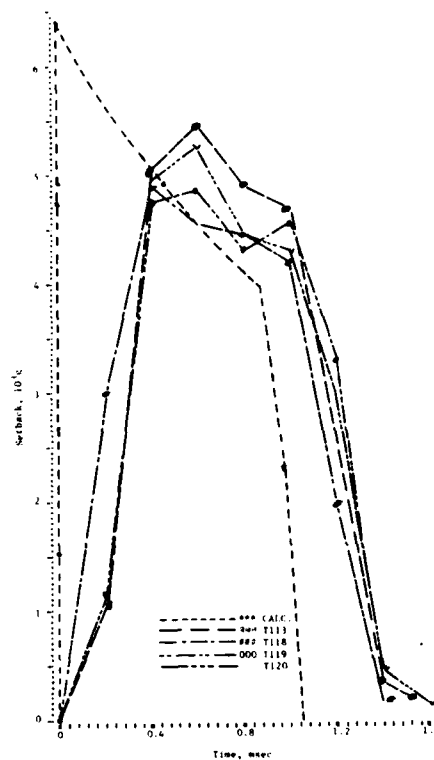


Figure 5 Comparison of calculated and experimental setback data for aluminum honeycomb mitigators. Shots 113, 118-120

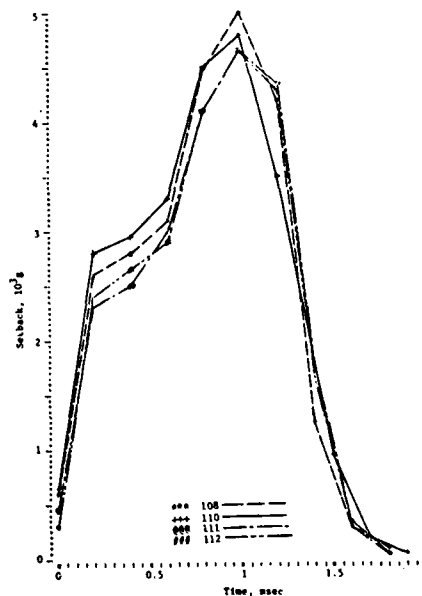


Figure 6 Experimental setback data for wood mitigators. Shots 108; 110-112.

The hydrodynamic crush force arising from acceleration of mitigator mass at the crush front is given by

$$R = \dot{M}_4 (U_1 - U_2)$$

where the time rate of mitigator crush is given by

$$\dot{M}_4 = \rho A S (U_1 - U_2).$$

The force (F+R) is transmitted to the mass (M1+M4), so that the setback acceleration experienced by the bird is

$$(1) A_1 = -(F+R)/(M_1+M_4).$$

The dynamic force F is transmitted to the mass (M2+M5), so that the MEM acceleration is

$$(2) A_2 = F/(M_2+M_5).$$

The spring constants of the mitigator, Z1=Z2, are determined at the time T=TC by the mitigator displacements C1=C2=0.01 and the force 1.05 F0 acting on both M1 and M2. No elasticity is assumed for T<TC, and setback ends when the forces acting on M1, M2, and M3 are simultaneously zero. Accordingly, for T>TC to the time at which A1=A2=A3=0, the bird and MEM accelerations were computed from the relations

$$(3) A_1 = -Z_1 X_1 / M_1 \text{ and}$$

$$(4) A_2 = Z_2 X_2 / M_2.$$

Computed values for the bird and MEM velocities and displacements were obtained by single and double integrations of the equations for A1 and A2.

3.2 DRAG

The drag force is determined entirely by the cavity and the ambient atmospheric pressures acting on the bird face. For the reasons discussed in section 4, it is sufficient to assume that the initial volume for the air in the cavity was 4.92 in.³ and the initial cavity air pressure was 20 psi for all test conditions. Table I shows the initial bird and MEM speeds for each test. The cavity pressure changes as a result of the air leakage into or out of the cavity and the change of the cavity volume arising from the relative motion between the bird and MEM. Incompressible air flow is assumed at a temperature of 530 °R and the leakage velocity U7 is computed from the relation

$$(5) U_7 = C \sqrt{2|P_0 - P|/D_7}, \text{ where}$$

C = 1 for Bernoulli (frictionless) incompressible flow, and

C = 0.5 for incompressible flow with friction.

The actual air leakage can be expected to have a value of C in the range 0.5<C<1. The mass rate of flow into or out of the cavity is given by

$$R_7 = D_7 U_7 A_7.$$

The cavity pressure is the sum of the partial pressures of the initial air in the cavity and the air leakage. The code DRAG computes the above quantities at small time intervals during the aerodynamic drag phase.

4. THEORETICAL AND EXPERIMENTAL RESULTS

Table I summarizes the tests run for setback and drag for the two types of mitigators and for the washer diameters of 2.483, 2.451, 2.401 and 2.350 in. Tests were also run without any washers, so that the obstructed area was that of the MEM cross section. The MEM has a diameter of 2.000 in. to which must be added the projected area 0.375 in.² of the four legs at each end of the MEM. The catch tube and bird diameters measured 2.503 and 2.483 in., which resulted in a leakage area of 0.0783 in.². The area A7 is the sum of the leakage areas about the bird and washer/MEM into the cavity. The table also gives the streak photo values for U0 and U1, and the values for U2 computed from momentum conservation. Both U1 and U2 are for the time denoting the termination of setback.

4.1 SETBACK

The streak camera was run at a comparatively slow speed so that both setback and drag could be recorded on a single photo. The photo covered a period of 20 ms, of which only about 1.5 ms consisted of setback. The setback displacement-time data was taken at 200 μs intervals. These time intervals are large compared with the setback pulse duration, so that the reduced data "smoothes" the actual pulse shape. Notably, the rise and fall times are lengthened and the A1_{max} is decreased.

Fig. 5 shows the reduced experimental setback data of four typical tests for A1 with aluminum honeycomb mitigators. If one allows for an uncertainty (shift of the time axis) of 50 μs in determining the beginning of the test pulse, the differences between experimental data are generally within about 10 percent of the average value of the A1 data for the given time. Fig. 5 also shows the calculated values for A1 based on the work of Pollin (Ref 1). Recalling that the experimental displacement data is read at 200 μs intervals, clearly, the calculated and experimental data can be brought into good agreement.

Fig. 6 shows typical experimental setback pulses with wood mitigators. The wood and aluminum mitigators yielded approximately equal peak accelerations, although the

wood gives longer pulse durations. Of course, having the same value for U_0 and approximately zero terminal velocity, the two sets of pulses have the same "area under the curve" since

$$U_0 = \int_0^{T_S} A_1 dt$$

where $T=T_S$ is the time of the setback pulse. The pulse time is larger for the wood mitigator because its curve is less rectangular. The test-to-test repeatability of A_1 for the wood mitigators is about the same as that noted above for the aluminum.

A reliable measure of the test data precision (which differs from that for drag) is given by the fluctuation of the data during the free flight bird travel over a distance of approximately 1.5 in. before setback begins. Accordingly, the average random error in determining setback velocity and acceleration was found to be 1 fps and 200 g.

4.2 DRAG

The bird velocity is generally less than 10 fps during the entire drag phase. To determine the measurement precision, three streak photos were obtained with the bird at rest. (That is, the bird was inserted into the slotted opening of the catch tube -- which is in the camera field of view -- and three streak photos were taken with the bird at rest in the same way as for an actual test for setback or drag). The test data precision is given by the fluctuation of the data for this condition. The average random error in determining velocity and acceleration during the drag phase was found to be 0.1 fps and 1 g. A few measurements were found to be in error by 2 g and one error amounted to 3 g. The timewise point-by-point fluctuation of the drag acceleration with the bird at rest is shown in figure 7. Although reduced test data of bird displacement were taken at time intervals of 400 μ s, calculations for the acceleration were made at intervals of 800 μ s, or four times larger than those used for setback. The test data shown in figure 7 are shown separated at 400 μ s intervals. This results from the fact that two overlapping sets of data points at 800 μ s time intervals, separated by 400 μ s, were prepared from each photo.

On the average, the wood and aluminum mitigators were each crushed 0.7 in. The variation of crush above or below 0.7 in. was within 5 percent. This is consistent with the previously noted less than 10 percent variation of setback acceleration. The initial bird impact with the mitigator occurred 0.25 in. aft of the slotted opening of the catch tube. Starting from the bird position at the edge of the slotted opening, the volume of air in the cavity was 9.99 and 5.44 in.³ for the wood and aluminum mitigators, respectively. At the termination of setback, the air volumes were 6.40 and 3.48 in.³. Thus, for both mitigators,

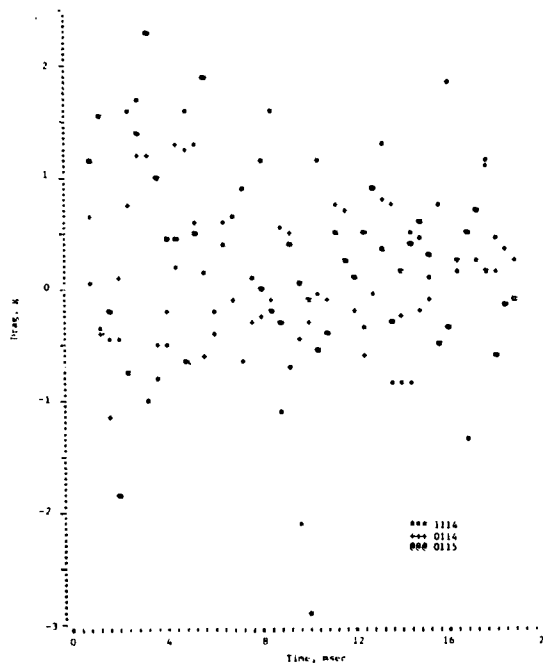


Figure 7 Precision of drag measurements

the compression ratio was 1.56. Assuming no leakage, isentropic or isothermal compression yields cavity air pressures of 27.4 or 22.9 psi. However, up to the termination of setback, there is a time interval of about 1.5 ms for leakage to occur, and the corresponding amount of the reduction of the cavity pressure depends on A_7 . If we assume a cavity volume of 4.92 in.³ (so that, in the absence of the mitigator, $L_0=1$ in.), table IIa shows the drag induced $A_1(T)$ for incompressible frictionless flow with cavity pressures at the beginning of drag of 20 and 30 psi for A_7 values of 0.117 and 1.068 in.². There is a small effect of cavity pressure on A_1 up to about 5 ms for $A_7=0.117$ and negligible effect on A_1 beyond 1 ms for $A_7=1.068$ in.². The net time effect is further reduced if we take into account the time required for setback.

The cavity volumes at the beginning of drag for the wood and aluminum mitigators were 1.3 and 0.7 times larger than the volume 4.92 in.³. If one assumes an initial cavity air pressure of 20 psi, table IIb gives the drag induced $A_1(T)$ for incompressible frictionless flow with L_0 values of 1.3 and 0.7 (corresponding values of L_0 for the above volumes) and for A_7 equal to 0.117 and 1.068 in.². The effect of initial cavity volume on A_1 is approximately the same as that found above for initial cavity pressure.

In the following comparisons between the predicted and experimental drag acceleration data given in figs. 8-15, the initial cavity air pressure and volume were taken as 20 psi

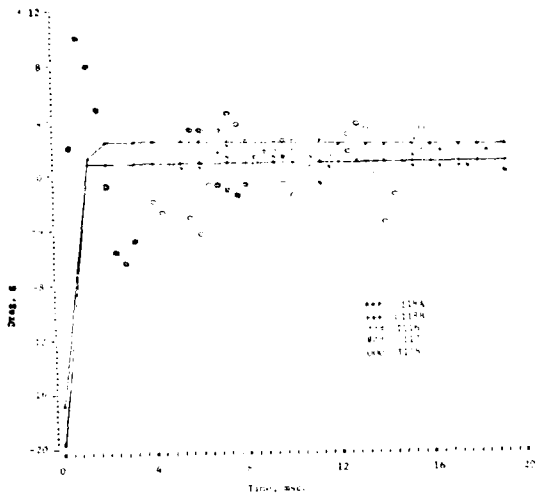


Figure 8 Comparison of calculated and experimental drag data with aluminum honeycomb mitigator. A7=.432 Shots 116-118

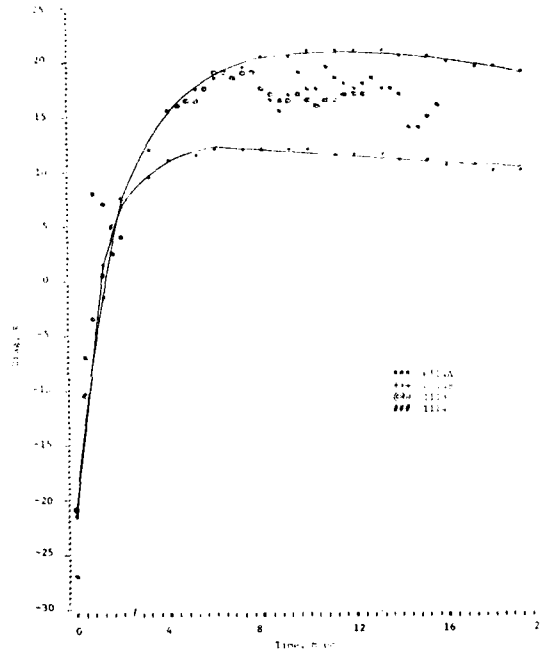


Figure 10 Comparison of calculated and experimental drag data with aluminum honeycomb mitigator. A7=.117 Shots 113, 114

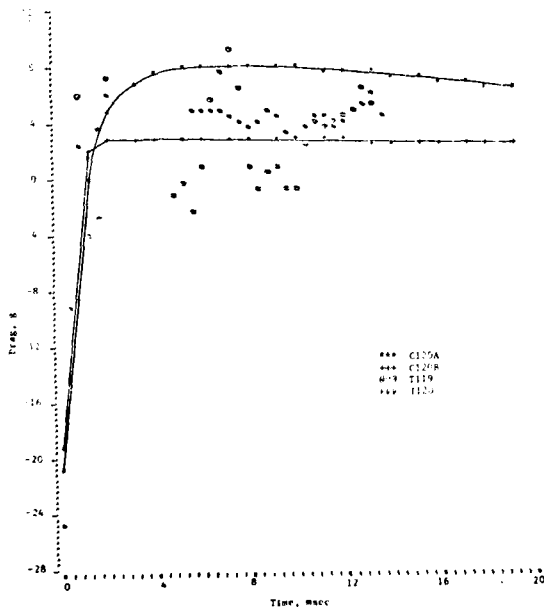


Figure 9 Comparison of calculated and experimental drag data with aluminum honeycomb mitigator. A7=.241 Shots 119, 120

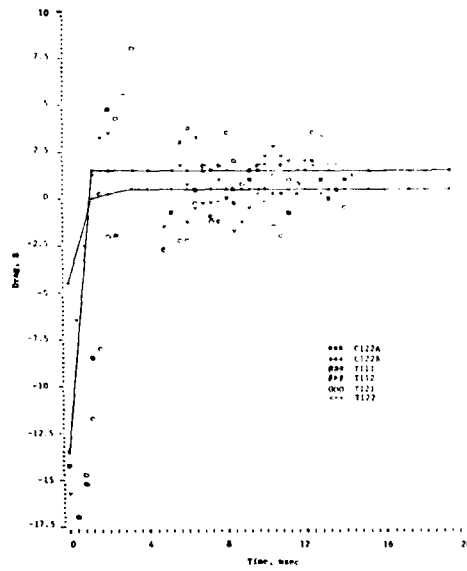


Figure 11 Comparison of calculated and experimental drag data with wood mitigator. A7=1.443 Shots 111, 112, 121, 122

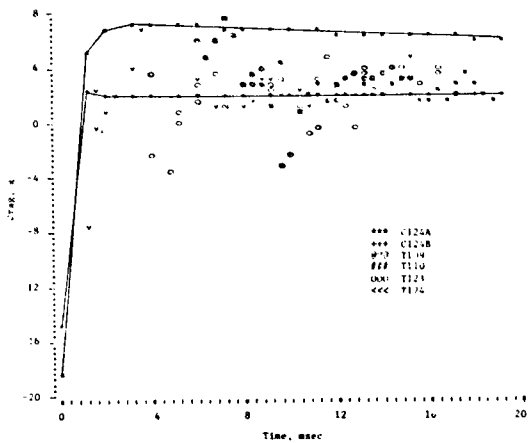


Figure 12 Comparison of calculated and experimental drag data with wood mitigator. $A7=.622$
Shots 109, 110, 123, 124

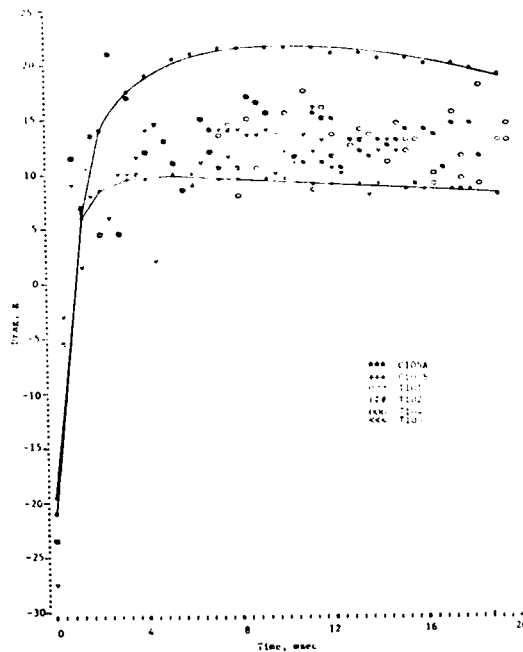


Figure 14 Comparison of calculated and experimental drag data with wood mitigator. $A7=.241$
Shots 101, 102, 104, 105

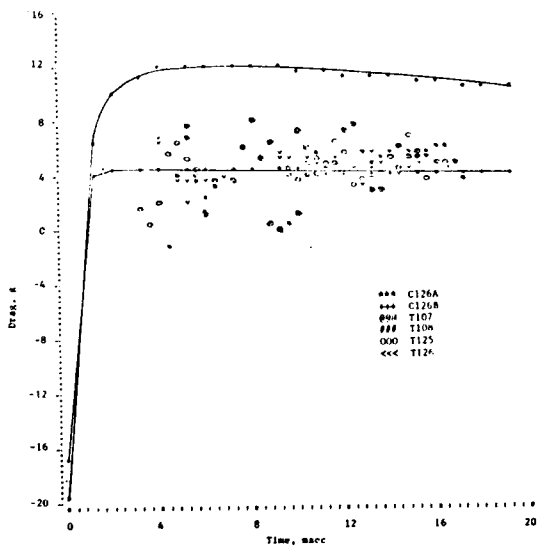


Figure 13 Comparison of calculated and experimental drag data with wood mitigator. $A7=.432$
Shots 107, 108, 125, 126

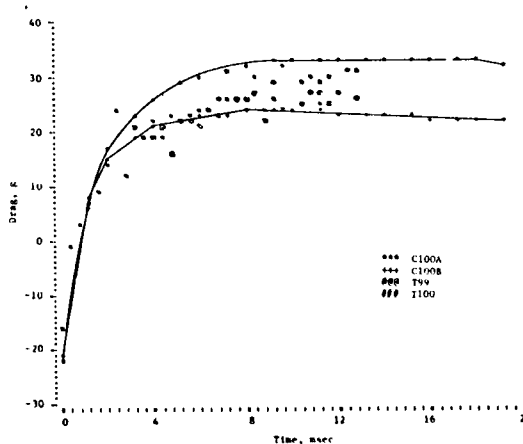


Figure 15 Comparison of calculated and experimental drag data with wood mitigator. $A7=.117$
Shots 99, 100

setbacks attained are assumed to be the same as those shown in figs. 5 and 6.* However, the diameter of the new bird was slightly smaller, so that the A7 value associated with each washer was slightly larger. Drags up to 9 g were obtained. The shapes of the drag pulses are shown in figs. 8 through 15. Streak photo data were available for a total time of 20 ms for each test, including setback. The calculated drag pulse duration (corresponding to the MEM speed and the time required for the washer to exit the catch tube) for the wood and aluminum mitigators was 21 and 91 ms, respectively.

Table III summarizes the test results on the S&A device. In all tests, the setbacks shown in figures 5 and 6 caused the device to proceed from safe to fail-safe position. Tests (not presented here) showed that the device would remain in the safe position when the bird impact speed was reduced to 95 fps and the mitigator was aluminum. For this speed, the pulse duration and/or magnitude of the setback were insufficient to cause the device to proceed to the fail-safe position, which agrees with the above-noted design requirement for the mechanism. Except in one out of 52 tests, (wood mitigator with $A7=0.48$) the test data of table III indicate that the device performed as expected. Otherwise, with proper setback the device armed as required when the drag was larger than 3 g and remained in the fail-safe position for drags not exceeding 1 g.

5. SUMMARY AND CONCLUSIONS

A description is given of the work performed to combine setback and drag into a single laboratory tester in order to simulate, in the proper time frame, the sequential setback and aerodynamic drag experienced by Army ordnance projectiles. In the present tests, maximum setback was about 5000 g and "steady" state drag commenced within 4 ms of the completion of setback. Aerodynamic drag up to 30 g was simulated for 20 ms and up to 17 g for 90 ms.

Differences between test-to-test setback acceleration data for both wood and aluminum mitigators are generally within about 10 percent of the instantaneous average value.

*In the chronological order of this work, the simulator tests on the S&A device were performed prior to the previously described measurements, and streak photo data was not obtained. However, on the basis of the precision and repeatability of the data shown in figures 5-15, the setback data can be assumed to be the same as those shown in figs. 5 and 6, and the predicted frictionless drag data ($C=1$) should adequately represent test data.

The predicted setback data for aluminum mitigators can be put into this same 10 percent agreement with the test data.

Finally, tests were performed on several units of a safety and arming device to demonstrate the feasibility of the simulator as a tester. The results of the simulator tests were found to be in good agreement with known design characteristics.

6. LIST OF SYMBOLS

A	instantaneous mitigator crush area (as measured at bird interface), in. ²
A0	maximum mitigator crush area, in. ²
A7	cavity leakage area, comprising the sum of leakages between catch tube and MEM, and between catch tube and bird, in. ²
AI	acceleration, ft/s ²
C	friction coefficient (=1.0 (frictionless), = 0.5 (with friction))
C1	mitigator elongation at the bird interface, arising from relaxing the force thereon at T=TC, in.
C2	mitigator elongation at the MEM interface, arising from relaxing the force thereon at T=TC, in.
D7	air density (=0.0749 lbm/ft ³)
F	mitigator dynamic crush force, lb
F0	mitigator static crush pressure, psi
I=1	bird
I=2	MEM
I=3	mitigator
I=4	crushed mitigator
I=5	remaining uncrushed mitigator
L	distance of bird penetration for which mitigator area increases linearly from 0 to A0, in.
L0	length of cavity at termination of setback, in.
L9	initial mitigator length, in.
MI	mass, lbm
M7	mass of air passing into cavity, lbm.
M4	time rate of mitigator crush, lbm/s
P	total air pressure in cavity, psi
P0	ambient atmospheric pressure (=14.7 psi)

TABLE III - TEST RECORD OF PERFORMANCE OF FUZE DEVICE

Aluminum Mitigator

Number of Tests	Cavity Leakage Area in ²	Fail-Safe	Armed	Drag Range g
16	.15	0	16	9 to 3
2	.20	0	2	4 to 2
6	.30	5	1	2
1	.39	1	0	1
2	.48	2	0	0.9
6	.67	6	0	0.4

Wood Mitigator

Number of Tests	Cavity Leakage Area in ²	Fail-Safe	Armed	Drag Range g
4	.30	0	4	7 to 5
8	.48	1*	7	4 to 3
3	.67	1	2	2
4	1.49	4	0	0.3

*Indicates malfunction of fuze device.

P7 partial pressure in cavity caused by air leakage into or out of cavity, psi
 R (=M4(U1-U2)) hydrodynamic crush force, lb

S ratio of crush front travel to depth of bird penetration

ρ density of uncrushed mitigator, lbm/in.³

T time, s

Superscript

TC time duration of the mitigator crush, s

(\cdot) denotes time differentiation of the given variable

U0 initial bird velocity, fps

ACKNOWLEDGEMENTS

U7 speed of air leakage passing into or out of cavity, (referred to area A7), fps

The concept of the simulator and much of its design are the work of Herbert Curchack. Preliminary tester construction and tests were done by Arthur Ball. Robert Kayser, Forrest Nelson and Don Mary operated the simulator and obtained the test data. Herbert Curchack and Don Mary reduced the streak photo data. Finally, I would like to thank Kathy Mott for her preparation of the typescript.

UI velocity, fps

V cavity volume, in.³

X1=C1-Y3+Y1>0, honeycomb elongation at bird interface, in.

X2=C2-Y2+Y3>0, honeycomb elongation at MEM interface, in.

REFERENCES

YI displacement, in.

1. Pollin, I., "Impact Pulse Shaping", Harry Diamond Laboratories TR-1710 (June 1975).

Z1(=-AIM1/C1), honeycomb spring constant at bird interface, where A1 is the acceleration at T=TC, lb/in.

Z2(=-AIM1/C2), honeycomb spring constant at MEM interface, where A1 is the acceleration at T=TC, lb/in.

δ depth of bird or MEM penetration, in.

ϕ washer diam, in.

DISCUSSION

Mr. Dyrdaahl (Boeing Company): What is the meaning of the term "set back"?

Mr. Pollin: "Set back" is the ballistic terminology for the negative acceleration that a projectile experiences when it is fired.

Voice: You can simulate the peak acceleration and the drag force but can you simulate the duration in flight?

Mr. Pollin: The catch tube was an 18 in. (.5m) long straight tube. The drag ends when the momentum exchange mass washer leaves the catch tube and I see no reason why the catch tube can't be made longer. We did nothing to try to profile the drag because we wanted to see whether our theory was correct. It was the first cut and it worked very well. The idea for the device came from Mr. Herbert Curchack of the Harry Diamond Laboratories.

Mr. Balsara (U.S. Army Engineer Waterways Experiment Station): Are you trying to simulate the acceleration, the steady flight and the deceleration of the missile?

Mr. Pollin: The set back itself is to simulate what happens inside a gun barrel. If we have a gun barrel 2 or 2½ ft (.6 or .76m) long, we know what type of accelerations this projectile should experience from pressure measurements made within the gun barrel. Then we can simulate exactly what happens in that gun barrel; we mount the components backwards and we get the projectile up the speed slowly. In our usual setback experiments we have a 100 ft. (30m) long gun in which we slowly accelerate the projectile up the speed. The test of the simulation begins when the mitigator begins to crush. We are able to simulate rise times on the order of one or two milliseconds. We are simulating the interior ballistic acceleration environment and that is the first set in the set back. The second part is the aerodynamic drag. When it leaves the gun barrel, it goes through a change from set back to aerodynamic drag. We are able to get within two to four milliseconds. This is what we know to be the real case. We are actually simulating the free flight aerodynamic drag.

BARREL-TAMPED, EXPLOSIVELY PROPELLED ROTATING PLASTIC PLATES*

F. H. Mathews, B. W. Duggin
Sandia Laboratories
Albuquerque, New Mexico 87115

A previous paper described the use of barrel-tamped explosive charges to accelerate aluminum plates to high velocity with slow rotation [1]. These plates were employed to study weapon fuzing under conditions simulating high-velocity oblique impact into hard-earth targets. In the present paper, small barrel-tamped explosive systems are modified to allow the launching of slowly rotating plastic plates with relatively efficient transfer from chemical to kinetic energy of the plate. This development was complicated by the tendency of plastic materials to fragment during acceleration. Several techniques are discussed that reduce the pressures experienced by the plate during acceleration. A successful design employing a detonation wave normally incident upon an expansion gap provides sufficient pressure reduction to project intact nylon-6 plates of small size. Velocities ranging from 2400 to 3800 m/s have been obtained. Parameters affecting the design are investigated, resulting in an empirical method for calculating terminal velocity.

Attempts to scale these results to larger systems suitable for full-scale fuze testing have been unsuccessful because of material failures in the nylon plates. Departures from scaling suggest the direction for future work.

INTRODUCTION

Ballistic missile warheads employ impact-actuated fuzes that function at contact velocities up to 4500 m/s. Development tests involve "turnaround" impacts where target materials are projected against stationary fuze assemblies. This reciprocal arrangement produces representative impact stresses while avoiding the high cost of flight experiments. Experimental methods suitable for velocities above 1800 m/s present a particular challenge because of the limited velocity or mass capability of such conventional devices as rocket sleds and powder guns.

* This work was supported by the United States Energy Research and Development Administration.

A previous paper [2] described a technique in which solid explosive initiated to produce grazing detonation accelerated a slowly rotating plate to high velocity. Appropriate positioning of the fuze along the flight path of the plate allowed the desired relation between the velocity vector and the surface of the plate. This has allowed impact experiments at oblique angles with simulants of both hard- and soft-earth targets.

Recent experience employing grazing detonation to propel nylon plates at velocities both above and below the 2350 m/s experiment previously described [2] has uncovered several problems. First, grazing detonation of C-4 explosive caused plate damage at velocities below about 1900 m/s. Second, at velocities above 2400 m/s, unacceptably large explosive quantities were necessary. The

useful velocity range for nylon plates using grazing detonation of C-4 explosive is presently severely limited. Accordingly, an experimental program was undertaken to develop a more acceptable explosive technique.

ONE-DIMENSIONAL ANALYSIS

Three configurations suitable for explosively accelerating plates are depicted in Fig. 1. Peak compressive stresses at the explosive plate interface are lowest for rearward detonation, increasing approximately twice for grazing detonation and twice again for normal detonation. If side losses are small; i. e., when the explosive is thin in comparison to lateral dimensions, plate terminal velocities can be predicted from one-dimensional theories. Thus, for the grazing configuration [3,4] the terminal velocity V is given by

$$V = \frac{\sqrt{2E}}{\left[\frac{1}{3} + \frac{5M}{3C} + \frac{4}{3} \left(\frac{M}{C} \right)^2 \right]^{1/2}} \quad (1)$$

where $\sqrt{2E}$ is an experimentally determined characteristic velocity for the explosive and C/M , the loading factor, is the ratio between explosive mass C and plate mass M .

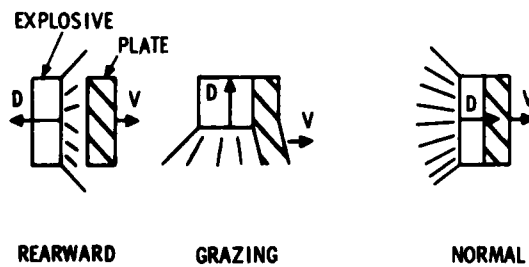


Fig. 1 - Geometries for explosive detonation

Terminal velocity for normal detonation [5] is given by

$$V = D \sqrt{\frac{8}{\gamma^2 - 1}} \left\{ \frac{\left(1 + \frac{32C}{27M} \right)^{1/2} - 1}{\left(1 + \frac{32C}{27M} \right)^{1/2} + 1} \right\} \quad (2)$$

where D is the detonation velocity and γ is the "effective" gas constant for explosion gases.

Terminal velocity for rearward detonation can be calculated numerically [6] from appropriate explosive properties.*

Final velocities are compared in Fig. 2 as a function of loading factor. Highest velocities are expected from forward detonation, provided difficulties associated with damage due to high pressure can be overcome. Significantly lower velocities are expected from rearward detonation, and even lower velocities result from grazing detonation. Side losses are important for most practical systems where low geometrical efficiency [1] tends to reduce final velocity below the values indicated. Because of axial symmetry, rearward detonation lends itself to side confinement and the possibility of improving geometrical efficiency in comparison to grazing detonation.

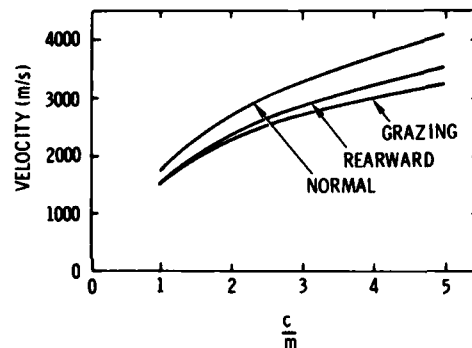


Fig. 2 - Terminal velocity as a function of loading factor for geometries of Fig. 1

REARWARD DETONATION

Two experiments were conducted with the geometry shown in Fig. 3. Initiation was provided by a thin multipoint exploding bridge-wire detonation [8] that generated 200 simultaneous initiations over the 100-mm diameter of the assembly. Results were disappointing. The nylon plate was shattered into many fragments, all moving at a nearly uniform but low velocity. Even with confinement, rearward detonation resulted in unacceptably low energy efficiencies. When rearward detonation is

* Properties used to describe Comp C-4 explosive [4, 7] are $\sqrt{2E} = 2750$ m/s, $D = 8040$ m/s, $\gamma = 2.7$, and density $\rho = 1.59$ Mg/m³.

compared to normal detonation, the lower pressures at the plate surface extend the time required for plate acceleration, permitting larger lateral losses. Our investigation of rearward detonation was terminated when faced with these problems.

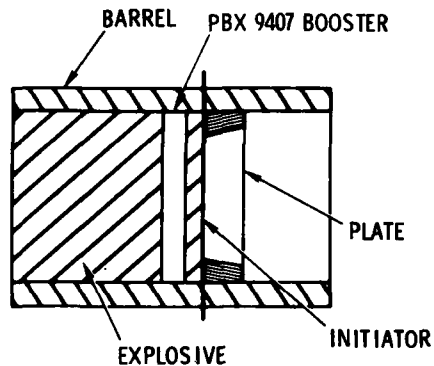


Fig. 3 - Explosive configuration for rearward detonation

NORMAL DETONATION

Normal detonation was investigated in numerous small experiments using the configuration illustrated in Fig. 4 where l , h and d are the explosive length, air gap and barrel inside diameter. Detonation is initiated at the rear surface and moves through the explosive, causing a pressure wave carrying the explosive gases to move across an air gap and accelerate both the flyer and guard plates. When the guard is loosely attached to the flyer, it affords protection from damaging edge relief waves. A slight taper cut across the width of the flyer-guard combination causes a modest-velocity gradient (< 5 percent) across the flyer width. This gradient when imposed upon translational velocity causes the rotation of the plate during flight.

Massive steel barrels, which are always fragmented, reduce side losses. Since pressures in the explosive gases depend upon the ratio of initial to instantaneous volume raised to approximately the third power, movement of the sidewalls tends to reduce the explosive pressure by approximately the ratio of initial to instantaneous radius raised to the sixth power. During the process of barrel expansion, a significant portion of the explosive energy is lost to barrel energy and becomes unavailable for plate acceleration. Considering the geometry of Fig. 4; with $h/l = 0.18$, $l/d = 1.9$ and a barrel weight per unit length that is 4.4 times

the explosive mass, about 70 percent of the explosive energy is lost to the side.

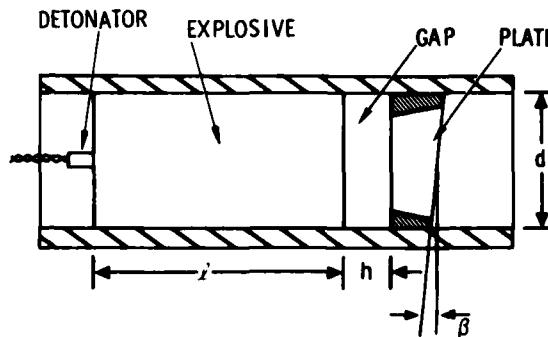


Fig. 4 - Barrel tamped systems

Two competing processes must be balanced to achieve a successful design. The driving pressure at the interface between explosion products and flyer can be reduced by increasing the gap, thus reducing the possibility of plate damage. However, increasing side losses tends to reduce plate velocity as the gap is enlarged. Since the plastic materials are fragmented when no gap is present, the smallest usable gap is optimum.

An approximate means of treating systems with side losses is to discount the total explosive C to a reduced value, the effective explosion C_e , which is assumed to act as if one-dimensional flow existed. Then $C_e = \alpha C$ where α is an experimentally determined discount factor. Then, using the effective explosive and combined guard and plate mass M , the one-dimensional analysis yields the terminal velocity of the plate. In this way, charge geometry (i. e., length and confinement) may be considered separately from plate velocity, mass and explosive properties that are treated by Eq. (2).

This approximation may be extended by using the discounted explosive mass in an appropriate one-dimensional shock-wave calculation. The influence of relative gap size upon driving pressures was computed [6] for several "discounted" one-dimensional geometries to yield the results plotted against a non-dimensional time in Fig. 5 for the case when the terminal velocity of a nylon plate is 3700 m/s. A purely hydrodynamic model was used for nylon [9]. Although side losses from the geometry of Fig. 4 account for approximately 70 percent of the explosive energy, this figure is thought to represent appropriate trends.

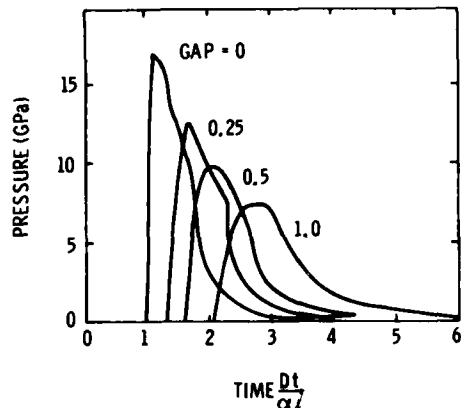


Fig. 5 - Computed pressure time histories at the explosive nylon interface as a function of relative gap size ($h/\alpha l$)

Terminal velocity was measured during several small experiments to determine the influence of gap size upon discount factor and whether a specific gap would yield intact nylon-6 flyer plates. The geometry is depicted in Fig. 4 where N is the barrel mass per unit length and M is the sum of flyer and guard mass. The results given in Table 1 and Fig. 6 were obtained by using the observed velocity in Eq. (2) to calculate an effective explosive mass and then the appropriate discount factor.

TABLE 1
Effect of Gap Size For $\frac{Nl}{C} = 4.4$

Shot No.	$\frac{l}{d}$	$\frac{h}{l}$	$\frac{C}{M}$	α	$\frac{h}{\alpha l}$	V m/s
1 (1)	1.5	0	4.6	0.43	0	2670
2 (2, 3)	1.5	0.5	8.4	0.23	2.2	2600
3 (2)	1.5	1.0	8.4	0.18	5.6	2300
- (1)	1.9	0	7.9	0.38	0	3300
4 (4)	1.9	0	12.4	0.35	0	3840
5 (5)	1.9	0.18	14.4	0.29	0.6	3780
6 (5)	1.9	0.33	14.2	0.21	1.6	3300
7 (6)	1.9	0.65	14.2	0.15	4.3	2750

Notes:

- (1) Aluminum plate
- (2) Nylon, no guard ring, front surface spalled
- (3) Sponge-rubber cushion between plate and explosive
- (4) Nylon plate fragmented
- (5) Nylon plate remained intact
- (6) Front surface spalled

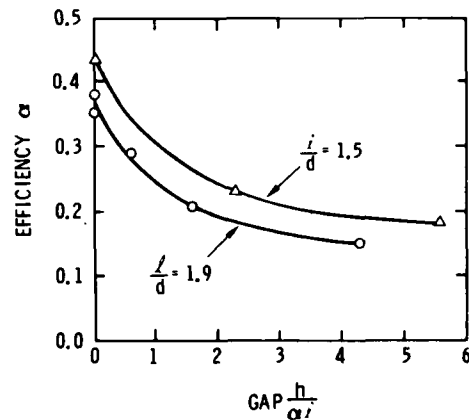


Fig. 6 - Discount factor α as a function of relative gap size for fixed confinement ($Nl/C = 4.4$) and two explosive lengths

In those cases where fragments were formed, an average velocity observed in pulse X-ray shadowgraphs was taken. These data indicate that only relatively small gaps may be considered before edge losses lead to a significantly reduced effective explosive mass.

Based upon previous experience with aluminum [1, 2] and these results, we concluded that a guard ring occupying half the barrel cross-sectional area was justified. The influence of gap upon plate damage is less clear. Small nylon plates could be propelled intact with gap sizes ($h/\alpha l$) from 0.6 to 1.6 when a guard ring was used. The damaged plate observed in Shot 7 is puzzling but was not investigated further due to a low discount factor obtained with this large gap.

An X-ray shadowgraph of an intact non-rotating nylon-6 plate propelled to a velocity of 2880 m/s is shown in Fig. 7. Relative gap size ($h/\alpha l$) was 0.96 with $\alpha = 0.27$. The image results from a triple exposure taken as the plate had moved approximately 0.75 m. Reference marks are placed 102 mm apart. Material visible behind the plate images is fragments from the nylon guard ring.

Other plastics besides nylon may be considered. We hoped to find materials more resistant to fragmenting. In addition to nylon, Lexan, Kevlar fiber-reinforced epoxy, and fiberglass-reinforced epoxy were tried. Fibers in the composites were directed to reinforce the thickness and circumferential directions

but did not strengthen the radial direction. All of these materials fragmented more extensively than did nylon.

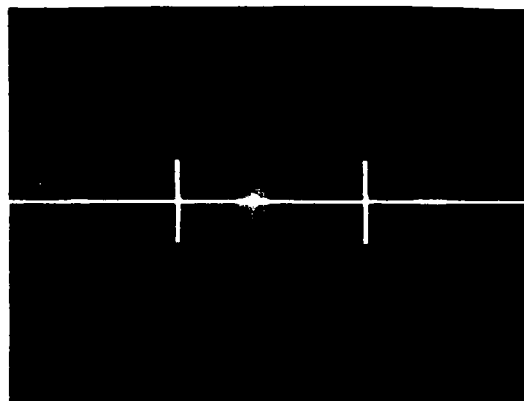


Fig. 7 - Pulse X-ray shadowgraph of a nylon plate at a velocity of 2880 m/s

With these results, a series of small experiments were conducted with Comp C-4 explosive and nylon-6 plates with fixed length ($l/d = 1.9$), fixed confinement ($lN/C = 4.4$) and fixed relative gap ($h/\alpha l = 0.60$) with a variable plate mass. Results are given in Table 2 and compared to a prediction from Eq. (2) using $\alpha = 0.29$ in Fig. 8. All nylon-6 plates remained intact over the velocity range from 2400 to 3810 m/s. Although the thinnest plate was bent forward, resulting in partial tear along its diameter, the resulting halves remained attached. The relatively good agreement between observed velocity and the discounted one-dimensional prediction establishes that this technique may be applied to barrel confined explosive systems with air gaps.

ROTATION

Rotation was caused by tapering the plate as indicated in Fig. 4 with typical values of β given in Table 2. Observed translation velocities were not affected by taper. This is not surprising since the rotational energy of the plate was never greater than 0.1 percent of its translational energy. Rotation velocities were always less than the value estimated from constant kinetic energy as a function of radius [1]. However, increasing the taper did increase rotation, while larger air gaps decreased rotation. The rotational rate for No. 5, Table 2, was 76 percent of the value

TABLE 2
Measured Velocity As A Function of Discounted Loading Factor⁽¹⁾

No.	Plate Thickness (mm)	$\frac{\alpha C}{M}$	Velocity (m/s)
1	9.6 ⁽²⁾	4.12	3810
2	13	3.02	3260
3	16	2.52	3030
4	16	2.48	3080
5	16 ⁽³⁾	2.47	3080
6	16 ⁽⁴⁾	2.46	2980
7	20	2.02	2730
8	24	1.66	2440

Notes:
 (1) $\alpha = 0.29$, $\frac{h}{\alpha l} = 0.60$, $\frac{lN}{C} = 4.4$
 (2) Plate torn due to bending
 (3) Tapered plate, $\omega = 4200$ rad/s, $\beta = 3.26^\circ$
 (4) Tapered plate, $\omega = 4400$ rad/s, $\beta = 4.94^\circ$

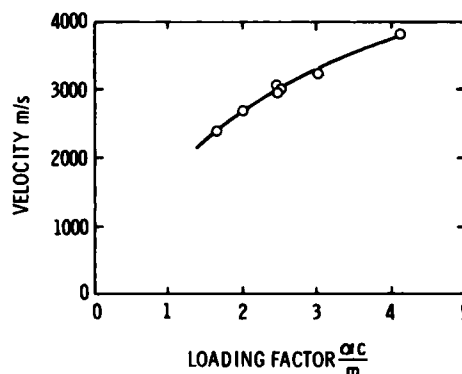


Fig. 8 - Observed nylon plate velocity compared to values calculated from Eq. (2) with $\alpha = 0.29$ and $h/\alpha l = 0.60$

calculated while No. 6, Table 2, yielded 60 percent of the calculated value. A relatively crude estimation of plate rotation is acceptable, because once rotation rate is known from small-scale experiments, appropriate scaling [2] can be used to find the value for larger tests. Then when full-scale testing is performed upon an impact fuze target, the fuze may be positioned along the plate trajectory to permit exactly the desired impact angle. An X ray of a small rotating plastic plate moving at 2880 m/s is given in Fig. 9 using an identical setup to that of Fig. 7.

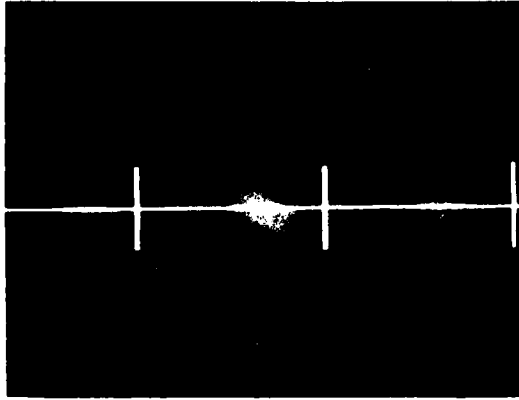


Fig. 9 - X-ray shadowgraph of a small rotating nylon plate

LARGE SYSTEMS

Development of a nylon flyer-plate system sufficiently large to accommodate fuze testing has been attempted at one velocity. This effort is presently unsuccessful, yielding the result depicted in Fig. 10. This experiment is a scaled enlargement (scale factor 4.25) of the small system employed for the result of Fig. 9 with a barrel inner diameter of 216 mm. Only the relative confinement was not scaled, being reduced from 4.4 to a value of 2.9. The appearance of fragments torn from the plate together with spall failures across the diameter of the plate indicate that tensile effects are producing failures not observed during the small experiments.



Fig. 10 - Rotating nylon-6 plate 173 mm in diameter moving at a velocity of 2700 m/s

Several possible avenues for further investigations with nylon 6 exist since rate-dependent properties, manufacturing stresses and many details of the material state; i. e., moisture content, do not scale or were not controlled during this experiment.

CONCLUSION

Techniques have been investigated for employing explosive to accelerate rotating nylon-6 plates suitable for impact-fuze testing. Poor energy efficiency coupled with plate damage restrict the explosive technique to barrel confined systems employing normally incident detonation. Air gaps reduce pressures sufficiently so that intact plates are obtained over a wide velocity range, provided the plates are relatively small. The efficiency of energy transfer between explosive and plate decreases with increasing gap size. A single empirical measure of performance called the "discount factor" was obtained. When this factor is applied with available one-dimensional theories, the terminal velocity of the plate can be predicted as a function of air spacing, explosive properties, and plate mass. An attempt to scale from successful small experiments to larger systems suitable for impact-fuze testing has been unsuccessful due to plate breakup. Several departures from scaling related to material strength suggest directions for further work.

REFERENCES

1. F. H. Mathews and B. W. Duggin, "Barrel Tamped, Explosive Propelled Plates for Oblique Impact Experiments," Shock and Vibration Bulletin, No. 46, Part 2, pp. 145-154, Aug. 1976
2. F. H. Mathews, "Explosively Propelled Rotating Plates for Oblique Impact Experiments," Shock and Vibration Bulletin, No. 45, Part 4, Jun. 1975
3. R. W. Gurney, "The Initial Velocities of Fragments from Bombs, Shells, and Grenades," BRL Report 405, 1943
4. J. E. Kennedy, "Explosive Output for Driving Metal," Behavior and Utilization of Explosives in Engineering Design, 12th Annual Symposium ASME, Published by The New Mexico Section ASME, Mar. 2-3, 1972

5. A. K. Aziz, H. Hurwitz and H. M. Sternberg, "Energy Transfer to a Rigid Piston Under Detonation Loading," Physics of Fluids, 4, pp. 380-384, 1961
6. R. J. Lawrence and D. S. Mason, WONDY IV - A Computer Program for One-Dimensional Wave Propagation with Rezoning, SC-RR-71 0284, Sandia Laboratories, Aug. 1971
7. B. M. Dobratz, "Properties of Chemical Explosives and Explosive Simulants," UCRL-51319, Dec. 1972
8. R. I. Butler, M. Cowan, B. W. Duggin and F. H. Mathews, "Mesh-Initiated Large Area Detonators," SAND75-0524, Sandia Laboratories, Nov. 1975
9. M. H. Rice, R. G. McQueen and J. M. Walsh, "Compression of Solids by Strong Shock Waves," Solid State Physics, Vol. 6, pp. 196-259. Academic Press, New York, 1958

DISCUSSION

Mr. Avrami (Picatinny Arsenal): What kind of explosives did you use?

Mr. Mathews: We used hand-packed charges of composition C-4 explosive exclusively.

Mr. Avrami: Did you try to determine the energy that was released from the explosive to impact the plate?

Mr. Mathews: Typically, the approach would be to use a sufficient quantity of explosive to obtain the desired result. However, the problem is that one would like to use as thick a plate as possible at as high a velocity as possible. The explosive charges required in that framework became larger than we could handle at our facility. The development of confined systems increased the efficiency at appropriate explosive amounts which turned out to be about 400 lbs.

SHOCK WAVEFORM TESTING
ON AN ELECTRODYNAMIC VIBRATOR

William E. Frain
Applied Physics Laboratory/The Johns Hopkins University
Laurel, Maryland

Digital Control systems provide an efficient method for transient waveform testing on electrodynamic shakers. These systems can generate a variety of acceleration-time history pulses including classical shock pulses and operator supplied waveforms. The type or pulse which can be accurately produced on an electrodynamic shaker is limited to that which yields, for both initial conditions and final conditions, zero value for the magnitude of acceleration, velocity, and displacement. In addition, force, velocity, and displacement are limited by the shaker design. To achieve the final end conditions, the classic pulse is conditioned. This paper studies the effect which the conditioning has on the ability of the shaker to produce the pulse and also examines the impact of conditioning on the Shock Response Spectrum.

INTRODUCTION

Digital Control systems afford an attractive capability for transient waveform (acceleration versus time) testing on electrodynamic shakers (see Figs. 1 thru 4). These systems, through the use of high speed transfer function measurements and subsequent shaping techniques, are capable of producing high quality and reproducible waveforms with minimum setup time. The process used to generate the waveform involves excitation with a pulse having a sharp rise followed by an exponential decay (Ref. 1), response measurement, and transfer function computation. A compensation waveform is then generated which has a signature, such that when operated on by the measured transfer function produces the desired waveform on the shaker.

The Applied Physics Laboratory is currently performing transient waveform testing using a 15,000 pound force shaker controlled by a commercially available digital vibration control system. The software package for transient waveform control was developed by the digital control system vendor (Ref. 6). This system can generate a variety of pulse shapes

including: half-sine, triangular, terminal peak sawtooth, rectangular, double-pulse rectangular, and operator supplied analog pulses.

NOMENCLATURE

- g_0 = peak acceleration expressed in units of g's;
- p = fraction of peak acceleration of classic pulse to be used in generating peak acceleration of conditioned sine wave;
- t = time variable;
- \ddot{X}_0 = peak acceleration;
- \dot{X} = velocity;
- X = displacement;
- τ_0 = period of classic pulse;
- τ_1 = period of pre or post half-sine.

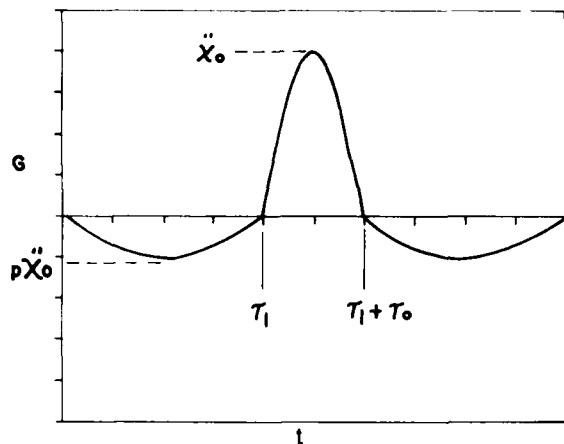


Fig. 1 - Conditioned half-sine pulse

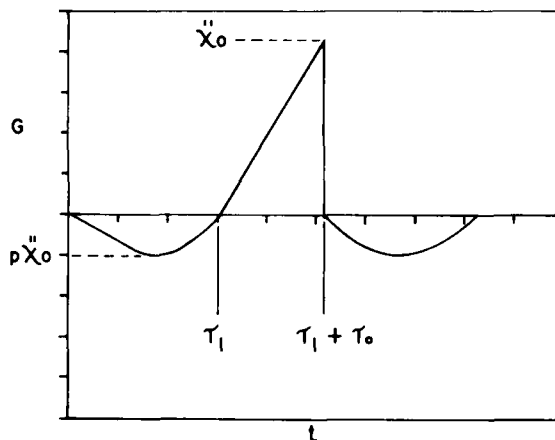


Fig. 2 - Conditioned triangular pulse

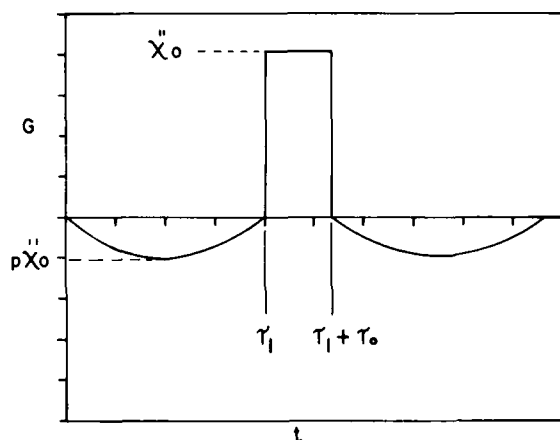


Fig. 3 - Conditioned rectangular pulse

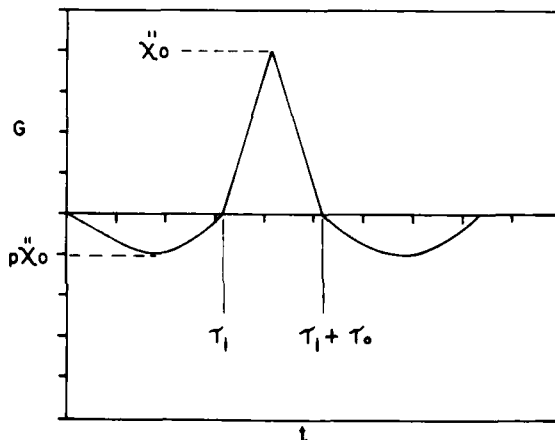


Fig. 4 - Conditioned terminal peak sawtooth pulse

SHAKER LIMITATIONS

The type of pulse which can be produced on an electrodynamic shaker is limited to that which yields, for both initial conditions ($t=0$) and final conditions ($t=\tau$), zero value for the magnitude of acceleration, velocity, and displacement (Ref. 2 and 3). In addition, a particular shaker has limitations of maximum force, velocity, and acceleration. For the shaker used at APL, the maximum force is 15,000 pounds while the maximum velocity and displacement ratings are 70 inches/second and 0.5 inches respectively. Clearly, for the unipolar pulses ($\ddot{X}(t) \geq 0$ for all t), the final conditions cannot be met with respect to final

velocity and displacement. As an example, a half-sine pulse has final conditions:

$$1) \dot{X}(t = \tau_0) = 2 X_0 \left(\frac{\tau_0}{\pi} \right) \neq 0$$

$$2) X(t = \tau_0) = \frac{\ddot{X}_0 \tau_0^2}{\pi} \neq 0$$

To achieve the final condition constraints, the transient waveform control software conditions the desired pulse by adding pre pulse and post pulse half-sine pulses of the proper amplitude and duration. These conditioning sine pulses are referred to as tails. Heuristically,

these tails provide a negative area under the acceleration-time history which is equal to the area of the requisite classical pulse assuring zero final velocity. The peak value of the tail ($p\ddot{x}_0$) is selectable upon input as a fraction of the peak value of the requisite waveform. The resulting duration of the conditioning sine pulses is depicted in Fig. 5 as the ratio of τ_1/τ_0 versus p for four types of classic pulses. The choice of the magnitude of p is usually governed by shaker displacement limitations.

For conditioned pulses, the maximum magnitude of velocity occurs at $t = \tau_1$ and at $t = \tau_1 + \tau_0$. These are the two zero crossings of the conditioned acceleration pulse. In the case of conditioned symmetric pulses, such as the half-sine, rectangular, and triangular, the maximum displacement occurs at $t = \tau_1 + \tau_0/2$. For conditioned unsymmetric pulses, the maximum displacement will occur at the time coinciding with the centroid (in the time domain) of the classic pulse. An example of this is the terminal peak sawtooth

pulse. This pulse has maximum displacement at $t = \tau_1 + \frac{2\tau_0}{3}$. It should be observed that for unsymmetric pulses, only the final velocity will be zero. Some residual displacement will exist. The residual displacement for the terminal peak sawtooth will be; $X_R = -\dot{X}_0\tau_0^2/12$.

Flexures on the electrodynamic shaker will return the specimen to the equilibrium position. Table I presents a compilation of the maximum velocity and maximum displacement which have been derived (see Appendix) for each of the available classic pulses conditioned by pre pulse and post pulse half-sines. From the equations of Table I, it can be seen that for a given peak acceleration the maximum velocity is a linear function of the duration of the classic pulse, τ_0 , and is independent of the magnitude of the conditioning pulse, $p\ddot{x}_0$, whereas, the maximum displacement varies with the sum of two terms; one involving τ_0^2 and the second as a function of both τ_0^2 and p .

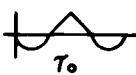
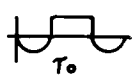

PULSE TYPE	MAX. VEL. IN/SEC.	MAX. DISP. INCHES
$\frac{1}{2}$ SINE	$\pm \frac{386.4 g \cdot \tau_0}{\pi}$	$-\frac{386.4 g \cdot \tau_0^2}{\pi} \left[\frac{1}{\pi} + \frac{1}{4p} \right]$
TRIANGULAR 	$\pm \frac{386.4 g \cdot \tau_0}{4}$	$-\frac{386.4 g \cdot \tau_0^2}{8} \left[\frac{2}{3} + \frac{\pi}{8p} \right]$
RECTANGLE 	$\pm \frac{386.4 g \cdot \tau_0}{2}$	$-\frac{386.4 g \cdot \tau_0^2}{8} \left[1 + \frac{\pi}{2p} \right]$
SAWTOOTH 	$\pm \frac{386.4 g \cdot \tau_0}{4}$	$-\frac{386.4 g \cdot \tau_0^2}{2} \left[.23457 + \frac{\pi}{32p} \right]$

TABLE I
Velocity and Displacement Maximax

Using the previously stated limitations of the shaker, maximum velocity equals 70 inches/second and maximum displacement equals 0.5 inches, these equations are expressed parametrically in p for each of the conditioned classic pulses in Figs. 6 through 9. For test laboratories having the same shaker limitations, these curves can be used directly for the purposes of determining capability for performing a test and for the selection of p . Of course, if the requisite test program exceeds the shaker displacement limitations, schemes such as armature D.C. biasing (Ref. 4) or armature mechanical biasing should be considered. It is noteworthy that increasing the magnitude of the conditioning half-sine pulse

(increasing p), has a dramatic effect on the maximum acceleration capability. Consider a half-sine classic pulse (Fig. 5) with a period of 0.020 seconds. With $p = 5\%$, a peak acceleration of 1.9g is permissible whereas, with $p = 50\%$, a peak acceleration of 12.5g can be achieved. Using p to advantage, a test conductor can then significantly increase capability by making p large. The value of conditioning the classic pulse is then two-fold: it preserves the requisite end conditions for an electrodynamic shaker and by increasing the peak amplitude of the conditioning sine waves, the shaker capability is significantly increased by decreasing the displacement of the conditioned waveform.

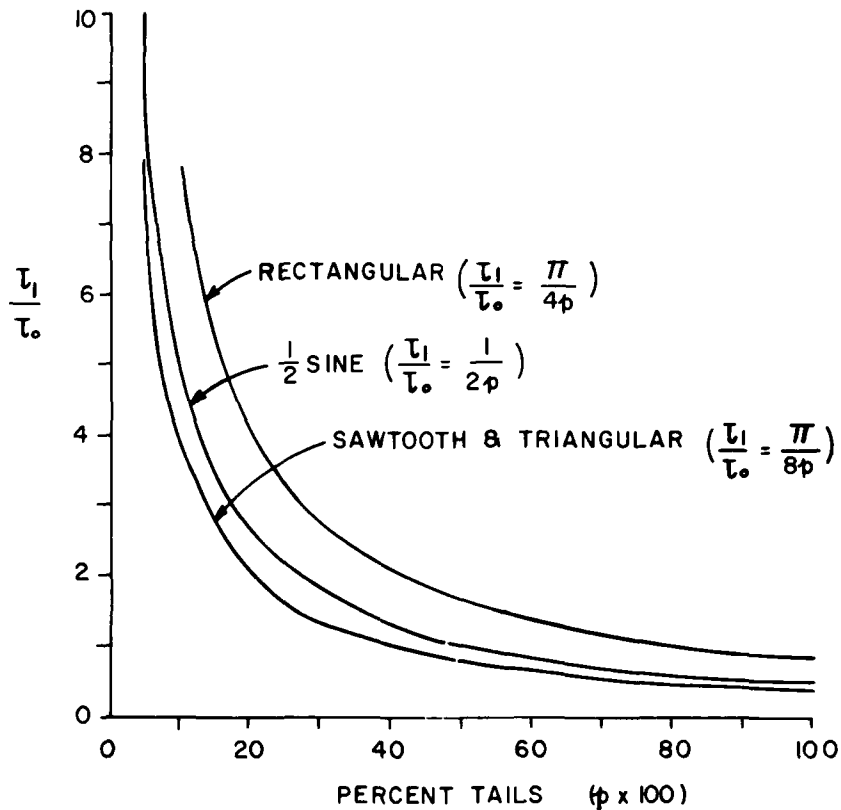


Fig. 5 - τ_1 versus percent tails

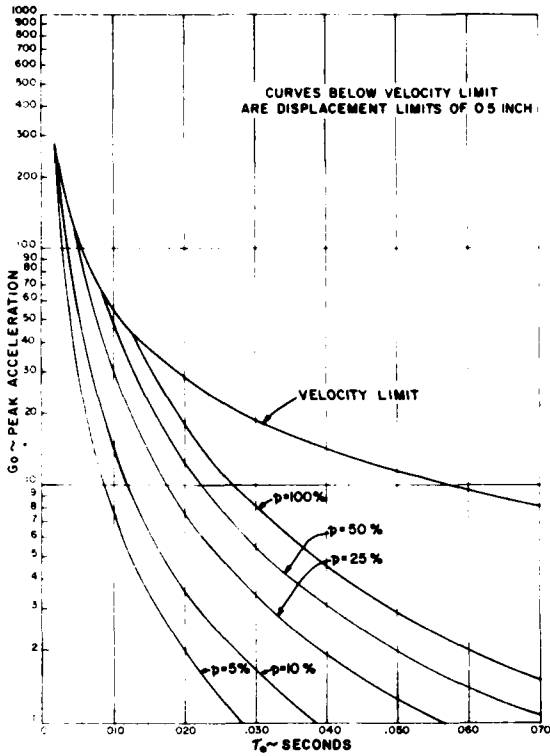


Fig. 6 - Shaker capability for conditioned half-sine pulse

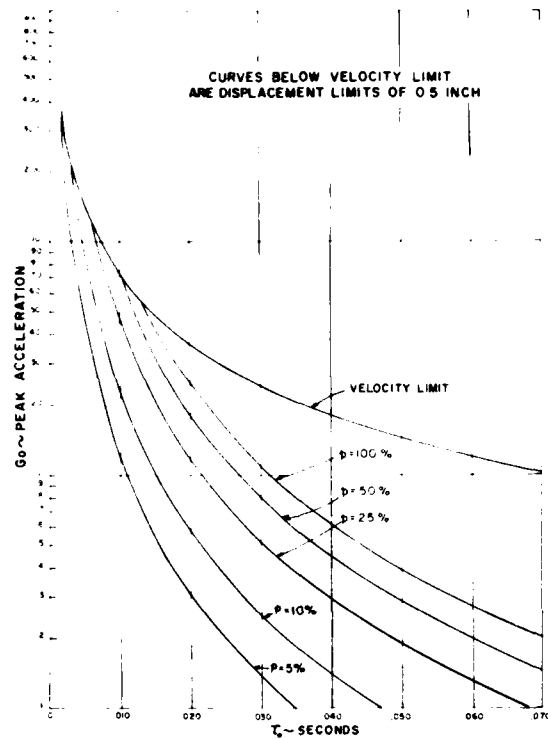


Fig. 7 - Shaker capability for conditioned triangular pulse

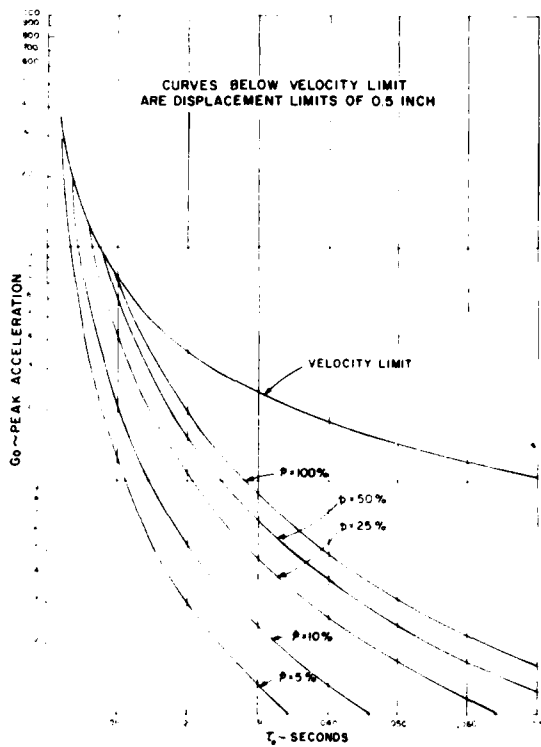


Fig. 8 - Shaker capability for conditioned terminal peak sawtooth pulse

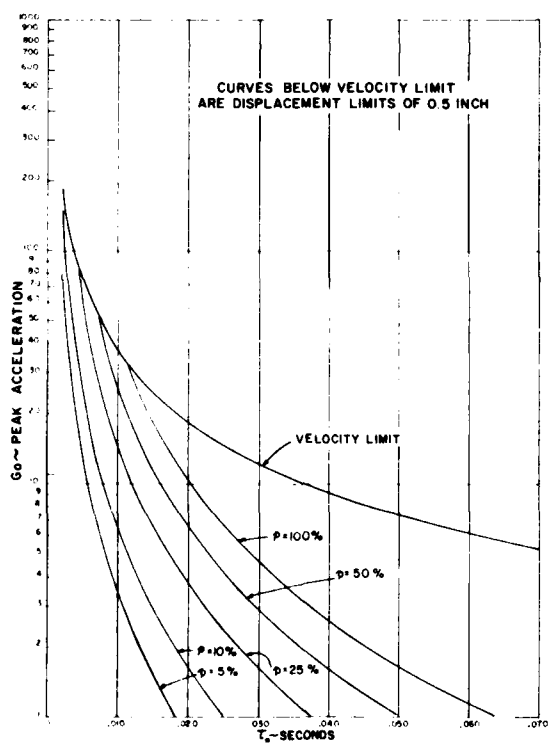


Fig. 9 - Shaker capability for conditioned rectangular pulse

CONSEQUENCES OF CONDITIONING

Although there is value derived from conditioning the classical pulses with tails, we need to know how this conditioning will alter the loading effect which is produced on a specimen which is subjected to this shock. Clearly, the pulses shown in Figs. 1 through 4 do not look like their classic counterparts. Also, they violate the shape tolerances given in MIL-STD-810B (Ref. 5). To evaluate this question, the Shock Response Spectrum (SRS) was used as a measure of severity of loading for each of the classic pulses and the classic pulses which were conditioned by the addition of tails. These data were generated experimentally using the digital control system in the closed loop mode. For the purpose of obtaining information regarding relative severity of the pulses, the maximax SRS with $Q = 10$ was selected. Figures 10 through 13 present these data for the available classic pulses. These data show a marked change on the SRS as p is increased. In many cases the SRS is

doubled for 50% and 75% tails. This strongly implies that the intent of the specification has been seriously jeopardized by increasing p . Alternatively, at lower frequencies, the SRS for conditioned pulses with large p is appreciably less than the SRS of the classic pulse. For high frequencies, the SRS of the conditioned pulses tends to equal the SRS of the classic pulse for all values of p . A comprehensive discussion of the effects which tailoring the pulse has on the shock response spectrum is developed in References 2 and 7. There is no one answer to the question of how large a value of p can be selected. In general, p should not exceed 10% to preserve a reasonable match to the SRS. If shaker displacement limits prohibit a test with $p \leq 10\%$, armature biasing should be considered in lieu of increasing p . On the other hand, if the specimen dynamics are well known and fragility is of greater concern in the high frequency range, p may be increased to generate enhanced shaker capability.

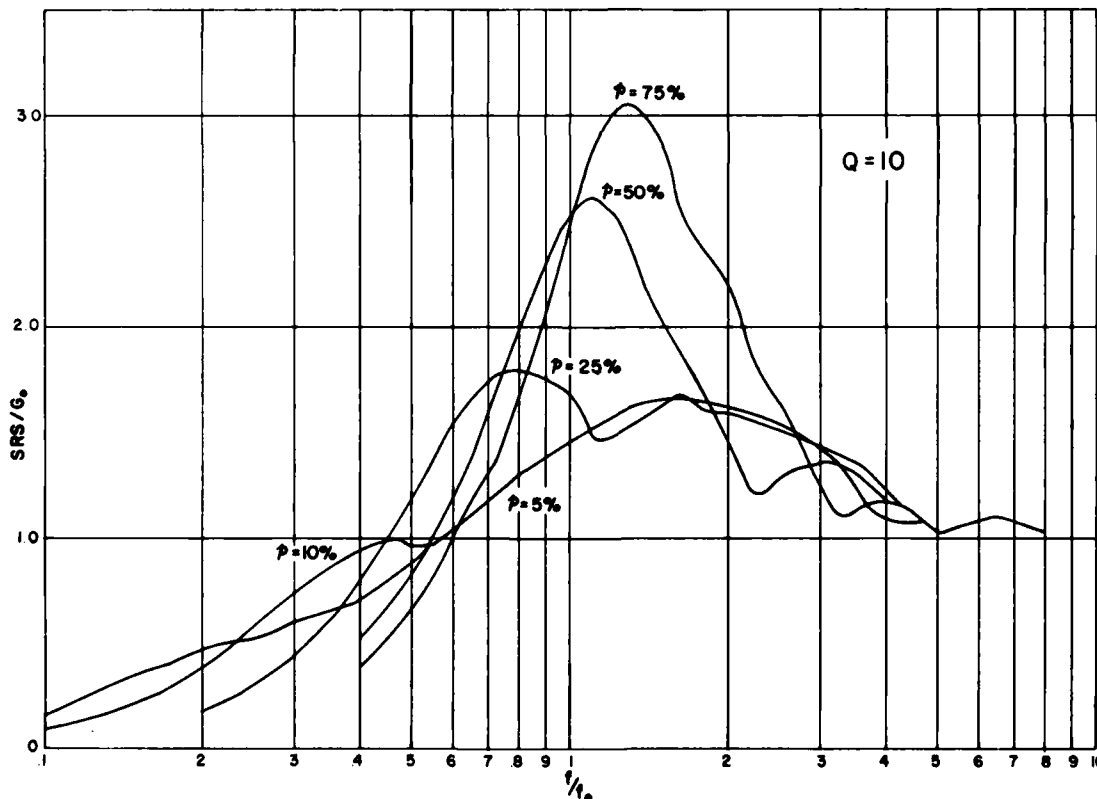


Fig. 10 - Maximax shock response spectra for conditioned half-sine pulse

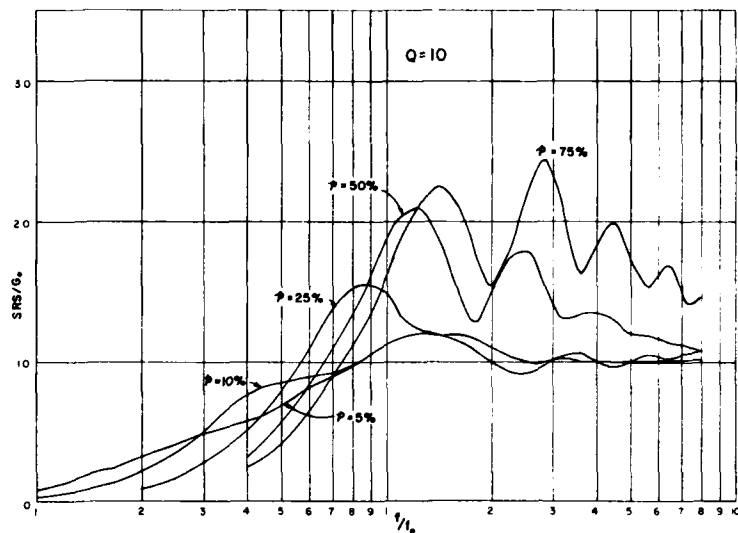


Fig. 11 - Maximax shock response spectra for conditioned terminal peak sawtooth pulse

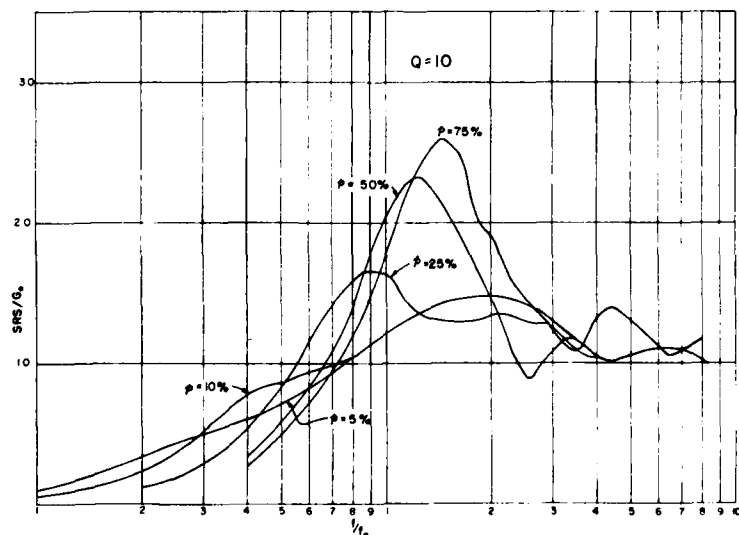


Fig. 12 - Maximax shock response spectra for conditioned triangular pulse

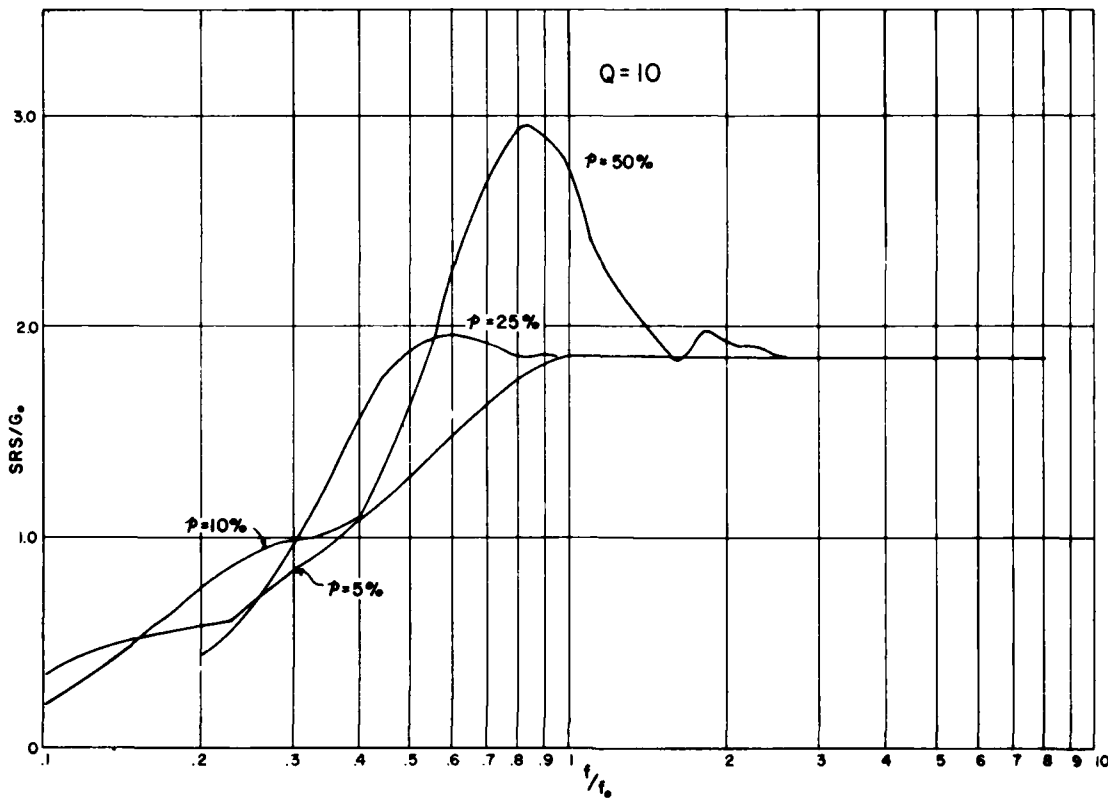


Fig. 13 - Maximax shock response spectra for conditioned rectangular pulse

CONCLUSIONS

The marriage of digital control systems to electrodynamic shakers affords test laboratories a reliable and efficient means of transient waveform control testing. Shaker displacement limitations restrict testing of significant acceleration levels to pulses having periods less than 0.020 seconds. Users should evaluate the damage severity of conditioning tails when it is required to condition the classic pulse with tails greater than 10%. Systems having software with equal duration tails should be changed so that zero residual displacement of unsymmetric pulses can be achieved.

The tolerances given in present specifications, MIL-STD-810B, are not

responsive to tolerances of pulses conditioned by this relatively attractive method. This poses a difficulty in demonstrating conformance to the test specification. New specifications should be generated with consideration given to tolerances on not only the parameters in the time domain, but on the shock spectra as well.

ACKNOWLEDGEMENT

The author is indebted to the assistance provided by James Bittner and Harvey Ward of the Environmental Test Laboratory at APL in the generation of much of the experimental data which appear in this paper.

REFERENCES

1. J. D. Favour and J. M. Lebrun, "Transient Waveform Control of Electromagnetic Test Equipment," Shock and Vibration Bulletin No. 40, Part 2, 1969.
2. D. O. Smallwood, "Time History Synthesis for Shock Testing on Shakers", "Seminar on Understanding Digital Control and Analysis in Vibration Test Systems," published by The Shock and Vibration Information Center, NRL, Washington, D.C., May 1975.
3. W. R. Miller, "Shaping Shock Acceleration Waveforms for Optimum Electrodynamic Shaker Performance," Shock and Vibration Bulletin No. 34, Part 3, 1964.
4. J. R. Fagan and J. M. McClanahan, "Extension of Shaker Shock Capabilities," Shock and Vibration Bulletin No. 35, Part 6, 1966.
5. "Military Standard Environmental Test Methods for Aerospace and Ground Equipment," MIL-STD-810B (USAF), June 1967.
6. J. P. Barthmaier, "Shock Testing Under Minicomputer Control," Proceedings of the Institute of Environmental Sciences, 1974.
7. D. O. Smallwood and A. F. Witte, "The Use of Shaker Optimized Periodic Transients in Matching Field Shock Spectra," Sandia Laboratory Development Report, SC-DR-710911, May 1972.

Appendix

DERIVATION OF MAXIMUM VELOCITY AND DISPLACEMENT FOR CONDITIONED CLASSIC PULSES

A.1 Conditioned Half-Sine

To evaluate the period of the conditioning pulse, τ_1 , we equate the integral of the classic pulse to the integral of the pre pulse and post pulse;

$$\int_0^{\tau_0} \ddot{x}_0 \sin \omega_0 t dt = 2 \int_0^{\tau_1} p \ddot{x}_0 \sin \omega_1 t dt$$

yielding, $\omega_1 = 2p\omega_0$
 substituting, $\omega = \pi/\tau$
 yields, $\tau_1 = \tau_0/2p$

The function is defined as,

$$\ddot{x}(t) = -p\ddot{x}_0 \sin \frac{2p\pi}{\tau_0} t$$

for $0 \leq t \leq \tau_1$

$$(1) \quad \ddot{x}(t) = \ddot{x}_0 \sin \frac{\pi}{\tau_0} (t - \tau_1)$$

for $0 \leq t \leq \tau_1 + \tau_0$

$$\ddot{x}(t) = -p\ddot{x}_0 \sin \frac{2p\pi}{\tau_0} \left[t - (\tau_1 + \tau_0) \right]$$

for $\tau_1 + \tau_0 \leq t \leq 2\tau_1 + \tau_0$

$$\ddot{x}(t) = 0; \text{ elsewhere}$$

for $0 \leq t = \tau_1$,

$$\dot{x}(t) = \int \ddot{x}(t) dt$$

$$(2) \quad \dot{x}(t) = -\frac{\ddot{x}_0 \tau_0}{2\pi} \left[1 - \cos \frac{2p\pi}{\tau_0} t \right]$$

$$x(t) = \int \dot{x}(t) dt$$

$$(3) \quad x(t) = -\frac{\ddot{x}_0 \tau_0}{2\pi} \left[t - \frac{\tau_0}{2p\pi} \sin \frac{2p\pi}{\tau_0} t \right]$$

for $\tau_1 \leq t \leq \tau_1 + \tau_0$

$$\dot{x}(t) = \int \ddot{x}(t) dt$$

$$(4) \quad \dot{x}(t) = -\frac{\tau_0 \ddot{x}_0}{\pi} \cos \left[\frac{\pi}{\tau_0} \left(t - \frac{\tau_0}{2p} \right) \right]$$

$$x(t) = \int \dot{x}(t) dt$$

$$(5) \quad x(t) = -\frac{\tau_0^2 \ddot{x}_0}{\pi} \left\{ \frac{1}{\pi} \sin \left[\frac{\pi}{\tau_0} \left(t - \frac{\tau_0}{2p} \right) \right] + \frac{1}{4p} \right\}$$

Observation of the zero crossings of $\ddot{x}(t)$ and $\dot{x}(t)$ produces the following maxima;

$$(6) \quad \dot{x}_{\max} = \pm \frac{\ddot{x}_o \tau_o}{\pi}$$

$$(7) \quad x_{\max} = - \frac{\tau_o^2 \ddot{x}_o}{\pi} \left[\frac{1}{\pi} + \frac{1}{4p} \right]$$

A.2 Conditioned Triangular

Evaluating τ_1 ,

$$2 \int_0^{\tau_1} p \ddot{x}_o \sin \omega_1 t dt = \frac{\ddot{x}_o \tau_o}{2}$$

$$\text{from which, } \tau_1 = \frac{\pi \tau_o}{8p}$$

The function is defined as,

$$\ddot{x}(t) = -p \ddot{x}_o \sin \frac{8p}{\tau_o} t$$

for $0 \leq t \leq \tau_1$

letting $T = t - \tau_1$

$$\ddot{x}(T) = \frac{2\ddot{x}_o}{\tau_o} T$$

for $0 \leq T \leq \tau_o/2$

for the purpose of establishing maxima, the function is uninteresting for $T > \tau_o/2$.

for $0 \leq t \leq \tau_1$

$$\dot{x}(t) = \int \ddot{x}(t) dt$$

$$(8) \quad \dot{x}(t) = - \frac{\ddot{x}_o \tau_o}{8} \left[1 - \cos \frac{8p}{\tau_o} t \right]$$

$$x(t) = \int \dot{x}(t) dt$$

$$(9) \quad x(t) = - \frac{\ddot{x}_o \tau_o}{8} \left[t - \frac{\tau_o}{8p} \sin \frac{8p}{\tau_o} t \right]$$

for $0 \leq T \leq \tau_o/2$;

$$\dot{x}(T) = \int \ddot{x}(T) dT$$

$$(10) \quad \dot{x}(T) = x_o \left[\frac{T^2}{\tau_o} - \frac{\tau_o}{4} \right]$$

$$x(T) = \int \dot{x}(T) dT$$

$$(11) \quad x(T) = \ddot{x}_o \left[\frac{T^3}{3\tau_o} - \frac{\tau_o T}{4} - \frac{\tau_o^2 \pi}{64p} \right]$$

\dot{x}_{\max} occurs at $t = \tau_1$ and

x_{\max} occurs at $T = \tau_o/2$.

$$(12) \quad \dot{x}_{\max} = \pm \frac{\ddot{x}_o \tau_o}{4}$$

$$(13) \quad x_{\max} = - \frac{\ddot{x}_o \tau_o^2}{8} \left[\frac{2}{3} + \frac{\pi}{8p} \right]$$

A.3 Conditioned Rectangular Pulse

To evaluate τ_1 ,

$$\ddot{x}_o \tau_o = 2 \int_0^{\tau_1} p \ddot{x}_o \sin \omega_1 t dt$$

$$\text{from which, } \tau_1 = \frac{\pi \tau_o}{4p}$$

Define the function for the first half of symmetry,

$$\ddot{x}(t) = -p \ddot{x}_o \sin \frac{4p}{\tau_o} t$$

for $0 \leq t \leq \tau_1$

and letting $T = t - \tau_1$

$$\ddot{x}(T) = \ddot{x}_o$$

for $0 \leq T \leq \tau_o/2$

for $0 \leq t \leq \tau_1$

$$\dot{x}(t) = \int \ddot{x}(t) dt$$

$$(14) \quad \dot{x}(t) = - \frac{\ddot{x}_o \tau_o}{4} \left[1 - \cos \frac{4p}{\tau_o} t \right]$$

$$x(t) = \int \dot{x}(t) dt$$

$$(15) \quad x(t) = - \frac{\ddot{x}_o \tau_o}{4} \left[t - \frac{\tau_o}{4p} \sin \frac{4p}{\tau_o} t \right]$$

for $0 \leq T \leq \tau_o/2$

$$\dot{x}(T) = \int \ddot{x}(T) dT$$

$$(16) \quad \dot{X}(T) = X_0 T - \frac{\ddot{X}_0 \tau_0}{2}$$

$$X(T) = \int \dot{X}(T) dT$$

$$(17) \quad X(T) = \frac{\ddot{X}_0}{2} \left[T^2 - \tau_0 T - \frac{\pi \tau_0^2}{8p} \right]$$

\dot{X}_{\max} occurs at $t = \tau_1$ and

X_{\max} occurs at $T = \tau_0/2$.

$$(18) \quad \dot{X}_{\max} = \pm \frac{\ddot{X}_0 \tau_0}{2}$$

$$(19) \quad X_{\max} = - \frac{X_0 \tau_0^2}{8} \left[1 + \frac{\pi}{2p} \right]$$

A.4 Conditioned Terminal Peak Sawtooth

Evaluating τ_1 ,

$$\frac{\ddot{X}_0 \tau_0}{2} = 2 \int_0^{\tau_1} p \ddot{X}_0 \sin \omega_1 t dt$$

$$\text{from which } \tau_1 = \frac{\pi \tau_0}{8p}$$

$$0 \leq t \leq \tau_1;$$

from equations 8 and 9,

$$(20) \quad \dot{X}(t) = - \frac{\ddot{X}_0 \tau_0}{8} \left[1 - \cos \frac{8p}{\tau_0} t \right]$$

$$(21) \quad X(t) = - \frac{\ddot{X}_0 \tau_0}{8} \left[t - \frac{\tau_0}{8p} \sin \frac{8p}{\tau_0} t \right]$$

for $0 \leq T \leq \tau_0$

$$\dot{X}(T) = \int \ddot{X}(T) dT$$

$$(22) \quad \dot{X}(T) = \frac{\ddot{X}_0}{2} \left[\frac{T^2}{\tau_0} - \frac{\tau_0}{2} \right]$$

$$(23) \quad X(T) = \frac{\ddot{X}_0}{2} \left[\frac{T^3}{3\tau_0} - \frac{\tau_0 T}{2} - \frac{\tau_0^2 \pi}{32p} \right]$$

\dot{X}_{\max} occurs at $t = \tau_1$ and

X_{\max} occurs at $T = \frac{2\tau_0}{3}$

$$(24) \quad \dot{X}_{\max} = \pm \frac{\ddot{X}_0 \tau_0}{4}$$

$$(25) \quad X_{\max} = - \frac{\ddot{X}_0 \tau_0^2}{2} \left[0.23457 + \frac{\pi}{32p} \right]$$

DISCUSSION

Voice: Did you consider anything besides a half sine pulse?

Mr. Frain: We are using a commercial system which presupposes the half sine waves as conditioning signatures for the pulses. We have not looked at other systems.

SEISMIC SHOCK WAVEFORM REPRODUCTION AND
SHOCK SPECTRA SYNTHESIS ON HYDRAULIC ACTUATOR

Robert S. Nichols
White Sands Missile Range, New Mexico

When using the Favour and LeBrun technique for digital computer control of an acceleration transient waveform on an electrohydraulic exciter, there are advantages in computing the required displacement time history and applying the control algorithm to it, rather than to the required acceleration time history. First, one avoids the nonlinear gain estimation techniques such as that employed by Norman Hunter (Sandia Laboratories, 1974), as electrohydraulic exciters are quite linear in this mode, particularly in the lower frequencies. Also, it is very easy to edit the Fourier transform of this required displacement time history to reduce the stroke requirements within available actuator capabilities. If the time history can not be reduced within stroke capabilities, then an iterative procedure for randomly juggling the phase portion of the required acceleration time history Fourier spectrum will generate an infinitude of other time histories with the same Fourier magnitude spectrum and shock spectrum. These time histories can be searched to locate one within available stroke capabilities.

NOMENCLATURE

X_t Calibration time history
 Y_t Acceleration response time history
 S_x Fourier transform of X_t
 S_y Fourier transform of Y_t
 $F()$ Fourier transform of argument
 $F^{-1}()$ Inverse Fourier transform of argument
 H_f Frequency response function
 R_t Required acceleration time history
 S_R Fourier transform of R_t
 S_D Frequency domain drive signal
 D_t Time history drive signal

A Acceleration
 K Coefficients of second-order gain equations
 V Voltage
 FFT Fast Fourier transform (forward)
 FFT^{-1} Inverse fast Fourier transform

INTRODUCTION

White Sands Missile Range (WSMR) has for many years been involved in virtually all phases of shock and vibration testing and simulation dealing with ground, rail, air, and ship environments. Recently, WSMR was tasked by Los Alamos Scientific Laboratories (LASL) with testing to seismic shock environments a large variety of items, some of which are quite massive. These requirements were placed in the form of time histories and shock spectra of an earthquake environment to be reproduced. Analysis of the required time

histories indicated that, with some minor modifications, the lower level time histories (and shock spectra) could be acceptably reproduced within the 10-inch displacement capability available from the WSMR electrohydraulic exciters. The high-level time histories, however, were far beyond this displacement capability, and simulation of the shock spectrum only was agreed on.

A brief investigation revealed that simulation using a decaying sinusoidal technique for shock spectrum simulation (1) also required excessive displacements. A new systematic technique for synthesis within specified displacement limits was required.

It has long been recognized that electrodynamic and electrohydraulic exciters (shakers) could be used to reproduce or simulate the transients from actual field environments. However, their use for this purpose has been quite limited until recently because the available control techniques have been inadequate to assure a high-quality reproduction or acceptable simulation.

In 1969, Favour and LeBrun of Boeing Aircraft published several papers (2, 3) on transient waveform control which revolutionized the thinking in the shock and vibration community concerning shock testing techniques. With their introduction of the use of the digital computer and the fast Fourier transform (FFT) as a control method, the ability to perform high-quality reproduction of the time history (and thus the shock spectrum) of an actual field transient came of age. Though their techniques were performed on an electrodynamic exciter and were dependent on time-invariant linear system assumptions, they did show that if a test system frequency response function could be defined accurately, then reproduction of an acceleration time history (within the exciter's capability) could be accomplished accurately. In 1974, Norman Hunter of Sandia Laboratories published a paper (4) extending the technique to electrohydraulic exciters by use of a nonlinear gain estimation scheme.

Minicomputer-based digital control systems are now readily available which can rapidly and accurately reproduce transient waveform time histories on linear systems by the Favour and LeBrun technique. This paper describes how, with some modification of the approach suggested by Hunter, the same control system technique can be extended to transient waveform control on electrohydraulic exciters. Also described is a technique for

deriving a second time history with the same shock spectrum as the first and within a required displacement capability.

REVIEW OF TRANSIENT WAVEFORM CONTROL

Linear System Technique (Electrodynamic Exciter)

A typical system for transient waveform control is shown in Figure 1. As can be seen, it is based on a linear system assumption. In tracing the flow path of action, a calibration transient time history X_t is output by the computer to the power amplifier. The power amplifier drives the exciter, producing an acceleration response transient time history Y_t . This response is measured by an accelerometer and signal conditioner system and returned to the computer. The FFT is computed for the two signals:

$$S_x = F(X_t) \quad (1)$$

$$S_y = F(Y_t) \quad (2)$$

and the system frequency response function is formed:

$$H_f = \frac{S_y}{S_x} \quad (3)$$

This system frequency response function is stored in the computer for later use. The FFT of the required transient acceleration time history is now computed:

$$S_R = F(R_t) \quad (4)$$

By use of the frequency response function previously stored, the frequency domain drive signal for the power amplifier to produce the required time history can be computed:

$$S_D = \frac{S_R}{H_f} \quad (5)$$

The time history of the drive signal is then obtained by computing the inverse fast Fourier transform of S_D :

$$D_t = F^{-1}(S_D) \quad (6)$$

This time history is then applied to the power amplifier, and the response of the test specimen is measured. If the system is linear, the reproduced time history and shock spectrum will match the required time history and shock spectrum within the accuracy and dynamic

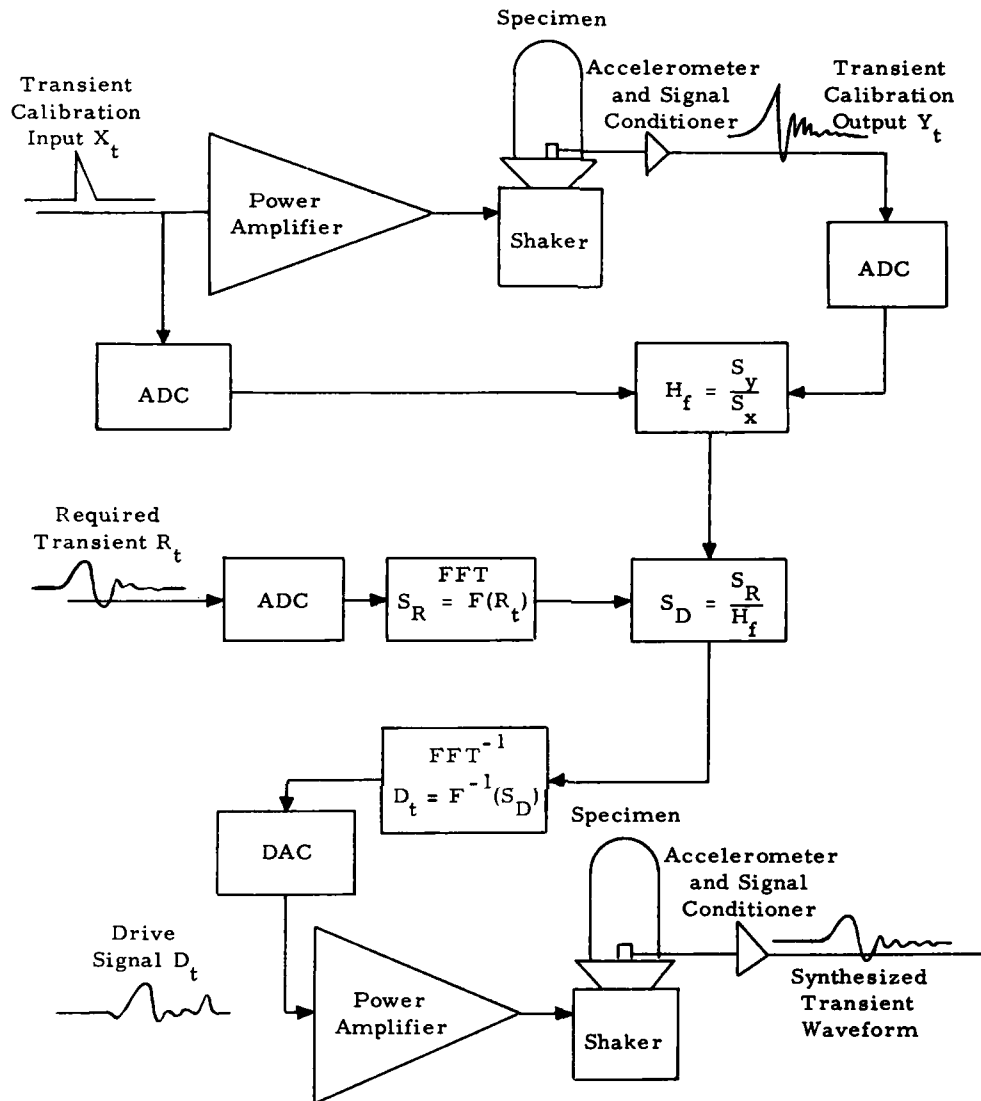


Fig. 1 - Transient Waveform Control System Block Diagram

range limits of the system.

It is quite feasible to use a previously determined frequency response function from an identical test setup to avoid imposing even the calibration pulse on the test specimen. This method obviously provides less accurate reproduction. Another technique used to advantage where multiple tests of the same specimen are conducted is to continuously update the estimate of the frequency response function.

Nonlinear System Technique (Electrohydraulic Exciter)

The nonlinear technique published by Hunter (4) required the gain characteristic at each frequency to be determined before the actual test from at least two calibration levels. A best-fit second-order approximation of the gain characteristic was then made, and this second-order equation was used to modify the drive signal spectrum.

As an example, at a single given frequency, the gain characteristics for actual data, a linear assumption, and a second-order assumption are illustrated in Figure 2. A zero acceleration has been assumed for a zero drive voltage. Two (different level) calibration pulses have been applied to the system. The input and output time history for each level Fourier transformed, the drive voltages V_1 and V_2 , and acceleration responses A_1 and A_2 were determined. Based on the second-order assumption:

$$A_1 = K_1 V_1 + K_2 V_1^2 \quad (7)$$

$$A_2 = K_1 V_2 + K_2 V_2^2 \quad (8)$$

Solving for the coefficients K_1 and K_2 gives:

$$K_1 = \frac{A_1 V_2^2 - A_2 V_1^2}{V_1 V_2 (V_2 - V_1)} \quad (9)$$

$$K_2 = \frac{A_2 V_1 - A_1 V_2}{V_1 V_2 (V_2 - V_1)} \quad (10)$$

Thus, at each frequency for a given required acceleration A_R , the required drive voltage V_D is related by:

$$A_D = K_1 V_D + K_2 V_D^2 \quad (11)$$

Solving for all the V_D 's from the different frequencies will yield the frequency domain drive

signal, which may then be inverse transformed to provide a time domain drive signal for input to the system.

DISPLACEMENT WAVEFORM CONTROL

With the realization that the electrohydraulic exciter system is a displacement controlled device which is quite linear with respect to displacement amplitude, and that Hunter's nonlinear compensation equation (11) would be linear if written in terms of displacement, it appeared feasible to compute the displacement of required acceleration time history and use it as the input to the electrohydraulic exciter control system.

The required vertical acceleration time history (Fig. 3) was integrated twice, with appropriate removal of dc offsets and reduction of end effects to allow for a smooth application of the transient without imposing a step function on the test specimen. It was also scaled into engineering units (inches). The required displacement was in excess of 40 inches because of the size of the very low frequency components (Fig. 4). The acceleration time history was then Fourier transformed, and some of the low-frequency components were removed and then inverse Fourier transformed. The displacement time history was again computed and scaled as before. This removal of low-frequency components continued until the displacement required was within the 10-inch stroke limit available at WSMR. The displacement time history is shown in Figure 5. Only the first five frequency lines, dc through approximately 0.025 Hz, had to be removed.

This displacement drive signal was scaled and used to drive the electrohydraulic exciter system with a dummy load mounted. The displacement time history was derived from the accelerometer return signal, and the Favour and LeBrun technique was used to compute a frequency response compensated displacement drive signal. This compensated drive signal varied little from the uncompensated. Additional testing showed that in this low-frequency range the compensation required varied little for a wide range of loads, making a single compensation for the basic hydraulic control system feasible. This technique was used to prepare displacement drive signals for three different transients. Figures 6 through 9 show the system block diagram, computer control system, hydraulic control system, electrohydraulic exciter, and actual test specimen. Data from an accelerometer mounted at the test specimen interface was recorded, and the acceleration time history and shock spectrum

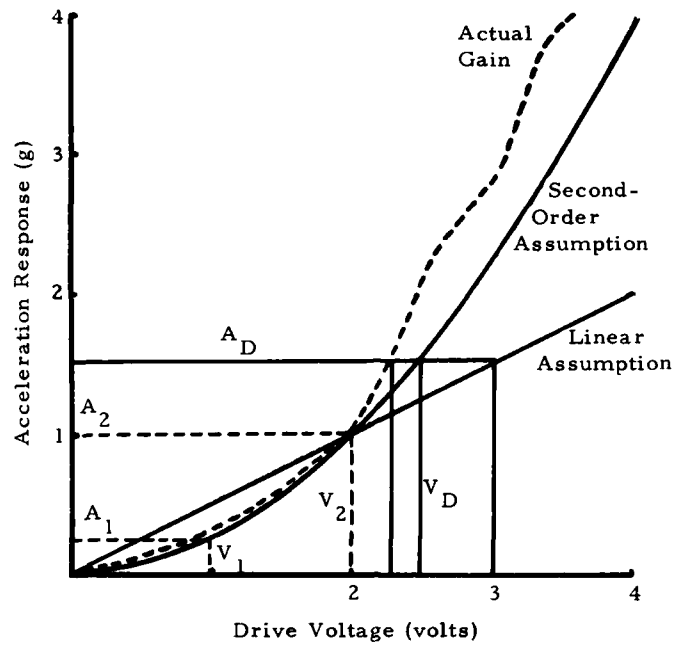


Fig. 2 - Gain Characteristics

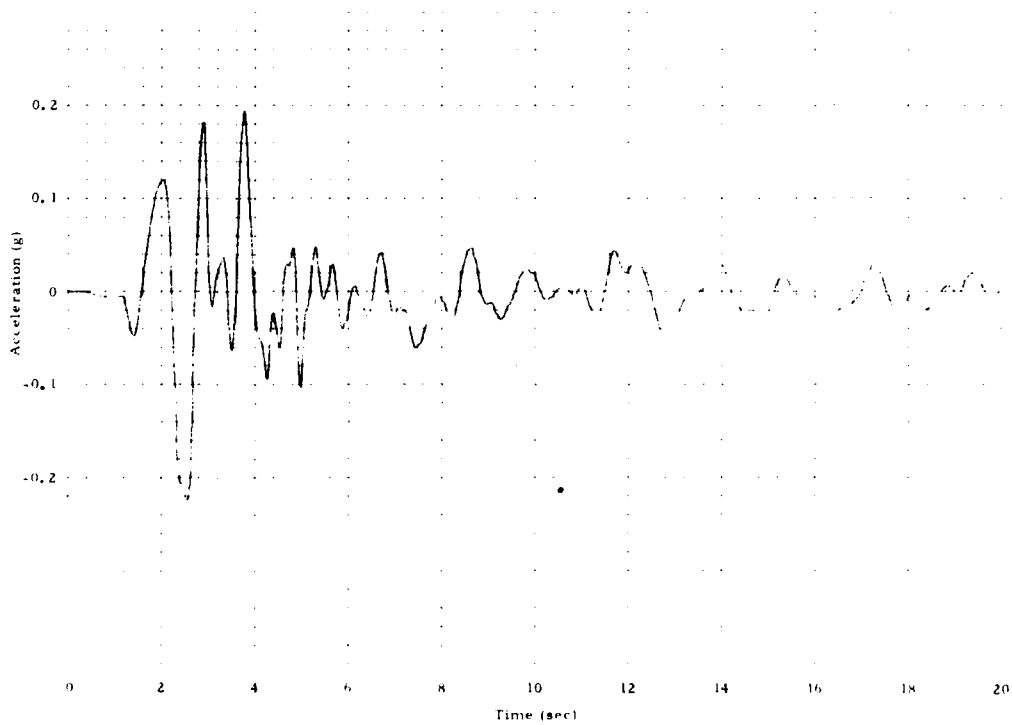


Fig. 3 - Required Acceleration Time History (Vertical)

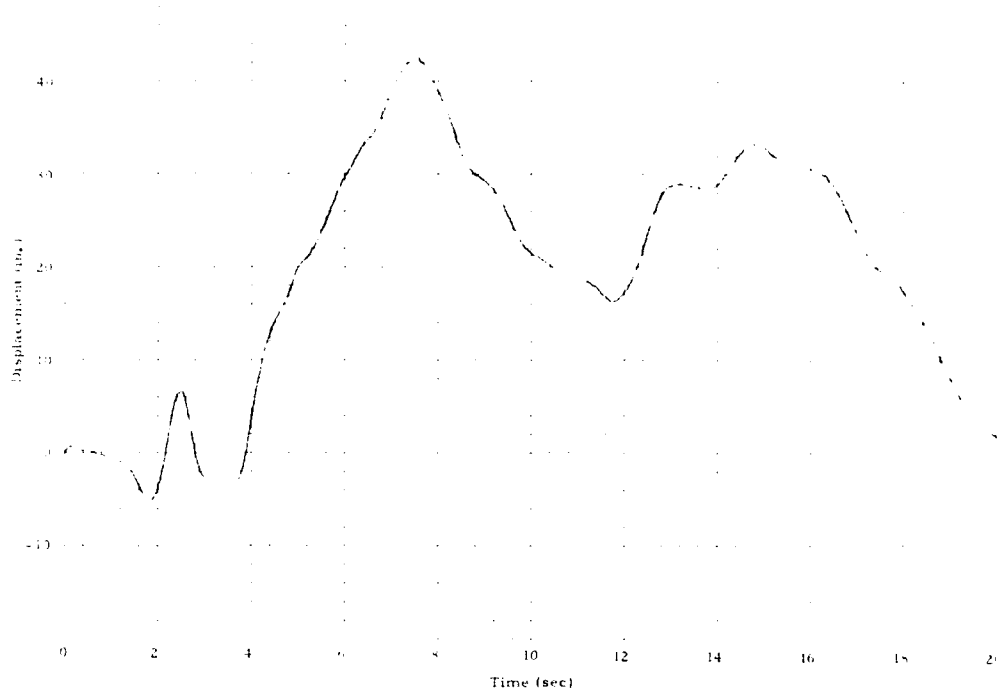


Fig. 4 - Required Displacement Time History (Vertical)

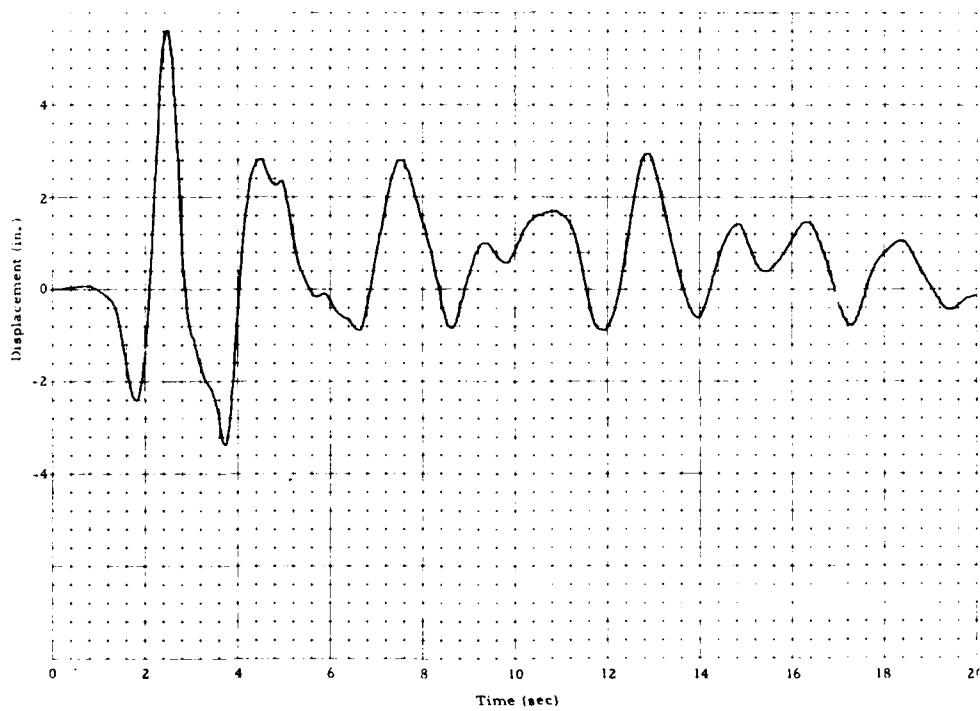


Fig. 5 - Compensated Required Displacement Time History (Vertical)

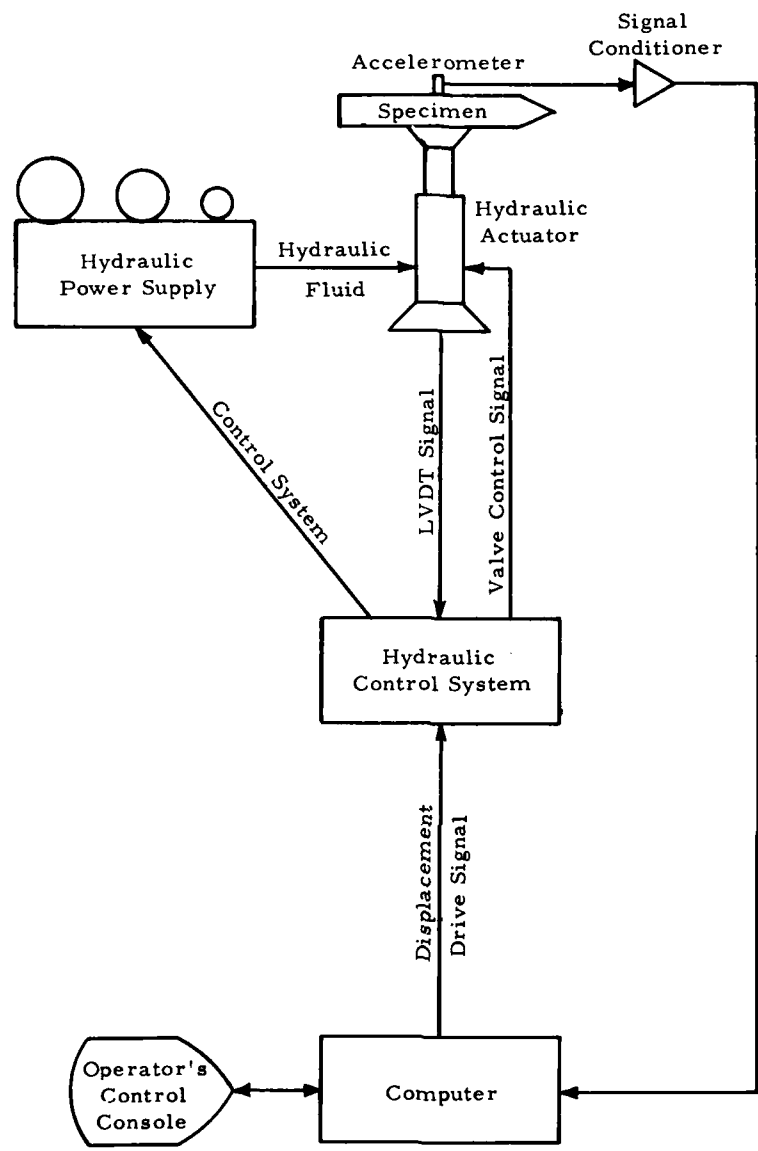


Fig. 6 - System Block Diagram



Fig. 7 - Computer Control System

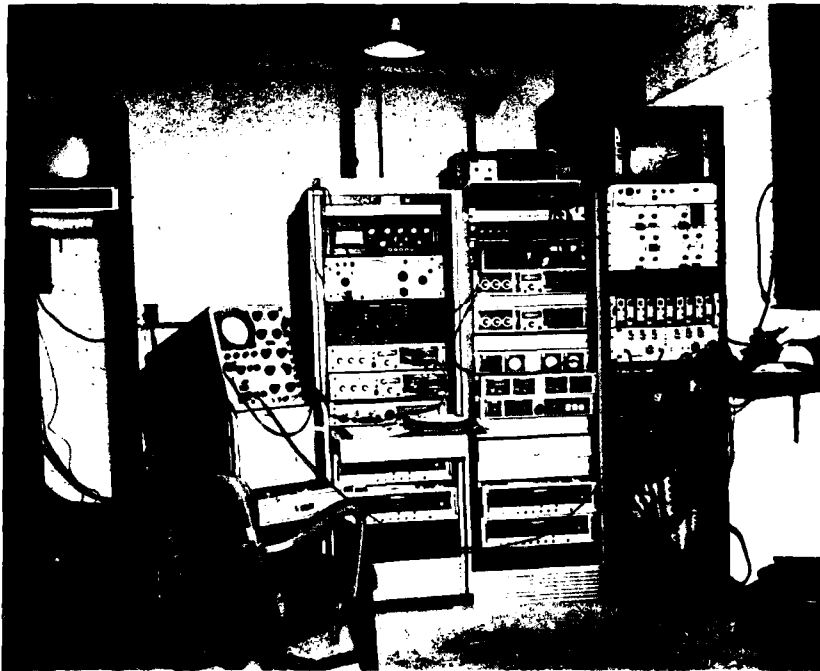


Fig. 8 - Hydraulic Control System

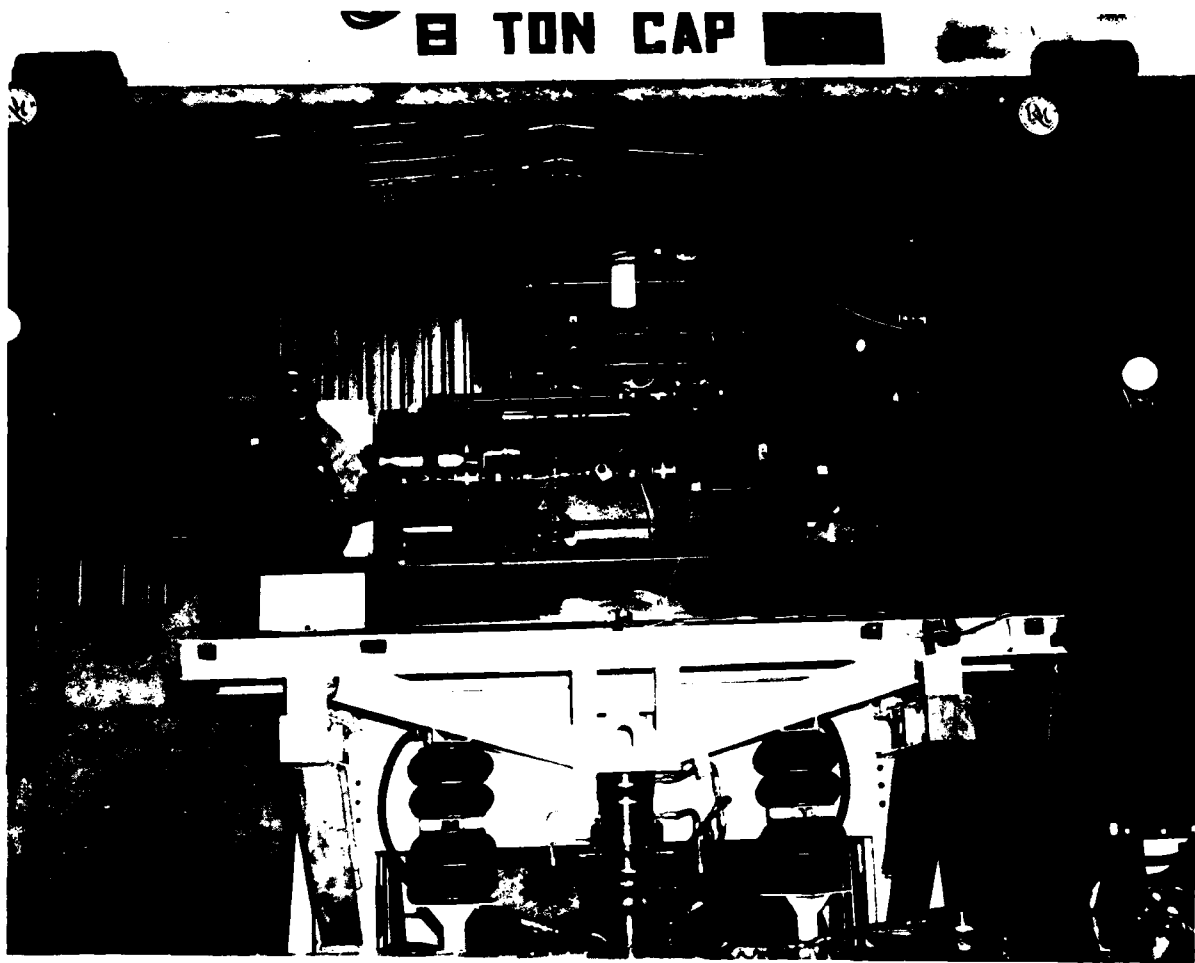


Fig. 9 - Electrohydraulic Exciter and Test Specimen

were computed. Figures 10 through 15 show comparisons of reproduced acceleration transients and shock spectra with actual transients and shock spectra.

WAVEFORM SYNTHESIS

In some cases, the transients to be reproduced cannot be successfully modified by removal of the low-frequency components to reduce the stroke requirements within the available displacement limits. The following procedure has been used successfully in deriving another time history which has the same shock spectrum but is within stroke capabilities. First, the required acceleration time history and a like-length, unity-magnitude, pseudo-random signal are Fourier transformed and multiplied (rectangular coordinates). The resulting spectrum is then inverse transformed, and the displacement time history is computed. This time history is then windowed (the Hanning window is ideal) to reduce the end effects toward zero. The resulting displacement time history is checked for the stroke requirement. If the stroke is too large, the initial pseudo-random time history is shifted one sample period in time, and the process is repeated. This continues until a time history is found that is within the available displacement capability. Figure 16 is a block diagram of the process, and Figures 17 through 21 show a comparison of an original acceleration time history, displacement requirement, and shock spectrum with the actual test results achieved by using a displacement drive signal derived by the above procedure and by using the described displacement waveform control.

The approach thus amounts to a random juggling of the phase components of the required acceleration time history's transform. The beauty of the approach is that it is systematic and easily automated on existing mini-computer control systems. While it is conceivable that no acceptable time history could be found by the approach, experience has shown that it usually produces an acceptable transient within a very small number of trials.

CONCLUSIONS

It is apparent that transient waveform control of electrohydraulic exciters can be accomplished readily in the displacement compensation mode. Accurate reproduction of acceleration waveform and shock spectrum has been demonstrated for low-frequency seismic shock requirements, and the technique is much easier to implement in most cases than the nonlinear gain estimation scheme. This does not

mean that the nonlinear gain estimation technique has been replaced; only that a simpler approach yields satisfactory results for at least some cases.

The technique presented for derivation of additional time histories with the same shock spectrum as a given time history is easy to automate on any computer. The requirement to search for time histories below a given displacement or velocity limit can be used to find a pulse within equipment limitations.

REFERENCES

1. D. O. Smallwood and A. R. Nord, "Matching Shock Spectra with Sums of Decaying Sinusoids Compensated for Shaker Velocity and Displacement Limitations," *Shock and Vibration Bulletin* No. 44, Part 3, pp. 43-55, Aug. 1974
2. J. D. Favour, J. M. LeBrun, and J. P. Young, "Transient Waveform Control of Electromagnetic Test Equipment," *Shock and Vibration Bulletin* No. 42, Part 2, pp. 45-53, Jan. 1972
3. J. D. Favour and J. M. LeBrun, "Feasibility and Conceptual Design Study - Vibration Generator Transient Waveform Control System," Final Report prepared for NASA under Contract NAS5-15171, Goddard Space Flight Center, Greenbelt, Maryland, by Aerospace Group, The Boeing Company, Kent, Washington, Jun. 1969
4. N. F. Hunter, "Transient Waveform Reproduction on Hydraulic Actuators Using a Non-Linear Gain Estimation Technique," *Proceedings of Environmental Sciences*, pp. 202-206, 1974

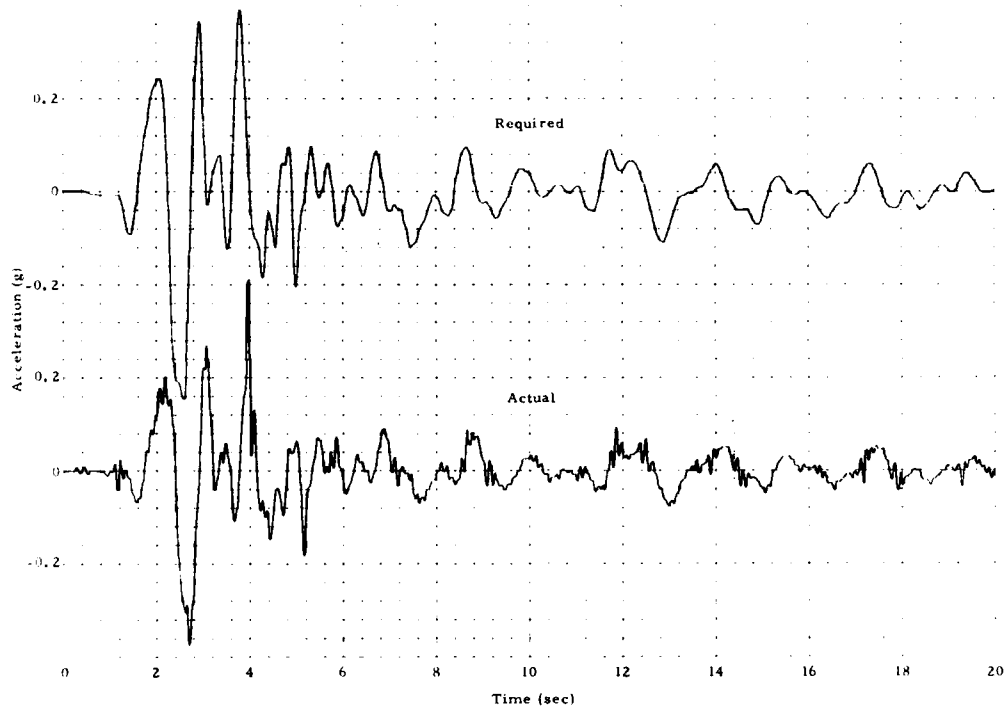


Fig. 10 - Acceleration Time History (Vertical)

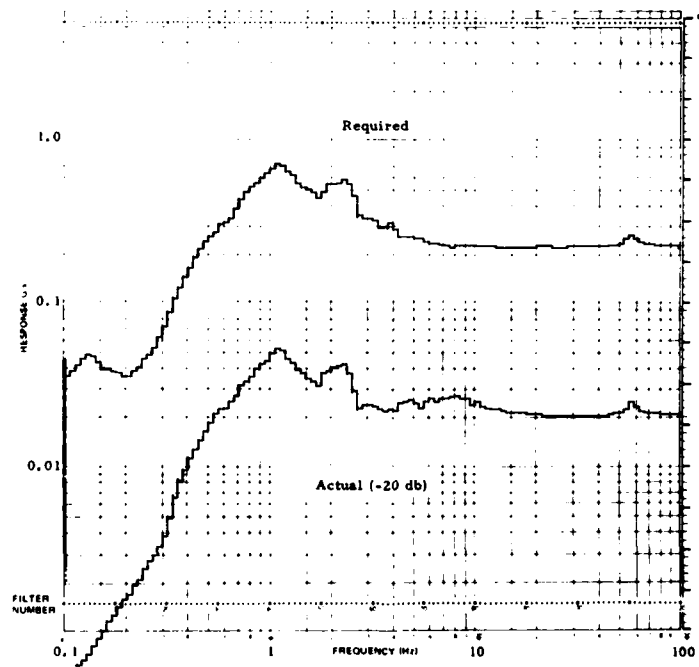


Fig. 11 - Shock Spectrum (Vertical; Q = 10)

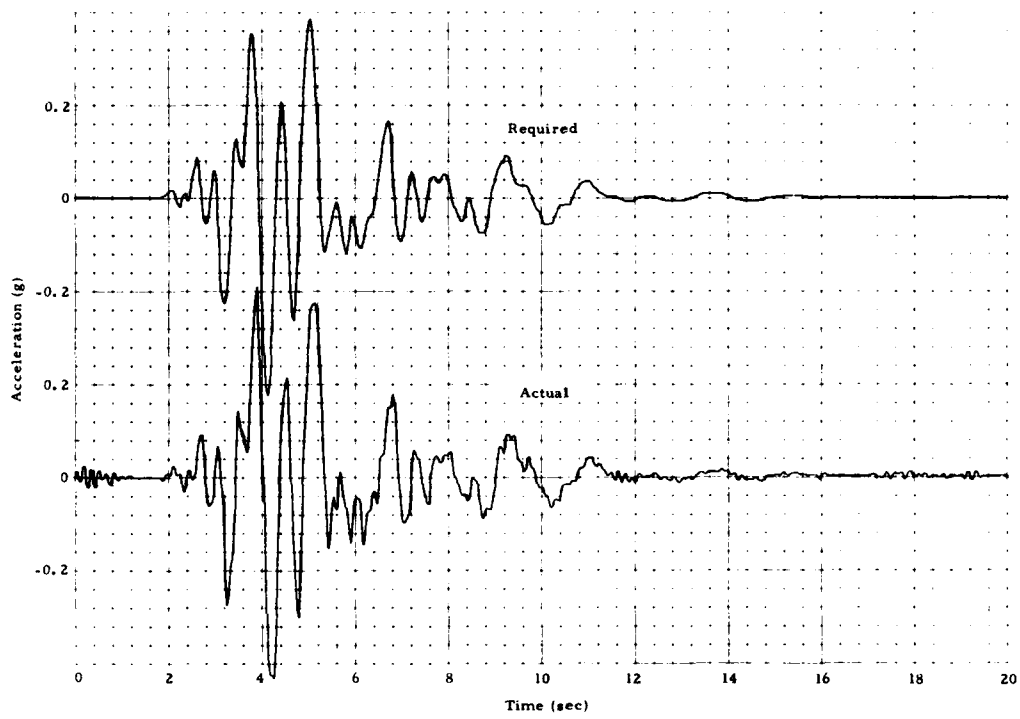


Fig. 12 - Acceleration Time History (Lateral)

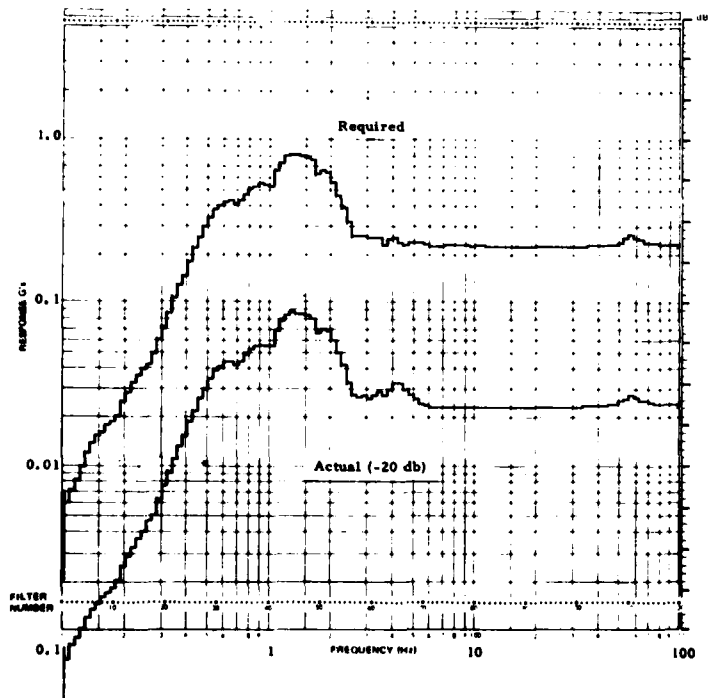


Fig. 13 - Shock Spectrum (Lateral; Q = 10)

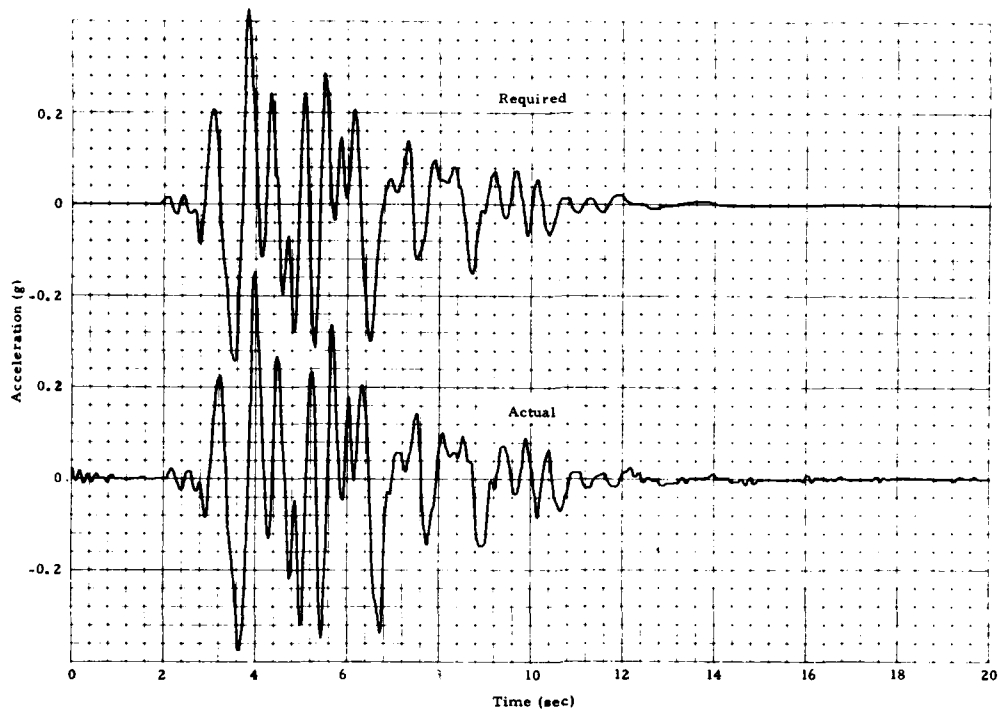


Fig. 14 - Acceleration Time History (Longitudinal)

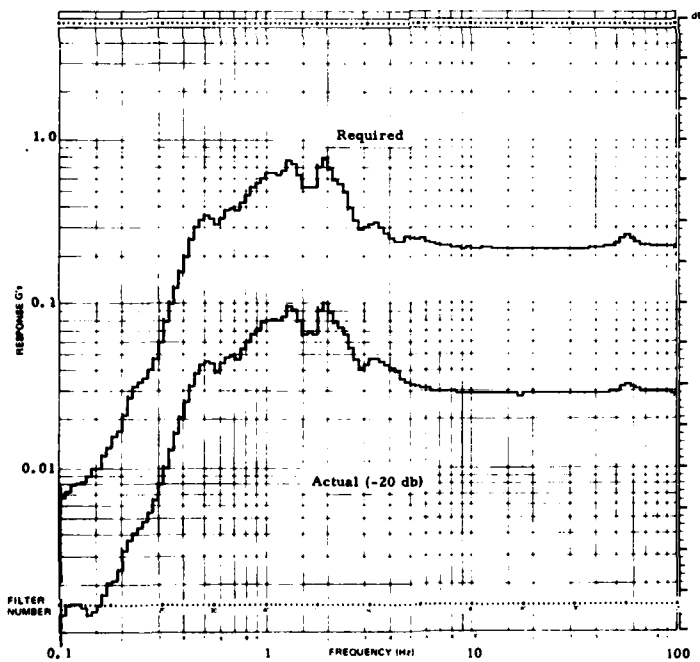


Fig. 15 - Shock Spectrum (Longitudinal; Q = 10)

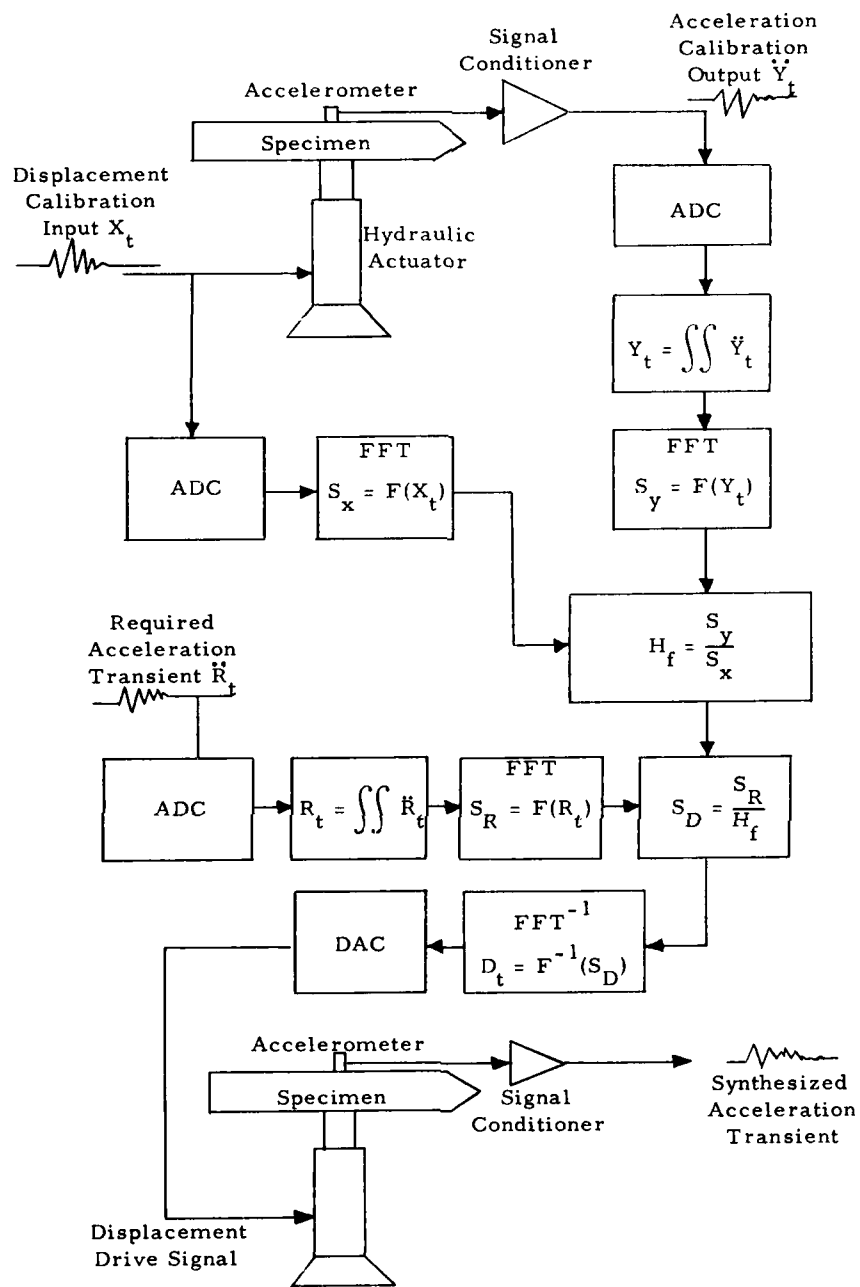


Fig. 16 - Displacement Waveform Control Block Diagram

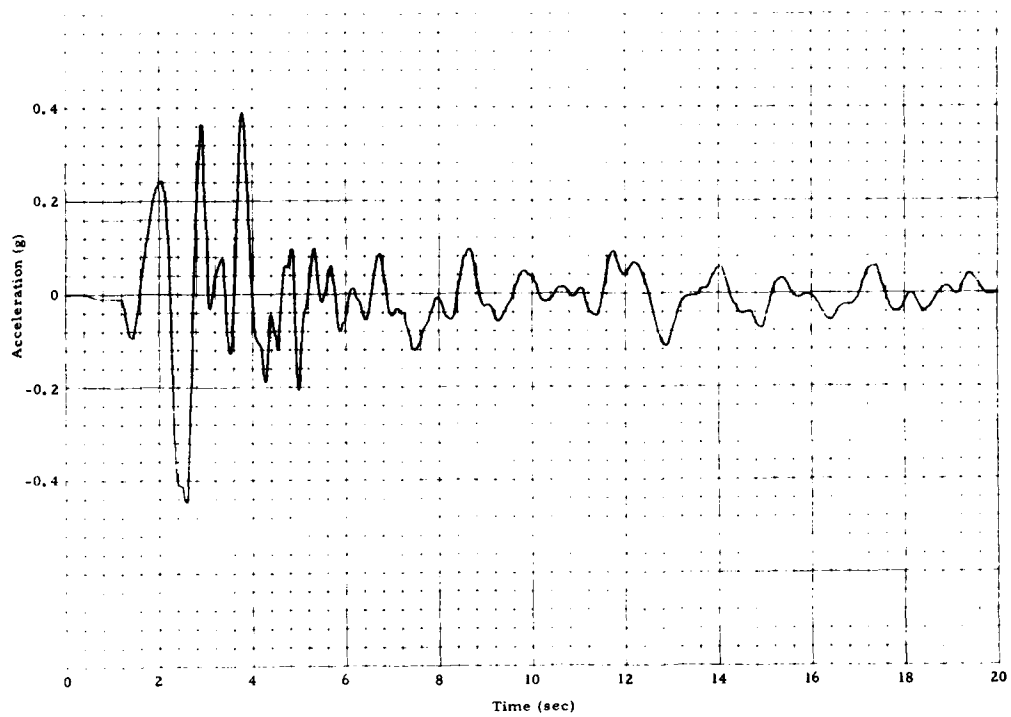


Fig. 17 - Acceleration Time History, Required

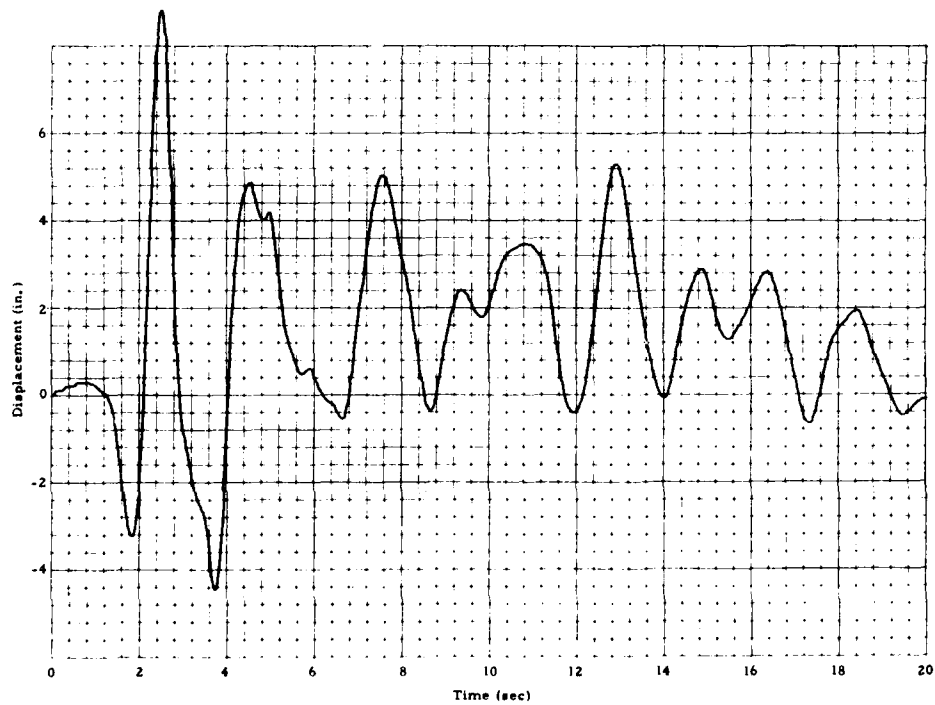


Fig. 18 - Displacement Time History, Required (Low-Frequency Compensated)

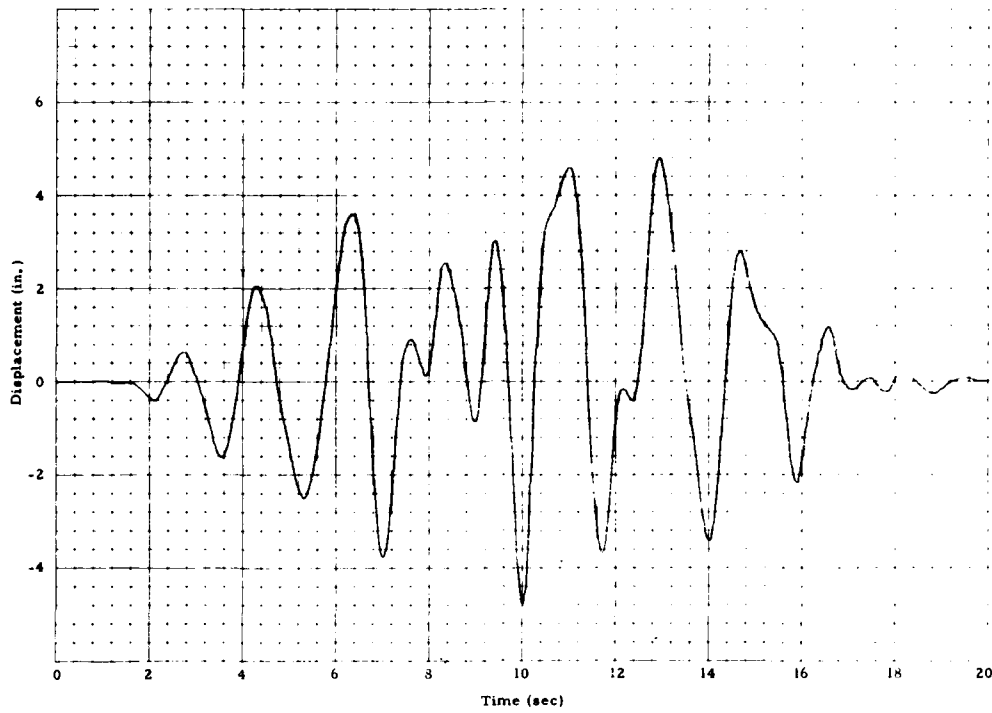


Fig. 19 - Displacement Time History, Actual (Phase Modified)

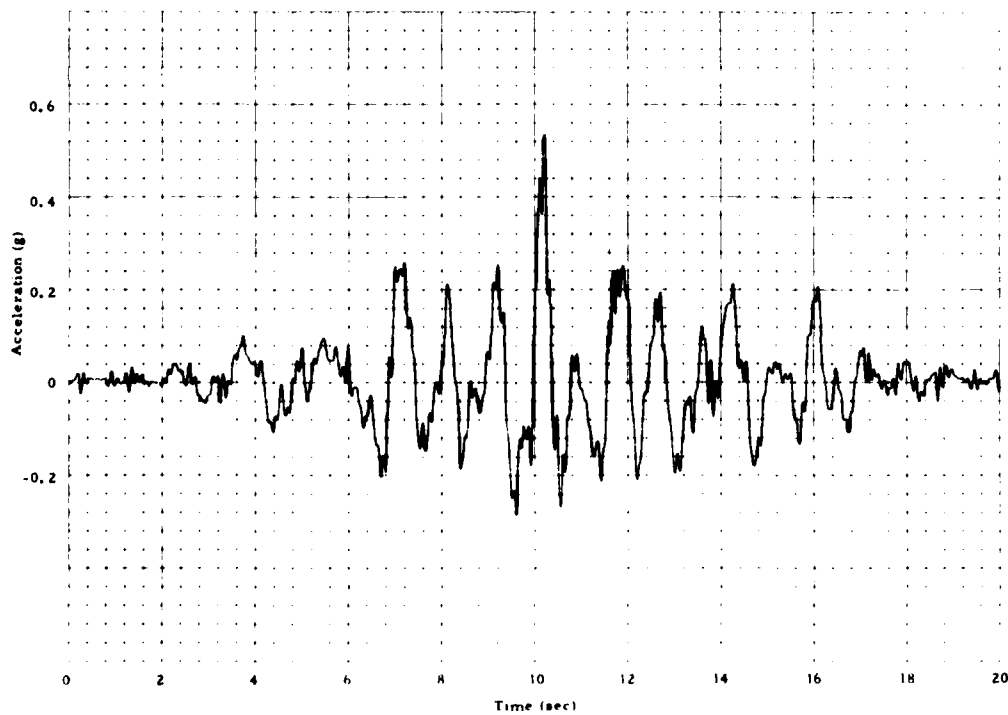


Fig. 20 - Acceleration Time History, Actual (Phase Modified)

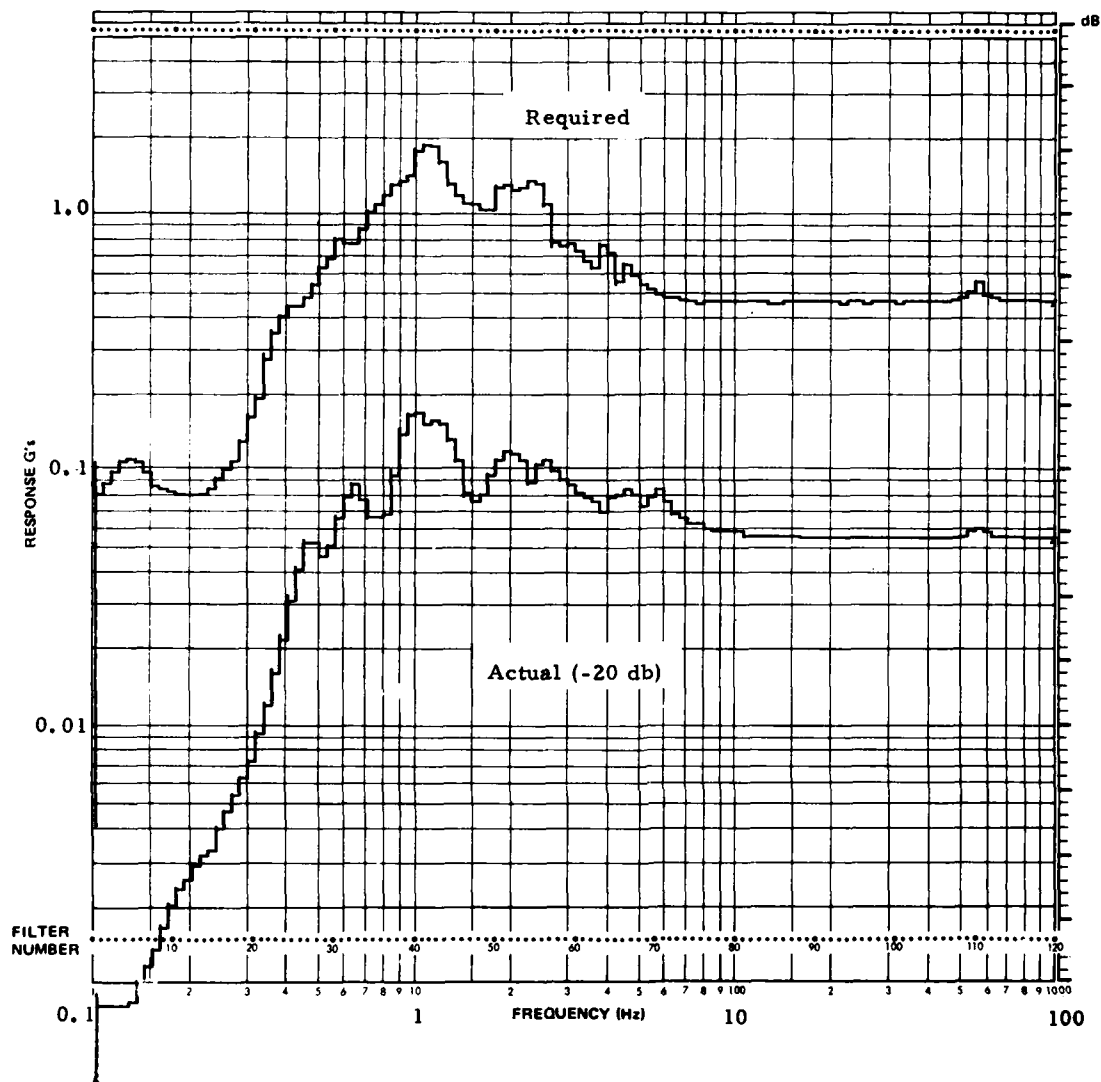


Fig. 2i - Shock Spectrum (Phase Modified; $Q = 10$)

Discussion

Mr. Fisher (Lawrence Livermore Laboratory):
You had a slide showing non-linear gain. How did you get that data and how do you appropriate that into your computation?

Mr. Nichols: I'll make no pretense that that non-linear gain looks like the real thing. The first and second order are computed, they are true. I drew the non-linear gain portion in.

Mr. Fisher: It was a single frequency test like sinusoidal test, I don't understand why the acceleration was not proportional to the displacement and why one was linear and the other was nonlinear.

Mr. Nichols: This is not a single frequency. This gain estimation technique is taking the gain and the drive signal, putting them in the frequency domain and looking at each individual frequency and the drive voltage that are required to generate that acceleration. You will not get a constant acceleration amplitude out of an electro-hydraulic shaker. In an electro-hydraulic system, which is a displacement controlled device, if you put in 1 volt you will get 1 inch, regardless of the frequency out to the limit where you begin to get into the roll-off characteristics of the system.

Mr. Gaberson (Naval Civil Engineering Lab.):
In this last technique where you multiplied the random cycle, was that your technique for removing the low frequency?

Mr. Nichols: No, there were two parts to it. One is the conversion to the frequency domain; that is removing the low frequency components until you can get the wave form within your displacement capabilities. Sometimes you can't remove enough of those components to the point that the customer is willing to tolerate the pulse.

ISOLATION AND DAMPING

EXPERIENCES ON SHOCK ISOLATION OF EQUIPMENT IN THE SAFEGUARD SYSTEM

M. A. Boyd and C. C. Huang
U. S. Army Engineer Division, Huntsville
Huntsville, Alabama

Shock protection of equipment is a major consideration for facilities that are hardened against nuclear weapons. In the SAFEGUARD Ballistic Missile Defense (BMD) System, large quantities of commercially available industrial grade equipment were used for which no fragility data were available. Shock isolation systems were provided to protect equipment critical to the BMD mission. The shock isolation effort involved determining which equipment needed shock isolation, developing shock isolation system criteria, design, fabrication, and installation of isolation systems, and verifying the performance of installed systems. An extensive shock test program was undertaken to qualify both hard-mounted and shock isolated equipment and required improved test methods and hardware. This paper highlights the approaches used and experience gained during the project and presents conclusions that could be of benefit to those who may be engaged in providing shock isolation protection in future weapon systems.

INTRODUCTION

Shock isolation systems for the SAFEGUARD Ballistic Missile Defense (BMD) System evolved during the period from 1968 to 1975. Three major aspects of the shock isolation effort were: establishing the need for equipment protection based on environments; equipment criticality and equipment fragility; development of criteria for the design, fabrication, and installation of shock isolation systems; and verification that the installed systems were in compliance with performance and survivability requirements.

Two categories of equipment in SAFEGUARD were: Weapon Systems Equipment (WSE) which consists of radars, data processors, and missiles and Tactical Support Equipment (TSE) which furnishes electrical power and environmental control for the WSE and life support systems. Both the WSE and TSE are housed in hardened facilities. This paper addresses TSE exclusively.

TSE was primarily commercially available high-grade industrial equipment. The decision to use commercial equipment instead of hardened equipment was based on the considerations of scheduling and equipment costs in the early SAFEGUARD (then called SENTINEL) program.

To decide which TSE required shock isolation and which could be hardmounted, the TSE subsystems were first screened to identify those having functions critical to the accomplishment of SAFEGUARD missions. The hardmount versus shock-isolate decision for mission critical equipment was then made based primarily on engineering judgment since fragility data on commercial equipment were not available at the time. Further, the procurement of TSE was based on performance specifications and by competitive bid; there was no prior knowledge of the manufacturer, equipment model, and component details that are essential to hardness estimates. The shock-isolate or hardmount decision process was carried out with

conservatism, i. e., when in doubt, shock isolation protection was provided because of the uncertainties involved. Ultimately, 107 shock isolation systems were specified, designed, and installed at the SAFEGUARD North Dakota Site for the protection of critical TSE.

SAFEGUARD TSE shock isolation systems are basically welded steel platforms supported by either base-mounted or pendulum-type shock isolators. The isolators reflect the state-of-the-art technology existing at that time. Helical mechanical springs with or without coulomb damping were used for base-mounted systems. Both helical mechanical springs and pneumatic springs [1] were used for pendulum systems. Considerations for selecting the type of isolators include the equipment type, size and weight, static load of each isolator, maintenance, and costs. The guidelines established were that mechanical springs would be used when the static load of each isolator was under 3000 lbs. Pneumatic springs would be used for static loads above 3000 lbs. A summary of the ranges of shock isolation system parameters is given in Table 1. Computer codes were developed for the design of the shock isolation system to account for three-dimensional large amplitude responses to time-dependent motions of the building in which the isolation systems were installed. The design philosophy, performance requirements, and computer code formulation of the TSE shock isolation systems are found in Reference 2. Typical shock isolation systems are shown in Figures 1 through

3. Figure 4 shows maximum input spectra (derived from building motions) to the TSE shock isolation systems and Figure 5 gives nominal platform environment.

Extensive shock testing was undertaken to verify the survivability of critical TSE, both hardmounted and shock isolated. Hardmounted equipment was tested on the basis of "go/no-go." Shock isolated TSE was tested in increasing levels to establish an approximate fragility level. The shock environment at the platforms under full threat was determined by combination of dynamic analysis [3], mechanical impedance tests of isolation system components [4] and in situ tests of a number of TSE shock isolation systems under operating conditions [5].

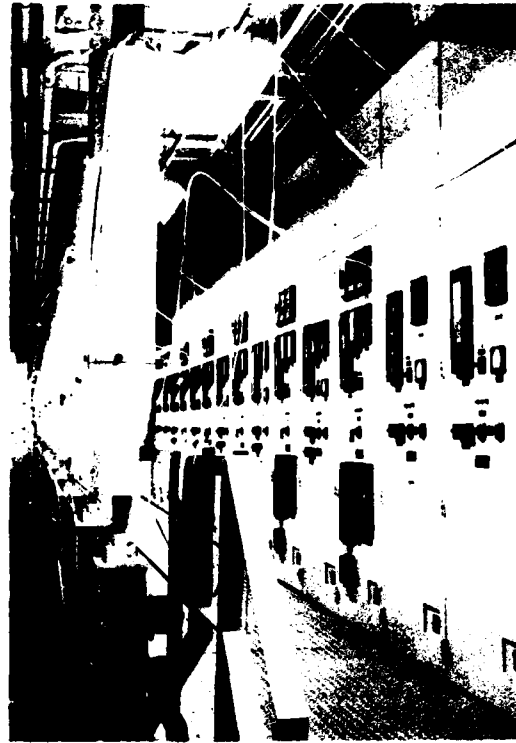
LESSONS LEARNED

The findings of the hardness assessment of the TSE installed at the Grand Forks site conclude that 99 percent of the mission critical TSE would survive and the remainder could survive with recommended retrofits [6]. Accordingly, the TSE shock isolation project for SAFEGUARD successfully met its objectives. From the perspective of hindsight the experience gained from this effort, whether satisfying or frustrating, could benefit those involved with shock isolating equipment in future weapons systems. While the overall results of the SAFEGUARD experience were satisfying, some of the lessons learned are reflected in the following considerations.

Table 1. Shock Isolation System Parameters

Parameter	Range	
	Minimum	Maximum
Platform Length (ft)	4.5	77.0
Platform Width (ft)	3.0	50.0
Aspect Ratio (L/W)	1.0	15.4
Platform Area (sq/ft)	15	3,136
Total Weight (lb)	1,400	284,000
Platform Weight (lb)	400	132,000
Weight Ratio (total wt/plat. wt)	1.5	11.8
Density (total wt/area) (lb/ft ²)	59	647
Moment of Inertia (in. ⁴)	40	20,095
Frequency (Modal, Hz)	0.6	91.7
Isolators (Numbers)*	4	60
Total Weight/Isolator	350	18,050
Isolator Static Loads (lb)	50	20,000
Isolator Stiffness (lb/in.)	5	1,675
Isolator Natural Freq (Hz)	0.6	2.0
Isolator Stroke (in.)	+4	+8
Isolator Damping (% of crit)	0	20

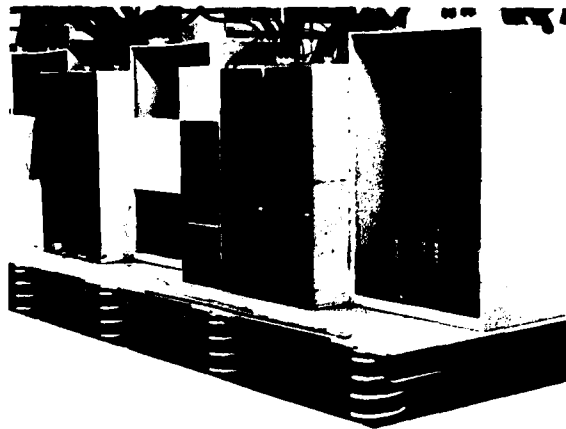
*For isolator mounted platforms. A number of electrical panels were individually isolated by hanging from two isolators.



NOTE:

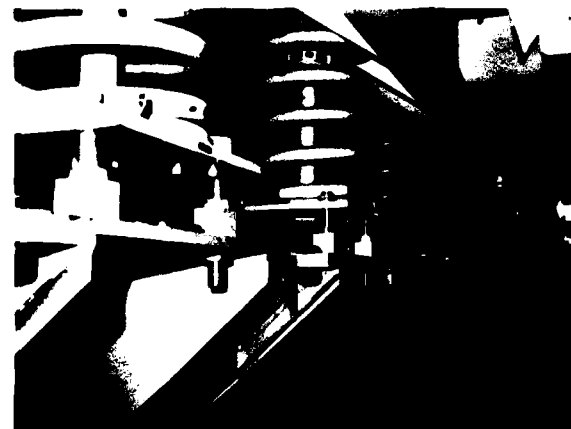
FOR HIGH VOLTAGE SWITCHGEAR USING PNEUMATIC PENDULUM ISOLATORS. PLATFORM SIZE APPROXIMATELY 15 FT BY 70 FT. WEIGHT APPROXIMATELY 240,000 LB. CABLES ARE FOR IN SITU SHOCK TEST INSTRUMENTATION.

Figure 1. Typical Pendulum Mounted TSE Shock Isolation System



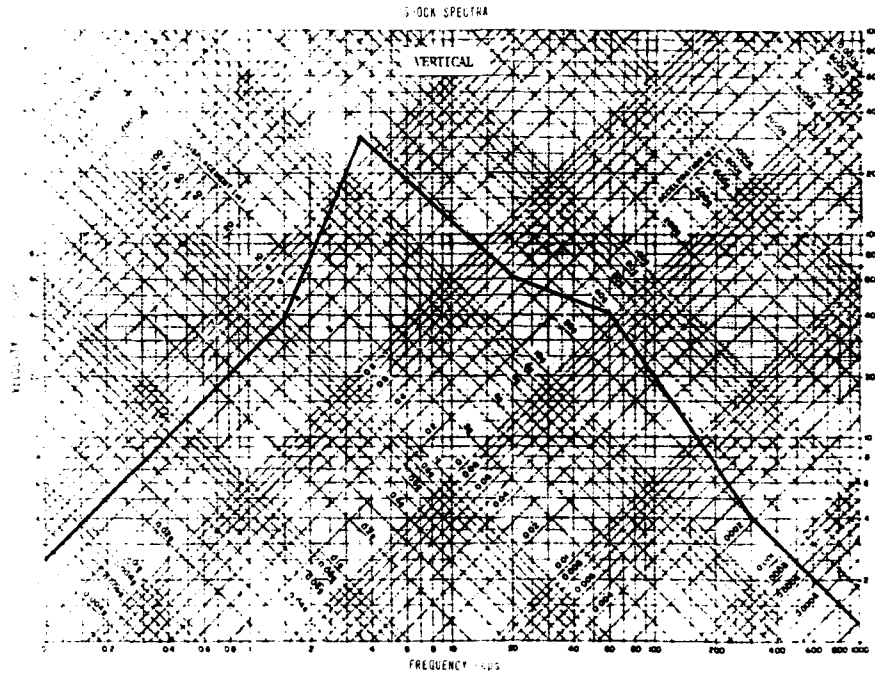
NOTE:
WITH UNDAMPED HELICAL SPRING ISOLATORS (DURING TSE INSTALLATION).

Figure 2. Typical Base Mounted TSE Shock Isolation System

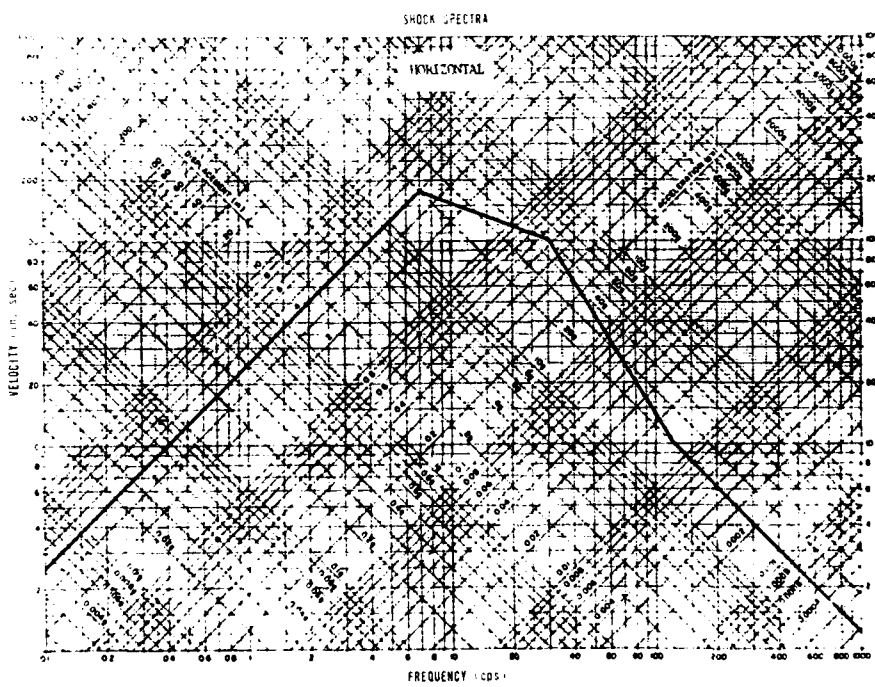


NOTE:
WITH COULOMB DAMPED MECHANICAL SPRING ISOLATORS. PLATFORM SIZE APPROXIMATELY 50 FT BY 40 FT. WEIGHT APPROXIMATELY 200,000 LB.

Figure 3. Close-up of Underfloor Shock Isolators for Power Plant Control Room Floor



Vertical Spectrum



Horizontal Spectrum

Figure 4. Examples of TSE Shock Isolation System Input (Building Motion) Shock Response Spectrum

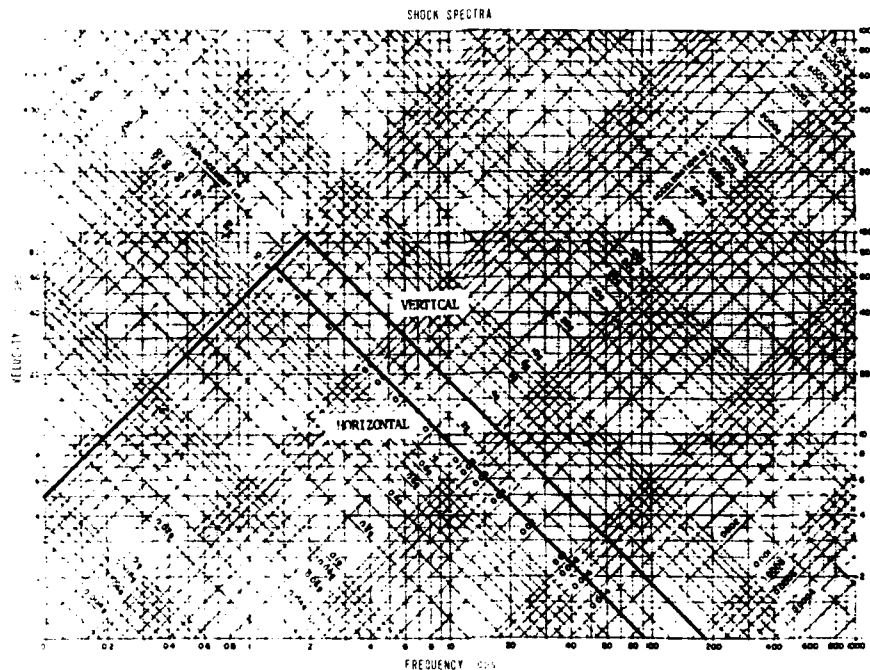


Figure 5. Nominal Isolation System Response Spectra (Platform Environments) for TSE Shock Isolation System Design

Criteria Development:

The active participation of facility designers should begin at the start, i. e., with the development of the basic nuclear weapon effects environmental criteria for weapons systems. This not only insures that the designer has a thorough understanding of the criteria, its assumptions, limitations and development, but helps provide for more reasonable and consistent criteria. Where possible criteria should avoid unique worst case conditions but should include a family of conditions consistent with the system's survivability requirements so that statistical approaches can be used for hardness verification.

Shock Isolate vs Hardmount Decision:

The decision to shock isolate or hardmount equipment involves a tradeoff among survivability, cost and schedule. SAFEGUARD experience has demonstrated that industrial grade equipment is a cost effective approach to TSE. However, there are a number of areas for improvement.

Equipment Procurement:

The approach to equipment procurement should be made as flexible as possible. For SAFEGUARD, TSE was procured by competitive bid and on performance specifications with no shock tolerance requirements. This decision was fully justified in the environment at that time. If a hardness requirement had been included in the equipment procurement specifications, it would have forced the suppliers to perform extensive testing to determine hardness tolerance of their product because such data were not available in most cases. Also, testing equipment was not readily available and refined testing techniques to simulate SAFEGUARD shock environments were yet to be developed. The added cost and time delay that would result from including hardness requirements in TSE procurement specifications would have been prohibitive. However, under the approach selected, the procurement procedures denied designers any knowledge of the make, model and details of equipment eventually to be acquired and the opportunity to pretest several candidates to establish the most desirable ones

from a hardness viewpoint. The designers, therefore, were forced to rely on their judgment in deciding whether or not shock protection was needed for a particular piece of critical equipment. In contrast to the late 1960s, the current demand for earthquake-proof equipment for nuclear power plants has stimulated manufacturers to become much more knowledgeable in the subjects of fragility and production of rugged equipment at a competitive price. Most of the minor failures encountered in SAFEGUARD shock testing such as broken welds, failure of secondary structural elements, or damage due to inadequate tie downs could be avoided by careful attention to design details, materials selection and quality control. No major equipment development is necessary to correct these types of weaknesses. An example of poor materials selection (cast aluminum) for mounting flanges of a wall-mounted transformer is shown in Figure 6. In a similar case, extensive retrofit was necessary for storage battery cases in a critical electrical back-up system. This retrofit could have been avoided if a more expensive impact resistant case material such as polycarbonate had been specified. The fluorescent light fixtures shown in Figure 7 illustrates another example of how minor changes can significantly improve shock resistance. Tests of typical fixtures from several manufacturers were performed early in the program prior to the facility design. These tests demonstrated

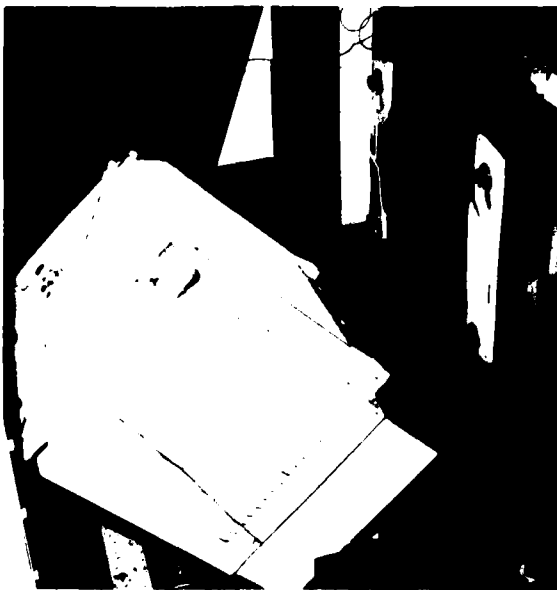


Figure 6. Example of TSE Failure During Shock Test

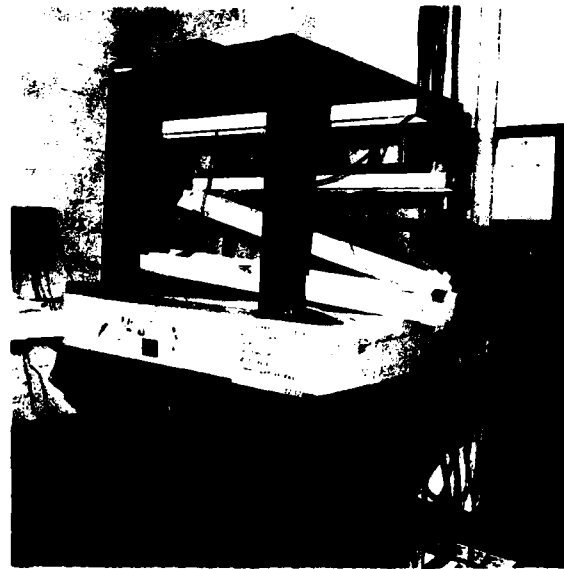


Figure 7. Failure of Fluorescent Light Fixtures During Shock Test

that use of positive fasteners, e.g., sheet metal or machine screws, to reinforce the usual snap-together type of fixture construction plus use of lamp locking sockets would prevent the fixtures from becoming a debris hazard in shock and vibration environments. Unfortunately, the simple ruggedization requirements were not included in the subsequent procurement specifications and the as-installed fixtures, which complied with the performance requirement, failed under shock tests and extensive retrofits were required to ruggedize the fixtures. Figure 8 shows an example of one type of fluorescent fixture "fix" being shock tested.

Preselection Shock Tests:

In the absence of fragility information and/or knowledge of manufacturer, model, etc., of installed TSE, shock tests of "typical" equipment items should be conducted for preselection of a number of candidate products. Such a test program should be coordinated with the equipment procurement schedule and facility design schedule, to the extent possible, to ensure that appropriate specimens are selected and simple ruggedization techniques, e.g., positive fasteners to reinforce or replace snap-in or other quick assembly connectors, are included in the procurement specifications to avoid costly retrofit. This approach is cost effective where large quantities of equipment are involved.



NOTE:

'MOD A' IS A SHEET METAL STIFFENER AND 'MOD B' IS A MACHINE SCREW FASTENER.

Figure 8. Example of "Fixes" to Ruggedize Fluorescent Fixtures Being Shock Tested

Shock Isolation Limitations:

Facility designers should be aware of the state-of-the-art of shock isolation systems and recognize that shock isolation is not always a panacea. If shock isolation is applied improperly, it could make matters worse. For example, some critical protective relays in several SAFEGUARD switchgear cabinets exhibited very low fragility at the frequencies near the rigid body frequencies of the shock isolation systems on which they were mounted.

Equipment Criticality Identification:

An important element in the shock-isolate versus hardmount decision is the identifi-

cation of critical components in equipment subsystems. In SAFEGUARD, because of the large quantity of components involved, time did not permit a thorough failure mode and effects analysis for each subsystem. As a result, it was discovered that some non-critical items were treated as critical. A more thorough identification process for subsystems to realistically assess the criticality of components should have been undertaken. Time and resources for this process should be allotted during the program planning. The cost and time saved in not treating non-critical items as critical should more than offset the cost and time invested in a thorough identification process.

Shock Isolation System Design:

Equipment Physical Data :

The lack of definitive equipment physical data, due to procurement lead-time, proved a major difficulty in the design of shock isolation systems. In many instances delivered equipment significantly deviated from estimated weights, thus improperly loading isolators as shown in Figure 9. Retrofit was accomplished exchanging under-loaded and overloaded isolators. On the other hand, improperly loaded pneumatic isolators could be adjusted by air pressure

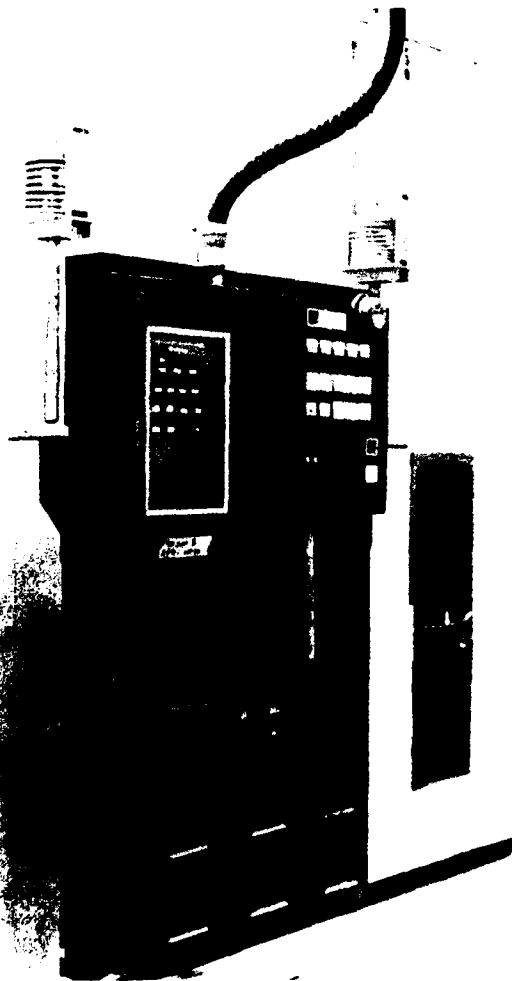


Figure 9. Example of Overloaded Mechanical Spring Pendulum Shock Isolators

to a new load without changing the natural frequency of the system. Whenever shock isolation systems must be designed without reliable equipment physical data the use of pneumatic isolators with their inherent load adjustability should be seriously considered. In SAFEGUARD, the pneumatic isolators use rolling sleeves to eliminate the need for seals around the shafts and pistons, which reduces isolator maintenance.

Rotating Machinery:

SAFEGUARD rotating machinery, particularly pumps and motor-generator sets, was found through analysis and testing to be inherently rugged. In the future such equipment should be carefully investigated before deciding to shock isolate it. Several critical SAFEGUARD motor-generator sets and control cabinets were shock isolated as shown in Figure 10. Two significant problems were encountered. First, the vibration induced by the rotating machines on the shock platform aggravated the shock sensitivity of some of the contacts, relays, etc., inside the control cabinets with resulting operational problems and premature failures. Second, when more than one rotating machine was mounted on a platform as in the case of the two motor-generator sets on the shock isolation platform shown in Figure 10, complex motions were created and caused operational problems and bearing failures. If shock isolation of rotating machines is necessary, vibration sensitive equipment such as control cabinets should be mounted on separate platforms from rotating machines. Redundant or multiple rotating machines, if shock isolated, should also be mounted on separate platforms. If group mounting on the same platform is necessary, careful attention to platform design is required to minimize the vibration cross-talk among machines that can degrade long term performance, reliability and survivability.

It was also learned that the isolators support platforms with rotating machines undergo low-level vibration continuously while the machines are operating. The constant working of isolators caused premature failures. A locking device should be considered to protect the isolators. The device would require fail safe features for quick release for periodic exercise or for switching the system from surveillance to alert mode.

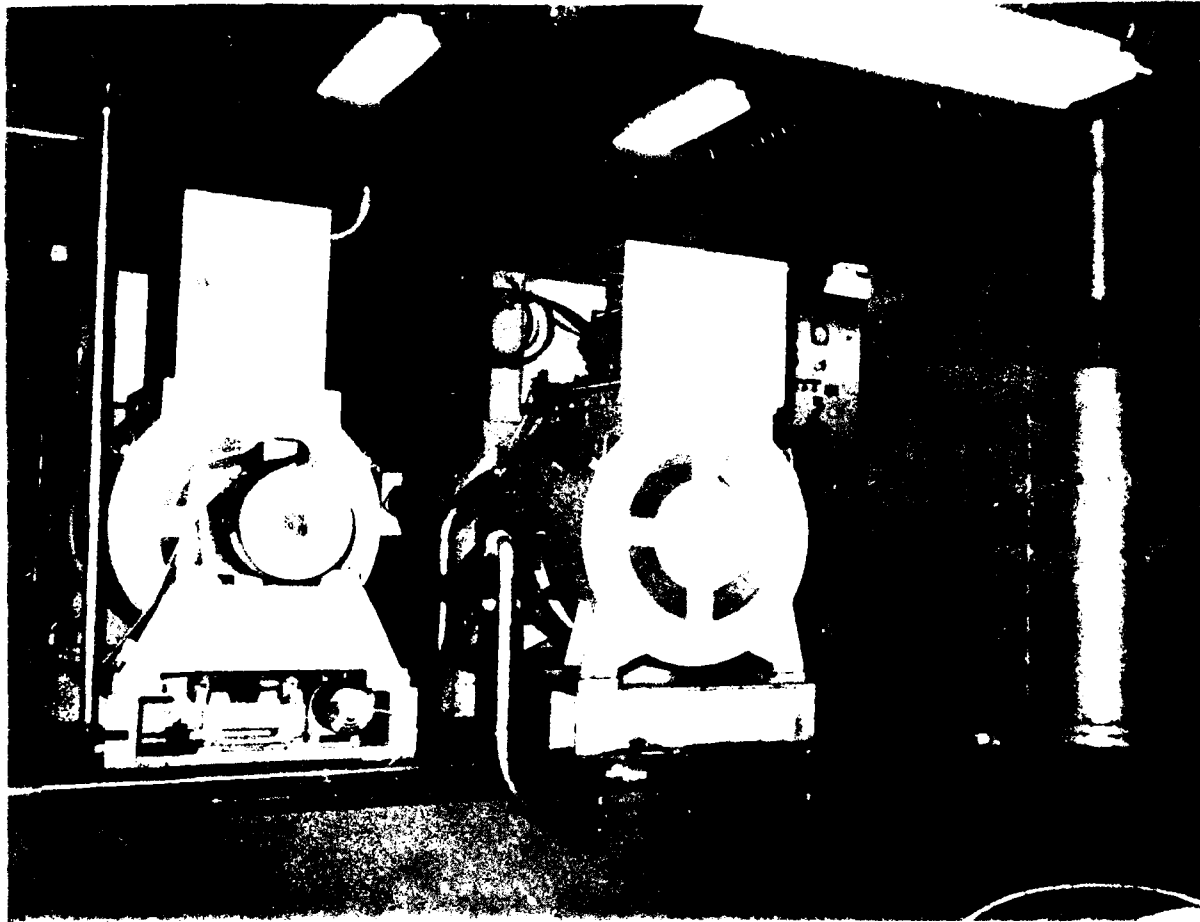


Figure 10. Example of Shock Isolated Motor - Generator Sets and Control Cabinets

Rattlespace:

Encroachment of rattlespace by conduits and pipes, or even by brackets and supports not called for on the drawings was found by hardness audit inspections. This reflects lack of understanding of the importance of rattlespace on the part of construction supervision, lack of explicit instructions on drawings or a combination of both. Shock isolation system rattlespace requirements should be clearly defined on design drawings and strictly complied with by construction crews.

Equipment Qualification Shock Testing:

The SAFEGUARD TSE shock test program placed new requirements on shock testing technology of the late 1960s. Shock spectrum testing was adopted for testing all TSE equipment in lieu of other existing conventional methods. The shock input to SAFEGUARD

equipment results from the response of the hardened structure to air blast and ground motion from nuclear weapons. Environments at different TSE locations are defined by undamped shock response spectra for the vertical and one horizontal direction. The time histories are complex waveform oscillations having a frequency content of 1 to 500 Hz, peak accelerations of less than 5-9 g, maximum displacements of 2-3 inches and a duration of 3-5 seconds. Equipment to be tested ranged in weight from a few pounds to about 10,000 pounds. For testing, equipment shock environment waveforms were simulated by superposition of outputs from pulsed 1/3 octave filters with amplitudes manually adjusted until the shock machine with a non-resonant dummy load attached duplicated the required shock spectrum. The specimen was then mounted on the machine and tested. For the test program a 1000-pound prototype biaxial hydraulic shock test machine capable of producing vibratory motions simultaneously in

the vertical and one horizontal direction was first built and successfully used at the Wyle Laboratories, Norco, California. Later, a 12,000-pound capacity biaxial shock table was built at the Corps of Engineers Construction Engineering Research Laboratory (CERL), Champaign, IL. This shock table is actuated by hydraulic cylinders and controlled by a dedicated minicomputer. Considerable effort was made during the test program to improve test methods and hardware. Digitally controlled hydraulic shock test machines proved cost effective through reduced calibration effort, improved accuracy in shaping test spectra and operational flexibility [7]. Now, machines of this type are available at other commercial and government test laboratories for both nuclear and seismic qualification.

Shock Isolation System Verification:

Verification of shock isolation system performance is a major element of an overall hardness verification program as experienced with SAFEGUARD. While analytical methods can approximate platform environments, the reliable answer is found in test data. The SAFEGUARD shock isolation system in-place test program has demonstrated the technology and feasibility of in situ dynamic testing of shock isolation systems by impedance measurement and pulse excitation. [5], [8], [9], and [11]. The major advantage of in situ tests over laboratory tests lies in the ability to test entire operating systems and subsystems with automatic inclusion of ill-defined phenomena such as effects of cable and piping connectors, isolator high frequency generation and transmission characteristics, friction, damping, etc. This increases the confidence in the hardness verification. In addition, in-situ tests can reduce the amount of laboratory testing of many individual pieces of equipment.

Hardness Maintenance:

Requirements for maintenance of shock isolation system performance throughout the operational life of the facility should be recognized early in the development of hardened facilities and made a part of the overall hardness program. The vibration signature technique used during SAFEGUARD was found useful for the prognosis of incipient anomalies in rotating machinery [10], and mechanical impedance techniques useful for checking the performance of shock isolation systems [5]. These techniques should be utilized in hardness surveillance activities throughout the service life of a system.

CONCLUSIONS

(1) Shock and vibration engineers should be called upon to participate in and contribute toward realistic design criteria. They should be delegated responsibility for overseeing proper design and construction from shock protection and rattlepace enforcement viewpoints.

(2) Experience with SAFEGUARD TSE indicates that standard industrial grade equipment can in many cases withstand the shock/vibration environment at the level predicted for SAFEGUARD or can be inexpensively ruggedized to withstand the environment.

(3) Since the early SAFEGUARD days in the late 1960s, equipment manufacturers have become much more knowledgeable in equipment ruggedization. They should be consulted as early as possible in a program to assess equipment fragility and to aid in the decision of shock isolation vs hardmounting.

(4) A flexible approach to TSE procurement should be taken to reduce avoidable retrofit costs. Certain readily attainable hardness requirements should be specified in the procurement specifications even though the basic requirements pertain to equipment performance.

(5) Equipment/component criticality should be determined using failure mode and effects analysis procedures and the limitations of current shock isolation technology recognized.

(6) Where equipment physical data are uncertain or unavailable, pneumatic shock isolators should be considered in preference to mechanical isolators because of the pneumatic isolator's inherent load adjustability.

(7) A variety of improved test methods and hardware are available both commercially and at Government facilities for qualification of equipment for nuclear or seismic environments and should be investigated early in the planning for hardness verification programs.

(8) Techniques such as impedance measurements and pulse tests of entire shock isolation systems are now available for accurate assessment of shock isolation system performance and should be planned early in the overall hardness verification programs.

REFERENCES

- 1 G. Fox, E. Steiner, "Transient Response of Passive Pneumatic Isolators," Shock and Vibration Bulletin, No. 42, pt. 4, Jan 1972, pp. 85-91.
- 2 "Shock Isolation Design Manual," HNDDSP-73-98-ED-R, 1 Aug 1973, U.S. Army, Corps of Engineers, Huntsville Division, Huntsville, AL.
- 3 W. Stea, J. Vellozzi, "Dynamic Analysis of a Typical PAR Shock Isolation Platform," Report No. PAR-CRI-A&W-96, U.S. Army Corps of Engineers, Huntsville Division, Huntsville, AL.
- 4 G. Kao, J. Cantril, G. Shipway, M. Boyd, "Prediction of Shock Environments by Transfer Function Measurement Techniques," Shock and Vibration Bulletin, No. 44, pt. 2, Aug 1974, pp. 65-81.
- 5 "In Place Testing of Shock Isolation Systems," HNDDSP-75-346-ED-R, 1 Mar 1975, U.S. Army Corps of Engineers, Huntsville, Division, Huntsville, AL.
- 6 "Subsystem Hardness Assurance Report," Vol. 1, Executive Summary, HNDDSP-72-156-ED-R, 30 June 1975, U.S. Army Corps of Engineers, Huntsville Division, Huntsville, AL.
- 7 G. C. Kao, K. Y. Chang, "Control of Electro-Hydraulic Shaker by Digital Iteration Techniques," SAE National Aerospace Engineering and Manufacturing Meeting, Oct 1972.
- 8 F. B. Safford, S. F. Masri, "Analytical and Experimental Studies of a Mechanical Pulse Generator," Journal of Engineering for Industry, Transactions of the ASME, Series B, Vol. 96, No. 2, pp. 459-470, May 1974.
- 9 S. F. Masri, G. A. Bekey, F. B. Safford, "Optimum Response Simulation of Multidegree Systems by Pulse Excitation," Transactions of the ASME, Paper No. 74-WA/Aut-5, Winter Annual Meeting, Nov 1974.
- 10 J. B. Catlin, "Improved Maintenance of Machinery," Transactions of the ASME, Paper No. 72-PEM-1, Plant Engineering & Maintenance Conference, Oct 1972.
- 11 S. F. Masri, F. B. Safford, "Earthquake Simulation Testing of Massive Structures by Pulse Techniques," ASCE National Structural Engineering Convention, April 1975.

ON THE DETERMINATION AND CHARACTERISTICS
OF THE CENTER OF ELASTICITY

Gary L. Fox
BARRY DIVISION
Barry Wright Corporation
Watertown, Massachusetts

By using the transformation properties of the flexibility matrix, the general solution to the problem of the elastic center is given for a rigid body mounted on a multiplicity of linear springs. It is shown that it is not possible, in general, to find a point that reduces all coupling terms in a flexibility matrix to zero, but that at least six of the nine terms may be guaranteed to vanish. It is proved that such a coordinate system always exists. A transformation is also derived which reduces the coupling terms to an RMS minimum. By proving a theory concerning the positive-definite characteristics of the flexibility matrix, it is shown that the RMS value of the coupling terms is invariant under a rotational transformation. A computer program is included.

NOMENCLATURE

- { } = 3 x 1 or 6 x 1 column vector
- [] = 3 x 3 or 6 x 6 matrix
- [+] = 6 x 6 matrix partitioned into 3 x 3 submatrices
- []^T, { }^T = transpose of matrix, column vector
- []⁻¹ = inverse of matrix
- [Q] = 6 x 6 coordinate transformation matrix
- [T] = 6 x 6 translation matrix
- [R] = 6 x 6 rotation matrix
- [r] = 3 x 3 rotation matrix
- [t] = 3 x 3 translation matrix
- [k_i], [K]_i = 6 x 6 spring stiffness matrix in local, global
- [A]_i = 6 x 6 spring flexibility matrix in global system
- [h]_i, [H]_i = 6 x 6 inertia matrix in local, global system
- |A| = The determinant of [A]
- [i]_i, [I]_i = 3 x 3 moment of inertia matrix in local, global system

- [1] = identity matrix
- [0] = null matrix, all elements zero
- [Λ] = diagonal matrix
- [K], [A] = system stiffness, flexibility matrix
- {f}, {F} = force in local, global system
- {x}, {X} = displacement in local, global system
- TR[A] = trace of [A], the sum of the diagonal components

IDENTITIES

- [Q] = [T][R]
- [T] = $\begin{bmatrix} 1 & 0 \\ t & 1 \end{bmatrix}$
- [R] = $\begin{bmatrix} r & 0 \\ 0 & r \end{bmatrix}$
- [K] = $\sum_i [K]_i$
- [A] = [K]⁻¹ = $\begin{bmatrix} U & W \\ W & V \end{bmatrix}$
- [H] = $\begin{bmatrix} M & J \\ J & I \end{bmatrix}$

INTRODUCTION

Small vibrations of a rigid body supported by a multiplicity of linear springs are completely defined by the total stiffness, $[K]$, and inertia matrices $[H]$. A number of authors [Refs. 1, 2, 3, 4] have used the properties of the stiffness matrix to calculate the spring stiffness and orientation so that the isolation system translational modes are completely decoupled from the rotational modes. The common technique used is: (a) to write the stiffness matrix relative to a coordinate system with the origin at the C.G. of the mass; and (b) to cause the coupling terms in the stiffness matrix, $[K]$, to vanish.

In many applications, however, constraints on the isolation system will destroy the symmetry assumed in previously solved cases. In these cases it may be practical for the Design Engineer to calculate the center of elasticity (C.E.) for an assumed case. By changing the mount characteristics an iterative procedure may be used to change the location of the C.E. The mass C.G. location may also be changed until the C.E. and C.G. coincide.

The following investigation will assume that only the flexibility matrix, $[A]$, is known in some reference coordinate system. The individual spring characteristics are not considered; indeed, $[A]$ may even represent a structure flexibility at the mounting points.

Writing the flexibility matrix as

$$[A] \equiv [K]^{-1} \equiv \begin{bmatrix} U & W^T \\ W & V \end{bmatrix} \quad (1)$$

then the off-diagonal submatrices (ODSM) $[W]$ and $[W]^T$ contain the coupling terms. In this representation a force, $\{F\}$, applied at the origin of the reference coordinate system causes a deflection, $\{X\}$, given by

$$\{X\} = [A]\{F\} \quad (2)$$

Recall that a force not applied at the origin must be transformed by the rule

$$\{F\} = [Q]\{F'\} \quad (3)$$

Equations (1) and (2) assume that the force and deflection vectors are written as

$$\{F\} = \begin{Bmatrix} F_t \\ F_r \end{Bmatrix} \sim \begin{Bmatrix} \text{TRANSLATIONAL} \\ \text{COMPONENTS} \\ \text{ROTATIONAL} \\ \text{COMPONENTS} \end{Bmatrix} \sim \begin{Bmatrix} X_t \\ X_r \end{Bmatrix} = \{X\} \quad (4)$$

where the right hand rule is assumed.

TRANSFORMATION PROPERTIES OF THE STIFFNESS AND FLEXIBILITY MATRICES

It has been shown [Ref. 5] that if a stiffness matrix, referenced to some global coordinate system, is known, then it can be referenced to a new coordinate system by a congruent transformation.

$$[K] = [Q][K'][Q]^T \quad (5)$$

Now, since $[K']$ is symmetric [Ref. 6], then it is easily shown that $[K]$ is symmetric. Taking the transpose of Eq. (5)

$$[K]^T = [Q][K']^T[Q]^T$$

since $[K']$ is symmetric

$$[K] = [K]^T$$

If the coordinates of the transformation are measured in the new system and the rotation is performed first (see Figure 1a)

$$[Q] = [T][R] \quad (6)$$

where

$$[R] \equiv \begin{bmatrix} r & 0 \\ 0 & r \end{bmatrix}$$

$[r]$ = the direction cosine or Euler angle 3 x 3 matrix

and

$$[T] \equiv \begin{bmatrix} 1 & 0 \\ t & 1 \end{bmatrix}$$

where

$$[t] = \begin{bmatrix} 0 & -P_3 & P_2 \\ P_3 & 0 & -P_1 \\ -P_2 & P_1 & 0 \end{bmatrix}$$

and

P_i = Location of old system measured in the new system

If the translation is performed first (Fig. 1b) then,

$$[K] = [Q'][K'][Q']^T \quad (7)$$

$$\text{and } [Q'] = [R'][T'] \quad (8)$$

The relationships between Eqs. (6) and (8) are

$$[R'] = [R] \quad (9a)$$

$$\text{and } [T'] = [R][T][R]^T \quad (9b)$$

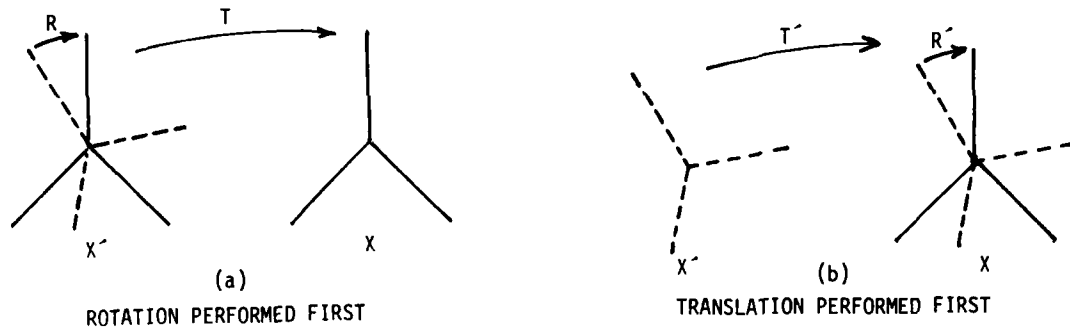


FIGURE 1

It will be advantageous to do the translation transformation first. By inverting Eq. (7) (the primes are no longer necessary) the transformation of the flexibility matrix is obtained

$$[A] = ([R]^T)^{-1} ([T]^T)^{-1} [A'] [T]^{-1} [R]^{-1} \quad (10)$$

Note that since $[R]$ is orthogonal $[R]^{-1} = [R]^T$ but $[T]^{-1} \neq [T]^T$. It has been shown [Ref. 5] that

$$([T]^T)^{-1} = \begin{bmatrix} 1 & t \\ 0 & 1 \end{bmatrix}$$

and

$$[T]^{-1} = \begin{bmatrix} 1 & 0 \\ -t & 1 \end{bmatrix}$$

DEFINITION OF THE CENTER OF ELASTICITY

If a transformation $[Q]$ can be found that reduces $[W]$ to zero, then the rotational and translational components are completely decoupled. This is illustrated as follows; by setting $[W]$ to zero, Eq. (2) becomes

$$\{X\} = \begin{bmatrix} U & 0 \\ 0 & V \end{bmatrix} \begin{Bmatrix} F_t \\ F_r \end{Bmatrix} \quad (11)$$

Inspection of Eq. (11) shows that in the absence of torques, $\{F_r\}$, there is no rotation regardless of $\{F_t\}$, and vice versa. This is a function of the coordinate system picked since $\{F_t\}$ is applied at the origin of the coordinate system. But, alas, $[W]$ cannot always be made to vanish! A simple example will convince the reader. Consider the isolation system shown in Figure II.

Clearly the elastic center must, by symmetry, lie in a plane formed by the elastic centers of the mounts and midway between them. The stiffness and flexibility matrices calculated at this point are

$$[K_1] = \begin{bmatrix} 262 & 0 & 0 & -495 & 0 & 0 \\ 0 & 262 & 0 & 0 & -671 & 0 \\ 0 & 0 & 195 & 0 & 0 & 1,166 \\ -495 & 0 & 0 & 1740 & 0 & 0 \\ 0 & -671 & 0 & 0 & 3210 & 0 \\ 0 & 0 & 1,166 & 0 & 0 & 11,800 \end{bmatrix}$$

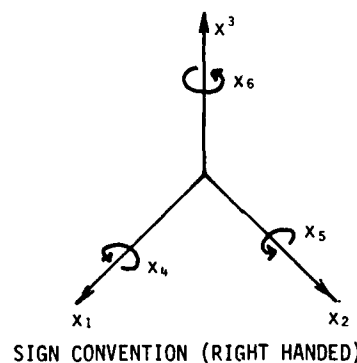
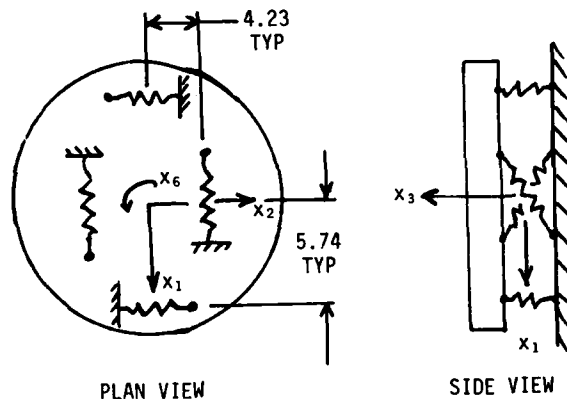


FIGURE II

ALL ISOLATORS ARE IDENTICAL AND INCLINED 60° TO THE VERTICAL

All the mounts are identical, their stiffness matrix is

$$[k_i] = \begin{bmatrix} 15 & 0 & 0 & | & 0 \\ 0 & 15 & 0 & | & 0 \\ 0 & 0 & 150 & | & 0 \\ \hline 0 & 0 & 0 & | & 0 \end{bmatrix}$$

and $[A_i] =$

$$\begin{bmatrix} .818 & 0 & 0 & | & +.232 & 0 & 0 \\ 0 & .818 & 0 & | & 0 & +.171 & 0 \\ 0 & 0 & 1.25 & | & 0 & C & -.123 \\ \hline +.232 & 0 & 0 & | & .123 & 0 & 0 \\ 0 & +.171 & 0 & | & 0 & .0668 & 0 \\ 0 & 0 & -.123 & | & 0 & 0 & .0206 \end{bmatrix} \times 10^{-2}$$

Inspection of $[A]$ shows that the diagonal terms in $[W]$ produce a rotation about the axis of the impressed force. Suppose a unit force is applied at the origin in the x_3 direction. Using Eq. (2)

$$\{X\} = [A] \begin{Bmatrix} 0 \\ 0 \\ 1 \\ 0 \\ 0 \\ 0 \end{Bmatrix} = \begin{Bmatrix} 0 \\ 0 \\ 1.25 \\ 0 \\ 0 \\ .123 \end{Bmatrix} \times 10^{-2}$$

it is seen that the translational force causes not only an x_3 displacement, but also an x_6 displacement, a rotation about the x_3 axis. There is no place on earth - or in the x_1 - x_2 plane anyway - that the force can be applied that prevents the x_6 displacement!

FINDING THE TRANSLATIONAL TRANSFORMATION TO THE ELASTIC CENTER

The preceding discussion leads one to believe that, although $[W]$ cannot be made to vanish, it can be made diagonal. There are six constraints, three translations and three rotation coordinates, to reduce the nine terms to zero. Now a diagonal matrix is just a special case of a symmetric matrix. If $[W]$ can be made symmetric, then a rotation transformation can make it diagonal [Ref. 6, Chapt. 5]. If $[W]$ is symmetric so is $[W]^T$, so that the ODSM's will be equal when $[A]$ is specified in that particular coordinate system, the origin being in fact the elastic center.

This leads to the definition of the Center of Elasticity (C.E.) and $[T]_{CE}$. The C.E. is that point at which the ODSM's are symmetric

and $[T]_{CE}$ is the transformation that reduces $[A]$ to this form. Written in terms of the submatrices Eq. (10) is

$$[A]_{CE} = \begin{bmatrix} U + t^T V t & | & W^T - t^T V \\ + W^T t^T + t^T W & | & \\ \hline W - V t & | & V \end{bmatrix} \quad (12)$$

Setting the ODSM's equal and noting that $[t]$ is anti-symmetric

$$[V][t] + [t][V] = [W] - [W]^T \quad (13)$$

Equation (13) is actually nine simultaneous equations, since each component of the 3×3 matrices must be equal. An interesting thing happens here. Equation (13) must be solved for $[t]$, but $[t]$ is anti-symmetric so there are only three independent elements, say p_1 , p_2 , and p_3 , to solve for. The p 's are the x_1 , x_2 , and x_3 coordinates of the elastic center. Inspection of Eq. (13) reveals that both sides are actually 3×3 anti-symmetric matrices, reducing the number of independent equations to three. These are

$$\begin{aligned} V_{13} p_1 + V_{23} p_2 - (V_{11} + V_{22}) p_3 &= A_{51} - A_{42} \\ -V_{12} p_1 + (V_{11} + V_{33}) p_2 - V_{23} p_3 &= A_{61} - A_{43} \\ -(V_{11} + V_{22}) p_1 + V_{12} p_2 + V_{13} p_3 &= A_{62} - A_{53} \end{aligned} \quad (14a)$$

or in matrix notation

$$[E]\{P\} = \{B\} \quad (14b)$$

The above equations when solved for $\{p_1, p_2, p_3\}$ give the unique location of the elastic center. It is shown in Appendix I that a unique solution to these equations always exists.

THE ROTATION TRANSFORMATION AT THE ELASTIC CENTER

As was mentioned earlier, transformation to the C.E. does not necessarily diagonalize the ODSM's. A rotation transformation, $[R]$, may also be required. The necessity of $[R]$ implies that the C.E. has tensor properties, there is not only a preferred point, but also a preferred set of axes. The physical interpretation of the C.E. and the principal elastic axes is very similar to the C.G. and principal axes of the inertia tensor. Recall that if a torque is applied about a principal axis of a body, then only rotation about that axis is induced. Similarly, a force acting along the principal axis of the C.E. will cause only translation and at most a rotation about the axis of the applied force. The case where the ODSM's vanish completely is similar to

the principal axes of a sphere; the axes may have an arbitrary orientation in space.

OTHER TYPES OF ELASTIC CENTERS

It is useful, at this point, to review the process of finding the center of elasticity. Writing out in detail the lower left ODSM in Eq. (12)

$$[W - Vt] =$$

$$\begin{bmatrix} W_{11} - V_{12} p_3 & W_{12} - V_{13} p_1 & W_{13} - V_{11} p_2 \\ + V_{13} p_2 & + V_{11} p_3 & + V_{12} p_1 \\ W_{21} - V_{22} p_3 & W_{22} - V_{23} p_1 & W_{23} - V_{12} p_2 \\ + V_{23} p_2 & + V_{12} p_3 & + V_{22} p_1 \\ W_{31} - V_{23} p_2 & W_{32} - V_{33} p_1 & W_{33} - V_{13} p_2 \\ + V_{33} p_2 & + V_{13} p_3 & + V_{23} p_1 \end{bmatrix}$$

In general, any three components may be made to vanish by setting them to zero and solving for $\{p_1, p_2, p_3\}$. If a "complete elastic center" exists, one that completely decouples the modes, then the ODSM's vanish and the equations have a unique solution; the actual elastic center. If the angular orientation of the coordinate system is also varied, then three more conditions can be imposed. These six conditions may be used to eliminate six of the nine elements. The procedure established above chose

those six to be the off-diagonal elements because a completely arbitrary system can be analyzed, the simplicity of the solution, and the physical interpretation of the results.

A "directional" elastic center may be found by requiring an entire row or column to vanish. A preferred direction may exist in the environment such as the spin axis of a gyroscope or the thrust axis of a missile.

Consider the isolation system in Figure III. The flexibility matrix written in a coordinate system centered in the plant of mounts is

$$[A_2] = \begin{bmatrix} 2.50 & 0 & 0 & 0 & 0 & 0 \\ 0 & 1.56 & 0 & .938 & 0 & 0 \\ 0 & 0 & 1.00 & 0 & 0 & 0 \\ 0 & .938 & 0 & 1.56 & 0 & 0 \\ 0 & 0 & 0 & 0 & 1.00 & 0 \\ 0 & 0 & 0 & 0 & 0 & .714 \end{bmatrix} * 10^{-2}$$

By inspection of $[A_2]$ it is clear that forces (at the origin!) in the x_1 and x_3 direction cause no rotations. To find what point, if any, that decouples the x_2 axis, the second column in Eq. (15) is set to zero.

$$\begin{aligned} .938 - 0. p_1 + 1.56 p_3 &= 0 \\ 0. - 0. p_1 + 0. p_3 &= 0 \\ 0. - .714 p_1 + 0. p_3 &= 0 \end{aligned}$$

Solution of the above implies $p_1 = 0$ and $p_3 = -.60$.

Each mount stiffness matrix is

$$[k_1] = \begin{bmatrix} 10 & 0 & 0 & 0 \\ 0 & 10 & 0 & 0 \\ 0 & 0 & 40 & 0 \\ 0 & 0 & 0 & 0 \end{bmatrix}$$

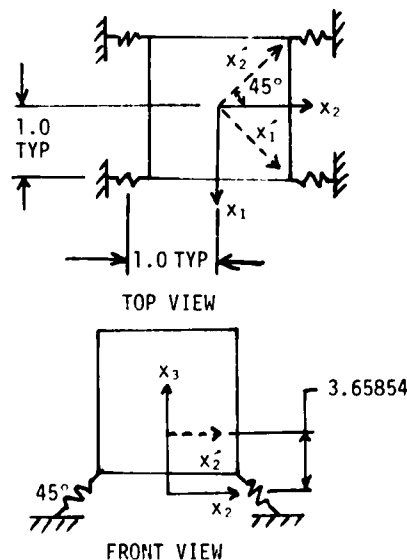


FIGURE III
(DASHED LINES SHOW THE CENTER OF ELASTICITY AND ELASTIC PRINCIPAL AXES)

Substitution of this result into Eq. (10) gives the flexibility matrix at the new location (0.6 in the + x_3 direction from the old origin).

$$[A_2] = \begin{pmatrix} 2.86 & 0 & 0 & 0 & .60 & 0 \\ 0 & 1.00 & 0 & 0 & 0 & 0 \\ 0 & 0 & 1.00 & 0 & 0 & 0 \\ \hline 0 & 0 & 0 & 1.56 & 0 & 0 \\ .6 & 0 & 0 & 0 & 1.00 & 0 \\ 0 & 0 & 0 & 0 & 0 & .714 \end{pmatrix} *10^{-2}$$

Inspection of the new matrix shows that indeed the x_2 forces will not cause rotation, but now x_1 forces will. Note that this procedure, if applied to the first example, would not result in a point that decouples a force in any direction because one is not guaranteed a solution to the equations since only two variables exist in any one column. To find the C.E., Eq. (14) is solved for $\{p\}_2 = \{0, 0, - .365854\}$. The flexibility matrix at the C.E. is

$$[A_2]_{CE} =$$

$$\begin{pmatrix} 2.634 & 0 & 0 & 0 & .366 & 0 \\ 0 & 1.00 & 0 & .366 & 0 & 0 \\ 0 & 0 & 1.00 & 0 & 0 & 0 \\ \hline 0 & .366 & 0 & 1.562 & 0 & 0 \\ .366 & 0 & 0 & 0 & 1.000 & 0 \\ 0 & 0 & 0 & 0 & 0 & .714 \end{pmatrix} *10^{-2}$$

A rotation of 45° about the x_3 axis diagonalizes the ODSM. The final flexibility matrix at the center of elasticity in the elastic principal axes is

$$[A_2]_{CE} =$$

(Principal Axes)

$$\begin{pmatrix} 1.86 & -.774 & 0 & .366 & 0 & 0 \\ -.774 & 1.86 & 0 & 0 & -.366 & 0 \\ 0 & 0 & 1.00 & 0 & 0 & 0 \\ \hline .366 & 0 & 0 & 1.28 & .281 & 0 \\ 0 & -.366 & 0 & .281 & 1.28 & 0 \\ 0 & 0 & 0 & 0 & 0 & .714 \end{pmatrix} *10^{-2}$$

This final coordinate system is shown in Figure III.

MINIMIZING THE RMS VALUE OF THE NINE COUPLING TERMS

Although the maximum number of coupling components have been reduced to zero by this procedure, there is another useful approach to 'minimize' the coupling terms. The method uses a procedure to reduce them to an RMS minimum. It will also be shown that the sum of the squares of the terms in the ODSM is invariant under a rotation transformation; for this type of solution there is no preferred axes.

Let the point in question be called $\{\hat{P}\}$. The nine terms in Eq. (15) can be written in matrix form.

$$\begin{pmatrix} 0 & V_{13} & -V_{12} \\ -V_{13} & 0 & V_{11} \\ V_{12} & -V_{11} & 0 \\ 0 & V_{23} & -V_{22} \\ -V_{23} & 0 & V_{21} \\ V_{22} & -V_{21} & 0 \\ 0 & V_{33} & -V_{32} \\ -V_{33} & 0 & V_{31} \\ V_{32} & -V_{31} & 0 \end{pmatrix} \begin{pmatrix} p_1 \\ p_2 \\ p_3 \end{pmatrix} = \begin{pmatrix} W_{11} \\ W_{12} \\ W_{13} \\ W_{21} \\ W_{22} \\ W_{23} \\ W_{31} \\ W_{32} \\ W_{33} \end{pmatrix} \quad (16a)$$

Defining the matrix terms in Eq. (16a) as

$$[\hat{E}]\{\hat{P}\} = [\hat{B}] \quad (16b)$$

The value of $\{\hat{P}\}$ that results in the RMS minimum of $[\hat{B}]$ is given [Ref. 8] by

$$\{\hat{P}\} = \left([\hat{E}]^T [\hat{E}] \right)^{-1} [\hat{E}]^T \{\hat{B}\} \quad (17)$$

In order to show that the coupling terms RMS value is not changed by a rotation transformation note that $\{\hat{B}\}$ is a vector consisting of the coupling terms. Now the sum of the squares of $\{\hat{B}\}$ can be written as

$$\sum_i (\hat{B}_i)^2 = \text{TR} ([W][W]^T) \quad (18)$$

The value of Eq. (18) after the flexibility matrix has undergone a rotation transformation is

$$\sum_i (\hat{B}_i')^2 = \text{TR} ([W'] [W']^T) \quad (19)$$

but the rotation results in [Ref. 5]

$$[W'] = [r][W][r]^T$$

so that Eq. (19) becomes

$$\sum_i (\hat{B}_i')^2 = \text{TR} ([r][W][W]^T[r]^T) \quad (20)$$

Now the matrix in Eq. (20) is a similarity transformation of the matrix in Eq. (19). Since the trace of a matrix is invariant under this operation [Ref. 9]

$$\sum_i (\hat{B}_i)^2 = \sum_i (\hat{B}_i')^2 \quad (21)$$

Equation (21) shows that the ODSM terms are minimized independently of the angular orientation of the coordinate system. This situation would be desirable, for instance, if the environment was characterized by an isotropic random vibration.

The solution of Eq. (17) for the case shown in Figure III, gives $\{P_2\} = \{0, 0, -.425653\}$. The flexibility matrix at this point is

$$[\hat{A}_2]_{\text{RMS}} =$$

$$\begin{pmatrix} 2.68 & 0 & 0 & 0 & .462 & 0 \\ 0 & 1.05 & 0 & .272 & 0 & 0 \\ 0 & 0 & 1.00 & 0 & 0 & 0 \\ \hline 0 & .272 & 0 & 1.56 & 0 & 0 \\ .426 & 0 & 0 & 0 & 1.00 & 0 \\ 0 & 0 & 0 & 0 & 0 & .714 \end{pmatrix} *10^{-2}$$

The RMS value of the ODSM terms for this point is $5.05 * 10^{-3}$ as compared to those for the C.E. of $5.17 * 10^{-3}$.

THE INERTIA MATRIX

A similar technique may be used to find the center of gravity and principal axes of a composite system of masses. Since the inertia matrix transforms like the stiffness matrix, [Ref. 5] at the total mass is the sum of the individual masses, it is clear that the resultant composite inertia matrix is given by an equation similar to Eq. (5) or (7) for i masses.

$$[H] = \sum_i [T_i][R_i][h_i][R_i]^T [T_i]^T \quad (22)$$

or

$$[H] = \sum_i [R_i][T_i][h_i][T_i]^T [R_i]^T \quad (23)$$

Because the mass is a scalar, the ODSM's in Eq. (22) or (23) are guaranteed to be anti-symmetric. From the form of $[H]$ it is clear that if the C.G. is located at $\{P'\}$, then

$$[t_{\text{C.G.}}] = \frac{1}{m} [J] = \begin{bmatrix} 0 & -P_3' & P_2' \\ P_3' & 0 & -P_1' \\ -P_2' & P_1' & 0 \end{bmatrix} \quad (24)$$

where m is the total mass (a scalar) and $[J]$ is defined by

$$[H] \equiv \begin{bmatrix} M & J^T \\ J & I \end{bmatrix} \quad (25)$$

The transformed inertia matrix

$$[H] = [T_{\text{C.G.}}][H][T_{\text{C.G.}}]^T \quad (26)$$

will cause the ODSM's to vanish. The rotation transformation that diagonalizes $[I']$ when applied according to Eq. (23), will give a diagonal inertia matrix.

DYNAMIC COUPLING

A coordinate system that simultaneously coincides with the C.G. and C.E. will exhibit the minimum coupling terms between the translational and rotational coordinates. This is true because a torque generated by an inertial translational force will be applied only about a principal axis of mass. Since the torque is applied only about a principal axis, then the induced rotation will be only about that axis.

COMPUTER PROGRAM

A computer program is listed in Appendix II that will calculate the C.E. or the RMS location from a system of springs, the stiffness matrix, or the flexibility matrix. The inertia matrix may also be calculated from a system of masses, as well as the C.G. location of the composite mass and the principal axes.

REFERENCES

- [1] Smollen, Leonard E., "Generalized Matrix Method for the Design and Analysis of Vibration Isolation Systems", The Journal of the Acoustical Society of America, Vol. 40, No. 1, pp 195-204, July 1966.
- [2] Derby, Thomas F., "Decoupling the Three Translational Modes From the Three Rotational Modes of a Rigid Body Supported by Four Corner-Located Isolators", The Shock and Vibration Bulletin, Bulletin 43, Part 4, pp 91-108, June 1973.
- [3] Doll, Robert W., "Modal Decoupling of Multi-Degree of Freedom Systems Using the Tensor Properties of the Stiffness Matrix", Qualifying Examination Report, University of California, Berkley, Professor G. W. Brown, Chairman, 1973.
- [4] Hannibal, A. J., "Focalization of Semi-Symmetric Systems", The Shock and Vibration Bulletin, Bulletin 46, Part 4, pp 253-268, August 1976.
- [5] Fox, Gary L., "Matrix Methods for the Analysis of Elastically Supported Isolation Systems", The Shock and Vibration Bulletin, Bulletin 46, Part 5, pp 135-146, August 1976.
- [6] Goldstein, Herbert, Classical Mechanics, (Addison-Wesley Publishing Co., Inc., Massachusetts, 1950) chapters 4 and 5.
- [7] Vernon, James B., Linear Vibration Theory, (John Wiley & Sons, Inc., New York, 1967), Section 8.3.
- [8] Mood, A. M.; and Graybill, F. A., Introduction to the Theory of Statistics, (McGraw-Hill Book Company, Inc., New York, 1963), Section 13.6.
- [9] Bellman, Richard, Introduction to Matrix Analysis, (McGraw-Hill Book Company, The Rand Corp., 1970), p 97.

APPENDIX I

PROOF OF THE EXISTENCE AND UNIQUENESS OF THE CENTER OF ELASTICITY

Writing the flexibility matrix in partitioned form

$$[A] \equiv \begin{bmatrix} U & W \\ W & V \end{bmatrix} \quad (I-1)$$

then [V] is a 3 x 3 symmetric matrix whose determinant is greater than zero. This is proved as follows: [V] is related to a diagonal matrix by an orthogonal rotation transformation, [R]

$$[V'] = [R][V][R]^T; [V'] \text{ is diagonal} \quad (I-2)$$

From the product rule of determinants

$$|V'| = |R'| |V| |R'^T| \quad (I-3)$$

but

$$|R'| |R'^T| = |R'| |R'^{-1}| = 1 \quad (I-4)$$

so that

$$|V'| = |V| \quad (I-5)$$

Now, since [V'] is diagonal and each of the elements must have positive values (negative or zero stiffness is not allowed)

$$|V'| = |V| = V'_{11} * V'_{22} * V'_{33} > 0 \quad (I-6)$$

Since [V] is symmetric, writing out the determinant

$$|V| = V_{11} V_{22} V_{33} - V_{11} V_{23}^2 - V_{22} V_{13}^2 - V_{33} V_{12}^2 + 2 V_{12} V_{13} V_{23} > 0 \quad (I-6a)$$

One more thing must be proved before proceeding; that is

$$V_{ii} V_{jj} - V_{ij}^2 > 0 \quad (I-7)$$

Equation (I-7) is a stronger condition than that [V] be positive definite. Writing the terms out in detail, by solving Eq. (I-2) for [V] and defining [R] ≡ [R']^T

$$[V] = [R][V'][R]^T$$

In the derivation, [R] is not assumed to be symmetric, although it may be. [V] is written in detail on the following page.

$$[V] = \begin{bmatrix} V_{11} r_{11}^2 + V_{22} r_{12}^2 + V_{33} r_{13}^2 \\ V_{11} r_{11} r_{21} + V_{22} r_{12} r_{22} + V_{33} r_{13} r_{23} \\ V_{11} r_{11} r_{31} + V_{22} r_{12} r_{32} + V_{33} r_{13} r_{33} \\ V_{11} r_{21} r_{11} + V_{22} r_{22} r_{12} + V_{33} r_{23} r_{13} \\ V_{11} r_{21}^2 + V_{22} r_{22}^2 + V_{33} r_{23}^2 \\ V_{11} r_{21} r_{31} + V_{22} r_{22} r_{32} + V_{33} r_{23} r_{33} \\ V_{11} r_{31} r_{11} + V_{22} r_{32} r_{12} + V_{33} r_{33} r_{13} \\ V_{11} r_{31} r_{21} + V_{22} r_{32} r_{22} + V_{33} r_{33} r_{23} \\ V_{11} r_{31}^2 + V_{22} r_{32}^2 + V_{33} r_{33}^2 \end{bmatrix} \quad (I-8)$$

Now for $i = 1$ and $j = 2$, or $i = 2$ and $j = 1$, since V is symmetric Eq. (I-7) becomes

$$\begin{aligned} & V_{11} V_{22} (r_{21} r_{12} - r_{11} r_{22})^2 \\ & + V_{11} V_{22} (r_{21} r_{13} - r_{23} r_{11})^2 \\ & + V_{22} V_{33} (r_{22} r_{13} - r_{23} r_{12})^2 > 0 \end{aligned} \quad (I-9)$$

If the terms in parentheses do not simultaneously vanish, then Eq. (I-9) is clearly greater than zero. Now the determinant of $[R]$ cannot vanish since it is orthogonal. Expansion of $|R|$ about the third row gives

$$\begin{aligned} |R| &= r_{33} (r_{21} r_{12} - r_{11} r_{22}) \\ &+ r_{32} (r_{21} r_{13} - r_{11} r_{23}) \\ &- r_{31} (r_{22} r_{13} - r_{23} r_{12}) \\ &= 1 \neq 0 \end{aligned} \quad (I-10)$$

Comparison of the terms in parentheses of Eq. (I-9) and (I-10) shows that Eq. (I-7) is indeed true for $i = 1, j = 2$. A similar argument holds for the other terms by a cyclic permutation of i, j, k . (This is equivalent to renaming the coordinate system while preserving its right-handedness.)

With the above characteristics of $[V]$ determined, the proof that $[E]^{-1}$ in Eq. (14b) exists can be given. If $|E|$ is not zero, then the inverse exists. Writing the determinant

$$\begin{aligned} |E| &= -(V_{11} + V_{22})(V_{11} + V_{33})(V_{22} + V_{33}) \\ &+ V_{12}^2 (V_{11} + V_{22}) + V_{13}^2 (V_{11} + V_{33}) \\ &+ V_{23}^2 (V_{22} + V_{33}) + 2 V_{23} V_{12} V_{13} \end{aligned} \quad (I-11)$$

Substituting Eq. (I-6a) for the last terms in Eq. (I-11)

$$\begin{aligned} |E| &+ |V| + V_{11} V_{22} V_{33} + V_{11} V_{23}^2 \\ &+ V_{22} V_{13}^2 + V_{33} V_{23}^2 \\ &= (V_{11} + V_{22})(V_{12}^2 - V_{11} V_{22}) \\ &+ (V_{11} + V_{33})(V_{13}^2 - V_{11} V_{33}) \\ &+ (V_{22} + V_{33})(V_{23}^2 - V_{22} V_{33}) \end{aligned} \quad (I-12)$$

Now the terms on the right are all negative from Eq. (I-7) and all terms on the left, except $|E|$, are positive so that

$$|E| + \text{Positive Terms} < 0 \quad (I-12a)$$

therefore

$$|E| < 0 \quad (I-13)$$

Since $|E|$ is not equal to zero, the inverse exists.

APPENDIX II

LISTING OF COMPUTER PROGRAM "CENTER"

A computer program that finds the center of elasticity and principal axes, the RMS minimum point, or the center of gravity and principal axes. Input may be of the system stiffness or flexibility matrix, the individual mount properties, or the individual mass properties.

The case shown in Figure III is used as an example of the program input and output.

TYPE OF INPUT
1=INDIVIDUAL SPRINGS
2=STIFFNESS MATRIX
3=FLEXIBILITY MATRIX
4=INDIVIDUAL MASSES
?1

INPUT NO. OF ELEMENTS, LOCATION, ORIENTATION, AND VALUES:
VALUES ARE DIAGONAL COMPONENTS OF MATRIX
?4, 1,1,0, -1,1,0, 1,-1,0, -1,-1,0

?0,-45,0, 0,-45,0, 0,45,0, 0,45,0

?10,10,40,0,0,0, 10,10,40,0,0,0, 10,10,40,0,0,0, 10,10,40,0,0,0

SYSTEM MATRIX

0.400E+02	0.	0.	0.	0.	0.
0.	0.100E+03	0.	-0.600E+02	0.	0.
0.	0.	0.100E+03	0.	0.	0.
0.	-0.600E+02	0.	0.100E+03	0.	0.
0.	0.	0.	0.	0.100E+03	0.
0.	0.	0.	0.	0.	0.140E+03

FLEXIBILITY MATRIX

0.250E-01	0.	0.	0.	0.	0.
0.	0.156E-01	0.	0.938E-02	0.	0.
0.	0.	0.100E-01	0.	0.	0.
0.	0.938E-02	0.	0.156E-01	0.	0.
0.	0.	0.	0.	0.100E-01	0.
0.	0.	0.	0.	0.	0.714E-02

INPUT TYPE OF SOLUTION
1=CENTER OF ELASTICITY
2=RMS MINIMUM POINT
?1

X(I)

0. 0. -0.365854E+00

F

0.100E+01	0.	0.	0.	0.366E+00	0.
0.	0.100E+01	0.	-0.366E+00	0.	0.
0.	0.	0.100E+01	0.	0.	0.
0.	0.	0.	0.100E+01	0.	0.
0.	0.	0.	0.	0.100E+01	0.
0.	0.	0.	0.	0.	0.100E+01

TRANSFORMED MATRIX

0.263E-01	0.	0.	0.	0.366E-02	0.
0.	0.109E-01	0.	0.366E-02	0.	0.
0.	0.	0.100E-01	0.	0.	0.
0.	0.366E-02	0.	0.156E-01	0.	0.
0.366E-02	0.	0.	0.	0.100E-01	0.
0.	0.	0.	0.	0.	0.714E-02

ROTATION MATRIX

0.707107E+00 -0.707107E+00 0.
0.707107E+00 0.707107E+00 0.
0. 0. 0.100000E+01

R

0.707E+00	-0.707E+00	0.	0.	0.	0.
0.707E+00	0.707E+00	0.	0.	0.	0.
0.	0.	0.100E+01	0.	0.	0.
0.	0.	0.	0.707E+00	-0.707E+00	0.
0.	0.	0.	0.707E+00	0.707E+00	0.
0.	0.	0.	0.	0.	0.100E+01

ROTATED MATRIX

0.176E-01	-0.774E-02	0.	0.366E-02	-0.873E-10	0.
-0.774E-02	0.186E-01	0.	0.873E-10	-0.366E-02	0.
0.	0.	0.100E-01	0.	0.	0.
0.366E-02	0.146E-10	0.	0.128E-01	-0.281E-02	0.
-0.146E-10	-0.366E-02	0.	-0.281E-02	0.128E-01	0.
0.	0.	0.	0.	0.	0.714E-02

CENTER 10/10/76

```
100 REAL K(6,6),KL(6,6),KINV(6,6),LABEL(3)
110 1 FORMAT(1X,6E11.3)
120 DIMENSION XP(3,2),XS(3,4),X(3),P(3,4)
125 &,SSK(6,6),TR(6,6),I1(6,6),SSK(6,4)
130 &,P1(3,3),P2(3,3),P3(3,3),I2(6,6),I3(6,6),P4(3),P5(3),A(9),CX(9,3)
140 101 FORMAT(1X"TYPE OF INPUT"/1X"1=INDIVIDUAL SPRINGS"/1X
150 &"2=STIFFNESS MATRIX"/1X"3=FLEXIBILITY MATRIX"/1X"4=INDIVIDUAL
160 & MASSES"/1X)
170 PRINT 101;INPUT,IPT
180 GO TO(102,103,103,102),IPT
190 102 CONTINUE
200 PRINT,"INPUT NO. OF ELEMENTS, LOCATION, ORIENTATION, AND VALUES:"
210 PRINT,"VALUES ARE DIAGONAL COMPONENTS OF MATRIX"
215 PRINT," "
220 INPUT,NM,((XS(I,J),I=1,3),J=1,NM),((P(I,J),I=1,3),J=1,NM)
230 &,((SSK(I,J),I=1,6),J=1,NM)
240 DO 10 L=1,NM
250 DO 15 I=1,6
260 15 SK(I,I)=SSK(I,L)
270 DO 11 I=1,3; XP(I,1)=XS(I,L)
280 11 XP(I,2)=P(I,L)
290 CALL TRAN(XP,TR)
300 CALL MIMPY(0,TR,SK,T1,6,6,6,6,6)
310 CALL MTMPY(0,T1,TR,KL,6,-6,6,6,6)
320 DO 12 I=1,6; DO 12 J=1,6
330 12 K(I,J)=K(I,J)+KL(I,J)
335 10 CONTINUE
340 GO TO 104
345 103 CONTINUE
350 PRINT,"INPUT STIFFNESS OR FLEXIBILITY MATRIX BY ROW OR COLUMN"
360 INPUT,K
370 104 CONTINUE
380 IF (IPT.EQ.3) GO TO 105
390 PRINT,"SYSTEM MATRIX"; PRINT 1,K
400 105 CONTINUE
980 GO TO(48,48,106,204),IPT
990 48 CONTINUE
1000 CALL MINV(K,6,6,6,P6)
1010 106 CONTINUE
1020 PRINT,"FLEXIBILITY MATRIX";PRINT 4,((K(I,J),I=1,6),J=1,6)
1030 PRINT 107; INPUT,IST; IF(IST.EQ.2) GO TO 50
1040 107 FORMAT(1X"INPUT TYPE OF SOLUTION"/1X"1=CENTER OF ELASTICITY"
1050 &"/1X"2=RMS MINIMUM POINT"/1X)
1060 P1(1,3)=K(4,6)
1070 P1(1,2)=K(5,6)
1080 P1(1,1)=-K(4,4)-K(5,5)
1090 P1(2,3)=-K(4,5)
1100 P1(2,2)=K(4,4)+K(6,6)
1110 P1(2,1)=-K(5,6)
1120 P1(3,3)=-K(6,6)-K(5,5)

1130 P1(3,2)=K(4,5)
1140 P1(3,1)=K(4,6)
1150 CALL MINV(P1,3,3,LABEL)
1160 LABEL(1)=K(4,2)-K(5,1)
1170 LABEL(2)=K(4,3)-K(6,1)
1180 LABEL(3)=K(5,3)-K(6,2)
1190 DO 145 I=1,3
1195 145 X(I)=0.
1200 DO 45 I=1,3
1210 DO 45 J=1,3
1220 45 X(4-I)=X(4-I)+P1(I,J)*LABEL(J)
```

```

1230 52 CONTINUE
1240 PRINT,"X(I)"; PRINT 3,X
1250 DO 46 I=1,3; DO 46 J=1,3
1260 F1(I,J)=0.
1270 F1(I,1)=1.; F1(I+3,I+3)=1.
1290 F1(I+3,J)=0.; F1(I,J+3)=0.
1300 46 CONTINUE
1310 F1(2,4)=X(3)
1320 F1(3,4)=-X(2)
1330 F1(1,5)=-X(3)
1340 F1(3,5)=X(1)
1350 F1(1,6)=X(2)
1360 F1(2,6)=-X(1)
1370 GO TO 47
2000 47 CONTINUE
2010 CALL MTMPY(0,T1,K,T2,6,6,6,6,6)
2020 CALL MTMPY(0,T2,F1,F3,6,-6,6,6,6)
2030 PRINT,"T"; PRINT 4,((T1(I,J),J=1,6),I=1,6)
2040 PRINT,"TRANSFORMED MATRIX"; PRINT 4,F3
2050 DO 57 I=1,3; DO 57 J=1,3
2060 57 RMS=RMS+F3(I,J+3)**2.
2070 IF(IST.EQ.2) PRINT,"RMS VALUE=",SQRT(RMS)
2080 IF(IST.EQ.2) GO TO 108
2090 4 FORMAT(1X,6E11.3)
2100 3 FORMAT(1X,3E14.6)
2110 DO 42 I=1,3; DO 42 J=1,3
2120 IF (IPT.EQ.4) P3(I,J)=T3(I+3,J+3)
2130 IF(IPT.EQ.4) GO TO 42
2140 P3(I,J)=T3(I+3,J); 42 CONTINUE
2150 CALL EIG1(P3,P2,3,1.0E-12,P4,P5,3,3)
2160 PRINT,"ROTATION MATRIX"; PRINT 3,((P2(I,J),J=1,3),I=1,3)
2170 DO 43 I=1,3; DO 43 J=1,3
2180 T2(I+3,J)=0.; T2(I,J+3)=0.
2190 T2(I,J)=P2(I,J); 43 T2(I+3,J+3)=P2(I,J)
2200 PRINT,"R"; PRINT 4,((T2(I,J),J=1,6),I=1,6)
2210 CALL MIMPY(0,T2,F3,I1,-6,6,6,6,6)
2220 CALL MIMPY(0,I1,I2,KINV,6,6,6,6,6)
2230 PRINT,"ROTATED MATRIX"; PRINT 4,((KINV(I,J),J=1,6),I=1,6)
2240 GO TO 108

```

```

2250 204 CONTINUE
2260 XP(1,1)=K(6,2)/K(1,1)
2270 XP(2,1)=K(5,1)/K(1,1)
2280 XP(3,1)=K(4,3)/K(1,1)
2290 XP(1,2)=0.
2300 XP(2,2)=0.
2310 XP(3,2)=0.
2320 CALL TRAN(XP,T1)
2330 GO TO 47
3000 50 CONTINUE
3010 CX(1,2)=K(4,6)
3020 CX(2,1)=-CX(1,2)
3030 CX(1,3)=-K(4,5)
3040 CX(3,1)=-CX(1,3)
3050 CX(2,3)=K(4,4)
3060 CX(3,2)=-CX(2,3)
3070 CX(4,2)=K(5,6)
3080 CX(5,1)=-CX(4,2)
3090 CX(4,3)=-K(5,5)
3100 CX(6,1)=-CX(4,3)
3110 CX(5,3)=K(5,4)
3120 CX(6,2)=-CX(5,3)
3130 CX(7,2)=K(6,6)
3140 CX(8,1)=-CX(7,2)
3150 CX(7,3)=-K(6,5)

```

```

3160 CX(9,1)=-CX(7,3)
3170 CX(8,3)=K(6,4)
3180 CX(9,2)=-CX(8,3)
3190 A(1)=-K(4,1)
3200 A(2)=-K(4,2)
3210 A(3)=-K(4,3)
3220 A(4)=-K(5,1)
3230 A(5)=-K(5,2)
3240 A(6)=-K(5,3)
3250 A(7)=-K(6,1)
3260 A(8)=-K(6,2)
3270 A(9)=-K(6,3)
3280 DO 53 I=1,3; DO 53 L=1,3
3290 DO 53 J=1,9
3300 53 F(I,L)=F(I,L)+CX(J,I)*CX(J,L)
3310 CALL MFINV(P,3,3,3,LABEL)
3320 DO 55 I=1,3; DO 55 J=1,9
3330 55 F4(I)=P4(I)+CX(J,I)*A(J)
3340 DO 54 I=1,3; DO 54 L=1,3
3350 54 X(I)=X(I)-F(I,L)*P4(L)
3360 GO TO 52
3370 108 STOP
3380 END
4000 SUBROUTINE TRAN(X,TR)
4010 DIMENSION X(3,2),K(6,6),I(6,6),TR(6,6),S(3),C(3),F(6,6)

```

```

4020 DO 14 I=1,6; DO 14 J=1,6; F(I,J)=0.
4030 14 R(I,J)=0.
4040 DO 10 I=1,6
4050 10 F(I,1)=1.
4060 F(4,2)=-X(3,1)
4070 F(5,1)=X(3,1)
4080 F(4,3)=X(2,1)
4090 F(6,1)=-X(2,1)
4100 F(5,3)=-X(1,1)
4110 F(6,2)=X(1,1)
4120 DO 11 I=1,3
4130 C(I)=COS(3.14159/180.*X(I,2))
4140 S(I)=SIN(3.14159/180.*X(I,2))
4150 11 CONTINUE
4160 R(1,1)=C(1)*C(3)+S(1)*S(2)*S(3)
4170 R(1,2)=C(2)*S(3)
4180 R(1,3)=-S(1)*C(3)+S(2)*S(3)*C(1)
4190 R(2,1)=-S(3)*C(1)+S(1)*S(2)*C(3)
4200 R(2,2)=C(2)*C(3)
4210 R(2,3)=S(1)*S(3)+S(2)*C(1)*C(3)
4220 R(3,1)=S(1)*C(2)
4230 R(3,2)=-S(2)
4240 R(3,3)=C(1)*C(2)
4250 DO 12 I=1,3; DO 12 J=1,3
4260 12 R(I+3,J+3)=R(I,J)
4270 CALL MIMPLY(0,T,R,TR,6,6,6,6,6)
4280 RETURN
4290 END

```

DESIGN OF ELASTOMERIC COMPONENTS
BY USING THE FINITE ELEMENT TECHNIQUE

Robert H. Finney, and Dr. Bhagwati P. Gupta
Lord Kinematics
Erie, Pennsylvania

High performance elastomeric components, in particular High Capacity Laminated (HCL) elastomeric components, present analysis problems which can only be solved using a finite element computer program having the capability of analyzing structures consisting of incompressible, or nearly incompressible materials such as rubber. An equally important required feature is accuracy in the solution. This paper describes the general features and capability of SARLAS (Stress Analysis of Rubber Laminated Structures), a finite element program used by Lord Kinematics to design elastomeric components. The validity of the analysis is supported by a comparison of the analytical results to test results. The elastomeric components selected for this analysis and test verification, include an HCL Spherical Thrust Bearing, an HCL Conventional Thrust Bearing used on a helicopter main rotor, a Marine Riser Flexjoint used in undersea drilling operations, plus other examples of how the technique can be utilized to solve other elastomeric design problems.

INTRODUCTION

Any system, that is subjected to shock loading, that undergoes vibrations, and that has a potential fretting problem, will need a device such as an elastomeric component for controlling the energy and vibrations so produced. If an elastomeric component of relatively simple and regular geometry is used under simple loading conditions, the simple closed form solutions available in MIL-HDBK-149A (Military Standardization Handbook Rubber and Rubber-Like Materials) or any elastomeric design textbook are usually sufficient. As long as the low stress/strain limits specified in these publications are observed, there is normally no fatigue performance problem.

Recent product specifications for elastomeric components specify, or imply, complex shapes such as cones, spheres and thrust bearings with shims of irregular cross section. These components are usually to be designed with highly-complex static and dynamic stress/strain patterns induced by a

three dimensional loading system. A fatigue analysis is also required to substantiate a life of 2000 or more hours at frequencies of 2.5 to 20 Hz. A typical helicopter main rotor spherical bearing is an example of the complex loading system which is normally required to accommodate the following loads and motions at 3 Hz for 2000 hours.

Loads:

Axial compression (centrifugal force)
- 266,893 \pm 22,241 Newtons
(60,000 \pm 5,000 pounds)

Radial shear - in the plane of the rotor
- 400 \pm 1,112 Newtons
(90 \pm 250 pounds)

Radial shear - perpendicular to the rotor
- 3,559 \pm 11,121 Newtons
(800 \pm 2500 pounds)

Motions:

Torsional shear - due to pitch motion
- 2.0° \pm 4.5°
Cocking shear - due to flap motion -
1.0° \pm 3.5°

Cocking shear - due to lead-lag motion - $0.5^\circ \pm 1.5^\circ$

Loads and motions are applied at various phases relative to each other.

Coupled with the highly complex analysis problem to determine the stress/strain levels is the need for valid fatigue data on the elastomer, since the number of fatigue cycles commonly applied is between 18 and 150 million. Elastomer fatigue data is generally unpublished, or unavailable, due to each individual elastomeric component manufacturer using a data base developed for proprietary elastomer blends which produce unique S-N curves and environmental properties. Therefore, an engineer could be faced with the problem of designing an elastomeric component using simple closed form textbook solutions to establish questionable stress/strain levels which will be used to enter incomplete S-N curves (or unavailable S-N curves) to determine if requirements such as a 2000 hour life will be satisfied.

FINITE ELEMENT ANALYSIS

The first part of the problem, therefore, to do the correct stress-deflection analysis of structures of complex shapes and under complex loadings, can be accomplished using proper finite element techniques and is the subject of this paper. By using a finite element computer program such as Lord Kinematics' "SARLAS" instead of the "cut and try" method, which is all too common in the industry, the costly redesign and retest required after a component does not meet the specification can be eliminated. When this precise analytical technique is coupled with a valid data base in elastomer fatigue, the result will be an optimized elastomeric component in terms of life, strength, and design integrity for use in highly critical applications.

This finite element program called "SARLAS" is a derivative of a finite element program called "TEXGAP" which was developed at the University of Texas by Professors E. B. Becker and R. S. Dunham. SARLAS is capable of analyzing a complex structure made of metal, composite and rubber-like materials without the simplifying assumptions of the metals being rigid or the loading patterns and shapes being simple and regular. The unique characteristic of this program is its ability of handling incompressible materials (Poisson's Ratio equal to 0.5), or nearly incompressible materials (Poisson's Ratio equal to say 0.49995).

For example, an error in Poisson's ratio in the fifth significant figure will change the shear modulus which will significantly affect the final results. Therefore, this program can handle correctly precise values of Poisson's Ratio. The program is essentially a two dimensional program capable of solving axisymmetric, modal and plane problems. The structure may be subjected to axisymmetric, torsional, thermal and asymmetric loadings including those due to spinning and accelerations.

SARLAS simultaneously solves the equations for the elastomer/shim interactions using unique and very accurate elements. The analysis by this program yields the information shown in Table I for each and every element. The interpretation of the symbols is provided in Figure 1. In addition to the detail information provided for each element, an additional valuable output is shown in Table II. This is called a Max-Min Sheet and locates, by numbers of the material and elements, the maximum and minimum stress/strain values within the elastomeric component. This eliminates the requirement of manually searching through each and every number to determine the points within the design that are the most likely to cause failure.

Therefore, this finite element program represents a quantum jump in the analytical capability of the elastomeric component designer to satisfy the requirements of today's high performance specification requirements. However, the vast amount of numbers generated by this technique and the significant amount of engineering plus computer time required to set up, analyze, and interpret the data is only justified if the numbers and their interpretation are correct. This technique has been applied at Lord Kinematics to numerous applications with good correlation and excellent test results which provide proof that the SARLAS program, when properly applied will produce valid analytical data.

ANALYTICAL/TEST RESULTS - EXAMPLES

The application of finite element analysis techniques, using the SARLAS program, on currently active elastomeric parts at Lord Kinematics illustrates the accuracy and versatility of this excellent design tool. It has been successfully applied to a helicopter main rotor elastomeric spherical thrust bearing to determine the shim

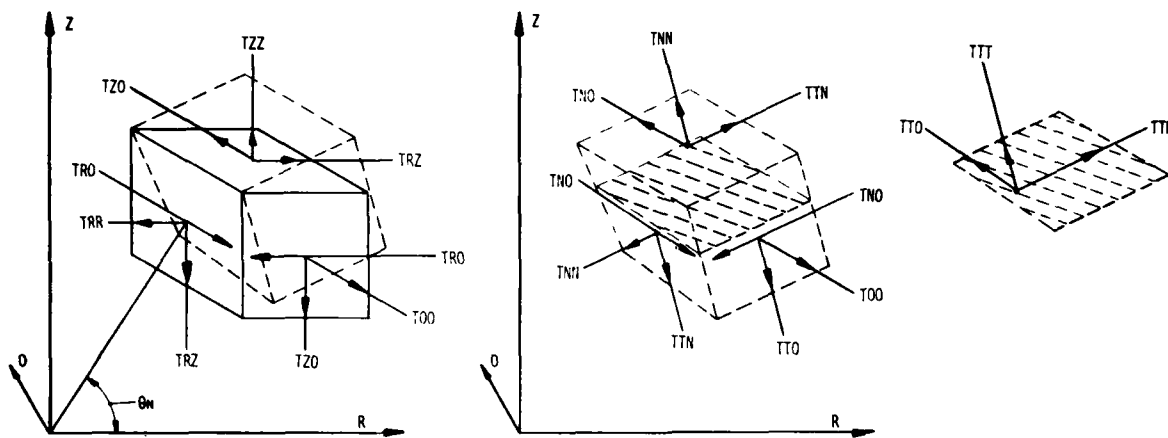


Fig. 1 - Coordinate system for SARLAS and stresses

DISPLACEMENTS FOR QUAD8 NO 16

J	RADIAL	AXIAL	HOOP
1	8	4.2961E-04	0.
2	8	-2.1980E-03	0.
3	8	-2.9233E-03	0.
3	9	-2.5187E-03	0.
2	9	-1.6633E-03	0.
		-2.4986E-03	0.
		-2.7104E-03	0.
		-2.0818E-03	0.
		-1.8960E-03	0.

MATERIAL NO 1

COMB STRESS	STR ENERGY DENS
8.3880E+03	6.2910E+00
5.5551E+04	2.7285E+02
4.9139E+04	2.0415E+02
1.3791E+04	1.1224E+01

NODAL POINT STRESSES AND STRAINS FOR QUAD8 NO 16

MATERIAL NO 1

IP	R	Z	TZR ERR TNN	TZZ EZZ TTT	TZO EZO TON	TRZ ERZ TTN	TRO ERO TOT	TZO EZO TON	MAX	MIN	TAUMAX
1	.722	2.175	8.921E+03	8.868E+03	5.870E+03	-4.517E+03	0.	0.	1.341E+04	4.377E+03	4.517E+03
			4.057E-04	3.987E-04	-2.198E-13	-1.202E-03	0.	0.	1.003E-03	-1.986E-04	1.202E-03
			4.969E+03	1.282E+04	5.870E+03	2.236E+03	0.	0.			
			8.821E+04	2.829E+04	3.844E+04	1.419E+02	0.	0.			
2	.921	2.060	4.314E+04	7.336E+04	3.844E+04	2.588E+04	0.	0.	8.821E+04	2.829E+04	2.996E+04
			6.251E-04	4.643E-03	-2.923E-13	6.884E-03	0.	0.	6.619E-03	-1.351E-03	7.971E-03
			3.237E+04	8.413E+04	3.844E+04	-1.511E+04	0.	0.			
			2.257E+04	7.586E+04	3.248E+04	1.254E+03	0.	0.			
3	.965	2.104	5.047E+04	4.796E+04	3.248E+04	2.665E+04	0.	0.	7.589E+04	2.254E+04	2.668E+04
			2.392E-03	2.059E-03	-2.519E-13	7.088E-03	0.	0.	5.773E-03	-1.322E-03	7.096E-03
			7.292E+04	2.551E+04	3.248E+04	1.224E+04	0.	0.			
			3.380E+03	1.331E+04	5.508E+03	6.006E+03	0.	0.			
4	.850	2.303	6.613E+02	1.603E+04	5.508E+03	-1.297E+03	0.	0.	1.614E+04	5.527E+02	7.792E+03
			-6.446E-04	1.399E-03	-1.663E-13	-3.449E-04	0.	0.	1.414E-03	-6.590E-04	2.073E-03
			9.641E+03	7.048E+03	5.508E+03	-7.683E+03	0.	0.			
			1.341E+04	4.377E+03	5.870E+03	2.638E+01	0.	0.			

TABLE I
Typical SARLAS Output for Each Element

stresses, identify the load paths and the mode of the bearing failure. A second application to a helicopter main rotor elastomeric conventional thrust bearing to determine the optimum shim shape illustrates another valuable aspect of this versatile analytical tool. A third application to a submarine deck link to evaluate the design for an impact load is also discussed

along with the analysis of a marine riser flexjoint for an underwater oil drilling pipe subjected to tremendous loads and pressures while accommodating motion about a spherical center.

MATERIAL NO. 1	QUANTITY	R	Z	ELEM	MAXIMUM	R	Z	ELEM	MINIMUM
	RADIAL STRESS	.965	2.104	16	5.0466479E+04	.905	.500	2	-3.2671205E+04
	AXIAL STRESS	.500	.500	1	8.0721257E+04	.905	.500	2	-6.6332446E+04
	HOOP STRESS	.500	.500	1	3.9758231E+04	.905	.500	2	-3.2671205E+04
	SHEAR STRESS	.965	2.104	16	2.6645767E+04	.631	2.915	19	-5.0180661E+03
	TAURO STRESS	2.739	2.968	27	0.	2.739	2.968	27	0.
	TAUZO STRESS	2.739	2.968	27	0.	2.739	2.968	27	0.
	MAX STRESS	.921	2.060	16	8.8214852E+04	.905	.500	2	-3.0157096E+04
	MIN STRESS	.500	.500	1	3.6020908E+04	.905	.500	2	-6.8846555E+04
	MAX SHEAR STRESS	.905	2.000	14	3.1840718E+04	1.109	2.662	19	7.5651465E+02
	NORMAL STRESS	.722	2.175	16	8.8214516E+04	.675	.500	2	-6.6332447E+04
	SURF SHEAR STRESS	.905	2.000	14	1.3086240E+04	.965	2.104	18	-1.8457691E+04
	RADIAL STRAIN	1.025	2.120	18	2.8081130E-03	.500	.750	3	-2.5444367E-03
	AXIAL STRAIN	.905	2.000	14	5.9727426E-03	.905	.500	2	-4.4769451E-03
	HOOP STRAIN	.894	3.370	24	4.0682338E-14	.500	.500	1	-2.0000000E-12
	SHEAR STRAIN	.965	2.104	16	7.0877741E-03	.631	2.915	19	-1.3348056E-03
	GAMRO STRAIN	2.739	2.968	27	0.	2.739	2.968	27	0.
	GAMZO STRAIN	2.739	2.968	27	0.	2.739	2.968	27	0.
	MAX STRAIN	.921	2.060	16	6.6193942E-03	.894	3.370	24	1.3598839E-04
	MIN STRAIN	1.109	2.662	19	9.4458312E-05	.905	.500	2	-4.8113215E-03
	MAX SHEAR STRAIN	.905	2.000	14	8.4696309E-03	1.109	2.662	19	2.0123290E-04
	COMBINED STRESS	.905	2.000	14	5.7540632E+04	1.109	2.662	19	1.9667824E+03
	STRAIN ENERGY	.921	2.060	16	2.7285409E+02	.894	3.370	22	2.2736023E-01

TABLE II

Largest and Smallest Stresses and Strains by Material Type

SPHERICAL THRUST BEARING

Figure 2 is a undeformed computer drawn x-y plot of the cross-section drawing of a Lastoflex[®] Spherical Thrust Bearing. This spherical thrust bearing was designed to support a 266,893 Newton (60,000 pound) compression load in the axial direction (F_A) while accommodating torsional shear motions (θ) and cocking shear motions (ϕ) about its spherical center. To attempt to analyze the shim stress in each shim using simple closed form solutions is an impossible task owing to the complex loading patterns, the different elastic foundations to which the shims are attached and the interaction from layer to layer that is present. By applying finite element analysis, the designer can determine the compression loading patterns and the hoop stress patterns, the elastomer edge compression strain profile and the elastomer edge compression induced shear strain profile.

Figure 3 presents the compression stress and hoop stress patterns, obtained from the finite element output, for selected shims within the bearing. Of significance in these two plots is the load path from the spherical center to the attachment point indicating a direct effect of the method

of major metal attachment on the shim loading patterns. The hoop stress patterns show a "warping" effect in the shims that is caused by the offset load path and marginal support of the shims due to insufficient cone angle. This information indicates either a redesign is required to provide adequate support or the shim strength should be sufficient to accommodate the adverse loading condition.

This spherical thrust bearing was built and strain gaged on five selectec shims with axial gages to measure the hoop strain due to axial loading and cocking shear (ϕ) motion. The results for two of these shims are presented in Figure 4 along with the finite element analysis results for the same axial (F_A) load. The excellent correlation is evident.

Figure 5 presents the finite element derived normal compression strain and the compression induced shear strain at the elastomer edge as a result of the axial (F_A) load being applied. A test specimen was subjected to an axial load of 155,688 + 155,688 Newton (35,000 ± 35,000 pounds) and the results shown in the test (Figures 6 and 7) correlated with the analysis results with the outside two layers (large end) showing signs of

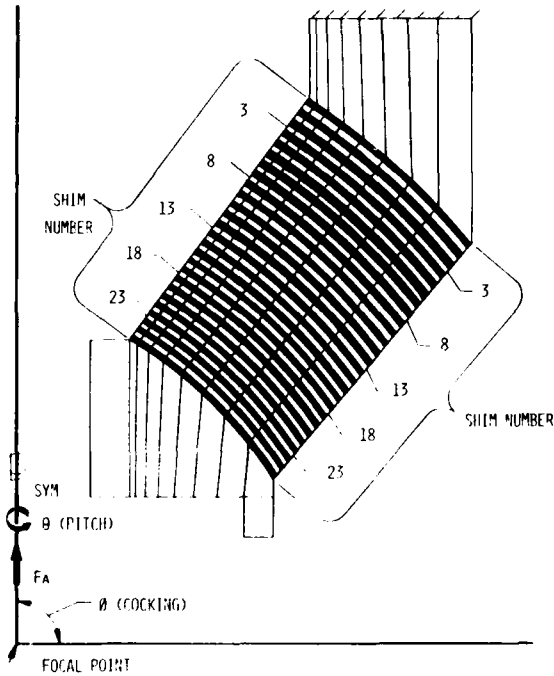


Fig. 2 - Computer plot of spherical thrust bearing

deterioration due to compression strain and the inside second layer from the large end extruding elastomer due to the peak compression induced shear strain indicated in the analysis. Therefore, this design would be marginal due to compression strain and compression induced edge shear strain without adding the prime source of fatigue, shear strain due to ϕ and Θ motion. Thus, a redesign would be indicated before any costly qualification testing was started. With this known correlation, future designs can be corrected and optimized even before the manufacturing stage is started.

CONVENTIONAL THRUST BEARING

The conventional thrust bearing shown in the computer drawn x-y deformed plot (Figure 8a) under a 266,893 Newton (60,000 pound) axial (F_A) load was designed to accommodate torsional shear (Θ) while reacting an axial load (F_A). The bulge pattern shown in the deformed plot was consistent with the pattern observed during testing and the areas of failure during dynamic torsional testing were consistent with the areas of highest bulge. An analysis using SARMAS revealed the compression loading pattern on the upper end to be skewed to the outside and on the lower end to be skewed to the inside. A plot of compression induced shear strain (Figure 9) at the

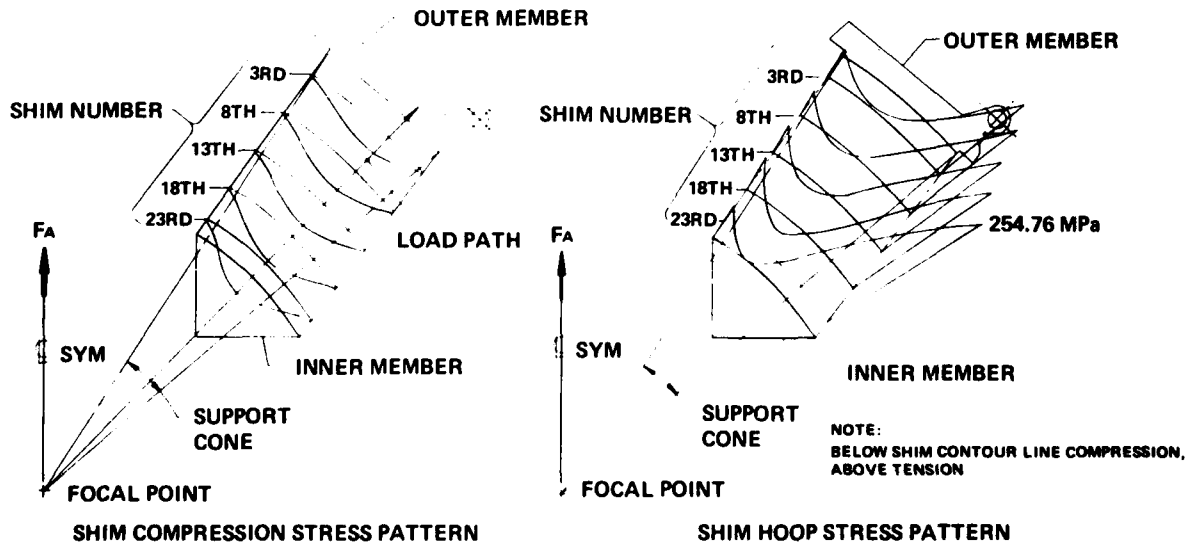


Fig. 3 - Spherical thrust bearing shim finite element results

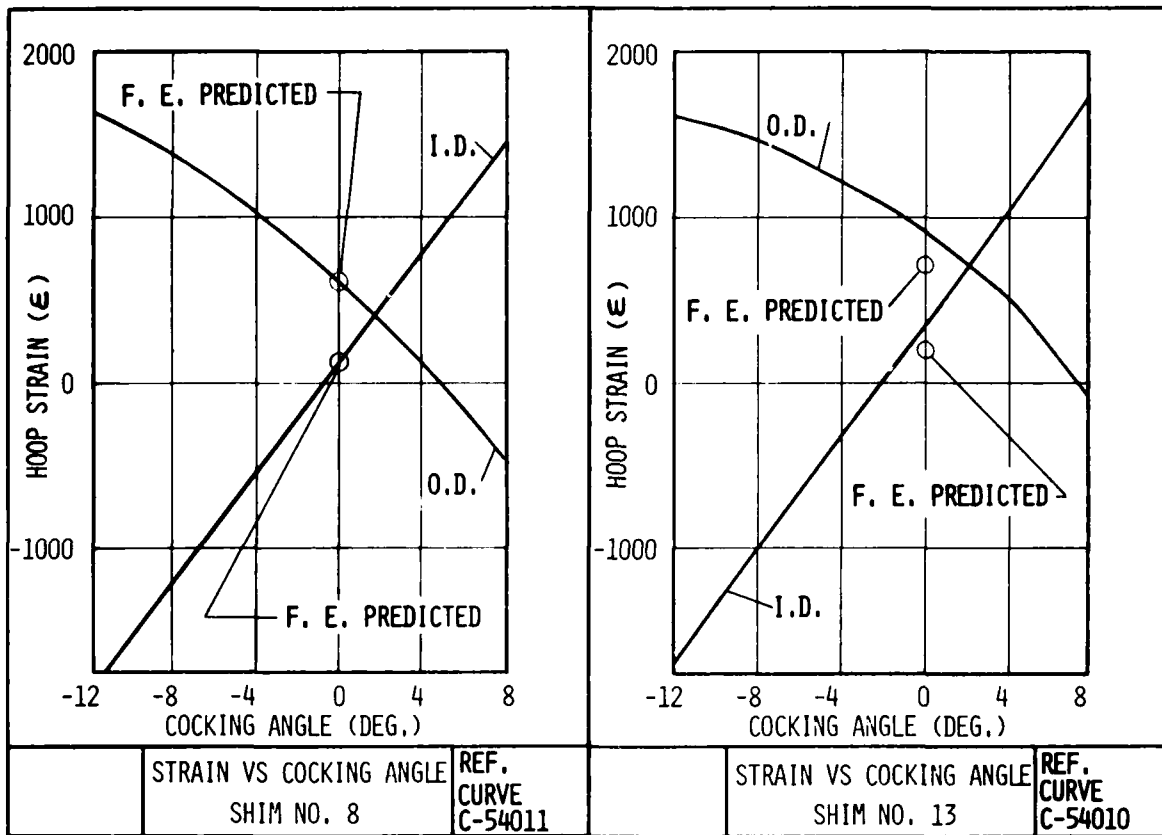


Fig. 4 - Spherical thrust bearing strain gage test results versus finite element analytical results

edge of the elastomer versus elastomer layer number revealed a very high peak shear strain at the upper end on the outer diameter and at the low end on the inner diameter.

A redesign of the shim profile was undertaken to eliminate the skewed compression loading pattern and to reduce the compression induced shear strain values to more acceptable limits. Figure 8b presents the redesigned bearing with the new shim profile as modeled in the finite element analysis under a 266,893 Newton (60,000 pound) axial (F_A) load. The more normalized compression stress loading pattern for this design resulted in a more uniform compression induced shear strain pattern as can be seen in Figure 9. Both designs were tested with an axial load of 155,688 ± 155,688 Newtons (35,000 ± 35,000 pounds). At 19,000 cycles, the original design was failing in the same regions that the specimens subjected

to dynamic torsional testing failed, and the specimen buckled. At 60,000 cycles, the redesigned specimen was exhibiting minor elastomer "fretting" in the first layer on the inside due to compression strain. The remainder of the specimen showed no signs of ever being tested. These two specimens are shown in Figures 10 and 11. It is significant to note that this quantum increase in performance was accomplished without increasing the size of the component or changing the spring rate outside the original tolerances.

AD-A148 079

THE SHOCK AND VIBRATION BULLETIN PART 1 OPENING SESSION
PANEL SESSION SHO. (U) NAVAL RESEARCH LAB WASHINGTON DC
SHOCK AND VIBRATION INFORMAT. SEP 77 BULL-47-PT-1

3/3

UNCLASSIFIED

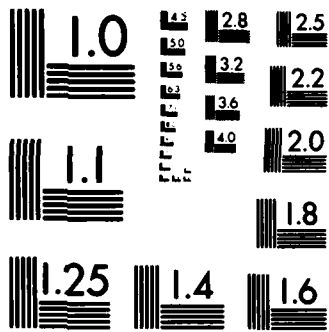
F/G 20/11

NL



END

END



MICROCOPY RESOLUTION TEST CHART
NATIONAL BUREAU OF STANDARDS-1963-A

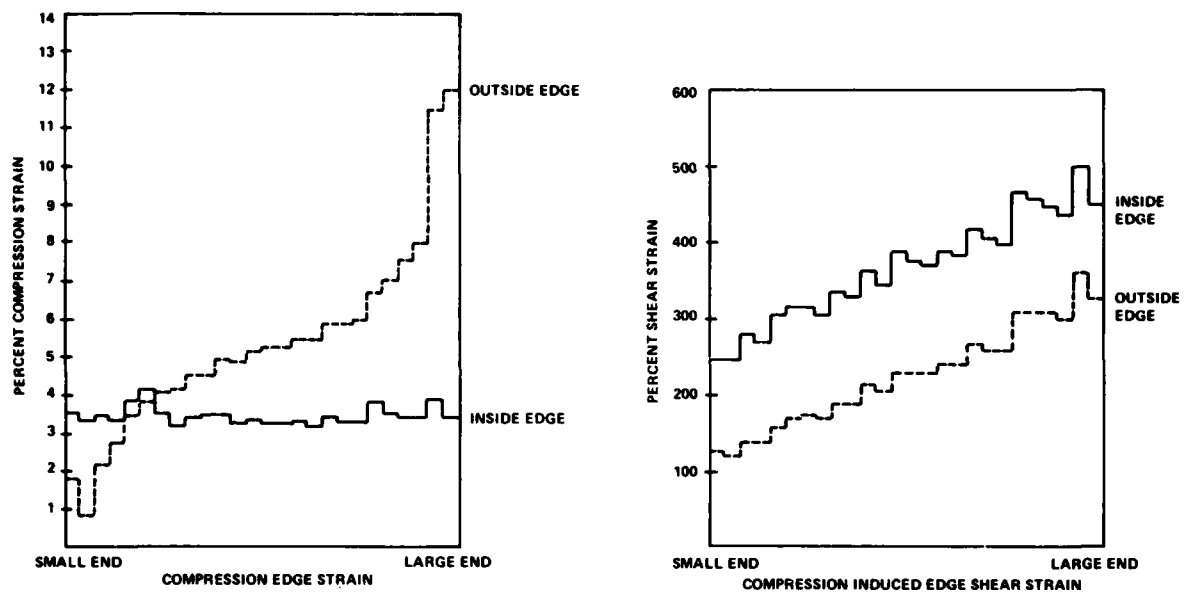


Fig. 5 - Spherical thrust bearing elastomer finite element results

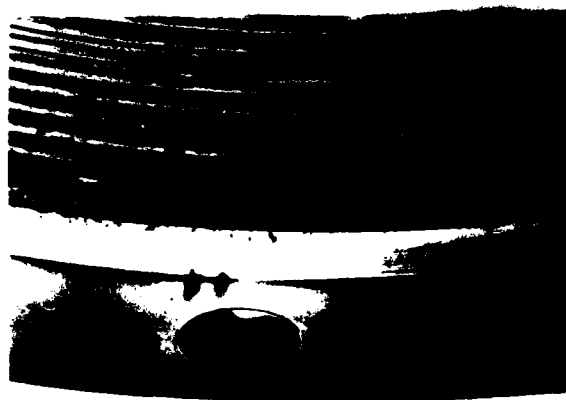


Fig. 6 - Outside layer (large diameter) failing due to edge compression fatigue

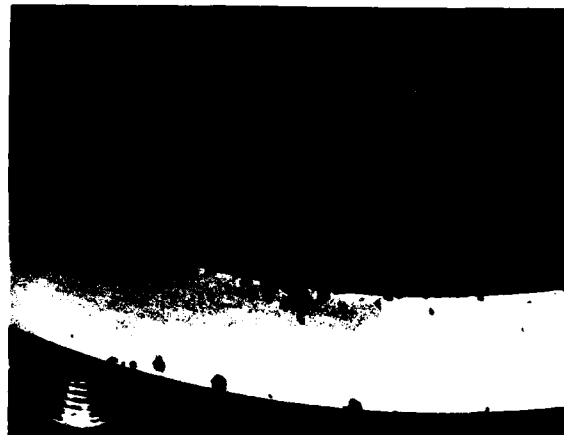


Fig. 7 - Inside layer (next to last) failing due to compression induced edge shear fatigue

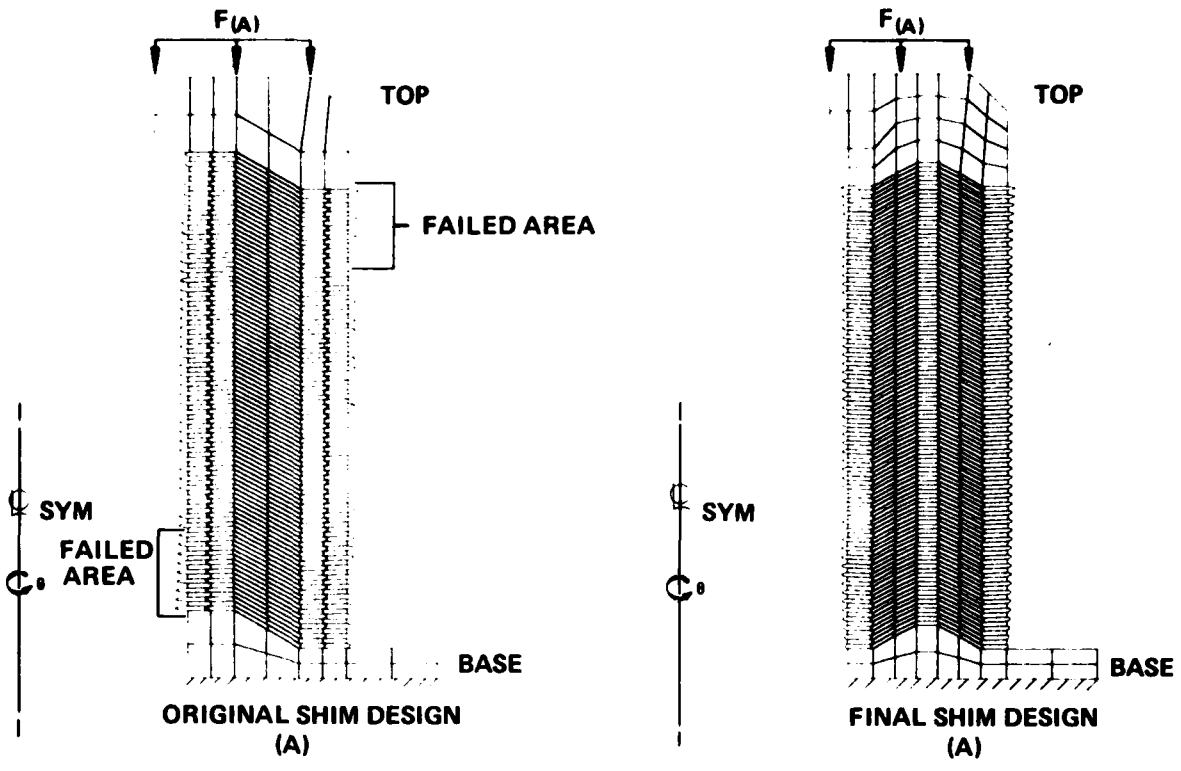


Fig. 8 - Thrust bearing deformed plots

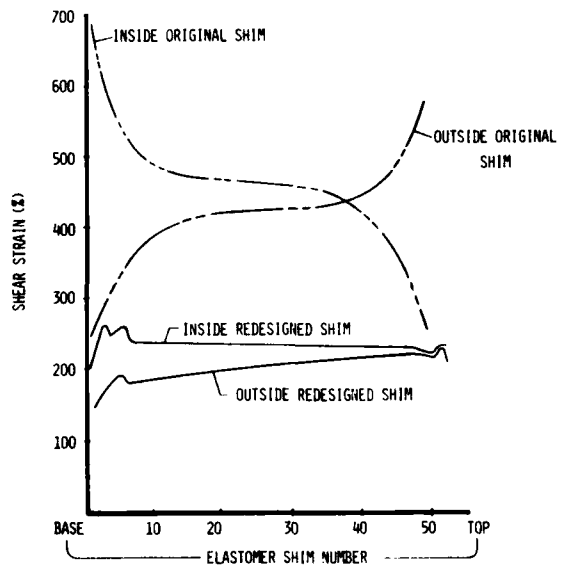
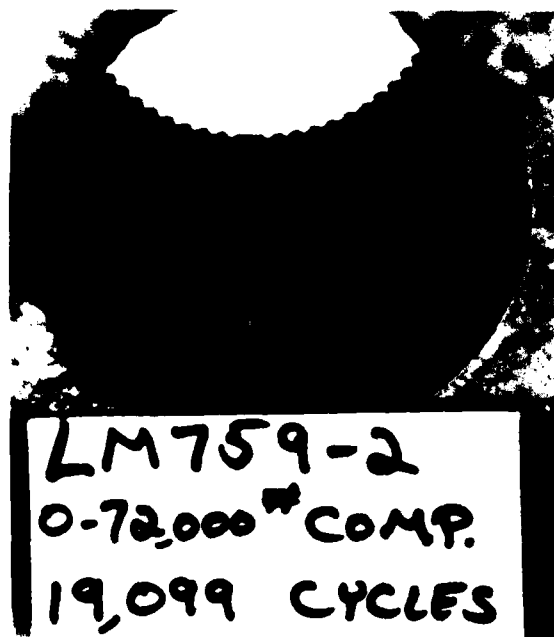


Fig. 9 - Thrust bearing compression induced edge shear strain

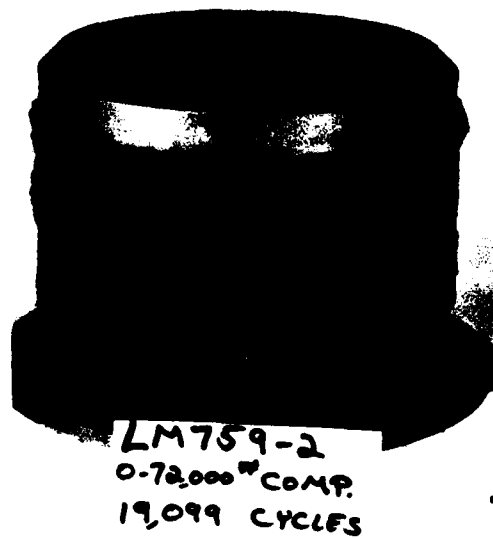
MARINE RISER FLEXJOINT

A marine riser flexjoint, for use beneath the sea in drilling operations, consists of two end terminations which include joint flanges and a central housing (see Figure 12). Each end termination has an interior bell end which accepts a laminated spherical thrust bearing between it and the housing. Between the interior surfaces of the bell, laminated elastomeric (HCL) seals are located.

The elastomeric (HCL) bearing is the primary load carrying member since forces from one end termination are carried through the bearing to the housing, and then through the other bearing to the other end termination. The bearing carries the following loads, which are additive:



(a) Inside

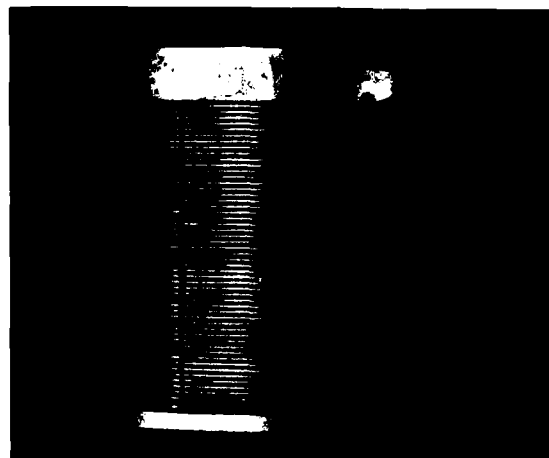


(b) Outside

Fig. 10 - Original thrust bearing design after 19,000 cycles of alternating compression



(a) Inside



(b) Outside

Fig. 11 - Redesigned conventional thrust bearing after 60,000 cycles of alternating compression. Note: No change in size from Fig. 10

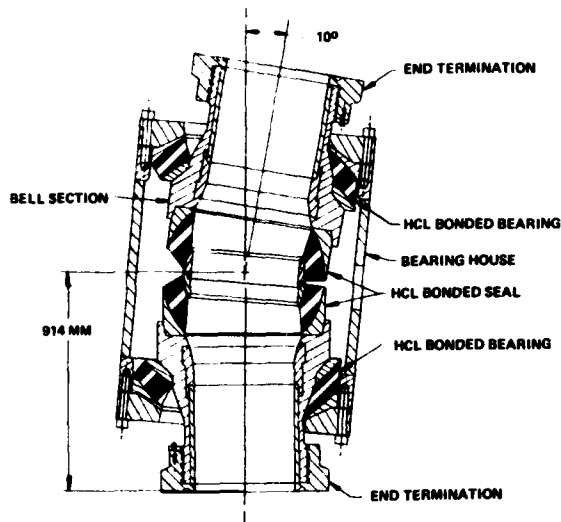


Fig. 12 - Flexjoint cross-section

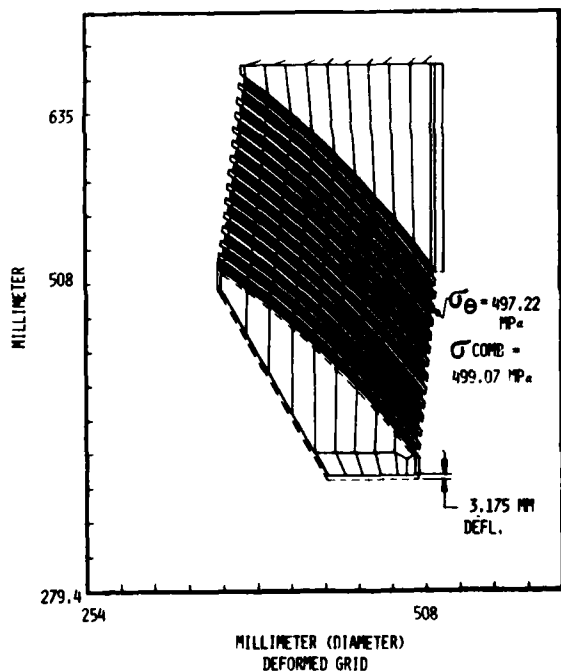


Fig. 13 - Flexjoint bearing with 3.175 mm axial deflection imposed (6,614,506 Newtons)

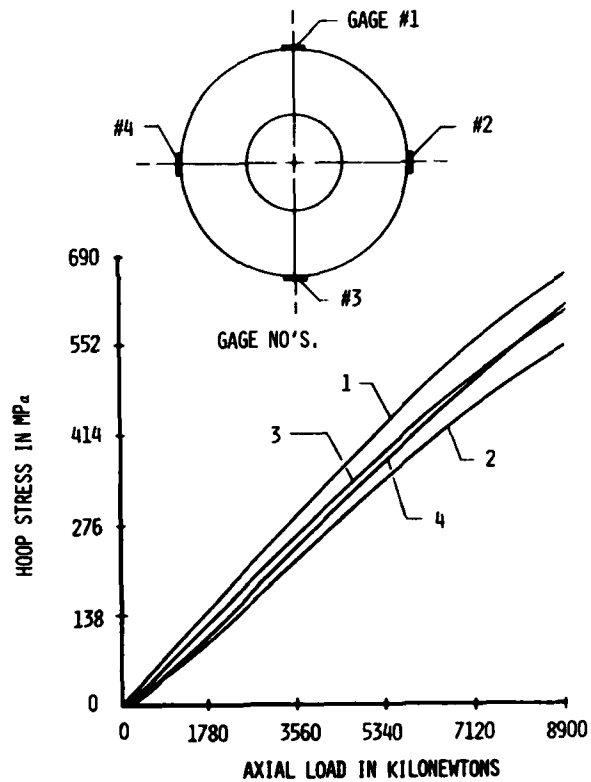


Fig. 14 - Strain gage test - third shim - Lord flexjoint bearing

1. Precompression - 756,198 Newtons (170,000 pounds)
2. Tension - 2,668,933 Newtons (600,000 pounds normal max.)
3. Piston Effect (due to internal diameter differences) - 5,604,760 Newtons (1,260,000 lbs.)
4. Seal Reaction - 1,027,539 Newtons (231,000 pounds)

In addition to carrying the above loads, angular cocking and torsional motion capability is also required. The required reliability of this type of HCL joint is obvious due to the hostile sea environment and depths in which it must function. This also is not a component where the "cut and try" method is applicable because of the high tooling costs associated with obtaining the first test article and the consequences if failure occurs during drilling operations. Finite element analysis was performed on both

the bearing and the seal prior to formal commitment to manufacture the component with data obtained from the previous spherical thrust bearing analysis and testing utilized during the design stage. Figure 13 is a computer drawn x-y plot of the cross-section of the resulting marine riser flexjoint spherical bearing with 3.175 mm (0.125 inch) axial deflection. This deflection is equivalent to 6,614,506 Newtons (1,487,000 pounds) of axial force and results in the hoop stress (maximum) of 497.22 MPa (72,116 psi) on the outer edge of the third shim as noted. The bearing was built, equipped with axial strain gages on the outside edge of the third shim and the shim hoop strain analysis verified. The four gages, located 90° from each other read between 427.47 MPa (62,000 psi) and 524 MPa (76,000 psi) with an average of 472.29 MPa (68,500 psi) (or an average 5% error between calculated and actual). This is shown in Figure 14.

Analytical data obtained by using SARLAS for the smaller elastomeric bearings in regards to elastomer stress and strain which has shown excellent correlation with test results can and is being used to evaluate the larger marine riser flexjoint elastomeric components. Due to the nature of the analytical technique, there is no size effect to account for in the application of data from one component to another.

ADDITIONAL APPLICATIONS

Numerous additional applications for SARLAS have been found to minimize risks to the customer and maximize the chances for success the first time in lieu of the "cut and try" method. Among these applications are:

Deck Link for the Trident Submarine - The analysis of a rod end designed to accommodate an impact load equivalent to 342,068 Newtons (76,900 pounds) radial load would normally require a series of assumptions based on past experience. This is risky in terms of both cost and time when a deck link of the size required for the TRIDENT submarine is considered. Therefore, due to the known accuracy of SARLAS, the TRIDENT Submarine Elastomeric Deck Link was analyzed with SARLAS using a sinusoidally distributed load of 13,467 Newtons per millimeter (76,900 pounds per inch) of the axial length. The maximum stress, based on the octahedral shear stress theory indicated a redesign (Figure 15a).

Repeating the analysis using an increased wall thickness of 38% (Figure 15b), the maximum octahedral stress showed a reduction of approximately 50%. Testing to date supports the validity of the analysis and the wisdom of a redesign while the design is still on the drawing board.

Combination Bearing System - Figure 16 illustrates an ideal application of SARLAS; the simulation of a system to determine its characteristics under load. In this system, the question is "Where should the elastomeric (HCL) conical bearing be located relative to the elastomeric (HCL) spherical bearing such that when pure radial shear is applied to the conical outer member, the inner member translates axially without cocking?". To design and build the test fixtures and test components required to determine the answer to this question would be extremely expensive and time consuming. By using SARLAS, the designer can determine the relative location and investigate the sensitivity of the solution with a high degree of confidence that when the system is built it will work the first time.

CONCLUSIONS

"SARLAS", a Lord Kinematics' modified version of the finite element program TEXGAP, can reduce the time and cost from design conception to production hardware of elastomeric components due to its capability to analyze structures consisting of incompressible or nearly incompressible materials such as rubber. The accuracy of this analytical technique has been demonstrated by experimental test data obtained by using strain gages and by actual endurance testing. The versatility of the analysis is only limited by the designers ingenuity since the cost in terms of time and money while significant, is less than the cost of tooling, test fixtures and the time required to iterate the "cut and try" method.

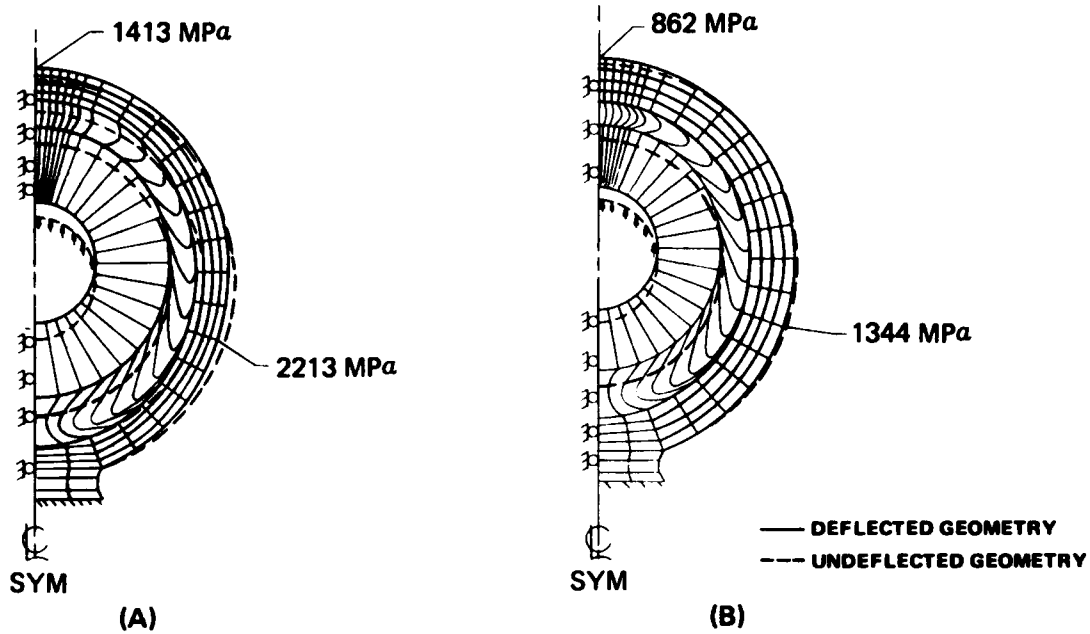


Fig. 15 - Trident Deck Link

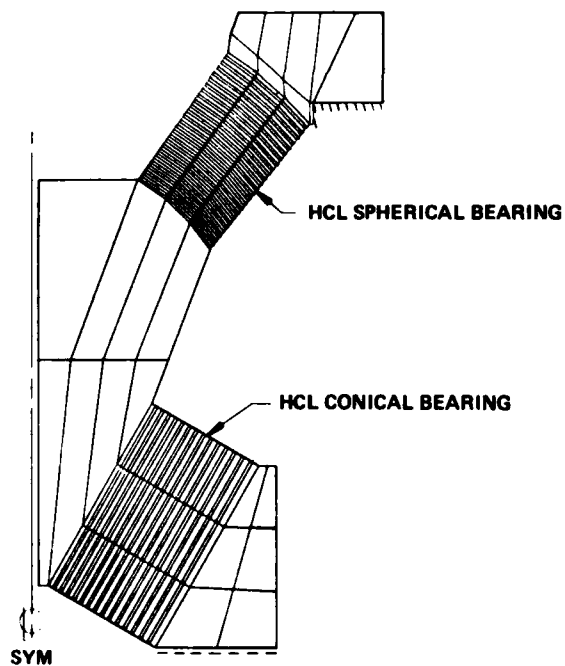


Fig. 16 - Combination Bearing System

ACKNOWLEDGEMENT

The authors wish to acknowledge the contributions of L. J. Schwemmer, Lord Kinematics, in obtaining the Marine Riser Flexjoint data presented herein.

CHARACTERIZATION OF BULK CUSHION MATERIALS
UNDER IMPACT LOADS USING VISCOELASTIC THEORY

Thomas L. Cost and James D. Dagen
The University of Alabama
Tuscaloosa, Alabama

and

John E. Jackson
Tennessee Valley Authority
Knoxville, Tennessee

The movement and storage of shock sensitive equipment requires the use of appropriately designed cushioning systems. Bulk cushion materials, such as foamed polyurethane and polyethylene, are used quite commonly in these systems to mitigate shock effects. Dynamic cushioning curves which illustrate peak deceleration values obtained for specific size bodies impacting specific cushioning systems are used extensively in the engineering design of such cushioning systems. Although the use of dynamic cushioning curves has proven beneficial, the large number of curves required to describe cushion data makes their use cumbersome. Also, the amount of testing required to develop the curves is large.

To reduce the amount of testing required and condense the data to be utilized in the cushion design process, a nonlinear viscoelastic stress-strain law was incorporated within a mathematical model of cushion systems under impact. After certain material parameters are determined from experimental data, the mathematical model can be used to predict the cushion response to impact loads associated with various drop heights, cushion thicknesses, and temperatures.

INTRODUCTION

Contemporary engineering package design procedures for impact loads rely on the use of cushion data presented in the form of curves displaying peak deceleration versus static stress, as illustrated in Figure 1. Values on the curves correspond to peak decelerations experienced by objects falling from a particular height onto a cushion of a given material and thickness and at a specific temperature. The static stress parameter corresponds to the ratio of body weight to body surface area in contact with the cushion. Separate curves are required for each unique combination of system parameters, i.e., drop height, cushion thickness, temperature, and, of course, material. The use of these dynamic cushioning curves has proven to be a useful design procedure. However, one limitation of the procedure has been the tremendous amount of testing required to generate the dynamic cushioning curves.

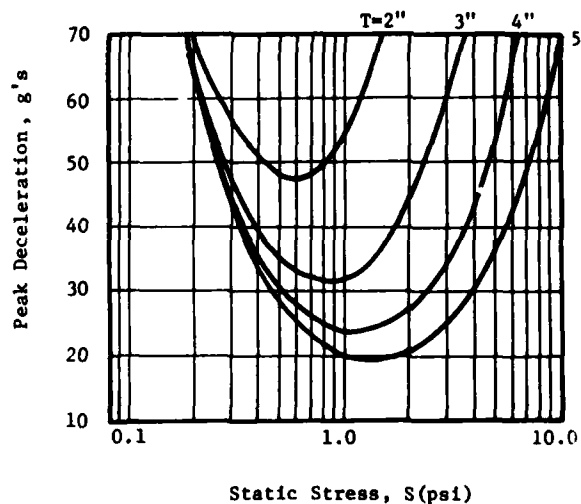


Figure 1. Typical Dynamic Cushioning Curve

Consider, for example, the number of tests required to develop the cushion data curves necessary to cover even a limited range of design conditions. Suppose cushions of three different thicknesses are to be tested at four different drop heights and at three different temperatures. To describe these parameters, a total of thirty six cushion data curves would be required for each material. To construct each deceleration versus static stress curve, assume testing must be conducted at seven different static stress levels. Finally, to obtain statistically meaningful data, at least ten tests would be required at each static stress level. This requires a grand total of 2,520 individual tests ($36 \times 70 = 2,520$) to characterize each material. Admittedly, this is a conservative estimate.

McDaniel [1,2] has developed a mathematical model which summarizes cushion data in the form of a polynomial equation. The data used to generate the equation would normally be presented in the form of dynamic cushioning curves. An optimization program has been developed [3] to search values of the equation and select the lightest cushion which meets the design specifications. Although this system represents a significant improvement in the design process, it still relies on the same large number of tests to construct the dynamic cushioning curves.

To alleviate the need for the numerous tests required to characterize a material, it appears desirable to attempt to describe the cushion material and test conditions in such a way that a limited number of test results would be sufficient to characterize a mathematical model which could then be used to predict the cushion system response under conditions other than those tested. This, of course, is the procedure followed in many other fields of engineering design. This basic technique was used by Cost [4] to generate the form of the McDaniel model [1].

An exploratory study was undertaken to investigate the feasibility of such an approach. The motion of the body has been described through the use of a one-dimensional equation of motion. The stress in the cushion which restricts motion of the body is described by a nonlinear viscoelastic constitutive relation. Details of the model and results of a preliminary study of the model are described in the following sections.

DESCRIPTION OF MATHEMATICAL MODEL

A mathematical model used to predict cushion response to impact loads involves two components: a description of the material response to imposed loads, independent of the material geometry, and a description of the motion of the falling object of a specific weight and size (static stress) as it impacts a cushion with a specific geometry (thickness) after falling

from rest from a particular height (drop height).

Material Response - Bulk cushions are typically manufactured from materials which in their solid polymer state are described by viscoelastic constitutive relations. It seems fruitful to extend the constitutive relations which apply to the solid polymers to their foamed states. This idea is not new. Meinecke and Clark [5] have presented a summary of several ideas related to the description of foamed materials with viscoelastic constitutive relations. Rusch [6] and Meinecke and Schwaber [7] have suggested two separate ideas related to the modification of classical viscoelastic relations to apply to foams.

For a one-dimensional stress state, classical linear theories of viscoelasticity allow the relation between stress and strain to be expressed as [8]

$$\sigma(t) = \epsilon(0)E(t) + \int_0^t E(t-\tau) \frac{\partial \epsilon}{\partial \tau} d\tau \quad (1)$$

where $\sigma(t)$ is the normal stress and $\epsilon(t)$ the normal strain in the material at any time t . The quantity $E(t)$ is referred to as a stress relaxation modulus whose value depends upon the particular material of interest. The linear relation (1) is limited to applications where the deformations are small and the stresses depend linearly on the magnitude of the loads and loading rates.

Bulk cushion materials under impact loads cannot be described by linear constitutive laws since the deformations are sufficiently large to permit the stiffness of the material (stress relaxation modulus) to increase as the deformation increases. This stiffening effect occurs when the voids within the foamed material are compressed to the stage of partial and, finally, total collapse. This effect is nonlinear in character. To account for this nonlinear behavior, it is assumed here that the linear relation (1) is modified by permitting the stress relaxation modulus $E(t)$ to depend not only on time but on magnitude of strain $\epsilon(t)$. Thus, the constitutive assumption employed in this work is

$$\sigma(\epsilon, t) = \epsilon(0)E(\epsilon, t) + \int_0^t E(\epsilon, t-\tau) \frac{\partial \epsilon}{\partial \tau} d\tau \quad (2)$$

The simplest form of stress relaxation modulus which represents actual material behavior is that of a "standard linear solid" [8]. For a linear material this relation is of the form

$$E(t) = (c_1/d_1)e^{-t/p_1} + c_0(1 - e^{-t/p_1}) \quad (3)$$

where the parameters c_0 , c_1 , d_1 , and p_1 are material constants. The parameters of Eqn. (3) can be related to the parameters of the spring-dashpot phenomenological model illustrated in Figure 2 as follows:

$$c_0 = k_2, c_1 = \frac{k_1 k_2}{k_1 + k_2}, d_1 = \frac{\eta}{k_1 + k_2}, p_1 = \frac{k_1 \eta}{k_1 + k_2} \quad (4)$$

The parameters k_1 , k_2 , and η have the physical significance of spring constants and a viscosity parameter, respectively.

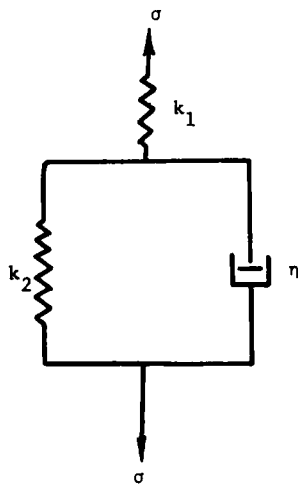


Figure 2. Standard Linear Solid Viscoelastic Model.

The constitutive assumption utilized in this study is derived from consideration of the relation of the mathematical relation (3) to the spring-dashpot model in Figure 2. To account for the nonlinear stiffening effect of the cushion material as it becomes compressed upon impact, it is assumed that the parameters related to the springs in the spring-dashpot model become strain dependent. This implies that the spring constants increase with increasing deformation. The parameter k_1 in Eqn. (4) is assumed to be of the form

$$k_1 = k_{10} + k_{11} \epsilon^{\alpha_{11}} + k_{12} \epsilon^{\alpha_{12}} \quad (5)$$

where k_{10} , k_{11} , k_{12} , α_{11} , α_{12} are parameters to be determined by matching the mathematical model to actual experimental data.

The parameters k_{10} , k_{11} , k_{12} , α_{11} , and α_{12} in equation (5) can be determined from test data. It is important to realize that the characterization tests do not necessarily have to be drop tests. To achieve the loading rates of interest, practical considerations do suggest that the tests should be impact in character. The loading rates associated with conventional uniaxial stress-strain tests are not adequate to characterize the material response. Also, the tests must be compressive in nature to include the nonlinear stiffening effect.

Cushion Impact Model - Consider the body illustrated in Figure 3a as it impacts a cushion supported on a rigid substrate. A free-body diagram of the body on the cushion is illustrated in Figure 3b. Application of Newton's second law to the body results in the equation

$$m\ddot{x} = W - \sigma(\epsilon, t)A \quad (6)$$

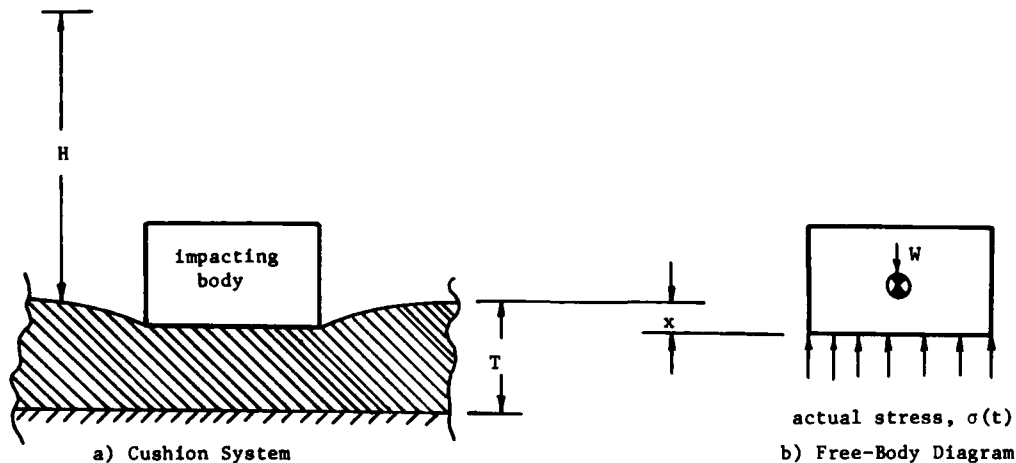


Figure 3. Schematic Diagram of Cushion Impact System

where m , W , and A are the mass, weight, and bottom surface area of the falling body, respectively, $\sigma(\epsilon, t)$ is the normal stress between the cushion and the body, and x is the position of the body relative to the body position at the time of initial contact. A dot over a variable denotes differentiation with respect to time. Equation (6) can be used to determine the position, velocity, and acceleration of the falling body at any time t . The model assumes that the cushion is massless and that the strain, defined as $\epsilon = x/T$, where T is the thickness of the cushion, is uniform throughout the cushion.

To describe the solution procedure for Eqn. (6), substitute the expression for the stress, Eqn. (2), into Eqn. (6) and use a second-order finite difference relation for the acceleration term \ddot{x} to obtain

$$m[x_{i+1} - 2x_i + x_{i-1}]/(\Delta t)^2 = W - A[\epsilon(0)E(\epsilon, t) + \int_0^t E(\epsilon, t-\tau) \frac{\partial \epsilon}{\partial \tau} d\tau] \quad (7)$$

In Eqn. (7), $x_i = x(t_i)$, where the time variable has been decomposed into a series of discrete time steps $t_1, t_2, t_3, \dots, t_n$, and $\Delta t = t_i - t_{i-1}$. By numerically integrating the integral in Eqn. (7), a recursion relation

can be developed for computing the displacement at any time t_{n+1} in terms of quantities at time t_n and t_{n-1} . This is a fairly common technique employed in solving transient dynamic problems [9]. The recursion relation can be expressed as

$$\left[\frac{m}{(\Delta t)^2} + E(0) \frac{A}{H} - \frac{A}{2T} [E(0) - E(\Delta t)] \right] x_{n+1} = W + \left[\frac{2m}{(\Delta t)^2} + \frac{A}{2T} [E(0) - E(\Delta t)] \right] x_n - \frac{m}{(\Delta t)^2} x_{n-1} + \frac{A}{2T} \sum_{i=1}^{n-1} (x_{i+1} + x_i) [E(t_{n+1} - t_{i+1}) - E(t_{n+1} - t_i)] \quad (8)$$

where the right hand side of this equation only involves known quantities at time t_{n+1} .

To start the step-by-step integration procedure for Eqn. (8), the velocity of the falling object at time zero is $\dot{x}(0) = \sqrt{2GH}$, where H is the drop height and G the gravitational constant. The position of the object at time zero is $x(0) = 0$. Repeated application of Eqn. (8) allows successive values of x, \dot{x} , and \ddot{x} to be calculated. Figure 4 contains a plot of typical displacement and acceleration histories obtained by repeated application of Eqn. (8).

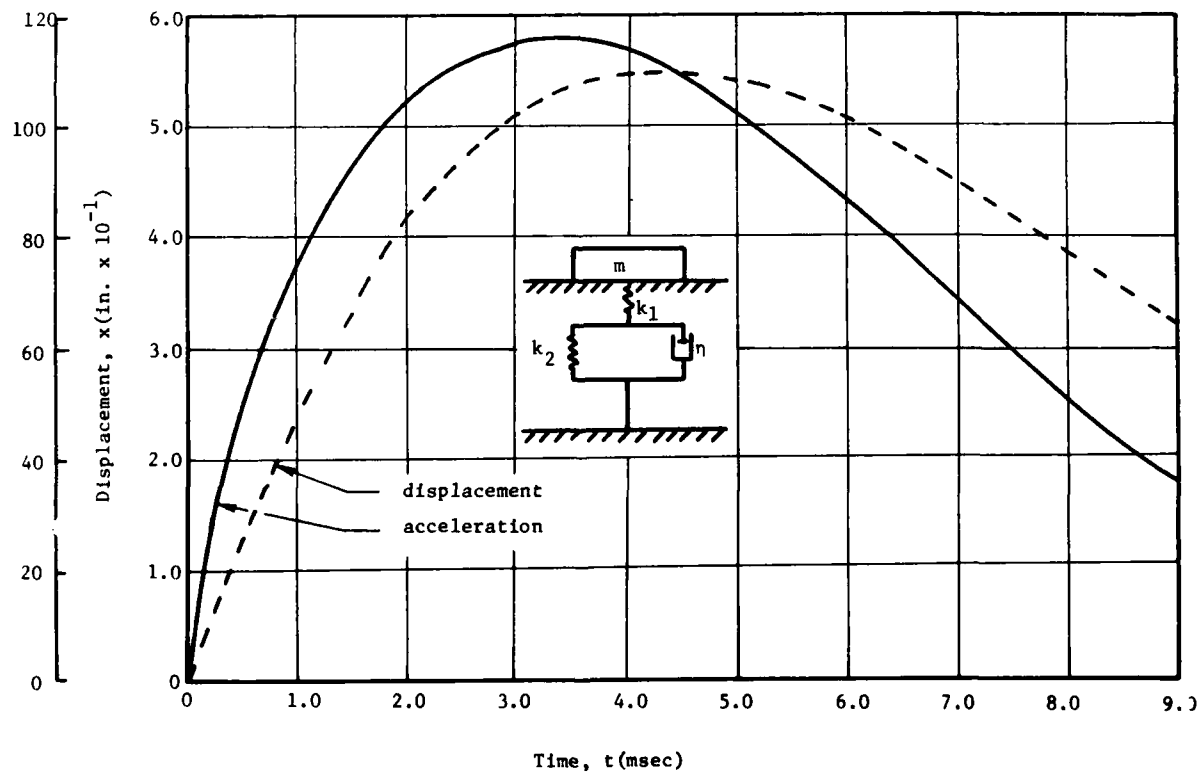


Figure 4. Displacement and Acceleration Histories of Impacting Body

If the total acceleration history of the falling object can be computed as in Figure 4, obviously the peak acceleration (deceleration) can be determined for particular values of the drop height H , cushion thickness T , static stress $\sigma_s = (W/A)$, and for a particular material. The strategy is to determine the cushion material parameters as described in Eqns. (3), (4), and (5) from material characterization studies and then to use Eqn. (8) to determine the peak deceleration value corresponding to a specific set of test parameters.

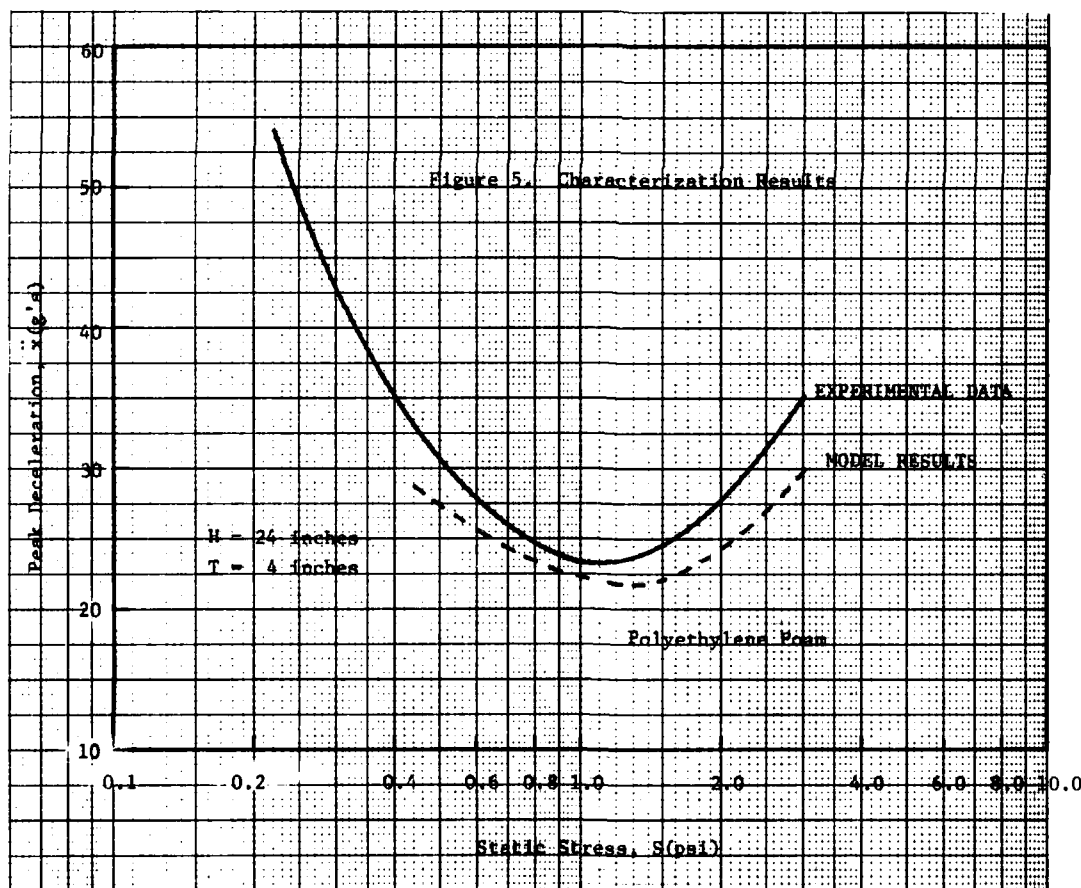
CHARACTERIZATION OF CUSHION MATERIALS

Before the mathematical model described in Section 2 can be used to predict response under a variety of conditions, the cushion material itself must be characterized by determining the material parameters in Eqn. (4). Although a drop test is not necessarily the best experiment to perform to characterize the cushion material, data from this type test was all that was available at the present time. Also, only drop test data in the form of dynamic cushioning curves was available. Detailed acceleration histories of the falling

object in a drop test would provide a better data base with which to characterize the material. However, such data was not available.

The dynamic cushioning curve data presented by Humbert and Hanlon [10] was selected as a commonly available set of data with which to work. It was decided to attempt to determine the desired material properties from the test results on the Humbert and Hanlon low-density polyethylene foamed material from a drop height of 24 inches and a cushion thickness of 4 inches. Based upon results of a parameter study, an initial guess for the desired material parameters was made and then a pattern-search optimization procedure employed to determine the parameter values which "best" correlated with the data.

The flexible tolerance optimization procedure developed by Himmelblau [11] was used to select the "best" set of parameters. In this case, "best" was defined as the parameters which resulted in the smallest variance between the predicted values and the actual data. The flexible tolerance optimization algorithm chooses various values of the desired parameters in a specific way and then



permits the dynamic cushion curve corresponding to these parameters to be produced. These predicted values are then compared with the actual data and the variance of two sets computed. If the variance is less than some arbitrarily defined acceptable value, the search procedure terminates. If the variance is greater than the acceptable value, the optimization procedure adjusts the parameters in an appropriate way and repeats the process. The optimization procedure attempts to minimize the variance between the predicted and actual data sets.

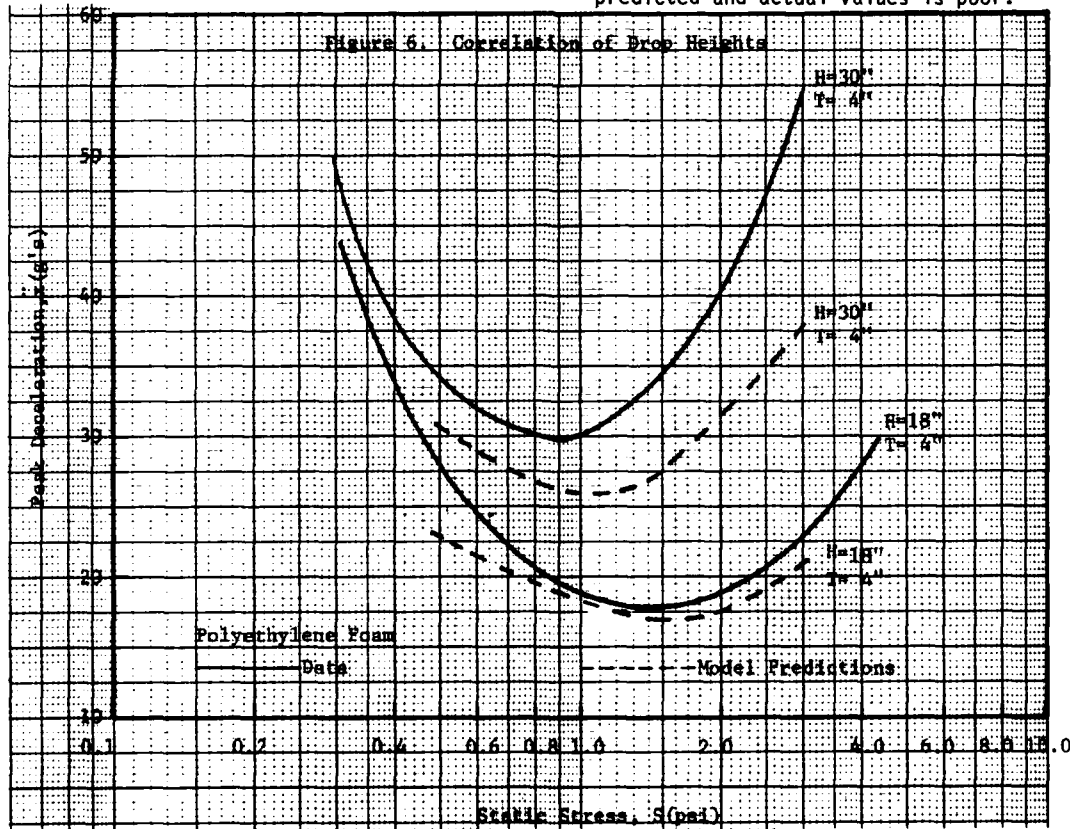
Figure 5 contains a graphical illustration of the "goodness of fit" obtained by determining the material parameters in the manner indicated. The curve again corresponds to the 24 inch drop height and 4 inch cushion thickness data. Values of the material parameters in Eqs. (4) and (5) corresponding to the results in Figure 5 are

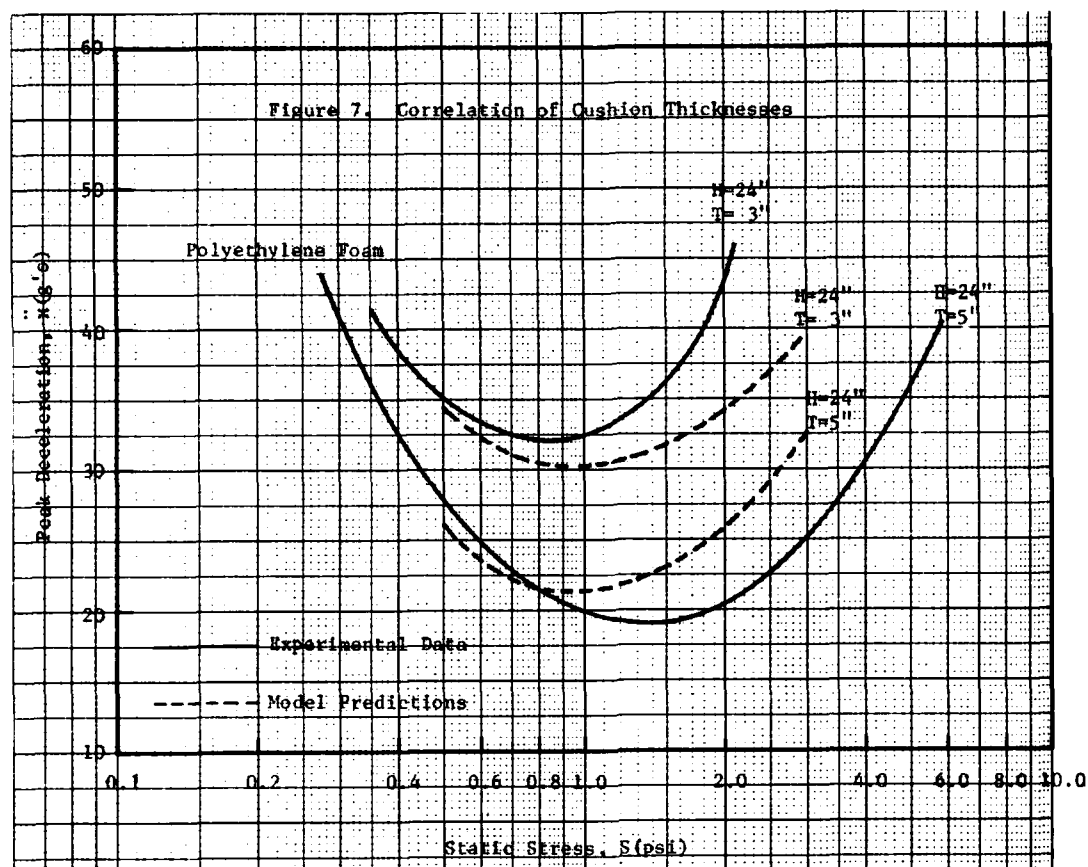
$$\begin{aligned}
 k_{10} &= -2.56660 \times 10^{+1} & a_{12} &= +4.19470 \times 10^{-1} \\
 k_{11} &= +2.94372 \times 10^{-6} & k_2 &= -3.65840 \times 10^{+1} \\
 k_{12} &= +3.60594 \times 10^{+1} & n &= +2.03597 \times 10^{+4} \\
 a_{11} &= +1.22488 \times 10^{+1}
 \end{aligned}$$

The parameters above were determined after searching 160 sets of values in the manner indicated. i.e., the optimization procedure went through 160 cycles.

RESULTS

Using the material properties determined in Section 3, the mathematical model described in Section 2 was used to predict dynamic cushioning curves for other thickness conditions. Correlation for different thicknesses was attempted by using the model to predict dynamic cushioning curves at 3 inch and 5 inch thicknesses. The predicted and actual curves are presented in Figure 6 for these conditions. The agreement seems fair for static stress values near the "optimum" or minimum value of the 3 inch thickness curve. However, agreement is not so good for extreme values of the static stress. Also, the predicted values for the 5 inch thickness cushion agree only in form with the actual data. The trends of the data are correct. However, the discrepancy in magnitudes would be unallowable in design. The ability to model drop height effects was attempted and the results are presented in Figure 7. Comparisons for the 18 inch and 30 inch drop heights agree only in form. The shapes of the curves are correct and the curves are in the proper relation to one another. However, agreement in magnitude between the predicted and actual values is poor.





DISCUSSION AND CONCLUSIONS

Based upon the limited results obtained to date it appears that the mathematical model, including the nonlinear viscoelastic constitutive equation, does represent the physics of the dynamic cushioning problem. It is obvious that if such a technique could be perfected, a large saving could be made in the amount of testing required to describe the behavior of cushions under impact loads. A relatively small number of tests could be used to characterize the material and the resulting characterization incorporated into the mathematical model and used to predict dynamic cushion response under a variety of conditions different than those tested.

The model at the present time may not have enough generality in the nonlinear behavior. Additional generality could be obtained by including more terms in Eqn. (5). Also, the mass of the cushion may need to be accounted for in the mathematical model. Initial attempts to include this effect through the use of the finite element method appear promising. Also, temperature effects can be modeled easily by utilizing the thermorheologically simple constitutive assumption used successfully on solid polymers [8] and on foamed materials [1].

Perhaps the greatest need at this stage of model development is for appropriate characterization tests. Detailed information related to the time-dependent stress and strain histories in the cushion under impact conditions is needed to determine the material properties.

REFERENCES

- 1) Donald M. McDaniel, "Modelling The Impact Response of Bulk Cushioning Materials", U. S. Army Missile Command, Redstone Arsenal, Alabama, Report No. RD-75-16, 1975.
- 2) Donald M. McDaniel, Richard M. Wyskida, and Mickey R. Wilhelm, "A Statistically Based Procedure for Temperature Sensitive Dynamic Cushioning Curve Development and Validation", The Shock and Vibration Bulletin, pp. 69-79, June 1975.
- 3) Donald M. McDaniel, and Bruce W. Fowler, "Impact Response Prediction Using the HP9830 System", U. S. Army Missile Command, Redstone Arsenal, Alabama, Report No. RE-76-7, June 1976.
- 4) Thomas L. Cost, "Dynamic Response of Container and Container Cushion Structures", Athena Engineering Co., Northport, AL,

Technical Report No. 74-003, October 1974.

- 5) E. A. Meinecke, and R. C. Clark, Mechanical Properties of Polymeric Foams, Technomic Publishing Co., Inc., Westport, Conn., 1973.
- 6) K. C. Rusch, J. Appl. Polymer Sci., 13, 2297, 1969.
- 7) E. A. Meinecke, and D. M. Schwaber, J. Appl. Polymer Sci., 14, 2239, 1970.
- 8) R. M. Christensen, Theory of Viscoelasticity, Academic Press, Inc., New York, N. Y., 1971.
- 9) N. M. Newmark, J. Eng. Mech. Div., ASCE, 85, 67, 1959.
- 10) W. G. Humbert, and R. G. Hanlon, Package Engineering, April, 1962.
- 11) D. M. Himmelblau, Applied Nonlinear Programming, McGraw-Hill Book Co., New York, 1972.

IMPACT RESPONSE MODELING OF BULK CUSHIONING SYSTEMS ON A PROGRAMMABLE DESK-TOP CALCULATOR

Richard M. Wyskida
Industrial and Systems Engineering Department
The University of Alabama in Huntsville
Huntsville, Alabama 35807

Don M. McDaniel
Research, Development, Engineering and Missile Systems Laboratory
U. S. Army Missile Command
Redstone Arsenal, Alabama 35809

and

James D. Johannes
Computer Science Program
The University of Alabama in Huntsville
Huntsville, Alabama 35807

This paper reports the results of the modeling efforts on four bulk cushioning materials. The model validation procedure, together with the available desk-top programmable calculator optimization programs, are described. Complete mathematical models are presented for those interested in viewing the basic coefficient/variable structure of the validated models. Specific cushioning application examples are also included.

INTRODUCTION

During the past four years, the Army Missile Command, in conjunction with the University of Alabama in Huntsville, has sponsored a bulk cushioning research program which has concentrated on the effect of temperature variation upon bulk cushioning materials. An extensive drop test program was initiated in 1973, based upon a rigorous experimental design, with initial drop testing conducted upon the Minicel bulk cushioning material [1,2]. Statistical analysis resulted in the development of design curves for each set of experimental conditions. These curves exhibited a statistically significant parabolic-logrithmic shape.

Based upon the encouraging results with the Minicel material, the research program was expanded to include two densities of polyethylene Ethafoam (32 and 64 kg/m³), and two types of polyurethane foam (64 kg/m³ polyester and 48 kg/m³ polyether). Statistically significant parabolic-logrithmic dynamic cushioning curves were developed for each material [3,4].

In 1974, initial modeling efforts began, with an ultimate objective of expressing the required cushion

thickness as a function of the temperature, drop height, fragility level, and static stress, in terms of an n-variable equation. The result was a 25 term Minicel model which was validated with statistical tests [5].

This paper reports the results of the modeling efforts upon the four additional bulk cushioning materials referenced above. The validation procedure is described, together with the available desk-top programmable calculator optimization programs.

MODEL DEVELOPMENT AND VALIDATION

The data base for the superimposed dynamic cushioning curves originally reported upon in [1] was utilized by McDaniel [6] in the development of a generalized model for the Minicel material. In a similar fashion, the data base for the Ethafoams [4], and the polyester and polyether type urethane [3] bulk cushioning materials, were utilized to develop an n-variable model for each new material. The complete model for Ethafoam-2, Ethafoam-4, Urether-3, and Urester-4 are shown in Tables 1 through 4, respectively.

TABLE 1
Ethafom 2 Model

Variable	Coefficient	θ	θ^2	θ^3	$h^{1/2}$	$T^{-1/2}$	$T^{-3/2}$	$(\ln \sigma_s)$	$(\ln \sigma_s)^2$
0	22.056000								
1	0.000000	X				X			
2	0.000000	X				X		X	
3	0.000000	X				X			X
4	-30.284966	X			X		X		
5	0.000000	X			X		X	X	
6	0.283549	X			X		X		X
7	9.951394	X			X	X			
8	-1.509574	X			X	X		X	
9	0.048203	X			X	X			X
10	0.000000		X			X			
11	0.000000		X			X		X	
12	0.000000		X			X			X
13	0.073399		X		X		X		
14	0.000000		X		X		X	X	
15	0.000000		X		X		X		X
16	-0.037576		X		X	X			
17	0.003939		X		X	X		X	
18	0.000000		X		X	X			X
19	0.000000			X		X			
20	0.000000			X		X		X	
21	-0.000001			X		X			X
22	0.000000			X	X		X		
23	0.000000			X	X		X	X	
24	-0.000001			X	X		X		X
25	0.000031			X	X	X			
26	0.000000			X	X	X		X	
27	-0.000003			X	X	X			X
28	-2983.204900	X					X		
29	490.060589	X					X	X	
30	-17.245423	X					X		X
31	18.028014		X				X		
32	-2.473188		X				X	X	
33	0.045148		X				X		X
34	-0.026779			X			X		
35	0.003078			X			X	X	
36	0.000000			X			X		X

NOTE: An X entry at any row and column intersection indicates that the variable identified by that column heading is included in that row variable term.

TABLE 2
Ethafom 4 Model

Variable	Coefficient	θ	θ^2	θ^3	$h^{1/2}$	$T^{-1/2}$	$T^{-3/2}$	$(\ln \sigma_s)$	$(\ln \sigma_s)^2$
0	33.845712								
1	- 23.858291	X				X			
2	0.000000	X				X		X	
3	0.000000	X				X			X
4	0.000000	X			X		X		
5	- 22.434815	X			X		X	X	
6	1.916798	X			X		X		X
7	7.613808	X			X	X			
8	- 0.639810	X			X	X		X	
9	0.000000	X			X	X			X
10	0.000000		X			X			
11	0.018726		X			X		X	
12	0.000000		X			X			X
13	0.000000		X		X		X		
14	0.091455		X		X		X	X	
15	- 0.006268		X		X		X		X
16	- 0.026303		X		X	X			
17	0.000403		X		X	X		X	
18	0.000124		X		X	X			X
19	0.000000			X		X			
20	0.000000			X		X		X	
21	- 0.000004			X		X			X
22	- 0.000169			X	X		X		
23	- 0.000036			X	X		X	X	
24	0.000000			X	X		X		X
25	0.000029			X	X	X			
26	0.000000			X	X	X		X	
27	- 0.000001			X	X	X			X
28	341.920818	X					X		
29	133.964130	X					X	X	
30	- 10.040600	X					X		X
31	0.568838		X				X		
32	- 0.639287		X				X	X	
33	0.000000		X				X		X
34	- 0.001811			X			X		
35	0.000000			X			X	X	
36	0.000129			X			X		X

NOTE: An X entry at any row and column intersection indicates that the variable identified by that column heading is included in that row variable term.

TABLE 3
Urether 3 Model

Variable	Coefficients	θ	θ^2	θ^3	$h^{1/2}$	$T^{-1/2}$	$T^{-3/2}$	$(\ln \sigma_s)$	$(\ln \sigma_s)^2$
0	13.555651								
1	0.000000	X				X			
2	0.000000	X				X		X	
3	0.319806	X				X			X
4	-8.900003	X			X		X		
5	0.000000	X			X		X	X	
6	0.000000	X			X		X		X
7	3.123866	X			X	X			
8	-0.327289	X			X	X		X	
9	-0.019270	X			X	X			X
10	0.000000		X			X			
11	0.008781		X			X		X	
12	-0.003297		X			X			X
13	0.007665		X		X		X		
14	0.010179		X		X		X	X	
15	0.000000		X		X		X		X
16	-0.013446		X		X	X			
17	0.000000		X		X	X		X	
18	0.000287		X		X	X			X
19	-0.000078			X		X			
20	0.000000			X		X		X	
21	0.000005			X		X			X
22	0.000000				X		X		
23	-0.000017			X	X		X	X	
24	-0.000005			X	X		X		X
25	0.000022			X	X	X			
26	0.000000			X	X	X		X	
27	-0.000005			X	X	X			X
28	54.828077	X					X		
29	-17.505666	X					X	X	
30	0.000000	X					X		X
31	0.000000		X				X		
32	0.000000		X				X	X	
33	0.002734		X				X		X
34	0.000000			X			X		
35	0.000000			X			X	X	
36	0.000000			X			X		X

NOTE: An X entry at any row and column intersection indicates that the variable identified by that column heading is included in that row variable term.

TABLE 4
Urester 4 Model

Variable	Coefficient	θ	θ^2	θ^3	$h^{1/2}$	$T^{-1/2}$	$T^{-3/2}$	$(\ln \sigma_s)$	$(\ln \sigma_s)^2$
0	- 60.879992								
1	0.000000	X				X			
2	0.000000	X				X		X	
3	0.000000	X				X			X
4	- 148.276080	X			X		X		
5	18.565089	X			X		X	X	
6	- 1.034744	X			X		X		X
7	10.752943	X			X	X			
8	- 0.982694	X			X	X		X	
9	- 0.039790	X			X	X			X
10	0.000000		X			X			
11	0.000000		X			X		X	
12	0.000000		X			X			X
13	0.487166		X		X		X		
14	0.000000		X		X		X	X	
15	0.000000		X		X		X		X
16	- 0.053289		X		X	X			
17	0.002101		X		X	X		X	
18	0.000529		X		X	X			X
19	0.000000			X		X			
20	0.000000			X		X		X	
21	0.000000			X		X			X
22	0.000000			X	X		X		
23	- 0.000207			X	X		X	X	
24	0.000013			X	X		X		X
25	0.000072			X	X	X			
26	0.000000			X	X	X		X	
27	- 0.000001			X	X	X			X
28	0.000000	X					X		
29	0.000000	X					X	X	
30	14.520064	X					X		X
31	6.557318		X				X		
32	- 1.681827		X				X	X	
33	0.000000		X				X		X
34	- 0.022919			X			X		
35	0.006071			X			X	X	
36	- 0.000215			X			X		X
37	- 2.185574	X							
38	0.000000	X						X	
39	0.065562	X							X
40	0.000000		X						
41	0.004620		X					X	
42	- 0.000735		X						X
43	0.000015			X					
44	- 0.000012			X				X	
45	0.000001			X					X

NOTE: An X entry at any row and column intersection indicates that the variable identified by that column heading is included in that row variable term.

It was hypothesized that the general model procedure developed by McDaniel [6], which provides dynamic cushioning curves for individual combinations of drop height, temperature, static stress, and cushion thickness, together with the prediction limit equation from [7],

$$\hat{y} \pm \frac{t_{\alpha}}{2} \sqrt{1 + \bar{a}^{-1} (x^T x)^{-1} \bar{a}^{-1}}$$

where

$$\hat{y} = b_0 + b_1 \ln x + b_2 (\ln x)^2,$$

could be combined to provide prediction limits for the developed models at selected static stress levels, drop heights, temperatures, and cushion thicknesses. Drop heights range from 304.8 to 762.0 mm, temperatures from 219 to 344 K, cushion thickness of 25.4 to 101.6 mm, and a static stress range of 345 to 35853 Pa. The individual dynamic cushioning curves [IDCC] developed in [1] would be compared with the developed prediction limits to ascertain whether the generalized model was predicting the IDCC in a consistent statistical fashion. In essence, the test of the generalized model is to determine if it can provide G-level values which include the significant static stress level portion of the IDCC and remain within the prediction limits for the particular conditions under consideration. For the purposes of the model validation, the significant portion of the IDCC are identified as the minimum IDCC G-level value bounded by + 6895 Pa. This significant portion may be truncated at the lower or upper static stress level if the bounds fall outside the standard static stress range of 345 Pa to 35853 Pa. For example, from Table 5, it is apparent that the minimum G-level for the IDCC is 34.38 G's at a static stress of 8274 Pa. Placing + 6895 Pa bounds on the identified static stress level gives a static stress range of 1379 Pa to 15169 Pa. This valid range is identified as a double asterisk (**) to the left of the MODEL column. Over this static stress range, it is seen that all model values are contained within the developed prediction limits for this case.

In Table 6, considering the Urester-4 model, immediately to the right of the values in the column entitled MODEL are seen several asterisks. These asterisks indicate the static stress levels at which the model values are outside of the IDCC prediction limits. For the IDCC, the minimum G's are 54.61 at a static stress of 1034 Pa. The lower static stress level of 345 Pa is utilized as the lower bound since it is the smallest static stress level on which drop test data is available. The upper bound becomes 8274 Pa. The comparison between the identified static stress range (indicated with double asterisk) and the model predicted values outside of the prediction limit (single asterisk), indicates the Urester-4 model is able to predict the IDCC value with the specified statistical accuracy. A complete documentation of the validation procedure for all five materials may be found in [8].

PROGRAMMABLE DESK-TOP CALCULATOR CUSHIONING MODELS

The validated models were programmed on the HP-9810A, based upon a search procedure which provides the bulk cushioning designer with an optimal cushion design that considers the effect of temperature variations.

The HP-9810A version of the developed container cushioning models can be utilized in one of two input modes: 1) magnetic card, or 2) cassette tape [9]. When using the magnetic cards, each model must be input separately and operated upon in an autonomous fashion. Consequently, if a particular material does not satisfy the specified fragility level, another model must be selected and input for consideration. The operator must select the model to be considered based upon his working knowledge of the bulk cushioning materials available. The cassette tape input mode requires the designer to select the model desired and merely acquire the desired program from the cassette tape.

All five models are based upon extensive drop test data which has been determined to be statistically significant at an alpha level of .05 [6]. The Minicel, Ethafoam 2, and Ethafoam 4 models span the 219 to 344 K temperature range. Consequently, these three models are capable of determining cushion requirements for these three materials over the above temperature range. The Urether 3 and Urester 4 models have been developed within a narrower temperature spectrum. Drop test experience indicated that both materials behaved erratically below 244 K suggesting that the materials were inconsistent at the extreme cold temperature. Therefore, these two models are valid only within the temperature range 244 to 344 K.

Two versions of the computerized models are available to the designer. The first, entitled "CUSHOP," is a tailored cushion design program, while the other, "ENCAP," is an optimal encapsulation program.

The "CUSHOP" program accepts from the designer the following inputs: the fragility level of the item to be protected (GLMAX); the temperature range to which the package will be exposed in its logistics environment ranging from the coldest, through ambient, to the hottest; the drop height requirement; and the material type from the library. The program then searches the static stress region from 345 to 34470 Pa at each thickness to determine compliance with the GLMAX requirement.

The "ENCAP" program is quite similar to "CUSHOP". The primary difference is the designer's intent to encapsulate the protected item in the cushion. Encapsulation consequently dictates that the

TABLE 5
Sample of Minicel Validation

304.8 mm D.H.		25.4 mm THICK		219 K TEMPERATURE	
STATIC STRESS Pa	DECELERATION (G)				UPPER-P
	IDCC	LOWER-P	MODEL		
345	186.72	156.91		193.03	216.52
689	128.03	98.70		128.64	157.37
1034	100.29	71.42		98.36	129.17
1379	83.55	55.12	**	80.19	111.98
1724	72.26	44.26	**	67.99	100.25
2068	64.12	36.55	**	59.24	91.69
2413	58.00	30.85	**	52.71	85.16
2758	53.28	26.52	**	47.69	80.03
3103	49.54	23.18	**	43.76	75.91
3447	46.55	20.56	**	40.63	72.53
3792	44.12	18.51	**	38.11	69.74
4137	42.15	16.89	**	36.08	67.41
4482	40.52	15.61	**	34.43	65.44
4826	39.19	14.61	**	33.10	63.77
5171	38.09	13.84	**	32.02	62.35
5516	37.20	13.25	**	31.15	61.14
5861	36.47	12.82	**	30.46	60.11
6205	35.88	12.52	**	29.93	59.23
6550	35.41	12.33	**	29.52	58.49
6895	35.04	12.23	**	29.22	57.86
8274	34.38	12.52	**	28.87	56.23
9653	34.58	13.52	**	29.44	55.63
11032	35.32	14.91	**	30.56	55.74
12411	36.41	16.50	**	32.05	56.33
13790	37.74	18.20	**	33.77	57.28
15168	39.22	19.95	**	35.64	58.49
16547	40.81	21.71		37.61	59.90
17926	42.46	23.48		39.65	61.45
19305	44.17	25.24		41.73	63.09
20684	45.90	27.00		43.82	64.80
22063	47.65	28.75		45.93	66.54
23442	49.40	30.50		48.03	68.30
24821	51.15	32.24		50.12	70.06
26200	52.90	33.99		52.20	71.81
27579	54.63	35.74		54.27	73.53
28958	56.36	37.49		56.31	75.23
30337	58.07	39.25		58.33	76.89
31716	59.76	40.99		60.33	78.53
33095	61.44	42.74		62.31	80.14
34474	63.10	44.46		64.26	81.73
35853	64.74	46.16		66.19	83.31

TABLE 6
Sample of Urester-4 Validation

457.2 mm D.H.		25.4 mm THICK		317 K TEMPERATURE	
STATIC STRESS Pa	DECELERATION			(G)	
	IDCC	LOWER-P	MODEL	UPPER-P	
345	71.75	20.58	** 62.63	122.02	
689	56.58	6.23	** 47.19	106.93	
1034	54.61	5.05	** 46.98	104.17	
1379	56.30	7.50	** 50.79	105.10	
1724	59.38	11.31	** 56.01	107.44	
2068	63.04	15.68	** 61.73	110.40	
2413	66.93	20.25	** 67.60	113.62	
2758	70.91	24.87	** 73.45	116.94	
3103	74.87	29.46	** 79.19	120.28	
3447	78.78	33.96	** 84.80	123.59	
3792	82.61	38.36	** 90.24	126.86	
4137	86.35	42.64	** 95.53	130.07	
4482	90.01	46.81	** 100.66	133.20	
4826	93.56	50.85	** 105.64	136.28	
5171	97.03	54.78	** 110.47	139.28	
5516	100.40	58.59	** 115.15	142.22	
5861	103.69	62.28	** 119.71	145.10	
6205	106.90	65.87	** 124.13	147.93	
6550	110.02	69.35	** 128.44	150.69	
6895	113.07	72.74	** 132.63	153.40	
8274	124.56	85.34	** 148.38	163.78	
9653	135.08	96.65	162.72	173.51	
11032	144.79	106.88	175.91	182.71	
12411	153.82	116.19	188.13	191.44	
13790	162.25	124.75	199.52	199.76	
15168	170.18	132.68	210.21 *	207.68	
16547	177.66	140.09	220.28 *	215.23	
17926	184.75	147.07	229.81 *	222.43	
19305	191.49	153.70	238.86 *	229.29	
20684	197.92	160.04	247.48 *	235.81	
22063	204.07	166.13	253.71 *	242.01	
23442	209.96	172.02	263.60 *	247.91	
24821	215.62	177.73	271.17 *	253.52	
26200	221.07	183.28	278.45 *	258.86	
27579	226.32	188.68	285.46 *	263.97	
28958	231.39	193.92	292.22 *	268.87	
30337	236.30	199.00	298.76 *	273.59	
31716	241.05	203.91	305.09 *	278.19	
33095	245.65	208.61	311.23 *	282.69	
34474	250.12	213.07	317.18 *	287.16	
35853	254.46	217.26	322.96 *	291.66	

static stress cannot be tailored to the values prescribed by "CUSHOP" using corner pads on other tailored designs. The stress levels are thus predetermined based on the surface area configuration and weight of the protected item. Consequently the "ENCAP" search technique accepts the static stress values for encapsulation in addition to the other parameters input in "CUSHOP". "ENCAP" then increments on thickness until the material response is below GLMAX at the static stress levels specified.

If the particular material model for "CUSHOP" or "ENCAP" is unable to satisfy the stipulated conditions, the hardcopy will be void of any superimposed dynamic cushioning curves. Consequently, the designer should select another material type for consideration.

The material cushion thickness range associated with the "CUSHOP" models begins at 25.4 mm and terminates at 114.3 mm. An indication of program termination occurs at 114.3 mm. Superimposed dynamic cushioning curves are not plotted since the upper limitation, 101.6 mm, on the basic drop test data, has been attained. In a similar fashion, the "ENCAP" models begin at a 25.4 mm cushion thickness, and have an upper limit of 317.5 mm. Any decisions associated with the "ENCAP" models which involve thicknesses greater than 101.6 mm, should be exercised with great prudence, since the range of the basic drop test data has been exceeded.

The materials currently available in the library are:

<u>Material No.</u>	<u>Material Name</u>
1	Minicel (Cross-linked polyethylene 32 kg/m ³)
2	Ethafoam 2 (Linear polyethylene 32 kg/m ³)
3	Ethafoam 4 (Linear polyethylene 64 kg/m ³)
4	Urether 3 (Polyether urethane 48 kg/m ³)
5	Urester 4 (Polyester urethane 64 kg/m ³)

"CUSHOP" OUTPUT INTERPRETATION

A typical output of the HP-9810A version of the "CUSHOP" model is shown in Figure 1. This output is associated with the Ethafoam-2 cushioning material encompassing the entire temperature spectrum considered essential to military packaging, namely 219 to 344 K. The drop height selected was 558.8 mm with a fragility level of 40 G's. All this information is input

by the designer, and is output under the heading on each hard copy.

The first plotting activity in the procedure draws a horizontal line at 40 G's to identify the specified fragility level for this example. The procedure then searches through the material cushion thickness, starting at 25.4 mm, until it acquires a material cushion thickness which provides a 1379 Pa static stress range at or below the 40 G fragility level. The variation which occurs as a function of temperature within the considered material is shown by the three parabolic shaped curves in Figure 1. The left upper most curve represents the cold temperature effect, the middle curve represents the ambient temperature effect, while the left lower most curve represents the hot temperature effect. The static stress range, indicated on the fragility level line by the intersection of the cold and hot superimposed dynamic cushioning curves, and identified in the heading as SSL = 4482 and SSU = 8617, represents the safe design limits for 50.8 mm of Ethafoam-2 cushion with a 558.8 mm drop height. TOPT represents the thickness of cushion required in millimeters.

It should be noted that any cushion thickness above 50.4 mm will result in excessive cushioning ability together with the attendant material cost and space requirements. Consequently, it is in the designers' best interest to utilize only the necessary amount of cushion in any container design.

"ENCAP" OUTPUT INTERPRETATION

A typical output of the HP-9810A version of the "ENCAP" model is shown in Figure 2. This output is similar to the "CUSHOP" output. However, two additional inputs are required, namely the upper static stress level and the lower static stress level. All other inputs remain the same.

The "ENCAP" model operates on the premise that the item to be packaged will be entirely surrounded by the proposed cushioning material. The amount of cushion required is a function of the temperature range, the drop height, the fragility level, and the static stress range. It should become immediately evident that the wider the static stress range, the greater the cushion thickness requirement.

The two vertical lines identified on Figure 2 represent the extremes of the selected static stress range. TOPT represents the thickness of cushion required in millimeters. It should be noted that the results are the same for both "CUSHOP" (Figure 1) and "ENCAP" (Figure 2), since the conditions are the same for both situations. Figure 3 illustrates completely different input conditions for the "ENCAP" model with the attendant output.

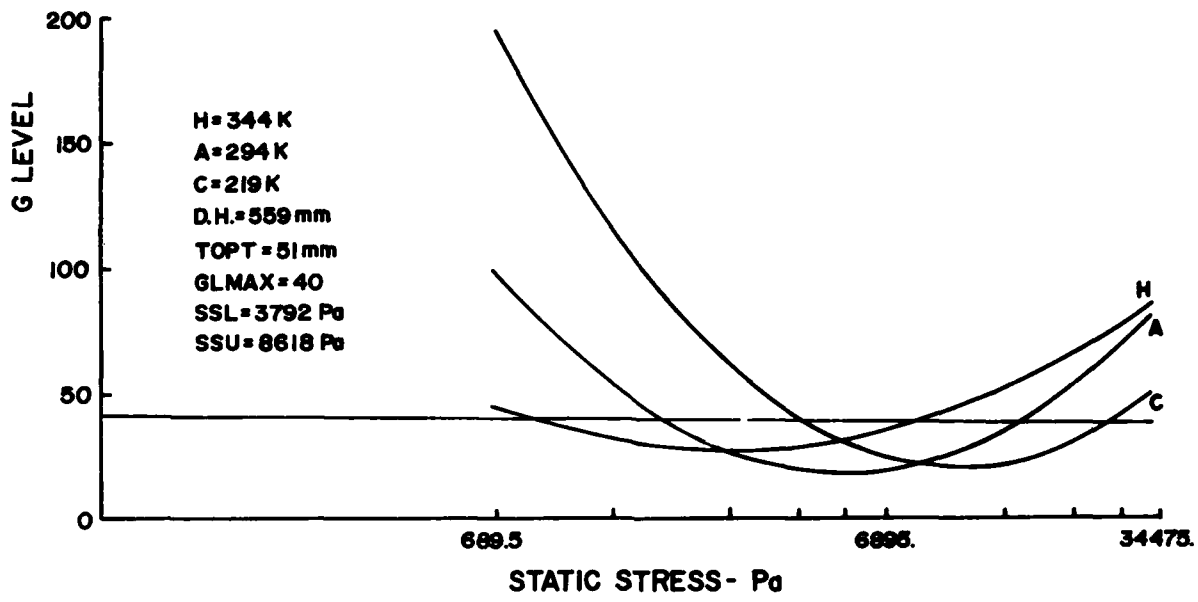


Fig. 1 - Ethafoam 2 "CUSHOP" Example

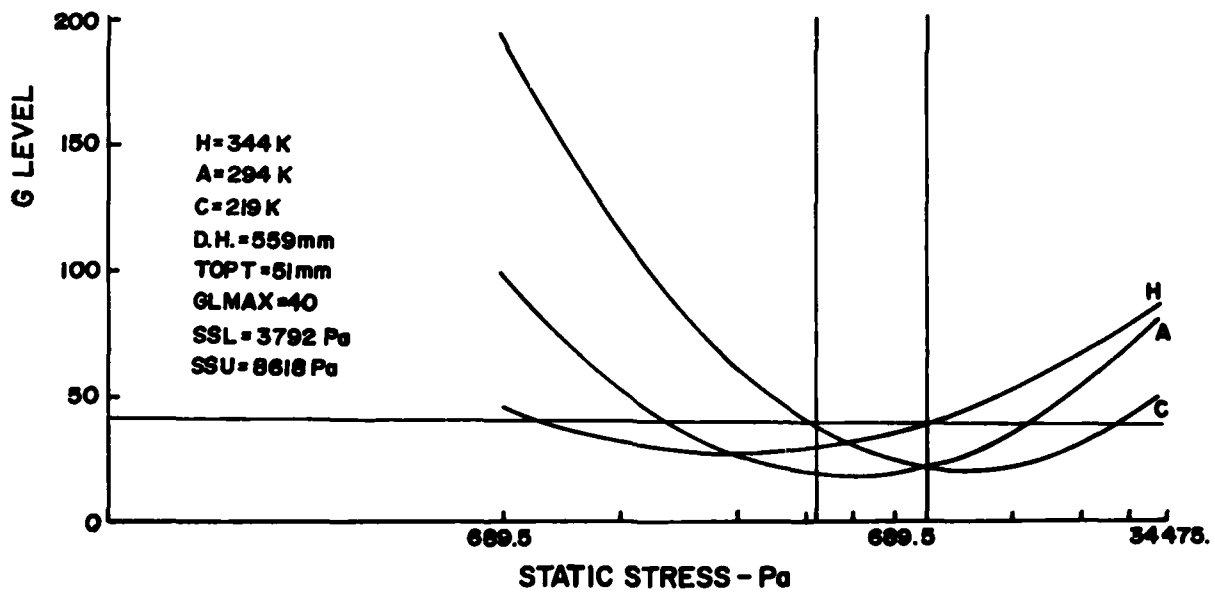


Fig. 2 - Ethafoam 2 "ENCAP" Example I

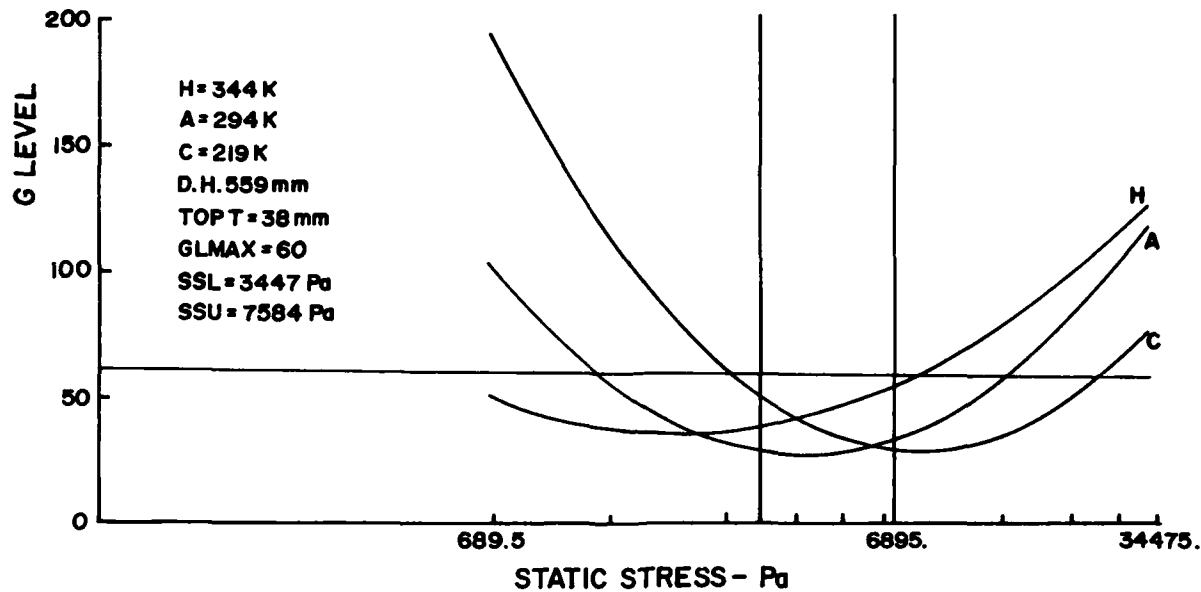


Fig. 3 - Ethafoam 2 "ENCAP" Example II

CONCLUSIONS

The material contained in this article describes the use of the Minicel, Ethafoam-2, Ethafoam-4, Urether-3, and Urester-4 bulk cushioning models which have been developed as part of the MICOM on-going research effort into bulk cushioning materials. These models may be utilized on programmable desk-top calculators in the "CUSHOP" or "ENCAP" modes. The "CUSHOP" model output identifies the cushion thickness, together with an appropriate static stress range, for given inputs of 1) hot, ambient, and cold temperature, 2) drop height, and 3) fragility level. The "ENCAP" mode output identifies only a cushion thickness, for given inputs of 1) hot, ambient, and cold temperature, 2) drop height, 3) fragility level, and 4) upper and lower static stress level. The "CUSHOP" model output results in a feasible cushion thickness requirement if superimposed dynamic cushioning curves are plotted. The "ENCAP" model results are valid only through 101.6 mm cushion thicknesses, although results may be plotted through 317.5 mm cushions.

The complete mathematical models are presented for those interested in viewing the basic coefficient/variable structure of the four validated models. In addition, a sample problem is provided, together with output interpretation, for the Ethafoam-2 model.

Additional models should be developed as new versions of commonly utilized bulk cushioning materials become available. Particular attention should be focused on the development of composite models utilizing thicknesses of material from the five materials already modeled.

The modeling effort is but one example of the improvement in utility and responsiveness derived from desk-top programmable calculator utilization. The nominal expense and relatively unsophisticated techniques should enhance the availability of this methodology to smaller enterprises engaged in package design. Larger enterprises should find that the background technology is sufficiently reliable to establish excellent confidence in the results derived. With the advent of Military Standard 648, in addition to other government and nongovernment specifications that require impact testing at temperature extremes, the necessity for the type of program that incorporates temperature effects becomes abundantly clear. Considerable cost savings can be projected in the avoidance of infeasible design, development and testing, better utilization of packaging and logistical resources, and a reduction in the failure of protected items.

REFERENCES

1. Wyskida, Richard M. and Wilhelm, Mickey R., Temperature Sensitive Dynamic Cushioning Function Development and Validation For Hercules Minicel Thermoplastic Foam, The University of Alabama in Huntsville, Huntsville, Alabama, UAH Research Report No. 159, Vol. I, (MICOM Report No. RL-CR-75-1), September, 1974.
2. McDaniel, Don, Wyskida, Richard M., and Wilhelm, Mickey R., "A Statistically Based Procedure For Temperature Sensitive Dynamic Cushioning Curve Development and Validation," The Shock and Vibration Bulletin, June, 1975.
3. Wyskida, Richard M., Wilhelm, Mickey R., and Bynum, Joseph D., Temperature Sensitive Dynamic Cushioning Function Development and Validation For Polyester and Polyether Type Polyurethane Foam, The University of Alabama in Huntsville, Huntsville, Alabama, UAH Research Report 159, Vol. III (MICOM Report No. RL-CR-75-1), December, 1974.
4. Wyskida, Richard M., Wilhelm, Mickey R., and Bynum, Joseph D., Temperature Sensitive Dynamic Cushioning Function Development and Validation For DOW Ethafoam Polyethylene Foam, The University of Alabama in Huntsville, Huntsville, Alabama, UAH Research Report No. 172, Vol. I, (MICOM Report No. RL-CR-75-4), July, 1975.
5. McDaniel, Don, and Wyskida, Richard M., "The Development of a Generalized Impact Response Model For a Bulk Cushioning Material," The Shock and Vibration Bulletin, June, 1976.
6. McDaniel, Don, Modeling The Impact Response of Bulk Cushioning Materials, U. S. Army Missile Command, Redstone Arsenal, Alabama, Technical Report RD-75-16, 1975.
7. Wyskida, Richard M., Wilhelm, Mickey R., Bynum, Joseph D., and Johannes, James D., Development and Application of Confidence Intervals and Prediction Limits on Dynamic Cushioning Functions For Selected Temperature Sensitive Cushioning Materials, UAH Report No. 180 (MICOM Report No. RL-CR-76-3), Vol. V, October, 1975.
8. Wyskida, Richard M., and Johannes, James D., Validation of Generalized Cushioning Models For Selected Temperature Sensitive Cushioning Materials, UAH Report No. 187 (MICOM Report No. RL-CR-76-7), Vol. I, October, 1976.
9. Wyskida, Richard M., Johannes, James D., and Wilhelm, Mickey R., Container Cushioning Design Engineer Users Manual, UAH Report No. 187, (MICOM Report No. RL-CR-76-7), Vol. II, October, 1976.

END

FILMED

12-84

DTIC

